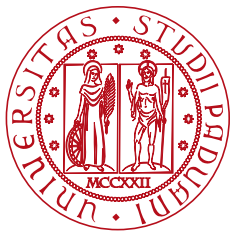

UNIVERSITÀ
DEGLI STUDI
DI PADOVA

Sede Amministrativa: Università degli studi di Padova

Dipartimento di Ingegneria Civile, Edile e Ambientale (ICEA)

SCUOLA DI DOTTORATO DI RICERCA IN
SCIENZE DELL'INGEGNERIA CIVILE ED AMBIENTALE
XXV CICLO

BIO-GEOMORPHIC PATTERNS IN TIDAL ENVIRONMENTS

Direttore della Scuola: Prof. Stefano Lanzoni

Supervisori: Prof. Marco Marani

Dr. Andrea D'Alpaos

Dottoranda: Cristina Da Lio

Ai miei genitori

Abstract

In times of natural and anthropogenic climate change, tidal bio-geomorphic systems are most exposed to possibly irreversible transformations with far-reaching ecological and socio-economic implications. It is thus of critical importance to develop models for predicting the evolution of such systems under varying forcings and, if present, their dynamically-accessible stable states.

The notion that freshwater and terrestrial ecosystems may switch abruptly to alternative stable states as a result of feedbacks between consumers and limiting resources is widely acknowledged. On the contrary, theoretical or observational proofs of the existence of alternative equilibrium states in intertidal ecosystems has until recently proven to be elusive.

This is due to a prevalent reductionist approach, which has until recently mostly produced either purely ecological or purely geomorphological models, while the coupled dynamics of landforms and biota in the intertidal zone has remained largely unexplored.

The presence and continued existence of tidal morphologies, and in particular of salt marshes, is intimately connected with biological activity, especially with the presence of halophytic vegetation. In fact, observations and models coupling geomorphological and biological processes indicate that vegetation crucially affects marsh equilibrium configurations through the production of organic soil, the capture of sediment, and the stabilization against erosion produced by wind waves. Often, different vegetation species live within very narrow elevation intervals, associated with similarly narrow ranges of environmental pressures, thus leading to the emerge of the *zonation* phenomenon. Here we present modeling analysis on the spatial distribution of geomorphological and vegetational spatial patterns in tidal landscapes arising as a result of two-way feedbacks between physical and biological processes. We challenge the traditional interpretation of zonation as a one–way relation between dominant processes in the intertidal frame (i.e. competition vs. edaphic controls), which fails to capture the active role played by vegetation in engineering its own environment.

We use a point model of the coupled elevation-vegetation dynamics, which retains the description of the chief processes shaping these systems, to show how competing stable states are responsible for the formation of characteristic large-scale bio-geomorphic features in tidal landscapes worldwide.

Our analyses extended to a one-dimensional context allows us to explore the mechanism that leads to the formation of well-known, smaller-scale patterns associated with marsh vegetation species distributions.

We develop and present a model that for the first time incorporates species competition, species mutations, sediment transport and soil accretion in a spatially-extended setting, emphasizing that the formation of smaller-scale intertwined topographic and vegetation patterns are driven by bio-geomorphic feedbacks.

We finally analyze the robustness of large-scale and marsh-scale bio-geomorphic features to changes in the forcings, with implications for marsh ecosystem resilience to climate change and anthropogenic pressures.

Sommario

I sistemi bio-geomorfologici a marea sono tra i sistemi più esposti a trasformazioni, anche irreversibili, a causa dei notevoli cambiamenti climatici generati da cause naturali o antropiche, con importanti conseguenze ecologiche e implicazioni socioeconomiche. É quindi di fondamentale importanza lo sviluppo di modelli per prevedere l'evoluzione di questi sistemi soggetti a forzanti variabili e, se presenti, studiarne i loro stati di equilibrio dinamicamente stabili.

L'idea che gli ecosistemi d'acqua dolce e terrestri possano essere soggetti a bruschi passaggi fra stati di equilibrio stabile alternativi, come risultato di retroazioni tra i diversi consumatori e le risorse limitanti, è ampiamente nota e riconosciuta. D'altro canto, dimostrazioni teoriche o osservazioni dirette della esistenza di tali stati di equilibrio negli ecosistemi intertidali non sono ancora consolidate o ampiamente discusse.

Ciò è dovuto ad un approccio prevalente riduzionista, finora principalmente basato su modelli puramente ecologici o puramente geomorfologici, mentre la dinamica accoppiata di morfologia e biologia nella zona intertidale è ancora in gran parte inesplorata.

La presenza e la sopravvivenza delle strutture morfologiche a marea, e in particolare delle barene, sono intimamente connesse con l'attività biologica, in particolare con la presenza di vegetazioni alofite. Infatti, le osservazioni e i modelli che accoppiano processi geomorfologici e biologici indicano che la vegetazione influenza in modo cruciale gli stati di equilibrio attraverso la produzione di suolo organico, la cattura di sedimenti, e la stabilizzazione contro l'erosione prodotta dalle onde da vento. Spesso, specie vegetali differenti vivono a quote altimetriche diverse ma molto ravvicinate fra loro, associate ad altrettanto diverse pressioni ambientali, determinando in tal modo l'emergere del fenomeno di *zonazione*. In questo studio si presentano alcune analisi modellistiche sulla distribuzione spaziale di strutture geomorfologiche e vegetali negli ambienti a marea come risultato di retroazioni bi-direzionali tra i processi fisici e biologici. Viene discussa e rielaborata l'interpretazione tradizionale che vede il fenomeno

di zonazione come una relazione univoca fra i processi presenti nella zona intertidale (cioè competizione fra specie e controlli edafici), che non riesce a cogliere il ruolo attivo svolto dalla vegetazione nel modellare questo ambiente.

Si utilizza così un modello puntuale che accoppia dinamiche fra elevazione e vegetazione, descrivendo i principali processi che portano alla formazione di tali sistemi, mostrando come gli stati di equilibrio stabile, in competizione fra loro, siano responsabili della formazione delle caratteristiche strutture osservate a grande scala negli ambienti a marea.

L'estensione delle analisi ad un contesto unidimensionale permette di esplorare il meccanismo che porta alla formazione delle ben note strutture a piccola scala, associate a diverse distribuzioni di specie vegetali sulle barene.

Il modello sviluppato, incorpora per la prima volta la competizione fra specie, la mutazione di specie, il trasporto di sedimenti e la produzione di suolo in un ambiente esteso nello spazio, evidenziando come la formazione a piccola scala di strutture topografiche e vegetali intrecciate fra loro, siano guidate da retroazioni bio-geomorfologiche.

Si analizza infine la robustezza a larga e piccola scala delle strutture biogeomofologiche al variare delle forzanti esterne presenti, con implicazioni sulla resistenza degli ecosistemi barenali al cambiamento climatico e alle pressioni antropiche.

Ringraziamenti

Desidero anzitutto ringraziare il mio supervisore, Prof. Marco Marani, che mi ha introdotto alla ricerca, invogliandomi ed incoraggiandomi sempre con entusiasmo e con nuovi stimoli alle sfide che si sono via via presentate durante il lavoro e soprattutto per aver con tenacia insistito nel permettermi di trascorrere un periodo all'estero.

Grazie al Dr. Andrea D'Alpaos, co-supervisore, per l'aiuto, gli utili suggerimenti, le idee sempre preziose che mi ha fornito durante il lavoro di ricerca.

Desidero ringraziare inoltre il Dr. Massimiliano Ignaccolo per le discussioni prettamente matematiche che mi hanno consentito di compiere quell'ultimo lungo gradino di salita e di aggiungere quel "quid" mancante: un incontro prezioso, oltre che piacevole sul piano personale.

Grazie al Professor Stefano Lanzoni per la direzione di questa Scuola di Dottorato e a tutti i professori che mi hanno insegnato.

Un grazie a tutti i miei colleghi di dottorato e compagni d'ufficio!

Infine, ma *in primis*, ringrazio i miei genitori che non solo in questi tre anni di dottorato, ma da sempre, mi hanno dato il loro appoggio incondizionato, i loro consigli e nulla mi hanno mai fatto mancare, grazie per la serenità con la quale mi hanno permesso di portare avanti il mio lavoro di ricerca.

E grazie Davide, per avere vissuto con me tutto questo!

Mai dire mai, finché non è sera

Contents

Introduction **1**

1 Large–scale and marsh–scale: eco–morphodynamic details of tidal environments **5**

1.1 Tidal environments: generality 5

1.2 Biotic components that shape the ecosystem 8

1.3 The Venice tidal environment: inorganic and organic characters 10

1.3.1 Lack of sediments: some causes 10

1.3.2 Salt marsh vegetation in the ecosystem evolution 11

1.4 Introductory notes to the 0–D and 1–D models: multiple stable equilibria and patterns formation 21

2 0–D: physical and biological large–scale processes shaping the tidal landscape **27**

2.1 Introduction 27

2.2 The point biogeomorphic model 29

2.3 Equilibrium-vegetation modeling 34

2.3.1 Synthetic forcings: general model behavior leads to different tidal patterns 34

2.3.2 Synthetic forcings: the role of the rate of RSLR and of organic production 37

2.3.3 Synthetic forcings: the role of the tidal range 39

2.3.4 Observed forcings: the role of the tidal regime 42

2.3.5 Observed forcings: the role of the wind regime 47
2.4 Dynamic-vegetation modeling 49
2.5 Observations 52

3 Bio-morphological 1D model 57
3.1 Deposition fluxes and climate change 57
3.2 Evolutionary vegetation model 62
3.2.1 Competition mechanism 62
3.2.2 Mutation mechanism 63
3.2.3 Discrete fitness function 64
3.2.4 Continuous fitness function 65

4 1–D: marsh–scale biogeomophic patterns formation 69
4.1 Discrete fitness functions: analysis 69
4.2 Training of zonation: general model behavior 77
4.3 The role of the rate of RSLR 85
4.4 The role of the sediment supply 90
4.5 The role of vegetation specialization 93
4.6 The role of the initial topography condition 100
4.7 The role of the settling velocity 101
4.8 The role of the maximum areal biomass productivity 104
4.9 The role of the tidal amplitude 107
4.10 Stochastic competition formulation 112
4.11 Mutation coupled with spatial competition 123
4.11.1 Analysis: 1 124
4.11.2 Analysis: 2 124
4.11.3 Analysis: 3 126
4.11.4 Analysis: 4 129
4.11.5 Analysis: 5 129
4.11.6 Analysis: 6 132
4.11.7 Analysis: 7 132

4.11.8 Analysis: 8 132
4.11.9 Analysis: 9 135
4.11.10 Analysis: 10 135
4.11.11 Analysis: 11 138
4.11.12 Analysis: 12 138
4.11.13 Analysis: 13 141
4.11.14 Analysis: 14 141
4.11.15 Analysis: 15 145
4.11.16 Analysis: 16 145
4.11.17 Analysis: 17 148
4.11.18 Analysis: 18 148
4.11.19 Analysis: 19 151
4.11.20 Analysis: 20 151
4.12 Observations 155

Conclusions **157**

Bibliography **171**

List of Figures

1.1 Patch of *salicornia veneta*, that dominates near a forming creek of about 10-20 cm large and 10 cm deep, where the soil elevations are lower between areas of *limonium* on the left and *sarcocornia fruticosa* on the right. 12

1.2 Transition from a mixed vegetation cover near a tidal creek (left and background) to a *limonium narbonense* patch. 13

1.3 Sharp transition between *limonium narbonense* (above) and *spartina maritima* (below). 14

1.4 Smooth transition from a *juncus acutus* patch (left), a *sarcocornia fruticosa* patch, and a *limonium narbonense* patch. 15

1.5 Transitions from a *spartina maritima* patch (above) to a *sarcocornia fruticosa* patch (middle), to a *pucinellia* patch (below). . 16

1.6 The spatial distribution of vegetation – Remote sensing – in the San Felice salt marsh, Venice Lagoon (Belluco *et al.*, 2006; Wang *et al.*, 2009) 18

1.7 Vegetation map of the San Felice salt marsh in the Venice Lagoon (geometric resolution is 0.5 m, channels and creeks are in blue (Marani *et al.*, 2006b) 18

2.1 Color-coded bathymetry of the Venice Lagoon with the locations of the anemometric, turbidimetric, and mareographic stations. . 35

2.2 Time derivative of platform elevation, dz/dt, as a function of platform elevation, z, (a) in the *multispecies vegetation* case and (b) in the *Spartina*-dominated case, when the system is forced with a sinusoidal tide of amplitude $H = 0.5$ m, period $T = 12$ hours, wind characteristics of the Chioggia station (see figure 2.1), rate of SLR $R = 3.5$ mm/yr, and SSC $C_0 = 20$ mg/l. The elevation z is computed with respect to the local MSL. 38

2.3 Bifurcation diagram showing equilibrium elevations, z_{eq}, as a function of the rate of RSLR, R, in the case of a *Spartina*-dominated system forced with a sinusoidal tide with period $T = 12$ hours, amplitude $H = 0.5$ m, and SSC $C_0 = 20$ mg/l. Two possible scenarios for organic production are also considered (namely $\gamma = 2.0 \cdot 10^{-3}$ m^3/yr/kg and $\gamma = 4.0 \cdot 10^{-3}$ m^3/yr/kg) together with the hypothetical case in which vegetation is absent. 40

2.4 a) Erosion rate, Q_E, and b) sub-tidal platform equilibrium elevations, z_{eq}, computed for different tidal amplitudes when the system is forced with a sinusoidal tide with period $T = 12$ hours, rate of SLR $R = 3.5$ mm/yr, wind characteristics at different stations (see figure 2.1), and different SSCs. Solid lines in figure 2.4a, computed by considering wind characteristics at the S. Leonardo station, represent the case in which MPB and vegetation are both present and increase the value of the critical shear stress for erosion; dashed lines show the case in which the polymeric biofilm due to MPB is disrupted by human activity or bioturbation (e.g., invertebrates) and only vegetation contributes to increase the threshold shear stress for erosion. Inset in figure 2.4a: Dependence of the bottom shear stress, τ, on water depth computed for a wind speed of 15 m/s. Solid gray circles in figure 2.4b are obtained when considering wind at the S. Leonardo station and $C_0 = 20$ mg/l; solid white circles: wind at the Chioggia station and $C_0 = 20$ mg/l; solid gray pentagons: wind at the S. Leonardo station and $C_0 = 10$ mg/l. 43

2.5 Salt-marsh and tidal-flat equilibrium elevations made dimensionless with the tidal amplitude, z_{eq}/H, versus the tidal amplitude, H, computed for different tidal amplitudes when system is forced with a sinusoidal tide with period $T = 12$ hours, rate of SLR $R = 3.5$ mm/yr, and SSC $C_0 = 20$ mg/l. 44

2.6 Stable equilibrium states in the oxygen-limited vegetation case with (a) tidal observations at “Murano”, wind at “Tessera” and suspended sediment concentration $C_0(t)$ at “Campalto”; (b) same as in (a) except that the astronomic tide (i.e. with no meteorological component) is prescribed; (c) same as in (a) except that tidal observations at “Saline” are used. 46

2.7 Probability density functions of Tidal levels for (a) observations at "Murano", (b) astronomic tide, (c) observations at "Saline". . 48

2.8 Probability of exceedance of wind velocity according to the Tessera, S. Andrea, S. Leonardo, and Chioggia anemometers. Inset: frequency distributions of wind velocity. 49

2.9 Effects of tidal regimes on the available equilibrium states. dz/dt vs. z and the associated stable equilibria on the basis of the astronomic tide, suspended sediment concentration $C_0(t)$ at Campalto, and wind velocity at Chioggia (a); S. Leonardo (b); S. Andrea (c); and Tessera (d). 50

2.10 Evolution in time of (a) platform elevations, (b) vegetation biomass, (c) accretion rates, and (d) phase portrait describing the dynamics of the system, for different initial conditions. We considered the case of a *Spartina*-dominated system forced with a sinusoidal tide with $T = 12$ hours, $H = 0.75$ m, $C_0 = 20$ mg/l, and $R = 3.5$ mm/yr, when both the reproduction and mortality rates vary as a function of marsh elevation (i.e. $r(z) = -0.5\ z/H + 1.0\ \mathrm{yr}^{-1}$ and $m(z) = 0.5\ z/H\ \mathrm{yr}^{-1}$). In all panels the depicted stable state correspond to a vegetated marsh with $z = 0.50$ m above MSL and $B = 500\ \mathrm{g/m^2}$. 53

2.11 Evolution in time of (a) platform elevations, (b) vegetation biomass, (c) accretion rates, and (d) phase portrait describing the dynamics of the system, for different initial conditions. We considered the case of a *Spartina*-dominated system forced with a sinusoidal tide with $T = 12$ hours, $H = 0.75$ m, $C_0 = 20$ mg/l, and $R = 3.5$ mm/yr, when the reproduction is assumed to be constant ($r = 1.0\ \mathrm{yr}^{-1}$) and the mortality rate increases with marsh elevation (i.e. $m(z) = z/H\ \mathrm{yr}^{-1}$). In all panels the depicted stable state correspond to a vegetated marsh with $z = 0.48$ m above MSL and $B = 350\ \mathrm{g/m^2}$. 54

2.12 Time required for marsh elevations to reach within 3% of the equilibrium elevation starting from different initial conditions, with the "dynamic vegetation" model (i.e. by solving equations (2.1) and (2.2)) and with the "equilibrium vegetation" model (e.g. based on eq. (2.11)) when the birth and the mortality rates are assumed to vary with elevation (as in figure 2.10) and when the birth rate is constant and the mortality rate increases with elevation (as in figure 2.11). 55

3.1 Sketch of the salt-marsh transect considered in the proposed 1-D model. The landscape-forming tide is assumed to be a sinusoidal tide with period $T = 12$ hours and amplitude $H = 0.5$ m. Bottom elevations, $z(x, t)$, and water surface fluctuations, $z_w(t)$, are computed with respect to the local mean sea level (MSL). The sketch, which portrays the biogeomorphic patterns of actual marshes, emphasizes the existence of intertwined vegetation and topographic patterns in which vegetation patches are shown to develop at different marsh elevations. Although salt marshes are commonly thought to as flat structures, field observations show the existence of small elevation differences associated to the encroachment of different vegetation types. 58

3.2 Representative discrete *fitness functions* 65

3.3 Representative continuous hyperbolic secant *fitness functions*. λ is the scale parameter (left or right), C is an optional prefactor from 0 to 1, to impose the maximum less or equal to one, index of the maximum possible areal biomass productivity, z_M is the function mode. 67

3.4 Schematic species mutations of the continuous *fitness function* describing the species characteristic. 68

4.1 Time constant topography linearly decreasing (left) and fitness function representation (right). Each color identifies a different species (red color for species adapted to high elevations, blue color for species adapted to low elevations). Spatial yearly selection mechanism and yearly mutation on. 71

4.2 Time constant topography exponentially decreasing (left) and fitness function representation (right). Each color identifies a different species (red color for species adapted to high elevations, blue color for species adapted to low elevations). Spatial yearly selection mechanism and yearly mutation on. 72

4.3 Time topography evolution (left) and fitness function representation (right). Starting constant topography condition. Each color identifies a different species (red color for species adapted to high elevations, blue color for species adapted to low elevations). Spatial yearly selection mechanism and yearly mutation on. 75

4.4 Representation of the species fitness shape after one thousand years, from species adapted to the low elevations (blue), to species adapted to high elevations (red). At the bottom of figure there are the transect topography (left) and the biomass production (right). 76

4.5 Reference case. Zonation patterns generated by the model. (a) The time evolution of transect topography was here started from a linear initial condition but several other initial conditions were explored with analogous results. Monospecific vegetation patches, very similar to observed zonation patterns (see inset), and terrace-like topographic structures emerge as a result of multiple stable states defined by $\partial z/\partial t = 0$ and $\partial/\partial z(\partial z/\partial t) < 0$. ($b$) Sites with initial elevation comprised between $z_i^{(u)}$ and $z_i^{(s)}$ move towards $z_i^{(s)}$, while sites whose initial elevation is located below $z_i^{(u)}$ move towards $z_j^{(s)}$, j being the species with optimal elevation located immediately below that of species i. (c) Shows the fitness function of the species populating the marsh, which defines the rate of organic soil production as $Q_o = \gamma \cdot B_0 \cdot f_i(z)$ (γ incorporates typical vegetation characteristics and the density of the organic soil produced, B_0 is the biomass density of a fully vegetated marsh). 80

4.6 Reference case. (a) Accretion rate dz/dt, function of elevation; (b) organic ($Q_o(x,t)$) and inorganic ($Q_s(x,t)$) fluxes along the transect; (c) organic flux compared with the inorganic one; (d) transect equilibrium topography 81

4.7 Reference case. (a) Accretion rate, function of elevation. Solid circles represent the stable elevation equilibria; (b) Shows the rate of inorganic soil production as Q_s almost linearly decreasing as the elevation increases. Solid circles represent the stable elevation equilibria; (c) Shows the rate of organic soil production as $Q_o = \gamma \cdot B_0 \cdot f_i(z)$ (γ incorporates typical vegetation characteristics and the density of the organic soil produced, B_0 is the biomass density of a fully vegetated marsh, $f_i(z)$ is the fitness function). Solid circles represent the stable elevation equilibria 82

4.8 Reference case: frequency density of the fitness functions 83

4.9 Reference case: frequency density of each species ("blue", "green", "red") fitness functions 84

4.10 Reference case. Inorganic and organic flux (left and right respectively); the red solid circle represents the last site colonized by the red species. 84

4.11 Perturbation N∘1. Inorganic and organic flux (left and right respectively); the red solid circle represents the last site colonized by the red species in the case in which we perturb the site equilibrium elevation z_{eq} from the equilibrium state $z = z_{eq} - 0.05$m decreasing the equilibrium elevation 86

4.12 Perturbation N∘2. Inorganic and organic flux (left and right respectively); the red solid circle represents the last site colonized by the red species in the case in which we perturb the site equilibrium elevation z_{eq} from the equilibrium state $z = z_{eq} + 0.05$m increasing the equilibrium elevation 86

4.13 Mean suspend sediment concentration over a tidal cycle in three different elevation topography configuration. In red solid circle we indicate the site#6 of the salt marsh transect, subjected to perturbation 87

4.14 (a) Equilibrium topography; terrace structures develop due to the existence of multiple stable states. As external forcings we assume $C_0 = 20$ mg/l and $R = 5.0$ mm/yr. The dashed line represents the equilibrium elevation state in figure 4.5a; (b) Accretion rate as a function of perturbations in the local elevation. Solid circles represent the stable elevation equilibria, open circles the unstable equilibria. External forcings assumed: $C_0 = 20$ mg/l and $R = 5.0$ mm/yr; (c) Fitness functions of the species populating the transect (scale parameter $\lambda = 5$) with $C_0 = 20$ mg/l and $R = 5.0$ mm/yr. Solid circles represent the stable elevation equilibria, open circles the unstable equilibria; (d) The same as (a) except $R = 7$ mm/yr; (e) The same as (b) except $R = 7$ mm/yr; (f) The same as (c) except $R = 7$ mm/yr; 91

4.15 Case RSLR=5 mm/yr. Deposition fluxes (inorganic and organic) over the salt marsh transect (left); relation between the organic and the inorganic flux (right) 92

4.16 Case RSLR=7 mm/yr. Deposition fluxes (inorganic and organic) over the salt marsh transect (left); relation between the organic and the inorganic flux (right) 92

4.17 (a) Equilibrium topography for $C_0 = 5$ mg/l and $R = 3.5$ mm/yr. The dashed line represent the equilibrium topography for the reference case (figure 4.5a); (b) Accretion rate as a function of perturbations in the local elevation. Solid circles represent the stable elevation equilibria. (c) Fitness functions of the species assumed to populate the transect (scale parameter $\lambda = 5$). Solid circles represent the stable elevation equilibria; (d), (g) and (l) The same as (a) with $C_0 = 30$, $C_0 = 40$, $C_0 = 50$ mg/l respectively; (e), (h) and (m) The same as (b) with $C_0 = 30$, $C_0 = 40$, $C_0 = 50$ mg/l respectively; (f), (i) and (n) The same as (c) with $C_0 = 30$, $C_0 = 40$, $C_0 = 50$ mg/l respectively; . . 94

4.18 Case $C_o = 5$ mg/l. Deposition fluxes (inorganic and organic) over the salt marsh transect (left); relation between the organic and the inorganic flux (right) 95

4.19 Case $C_o = 30$ mg/l. Deposition fluxes (inorganic and organic) over the salt marsh transect (left); relation between the organic and the inorganic flux (right) 95

4.20 Case $C_o = 40$ mg/l. Deposition fluxes (inorganic and organic) over the salt marsh transect (left); relation between the organic and the inorganic flux (right) 96

4.21 Case $C_o = 50$ mg/l. Deposition fluxes (inorganic and organic) over the salt marsh transect (left); relation between the organic and the inorganic flux (right) 96

4.22 (a) Equilibrium topography with terrace structures developing. Multiple stable states emerge assuming $C_0 = 20$ mg/l and $R = 3.5$ mm/yr. The dashed line represent the equilibrium elevation state in figure 4.5a; (b) Accretion rate as a function of perturbations in the local elevation. Solid circles represent the stable elevation equilibria. External forcings assumed: $C_0 = 20$ mg/l and $R = 3.5$ mm/yr; (c) Fitness functions of the species populating the transect with scale parameter $\lambda = 10$, $C_0 = 20$ mg/l and $R = 3.5$ mm/yr. Solid circles represent the stable elevation equilibria; (d) The same as (a) considering the scale parameter $\lambda = 2$; (e) The same as (b) considering the scale parameter $\lambda = 2$; (f) The same as (c) considering the scale parameter $\lambda = 2$; 98

4.23 Case $\lambda = 10$. Deposition fluxes (inorganic and organic) over the salt marsh transect (left); relation between the organic and the inorganic flux (right) 99

4.24 Case $\lambda = 2$. Deposition fluxes (inorganic and organic) over the salt marsh transect (left); relation between the organic and the inorganic flux (right) 99

4.25 (*a*) Equilibrium topography with terrace structures developing. Multiple stable states emerge assuming $C_0 = 20$ mg/l, $R = 3.5$ mm/yr and a constant ($z = 0.20$ m above MSL) initial topography (black dashed line). Dashed line represent the equilibrium topography (colour line) and the initial topography (black line) of the reference case; (*b*) Accretion rate as a function of perturbations in the local elevation. Solid circles represent the stable elevation equilibria; (*c*) Fitness functions of the species populating the transect with scale parameter $\lambda = 5$. Solid circles represent the stable elevation equilibria; (*d*) and (*g*) The same as (*a*) considering a random initial topography from a uniform distribution and from a normal distribution respectively (black dashed line); (*e*) and (*h*) The same as (*b*) considering a random initial topography from a uniform distribution and from a normal distribution respectively (black dashed line); (*f*) and (*i*) The same as (*c*) considering a random initial topography from a uniform distribution and from a normal distribution respectively (black dashed line) 102

4.26 Case constant initial topography. Deposition fluxes (inorganic and organic) over the salt marsh transect (left); relation between the organic and the inorganic flux (right) 103

4.27 Case random initial topography from a uniform distribution. Deposition fluxes (inorganic and organic) over the salt marsh transect (left); relation between the organic and the inorganic flux (right) 103

4.28 Case random initial topography from a normal distribution. Deposition fluxes (inorganic and organic) over the salt marsh transect (left); relation between the organic and the inorganic flux (right) 104

4.29 (*a*) Equilibrium topography with terrace structures developing. Multiple stable states emerge assuming $C_0 = 20$ mg/l, $R = 3.5$ mm/yr and $w_s = 0.1$ mm/s. In dashed line we represent the equilibrium elevation state in figure 4.5*a*; (*b*) Accretion rate as a function of perturbations in the local elevation. Solid circles represent the stable elevation equilibria. External forcings assumed: $C_0 = 20$ mg/l, $R = 3.5$ mm/yr and $w_s = 0.1$ mm/s; (*c*) Fitness functions of the species populating the transect (scale parameter $\lambda = 5$) with $C_0 = 20$ mg/l, $R = 3.5$ mm/yr and $w_s = 0.1$ mm/s. Solid circles represent the stable elevation equilibria; (*d*) The same as (*a*) with $w_s = 0.4$ mm/s; (*e*) The same as (*b*) with $w_s = 0.4$ mm/s; (*f*) The same as (*c*) with $w_s = 0.4$ mm/s; 105

4.30 Case $w_s = 1$ m/s. Deposition fluxes (inorganic and organic) over the salt marsh transect (left); relation between the organic and the inorganic flux (right) 106

4.31 Case $w_s = 4$ m/s. Deposition fluxes (inorganic and organic) over the salt marsh transect (left); relation between the organic and the inorganic flux (right) 106

4.32 (*a*) Equilibrium topography with terrace structures developing. Multiple stable states emerge assuming $C_o = 20$ mg/l, $R = 3.5$ mm/yr and $B_0 = 500$ g/m^2. Dashed line represent the equilibrium elevation state in figure 4.5*a*; (*b*) Accretion rate as a function of perturbations in the local elevation. Solid circles represent the stable topography. External forcings assumed: $C_0 = 20$ mg/l, $R = 3.5$ mm/yr and $B_0 = 500$ g/m^2; (*c*) Fitness functions of the species populating the transect (scale parameter $\lambda = 5$) with $C_0 = 20$ mg/l, $R = 3.5$ mm/yr and $B_0 = 500$ g/m^2. Solid circles represent the stable topography; (*d*) The same as (*a*) with $B_0 = 2000$ g/m^2; (*e*) The same as (*b*) with $B_0 = 2000$ g/m^2; (*f*) The same as (*c*) with $B_0 = 2000$ g/m^2; 108

4.33 Case $B_o = 500$ g/m^2. Deposition fluxes (inorganic and organic) over the salt marsh transect (left); relation between the organic and the inorganic flux (right) 109

4.34 Case $B_o = 2000$ g/m^2. Deposition fluxes (inorganic and organic) over the salt marsh transect (left); relation between the organic and the inorganic flux (right) 109

4.35 (a) Equilibrium topography with terrace structures developing. Multiple stable states emerge assuming $C_o = 20$ mg/l, $R = 3.5$ mm/yr and $H = 0.25$ m. In dashed line we represent the equilibrium elevation state in figure 4.5a; (b) Accretion rate as a function of perturbations in the local elevation. Solid circles represent the stable elevation equilibria. External forcings assumed: $C_0 = 20$ mg/l, $R = 3.5$ mm/yr and $H = 0.25$ m; (c) Fitness functions of the species populating the transect (scale parameter $\lambda = 5$) with $C_0 = 20$ mg/l, $R = 3.5$ mm/yr and $H = 0.25$ m. Solid circles represent the stable elevation equilibria; (d) The same as (a) with $H = 2.00$ m; (e) The same as (b) with $H = 2.00$ m; (f) The same as (c) with $H = 2.00$ m; 110

4.36 Time interval of submersion with different tidal amplitudes for a fixed elevation $\hat{z}$ (dashed line). 111

4.37 Case $H = 0.25$ m. Deposition fluxes (inorganic and organic) over the salt marsh transect (left); relation between the organic and the inorganic flux (right) 112

4.38 Case $H = 2.00$ m. Deposition fluxes (inorganic and organic) over the salt marsh transect (left); relation between the organic and the inorganic flux (right) 113

4.39 Case "stochastic formulation". Deposition fluxes (inorganic and organic) over the salt marsh transect (left); relation between the organic and the inorganic flux (right) 114

4.40 (a) Multiple stable states assuming as external forcings $C_0 = 20$ mg/l, $R = 3.5$ mm/yr. "Stochastic formulation" is assumed as spatial competition mechanism. In dashed line we indicate the topography reference case (figure 4.5a), where we adopted the "fittest-takes-it-all formulation"; (b) Multimodal frequency distribution of topographic elevations. Each peak (color-coded, according to the most abundant species in each interval) is associated with the unique species that generates it; 115

4.41 (a) Multiple stable states assuming as external forcings $C_0 = 20$ mg/l, $R = 3.5$ mm/yr. "Stochastic formulation" is assumed as spatial competition mechanism. In dashed line we indicate the topography reference case (figure 4.5a), where we adopted the "fittest-takes-it-all formulation"; (b) Frequency distribution of topographic elevations considering no organic deposition flux. Each peak (color-coded, according to the most abundant species in each interval) is associated with the unique species that generates it. 116

4.42 Case "stochastic competition": frequency density of the fitness functions considering one year sample 117

4.43 Case "stochastic competition": frequency density of each fitness functions 117

4.44 Case "stochastic competition": frequency density of the fitness functions considering ten years sample 118

4.45 Case "stochastic competition" considering less specialized species ($\lambda = 2$): frequency density of the fitness functions considering one year sample 118

4.46 Case "stochastic competition" considering less specialized species ($\lambda = 2$): frequency density of the fitness functions considering ten years sample 119

4.47 Case "stochastic competition" considering less specialized species ($\lambda = 2$): frequency density of each fitness functions 119

4.48 PART I (*a*–*b*) Observed zonation patterns. An accurate topographic survey (uncertainty smaller than 1 mm) reveals a multimodal frequency distribution of soil elevation, highly suggestive of the major role played by the biomass-elevation feedback in tuning marsh topography. Each bar is color-coded according to the vegetation species which is most abundant within the pertinent elevation interval, showing that indeed elevation ranges are characteristic of the vegetation species (or of a typical mix of species at high elevations) which maintain them. 121

4.49 PART II (*c*–*d*) Observed zonation patterns. An accurate topographic survey (uncertainty smaller than 1 mm) reveals a multimodal frequency distribution of soil elevation, highly suggestive of the major role played by the biomass-elevation feedback in tuning marsh topography. Each bar is color-coded according to the vegetation species which is most abundant within the pertinent elevation interval, showing that indeed elevation ranges are characteristic of the vegetation species (or of a typical mix of species at high elevations) which maintain them. 122

4.50 Analysis: 1. Time evolution of topography (left) and species (right). Rate of mutation adopted: 50 years. Mutation based on changing the fitness function mode and the maximum value. More details in the supplementary material. 125

4.51 Analysis: 2. Time evolution of topography (left) and species (right). Rate of mutation adopted: 10 years. Mutation based on changing the fitness function mode and the maximum value. More details in the supplementary material. 127

4.52 Analysis: 3. Time evolution of topography (left) and species (right). Rate of mutation adopted: 50 years. Mutation based on changing the fitness function mode (different from Analysis 1) and the maximum value. More details in the supplementary material 128

4.53 Analysis: 4. Time evolution of topography (left) and species (right). Rate of mutation adopted: 50 years. Mutation based on changing the fitness function mode and the maximum value. Initial species differ from Analysis 3. More details in the supplementary material 130

4.54 Analysis: 5. Time evolution of topography (left) and species (right). Rate of mutation adopted: 5 years. Mutation based on changing the fitness function mode and the maximum value. More details in the supplementary material 131

4.55 Analysis: 6. Time evolution of topography (left) and species (right). Rate of mutation adopted: 5 years. Mutation based on changing the fitness function mode and the maximum value. Initial species differ from Analysis 5. More details in the supplementary material 133

4.56 Analysis: 7. Time evolution of topography (left) and species (right). Rate of mutation adopted: 5 years. Mutation based on changing the fitness function mode and the maximum value. Initial species differ from Analysis 5 and 6. More details in the supplementary material 134

4.57 Analysis: 8. Time evolution of topography (left) and species (right). Rate of mutation adopted: 50 years. Mutation based on changing the fitness function mode (more than Analysis 3) and the maximum value. More details in the supplementary material 136

4.58 Analysis: 9. Time evolution of topography (left) and species (right). Rate of mutation adopted: 50 years. Mutation based on changing the fitness function mode (like Analysis 8) and the maximum value. Initial species differ from Analysis 8. More details in the supplementary material 137

4.59 Analysis: 10. Time evolution of topography (left) and species (right). Rate of mutation adopted: 2 years. Mutation based on changing the fitness function mode and the maximum value. $C_0 = 40$ mg/l. More details in the supplementary material . . . 139

4.60 Analysis: 11. Time evolution of topography (left) and species (right). Rate of mutation adopted: 10 years. Mutation based on changing the fitness function mode and the maximum value. $C_0 = 40$ mg/l. More details in the supplementary material . . . 140

4.61 Analysis: 12. Time evolution of topography (left) and species (right). Rate of mutation adopted: 50 years. Mutation based on changing the fitness function mode and the maximum value. Linear stochastic formulation adopted in the spatial competition. More details in the supplementary material 142

4.62 Analysis: 13. Time evolution of topography (left) and species (right). Rate of mutation adopted: 50 years. Mutation based on changing the fitness function mode and the maximum value. Non-linear stochastic formulation adopted in the spatial competition (differ from Analysis 12). More details in the supplementary material 143

4.63 Analysis: 14. Time evolution of topography (left) and species (right). Rate of mutation adopted: 50 years. Mutation based on changing the fitness function mode and the maximum value. Non-linear stochastic formulation adopted in the spatial competition (differ from Analysis 12 and 13). More details in the supplementary material 144

4.64 Analysis: 15. Time evolution of topography (left) and species (right). Rate of mutation adopted: 50 years. Mutation based on changing the fitness function mode and the maximum value. Non-linear stochastic formulation adopted in the spatial competition (differ from Analysis 12, 13 and 14). More details in the supplementary material 146

4.65 Analysis: 16. Time evolution of topography (left) and species (right). Rate of mutation adopted: 1 years. Mutation based on changing the fitness function mode. More details in the supplementary material 147

4.66 Analysis: 17. Time evolution of topography (left) and species (right). Rate of mutation adopted: 1 years. Mutation based on changing the fitness function mode and the maximum value. More details in the supplementary material 149

4.67 Analysis: 17 – time sequence. Time evolution of topography (left) and species (right). Time sequence when the elevation of the last site goes down under the mean sea level. More details in the supplementary material 150

4.68 Analysis: 18. Time evolution of topography (left) and species (right). Rate of mutation adopted: 100 years. Mutation based on changing the fitness function mode and the maximum value. More details in the supplementary material 152

4.69 Analysis: 19. Time evolution of topography (left) and species (right). Rate of mutation adopted: 50 years. Mutation based on changing the fitness function mode, the maximum value and the variation value. More details in the supplementary material . . . 153

4.70 Analysis: 20. Time evolution of topography (left) and species (right). Rate of mutation adopted: 50 years. Mutation based on changing the fitness function mode, the maximum value and the variation value. Initial species differ from Analysis 19. More details in the supplementary material 154

List of Tables

4.1 Inorganic deposition, organic deposition and mean SSC in three different elevation topography configurations. We perturb the elevation of a site of the salt marsh transect to see the effect on the deposition fluxes 88

Introduction

This work focuses on intertidal systems, i.e. coastal and estuarine systems which are subject to fluctuating water levels forced by tides. These systems are characterized by the presence of bio-geomorphic structures, such as marshes, tidal flats, and sub-tidal platforms, which are possible equilibrium states resulting from the interplay of physical and biological processes.

The objectives of the present Thesis are the development of a 0–D and 1–D bio-geomorphological models to analyze the complex interplay between physical and biological components of intertidal environments and their dynamics.

In this Thesis, these tidal landscape structures are shown to be bio-geomorphic in nature, as they emerge from the coupled dynamics of biotic and abiotic processes. At large scales, tidal landforms and the associated ecosystems are shown to emerge as multiple, competing, equilibrium states from the interplay of erosion and deposition processes and biostabilization produced by vegetations and the benthic microalgae. The existence of these competing stable states represents the large-scale pattern formation mechanism for characteristic and ubiquitous biogeomorphic features of tidal landscapes. At a smaller scale, biogeomorphic features in tidal marshes are actively engineered by the ability of vegetation species of tune soil elevation within preferential ranges. We propose here a novel interpretation, based on new detailed observations, which, for the first time, couples geomorphic dynamics and species competition/mutation in a spatially extended setting.

In Chapter 1 we present some of the main features of the tidal environment, focusing in particular on salt marshes, which are usually thought to as

characterized by a flat topography. Actually, these platforms display small topographic gradients, associated with the presence of different vegetal species which encroach the tidal landscape at different elevations.

In Chapter 2 using a 0–D model we show how competing stable states are responsible for the formation of ubiquitous characteristic large-scale biogeomorphic features in tidal landscapes. We develop a point model of the joint evolution of tidal landforms and biota including the dynamics of intertidal vegetation, benthic microbial assemblages, erosional and depositional processes, local and general hydrodynamics, and relative sea-level change. Alternative stable states and punctuated equilibrium dynamics emerge, characterized by possible sudden transitions of the system, governed by vegetation type, disturbances of the benthic biofilm, sediment availability and changes in the rate of relative sea level rise. Multiple equilibria highlight the importance of the coupling between biological and sediment transport processes in determining the evolution of a tidal system as a whole. A sensitivity analysis is carried out in order to study the influence of the governing processes on tidal landscape equilibria and dynamics.

Chapter 3 we present a biomorphodynamic 1–D model that describes the time evolution of a marsh transect, and we detail its structure and most relevant features. Changes in soil elevation are everywhere dictated by the local balance among the rate of inorganic soil deposition, determined by the hydro-dynamic circulation/sediment transport processes and the rate of organic soil production by vegetation, modulated by a fitness function describing how biomass production of species varies depending on its adaptation to the edaphic conditions associated with elevation. The evolutionary vegetation model includes also the interspecific spatial competition and the mutation, as mechanisms that allow the self–development and self–colonization of the species in relation with the edaphic conditions.

In Chapter 4 we explore through the 1–D model, the mechanisms that lead to the formation of well-known vegetation patterns associated with marsh veg-

etation species distributions corresponding to competing stable states. At the marsh–scale, we find that zonation is a bio-geomophological pattern, rather than simply a biological one, with visible symptoms that underly feedbacks between biomass productivity and soil accretion. We carry out a sensitivity analysis to explore the model response and the resilience of pattern–structures to changes in external forcings. Two different evolutionary vegetation mechanisms are explored with a significant number of analyses: the competition mechanism (i.e. spatial competition among fixed species over time) and the coupled competition–mutation mechanisms (i.e. spatial competition among variable species over time).

Finally, a Conclusion Chapter draws a set of the main findings and conclusions.

Chapter 1

Large–scale and marsh–scale: eco–morphodynamic details of tidal environments

In this Chapter we provide a general introduction to the morphological and biological characteristics of tidal areas and a description of the study area highlighting the importance and novelty of the study presented.

1.1 Tidal environments: generality

The long-term morphological evolution of tidal landscapes is the result of complex and delicate balance between hydrodynamic processes, morphodynamic, ecological and anthropogenic interventions. As a result of these forcings, the tidal landscape morphology evolves and organizes in a strong relation with the ecological dynamics showing complex feedback mechanisms between hydrodynamic, physical and ecological processes.

In the tidal environment we can distinguish, from a morphological point of view, several characteristic structures: the *salt marshes*, the *tidal flats*, the *subtidal flats* and the networks of *channels*, whose hydrodynamic behavior is different because of the different roles of the forcings that govern the propagation

of tidal currents.

The behavior of the *salt marshes* is particularly interesting. These morphological characteristics formations are usually located on the margins of the tidal platform, although sometimes, as in the case of Venice Lagoon, these structures interpose themselves between the areas of the lagoon next to the inlets and the areas far from the edge of the tidal platform.

The salt marshes are the topographically highest vegetated areas of the tidal platform subject to periodic flooding as a result of fluctuating water levels of adjacent saline water bodies; being higher than the average sea, they emerge for the most of the tidal cycle and are submerged only in particular conditions of high tide (sigizia) that flows and covers during phase of flux and uncovers during the subsequent phase of reflux (Adam, 1990). They occur in temperate and high latitudes along estuaries, bays and tidal rivers, where wave energy is sufficiently low to allow establishment of salt tolerant grasses (*Halophytes*) in the intertidal zone (Allen and Pye, 1992). Because of the rich variety halophytic vegetation, capable to grow in areas subject to prolonged periods of flooding and in soils with high salt content, there are important interactions between hydrodynamic and transport morphodynamic processes (Marani *et al.*, 2004, 2007; Day *et al.*, 1999) together with, not negligible, processes of production of organic soil. Generally, salt marshes are flat structures, carved by a widespread network of small creeks that influence or enable the tide periodical flooding. The salt marshes have an important role in the tidal ecosystem: they play specific and diverse functions that can be divided into two main types:

- Morphological function: marshes are important natural dissipators of tidal currents and waves, thus protecting landward sea defences from scour and wave erosion; they also act as sediment trapping zones, and play a central role in determining water quality and in buffering nutrient fluxes from the land;
- Naturalistic function: host the highest organic, vegetable and bacterial production and represent favorable habitats to the settlement of benthic

communities and are areas of transit, parking and reproduction areas for many species of birds.

Tidal flats are sand or mud coastal habitats characterized by lower elevations when compared to salt marshes, and are thus not colonized by halophytic plants. They are flooded during the most of the tidal fluctuations and despite the extreme edaphic conditions due to periodic exposure to air and variations in salinity, they are colonized by marine phanerogams (seagrasses, e.g. Zostera marina, Zostera noltii, Cymodocea nodosa for the Venice Lagoon), algae (e.g. Ulva rigida), small crustaceans, and various benthic microbial assemblages. These zones are even more exposed to the erosive action of the wave motion generated by wind that produces altimetrical instability also because of the periodical frequent tidal floods.

The *subtidal platforms*, the last tidal morphological structure, develop below the minimum tidal level and are always submerged by the water.

The environments described above are strongly correlated and interdependent. Therefore it seems important to understand how these environments can or not evolve to stable equilibrium states and what is the mechanism that leads to their formation.

Climate changes, human interventions and natural changes occurred over the centuries in tidal areas, such as those that occurred in the Venice lagoon, profoundly influenced their evolution with mutations sometimes irreversible. It is therefore of critical importance to test predictive models that simulate the geomorphological evolution of the tidal systems: this issue is closely linked to ecological, socio-cultural but also economic issues.

We will focus on salt marsh, tidal flat and subtidal flat evolution, subjected to different external forcings; it is also of strategic importance to understand how the salt marshes develop, what is the biological-morphological mechanism that leads to their growth and shape and what is the important link with the vegetation.

1.2 Biotic components that shape the ecosystem

Tidal enviroments are characterized by the presence of halophytic vegetation, macrophytes which can complete their entire life cycle in environments with high soil salinity and saturation (Adam, 1990) and of sediment inhabiting macrofauna and microbes (*microfitobenthos*, MPB) that engineer and structure the landscape or substrate at different scales.

Microphytobenthos assemblages have an important role in the tidal system dynamics as ecological or bio-engineers (Widdows and Brinsley, 2002). They are composed of benthic microalgae that live in and on sediments of intertidal areas where light reaches the sediment surface. They drive biogeochemical processes contributing to the carbon flux (Middelburg *et al.*, 2000), primary productivity, exchanges of nutrients between sediments and the water-column (Sundbäck and Granéli, 1988), and sediment dynamics (oxygenation and stabilization). They strongly enhance the stability of mudflats by directly and indirectly altering the properties of the surface, making it more resistant to erosion (Yallop *et al.*, 1994; Miller *et al.*, 1996).

The *halophytes*, salt tolerant grasses, have a crucial importance in the development of intertidal environments. The main characteristic of the marshes vegetation is its spatial distribution of stable and monospecific communities, that create the particular phenomenon called *zonation* (Adam, 1990) linked to the different environmental gradients as well as biological interactions. The different elevations are very close to each others but few centimeters are sufficient to change from a species colonization to another one.

A striking characteristic of salt marshes is their apparent tabular shape, with a slight depression towards the inner of the area of about 10-20 cm (slopes of about one per thousand) and visibly appreciable just because the vegetation changing (Pignatti, 1966).

Salt-marsh vegetation is largely responsible for the stability of these areas,

through feedbacks involving hydrodynamic and sediment circulations. Plant roots, in fact, stabilize the soil, while the aboveground biomass importantly reduces water flow velocity and dampens wind-induced waves, thus effectively impeding sediment resuspension and erosion. Furthermore, the biomass produced by halophytes often constitutes the largest contribution to the local incoming flux of soil and thus is crucial in allowing marsh accretion to keep pace with soil compaction, subsidence and sea-level rise (Day *et al.*, 1999).

On the other hand, the net effect of deposition and erosion processes determines local topography, which, together with tidal forcing and subsurface water flow, in turn determines the edaphic conditions constraining vegetation development and selecting halophytic species (Silvestri *et al.*, 2005).

Vegetation cover, over the marsh surface, has a dual role. Firstly, vegetation reduces the velocity of water flow near the marsh surface increasing the opportunities for accretion, and secondly, the root mass helps to increase the stability of the material already deposited.

The origin of salt marshes within an intertidal zone is usually attributed to increased deposition rates in tidal flats causing an increase in topographic elevation and thus less frequent flooding of the soil, which may then be colonized first by microbiota and then by pioneer vascular plants of the resulting more elevated area (i.e. pioneer zone).

The pioneer zone, which is covered by most tides, is where the rate of accretion is greater because of the duration of tidal inundation, when sediment deposition may take place. As the level of the marsh surface rises, the duration of inundation decreases and a wider range of species is able to colonize the middle and high marshes becoming progressively more floristically various.

We think that an understanding of salt marsh dynamics still lacks a comprehensive and predictive theory, mainly because many of the linkages between the relevant ecological and geomophological processes (vegetation patterns formation and patterns distributions) are poorly understood.

1.3 The Venice tidal environment: inorganic and organic characters

1.3.1 Lack of sediments: some causes

The Venice lagoon is the most extended wet environment in Italy, it covers an area of about 550 km^2 and 40 km^2 of these are made up of salt marshes covered by halophytes and periodically flooded by high tides. The lagoon is the result of a coevolution of human and natural processes that have repeatedly changed the hydrodynamic and morphological characters. It is subject to intense erosion processes, which have radically changed the character of its biomorphological structures.

The lagoon is in a non equilibrium state that causes a general tendency to erosion, evident in the alignment of the subtidal flats, in the deepening of the tidal flats, in the loss of the morphological variability and in the gradual disappearance of the salt marshes. During the centuries, the reduction of sediment input in the lagoon due to natural and anthropogenic causes has been the main problem for the lagoon morphology.

Wave motion due to wind and boats, the eustatism, the subsidence, the reduced availability of river sediments, the human intervention, the activities of illegal fishing, were and continue to be the main responsible of erosion and/or sedimentary processes able to significantly change the lagoon structure.

The transport of goods and passengers by water is one of the activities that more typically characterize the area of the Venice lagoon. The high flow of energy on the channel sides due to the passage of boats, involves a progressive silting up as a result of the continuous transport of sediments from the surrounding tidal flat, which then will tend to further deepen. The periodic dredging of the channel, which is required in order to maintain the navigability, keeps this mechanism active and constantly contributes to the deepening of the areas crossed by the channels.

The resuspension of bottom sediments is also determined by fishing activities.

They deliver to the already precarious balance of the lagoon sediment, further negative contribution. The activities of fishermen, whether authorized or illegal, produce irreversible damage to the integrity of the sediment in the tidal flats, producing not only an increase in the available sediment to an easier resuspension and transport to the sea but also the removal of the stabilizing biofilm on the surface.

The diversion of the rivers that flowed into the Venice lagoon, which took place in the past centuries, to prevent the silting up of the lagoon, almost eliminated the amount of sediment from the drainage basin. At the time of "Repubblica Serenissima di Venezia", the evolutionary trend of the lagoon was opposite of the current one and the problem was the silting promoted by the major contribution of sediment by rivers that flowed into the lagoon. The evolution of the lagoon after the diversion of the main rivers, led to an increase in the average depth of the seabed with a consequent increase in the amplitudes of the wind waves. In this way it established a positive feedback mechanism, in such a deepening of the bathymetry corresponds to an increase of wave energy, which then induces a further and more rapid deepening of the bathymetry because of the increased energy of the waves, which favors erosion of both the tidal flat and the edge of salt marshes. The fine sediments carried in suspension by the waves, being characterized by a low settling velocity, also tend to be gradually carried toward the inlets by tidal currents.

1.3.2 Salt marsh vegetation in the ecosystem evolution

The spatial distribution of vegetation over the salt marshes is not spatially uncorrelated, it is instead organized in characteristic spatial patches, whose observation is currently promoting a growing interest in the study of the phenomenon (Pignatti, 1966; Marani *et al.*, 2003).

The salt marsh soil appears to be covered by a mosaic of patches and each of them is formed by a single vegetation species or by a charachteristic association of a few species as we can observe in figures 1.1–1.5.

Figure 1.1: Patch of *salicornia veneta*, that dominates near a forming creek of about 10-20 cm large and 10 cm deep, where the soil elevations are lower between areas of *limonium* on the left and *sarcocornia fruticosa* on the right.

Figure 1.2: Transition from a mixed vegetation cover near a tidal creek (left and background) to a *limonium narbonense* patch.

Figure 1.3: Sharp transition between *limonium narbonense* (above) and *spartina maritima* (below).

Figure 1.4: Smooth transition from a *juncus acutus* patch (left), a *sarcocornia fruticosa* patch, and a *limonium narbonense* patch.

Figure 1.5: Transitions from a *spartina maritima* patch (above) to a *sarcocornia fruticosa* patch (middle), to a *pucinellia* patch (below).

The elevation-based zonation model persists in salt marsh ecology (Adam, 1990; Pennings and Callaway, 1992; Silvestri *et al.*, 2005). Many halophytes seem to better live in a preferred elevation range and this is an obvious constraint for their development.

Silvestri *et al.* (2005) observed that this reference elevation range change, considering different salt marshes even within the same tidal environment (i.e the Venice lagoon), even if the sequence of adaptation to the different ranges of elevation is the same, only rigidly shifted.

The *zonation* is generally linked to the concept of "succession" i.e. the replacement of plant species in an orderly sequence of colonization and development. This hypothesis is based on the assumption that, on emerging salt marshes, after an initial colonization phase, the substrate would be more stable and sediments would be trapped by the vegetation. This would allow other species to invade the marsh, producing changes directed towards a mature and stable climax ecosystem (Silvestri *et al.*, 2005). Results of long-term monitoring, however, reveal that the dynamics of salt marsh vegetation does not always proceed according to succession schemes (Leeuw *et al.*, 1993).

A number of authors (Chapman, 1976; Bockelmann *et al.*, 2002; Costa *et al.*, 2003; Rogel *et al.*, 2001) have described plant zonation in salt-marsh environments and have evaluated the environmental factors affecting the distribution of halophytes.

The reproduction, germination and development of halophytes depend on a number of physiological needs, broadly related either to a sufficient input of energy and vital substances (e.g. water, oxygen, light, salt ions, macronutrients and micro-nutrients, etc.) or to the limitation of stressing factors (e.g. soil waterlogging, toxic substances in soils, sudden thermal changes, interand intra-specific competition).

Hence, the distribution of halophytes seems to be dictated also by location and size of tidal channels, since tidal networks largely control the distribution of tidal flooding within the marsh (Sanderson *et al.*, 2000).

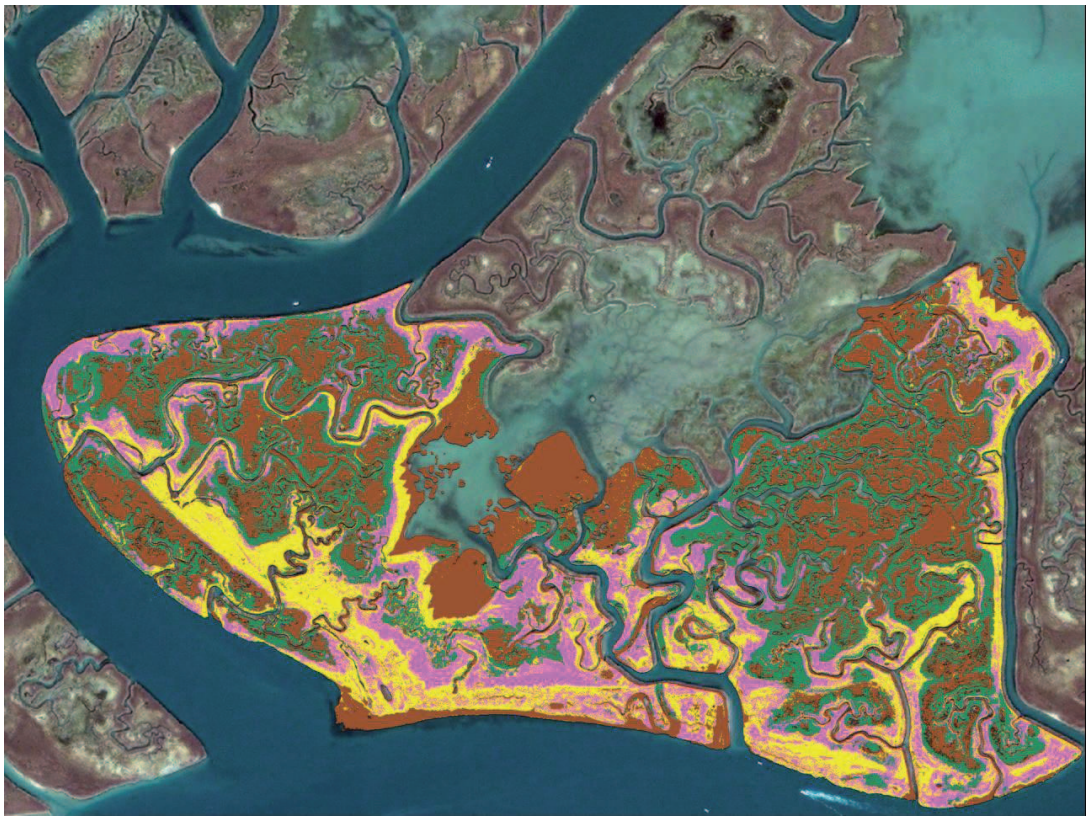

Figure 1.6: The spatial distribution of vegetation – Remote sensing – in the San Felice salt marsh, Venice Lagoon (Belluco *et al.*, 2006; Wang *et al.*, 2009)

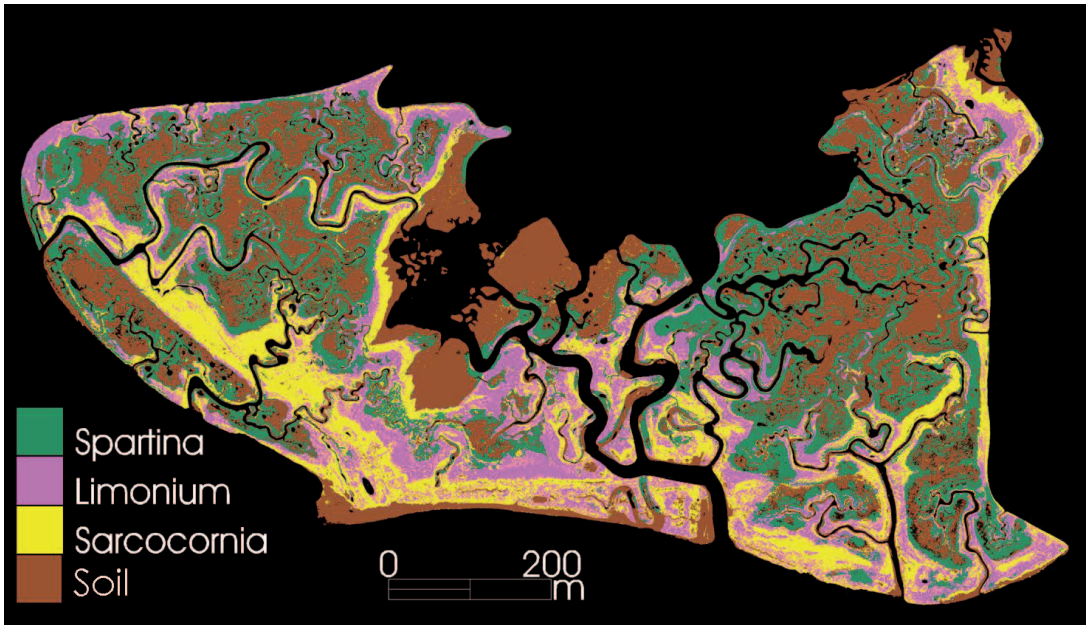

Figure 1.7: Vegetation map of the San Felice salt marsh in the Venice Lagoon (geometric resolution is 0.5 m, channels and creeks are in blue (Marani *et al.*, 2006b)

Also numerous edaphic and biotic factors have been found to be related to saltmarsh plant distribution, for example, nutrient availability (Rogel *et al.*, 2001), wave disturbance, temperature, salinity, frequency and duration of tidal inundations (Callaway *et al.*, 1990), human management (Adam, 1990).

Studies in many natural environments have shown that variations in species distributions may also reflect biotic interactions, in particularly interspecific interactions (competition and/or facilitation) (Costa *et al.*, 2003; Pennings and Callaway, 1992).

Numerous experimental studies have found evidence to support the importance of interspecific competition in shaping wetland zonation patterns (Grace and Wetzel, 1981; Wilson and Keddy, 1985; Bertness *et al.*, 1992; Levine *et al.*, 1998). Most experimental field studies of zonation in salt marsh plants have been conducted at middle and high latitudes of the northern hemisphere and in regularly inundated tidal marshes pointing to trade-offs between the ability of a species to tolerate stress and competitive ability and a competitive displacement of subordinate species to physically stressful habitats.

In this Thesis, we will present the spatial *competition* concept as spatial interaction among two or more species that can potentially occupy the same habitat unit; the spatial competition will be applied following two main criteria, the first one will prefer the best fit species to specific elevation and the second one will be a stochastic formulation randomly selecting a species. The *mutation* is the second concept presented here as a random speciation that may happen in the species, changing some characters of phenotype or genotype. These two concepts are the base of the ecosystem *evolution*.

It is well accepted by ecologists that organisms not only adjust their properties to the physical environment, but they also modify and in a certain case create it. In parallel, the mechanism by which species modify their physical environment, encompassing geomophologic components in ways to create or maintain suitable niche conditions for other species, have received growing attention among the ecological community (Bruno *et al.*, 2003; Corenblit *et al.*,

2011). The idea of facilitation describes species interactions that benefit at least one of the participants and cause harm to neither (Stachowicz, 2011). This process has become a central concept in ecology for describing ecosystem structure and function through the consideration of positive interactions between species mediated by habitat changes or constructions. A formalization of such dependency between organisms mediated by the physical components of ecosystems was proposed in ecology by Jones *et al.* (1994, 1997) in their concept of "ecosystem engineers". Physical ecosystem engineers are organisms that directly or indirectly control the availability of resources to other organisms by causing physical state changes in biotic or abiotic materials. Physical ecosystem engineering by organisms is the physical modification, maintenance or creation of habitats. The ecological effects of engineering on other species occur because the physical state changes directly or indirectly control resources used by these other species (Jones *et al.*, 1997). Engineers are found in all ecosystems (Jones *et al.*, 1994), more important in some ecosystems than others. The ecosystems engineering, effect of organisms, could have a broad range of impacts on ecosystem functions (Matthews *et al.*, 1997). The concept of facilitation has improved in ecology the understanding of the relationship between biodiversity and ecosystem function by considering more explicitly the effects of engineer species on habitat properties (Bruno *et al.*, 2003). It is suggested that increasing engineer species diversity may increases community structural and functional complexity. The presence of habitat patches created by engineer plants or animals increases species richness at the landscape level. Evidence for such positive landscape-level effects of engineer animal and plant species on biodiversity has been found within fluvial and terrestrial systems, for example in association with beaver activities (Corenblit *et al.*, 2011). The concept of "niche construction" also refers to the modification of the physical environment by organisms. Niche construction is an analog of ecosystem engineering, although this latter term is used mainly at the scales of ecosystem dynamics, while niche construction operates both at scales of ecological dynamics and the evolution of organisms. Numerous

examples of niche construction by organisms can be found in the ecological literature (Corenblit *et al.*, 2011), demonstrating the usefulness of the concept for describing co-evolutionary dynamics between species mediated by engineered or constructed physical environments.

In this Thesis we will present the ecological phenomenon of patterns formation from a new point of view. The patterns are traditionally explained as the result of the spatial distribution of edaphic conditions (dominant in the lower areas of the marsh, where physical conditions are harshest) and of interspecific competition (dominant in the higher zones, where stress is low). Importantly, the existing interpretative paradigm, which has not produced a predictive modeling formulation, takes the topography, and the associated environmental conditions, as a fixed constraint set a priori.

We show here, using modeling and observations, that the importance of biomass production in determining equilibrium elevations in a salt marsh naturally leads to zonation patterns that are both vegetational and geomorphic: these patterns are not the sign of a passive adaptation of vegetation species to the environment, but, rather, the signature of a positive feedback in which vegetation species tune soil elevation within a favorable range and elevation changes, in turn, affect the rate of biomass production.

1.4 Introductory notes to the 0–D and 1–D models: multiple stable equilibria and patterns formation

Salt marshes display the complex ecological and physical interactions and thus require an interdisciplinary approach to discern the mechanism by which they function (Fagherazzi *et al.*, 2004; Kirwan and Murray, 2007; Marani *et al.*, 2007). Numerical modeling is one powerful tool that can be used to quantify the nonlinear feedbacks, morphology and sediment transport processes.

Numerical models can be used to test hypotheses regarding salt marsh processes, quantify the exchanges of energy and material across the intertidal landscape, and shed light on the long-term evolution and resilience of these systems (Fagherazzi *et al.*, 2012).

At the large–scale there are the zero-dimensional models that simulate processes (i.e., net primary production and elevation change) at a single point within a marsh.

Next are the models that simulate morphodynamics (i.e., sedimentation, channel development, and erosion) across a marsh transect (a one-dimensional model). These models are said to be "ecogeomorphic" if they additionally consider the feedbacks between marsh vegetation and physical processes such as sedimentation and erosion.

In the Chapter 2 we will describe, apply and subsequently improve a point model that describes the time evolution of the bottom elevations considering the complex interactions between the halophytic vegetations, the microbes colonies, the sediment deposition and erosion processes, the hydrodynamic and the rate of the relative see level rise.

This bio-morphodynamic model introduces a coupled relation between the geomorphological and the biological processes, considering both a steady state vegetation model and a dynamic vegetation model.

In this work, we resume the results of recent contributions in the study of the lagoon morphodynamics (Marani *et al.*, 2007; Fagherazzi *et al.*, 2006), in which was highlighted the complex link between the deposition of sediment and the erosion process that may occurs within the lagoon basin, closely related to hydrodynamic conditions assumed and the presence or absence of the vegetative component that plays a key role in limiting the contribution of erosion. The model adopted here is further tested with real data of forcing providing observations and assessments. We explore the stable equilibria that can be reached, the dynamics to achieve, transients and the weight of the physical and biological

factors that control the transition through these different stable equilibria.

Although the problem of the deficit of the lagoon sediments is of great importance for many aspects highlighted, the development of predictive models and an organic theory is still in the early stages of development (D'Alpaos *et al.*, 2007; Fagherazzi *et al.*, 2006; Kirwan and Murray, 2007; Marani *et al.*, 2007, 2010), as a result of the overlapping of various processes, whose dynamics are poorly understood, which operate on different spatial and temporal scales. These trends can be explained more thoroughly, knowing the morphodynamic processes responsible of the development of the major geomorphological structures, and understanding the relative roles and interactions between physical and biological components, as part of a coupled description of the evolution of the eco–geomorphological system.

In this work we describe a long-term bio–morphodynamic model of evolution of tidal basins, obtained by coupling a model which describes the bathymetry variations as result of a mass balance between the amount of deposited sediment and the erosion because of wave motion, to a model which describes the dynamics of halophytic vegetation considering the forcing action of tides, different inputs of sediments and variations of the sea level, including also the effects of biological processes that contribute to the production of organic soil.

The current understanding of intertidal bio-gemorphology, recognized the central role of vegetation primary productivity in leading to different large-scale topographic equilibria, and coexisting alternative stable states (Morris *et al.*, 2002; Marani *et al.*, 2007, 2010). At intermediate scales, tidal landforms and the associated ecosystems are shown to emerge as multiple, competing, equilibrium states from the interplay of erosion, deposition, and biostabilization (Marani *et al.*, 2007). Here we show how smaller-scale marsh biogeomorphic features, zonation and the associated geomorphic patterns (Silvestri *et al.*, 2005; Marani *et al.*, 2006b) emerge.

In the Chapter 4, using modelling and observations, we present the impor-

tance of biomass production in determining equilibrium elevations in a marsh that naturally leads to zonation patterns that are both vegetational and geomorphic.

We will show that the zonation patterns are a striking and widespread salt marsh characteristic (Adam, 1990) combined with multimodal distributions of bottom elevations that illustrate how this is a symptom of multiple stable equilibrium states generated by the competition of the different plant species that tune the topographic bathymetry.

These patterns are historically explained as a passive adaptation of vegetation species to the environment and the different edaphic conditions (Bertness and Ellison, 1987; Bockelmann *et al.*, 2002; Marani *et al.*, 2006b; Pennings and Callaway, 1992; Silvestri *et al.*, 2005) supposing the topography and the edaphic conditions as a constraint fixed a priori.

We suggest here a new interpretation according to new detailed observations: the signature of a positive feedback in which vegetation species tune soil elevation, in turn, affect the rate of biomass production. We challenge the traditional interpretation of zonation as a tradeoff between dominant processes in different parts of the intertidal frame, which fails to capture the active role played by vegetation in engineering its own environment.

For the first time we couple geomorphic dynamics and species competition in a spatially extended setting. In fact, previous models were either 0D (Morris, 2006) or did not include a description of interspecific competition (D'Alpaos *et al.*, 2007; Fagherazzi *et al.*, 2012; Kirwan and Murray, 2007; Mudd *et al.*, 2004; Temmerman *et al.*, 2007) and were thus intrinsically incapable of providing insight into zonation-generating mechanisms.

Furthermore we explore the response of tidal landscapes to variations in the governing physical and biological forcings, such as rates of relative sea level rise, sediment supply concentrations, types of vegetation, different tidal amplitudes, different maximum areal biomass productivity, different settling velocities and different spatial vegetation species competition dynamics.

We focus on the biogeomorphic dynamics of a marsh transect oriented in a direction perpendicular to the nearest channel that feeds the marsh with inorganic sediment. Changes in bottom elevation are governed by the local balance among the rate of inorganic soil deposition determined by the hydrodynamic circulation/sediment transport processes; the rate of organic accretion by vegetation modulated by a *fitness function* which describes how biomass production of species i varies depending on its adaptation to the edaphic conditions associated with elevation (Silvestri *et al.*, 2005; Morris, 2006; Marani *et al.*, 2010) and the relative rate of sea level rise, R.

Changes in bottom elevations along the transect are coupled, through a two-way feedback, to changes in the spatial distribution of different vegetation species as a consequence of inter-specific competition, which may occur either i) by selecting, at each site the species which displays the maximum fitness function for the elevation of the considered site ("fittest-takes-it-all") or ii) by randomly selecting a species with a probability proportional to the *fitness function* ("stochastic competition" mechanism). Furthermore we introduce a mutation mechanism that contributes to the different spatial distribution of species and also allows the growth of new species.

Chapter 2

0–D: physical and biological large–scale processes shaping the tidal landscape

2.1 Introduction

The dynamics of tidal biogeomorphological systems is governed by interacting ecological, hydrological, and geomorphological processes, which exhibit fast responses and possibly irreversible transformations as a result of environmental changes and increasing human pressures (Schneider, 1997; Bohannon, 2007; Day *et al.*, 2007). A thorough quantitative understanding of the many linkages between the dominant biological and geomorphological processes in tidal environments is still lacking (Rinaldo *et al.*, 1999a,b; Feola *et al.*, 2005; Marani *et al.*, 2006a; Murray *et al.*, 2008), such that a comprehensive and predictive theory of tidal landscape evolution is still proving elusive. Such a lack of a predictive understanding of tidal morphodynamics can be ascribed, to a large extent, to our quite recent awareness that biological dynamics in intertidal areas are not just an epiphenomenon of physical geomorphological transformations (Reinhardt *et al.*, 2010). As in many other fields of science, the long-standing paradigm of physical processes carving the landscape and dictating

the constraints for biological agents, forced to live within those constraints, is being abandoned, in favor of a new view in which biota feedbacks on, directly alters, and contributes to shape the landscape (Viles, 1988; Jones *et al.*, 1994; Yoo *et al.*, 2005; Muneepeerakul *et al.*, 2008; Murray *et al.*, 2008; D'Odorico *et al.*, 2010; Reinhardt *et al.*, 2010). The explicit description of interacting biotic and abiotic dynamics is therefore a key requirement to understand, and model, the evolution of intertidal systems and recent contributions in the field of tidal biomorphodynamic modelling have indeed proposed formulations which account for the intertwined effects and the mutual influence of biotic and abiotic components (Morris *et al.*, 2002; Mudd *et al.*, 2004; van de Koppel *et al.*, 2005; D'Alpaos *et al.*, 2006; Morris, 2006; D'Alpaos *et al.*, 2007; Kirwan and Murray, 2007; Marani *et al.*, 2007; Temmerman *et al.*, 2007; Kirwan *et al.*, 2008; Mudd *et al.*, 2009; Larsen and Harvey, 2010; Mudd *et al.*, 2010; D'Alpaos, 2011; D'Alpaos *et al.*, 2011b). Here, we build on such recent approaches to further explore the response of tidal landscapes to variations in the governing physical and biological forcings, such as tidal range, wind climate, sediment supply, vegetation and microphytobenthos colonization, and rates of relative sea-level rise (RSLR). In particular we focus on the mutual influence exerted by bio-physical processes in controlling the biomorphodynamic evolution of tidal systems, giving rise to the possible existence of multiple stable states corresponding to characteristic and widespread geomorphic features.

To this end we refine the model proposed by Marani *et al.* (2007, 2010), which formalizes a description of the chief biological and physical land-forming processes responsible for the long-term evolution of tidal unchanneled morphologies. The model treats soil elevation and vegetation biomass as separate dependent variables, and describes their evolution in terms of two coupled dynamic equations leading to stable and unstable equilibria. In the original formulation the platform is subjected to a sinusoidal tide and to a constant forcing suspended sediment concentration (SSC), representing the available sediment due to wave activity on adjacent areas, and possible fluvial or marine inputs. Here, we relax some of the simplifying assumptions and explore the response of intertidal ge-

omorphologies, mediated by vegetation, to realistic tidal forcings, time-varying SSCs, and wind characteristics obtained from observations from the Venice Lagoon. We furthermore explore the full extent of the arising alternative equilibria, their dynamic accessibility, and the biological and physical factors controlling the possible abrupt transitions among them.

The Chapter is organized as follows. In Section 2.2 we briefly summarize the structure and features of the biomorphodynamic model and provide some information on the data used to force the model. Section 2.3 and 2.4 analyzes the role of physical and biological factors shaping the tidal landscape, subject to synthetic and realistic forcings, under the assumptions that: i) biomass is at all times in equilibrium with the current soil elevation ("equilibrium vegetation model"), or ii) biomass evolves according to its own time scales ("dynamic-vegetation model"). Finally, Section 2.5 draws a set of the main observations.

2.2 The point biogeomorphic model

The model describes the coupled time evolution of the elevation, $z(t)$, of a tidal platform, computed with reference to the (variable) relative mean sea level (RMSL), and of the vegetation biomass, $B(t)$, possibly colonizing it. The biogeomorphic evolution of the tidal platform is described by two coupled dynamic equations:

$$\frac{dz}{dt} = Q_S(z,B) + Q_T(z,B) + Q_O(B) - Q_E(z,B,\mathrm{MPB}(z)) - R \tag{2.1}$$

$$\frac{dB}{dt} = r(z)\,B\left(1 - \frac{B}{B_{max}}\right) - m(z)\;B \tag{2.2}$$

Equation (2.1) is the sediment continuity equation in which Q_S, Q_T, and Q_O are the annually-averaged sediment fluxes due to settling, trapping, and production of organic soil, respectively; Q_E is the annually-averaged erosion rate, mainly due to wind-induced waves in micro- and meso-tidal environments;

MPB(z) indicates the dependence of microphytobenthos (and of the associated sediment-stabilizing biofilm) on soil elevation; and R is the rate of RSLR (sea level variations plus local subsidence), which need be included in equation (2.1) to keep track of the moving sea level. Equation (2.2) governs the time evolution of the annually-averaged above-ground halophytic vegetation biomass, B (Levins, 1969), in which $r(z)$ is the reproduction rate, $m(z)$, is a mortality rate, and B_{max} is the maximum biomass density of a fully vegetated marsh.

The annually-averaged settling and trapping rates, Q_S and Q_T, are expressed as

$$Q_S(z,B) = \frac{1}{n_Y T}\frac{w_s}{\rho_b}\int_T \mathcal{C}(z,B,t)dt \tag{2.3}$$

$$Q_T(z,B) = \frac{1}{n_Y T}\frac{\alpha B^\beta}{\rho_b}\int_T \mathcal{C}(z,B,t)dt \tag{2.4}$$

where T is the period over which averaging is performed (a multiple or a fraction of one year), n_Y is the number of years in T (such that Q_S and Q_T are the annually-averaged rates); w_s is the settling velocity (here estimated as $w_s = 0.2$ mm/s for a median sediment diameter $d_{50} = 50$ μm (Gibbs, 1985)); $\rho_b = \rho_s \cdot (1-p)$ is the bulk density, with $\rho_s = 2650$ kg/m^3 and sediment porosity p =0.5, implicitly accounting for compaction processes; $\beta = 0.382$ and $\alpha = 1.02 \cdot 10^6\ d_{50}^2\ U^{1.7}$ m/s (m^2/g)$^\beta$, with U being an average flow velocity during a tidal cycle (Mudd *et al.*, 2004; D'Alpaos *et al.*, 2007); $\mathcal{C}(z,B,t)$ is the instantaneous SSC, in turn determined by solving a sediment balance equation in this 0D context that describe the exchange of water and sediment between the channel (where the tidal wave propagates and suspended sediments are transported) and the tidal platform (Krone, 1987; Temmerman *et al.*, 2003).

This is done according to the following conservation equation:

$$\frac{d}{dt}(DC) = -w_s C - \alpha B^\beta C + \tilde{C}\frac{dh}{dt} \tag{2.5}$$

where $h(t)$ is the instantaneous tidal elevation with respect to local MSL, $D(t) = h(t) - z$ is the instantaneous water depth, and

$$\tilde{C}(z,B,t) = \begin{cases} C_0 & \text{when} \quad dh/dt > 0 \\ C(z,B,t) & \text{when} \quad dh/dt < 0 \end{cases} \tag{2.6}$$

The concentration in the channel is fixed at C_0, while $h(t) = H \cdot sin(2\pi t/T)$ (T = 12 hrs, the main tidal period, H being the tidal amplitude). Note that $w_s\, C(t)/\rho_b$ and $-\alpha B^{\beta} C(t)/\rho_b$ are the instantaneous settling and trapping fluxes, respectively, which, by integration over all tidal cycles in one year yield the yearly mean total inorganic flux.

Although belowground biomass production plays a key role in maintaining marsh surface elevations (e.g., Turner *et al.*, 2004; Nyman *et al.*, 2006; Neubauer, 2008), the model does not address an explicit representation of below-ground processes (e.g., Mudd *et al.*, 2009), and assumes the production of organic matter, Q_O, to be proportional to the annually-averaged aboveground biomass, B, an assumption commonly adopted in salt-marsh ecomorphodynamic models (e.g., Randerson, 1979; Morris *et al.*, 2002; Mudd *et al.*, 2004; D'Alpaos *et al.*, 2006, 2007; Kirwan and Murray, 2007):

$$Q_O = \gamma B \tag{2.7}$$

where $\gamma = 2.0 \cdot 10^{-3}$ m^3/yr/kg incorporates typical vegetation characteristics and the density of the organic soil produced.

The erosion flux, Q_E, is computed on the basis of the wind-wave induced bottom shear stress (BSS), estimated using a point wave model (Carniello *et al.*, 2005; Fagherazzi *et al.*, 2006; Carniello *et al.*, 2011). The effective BSS due to wind-wave action, τ, is thus a function of water depth, $\mathcal{D}$, and wind velocity, u_w (Fagherazzi *et al.*, 2006; Defina *et al.*, 2007). The computation of the erosion flux for a value, z, of the platform elevation is performed by selecting a value of wind velocity, U_w, and computing the instantaneous erosion flux as (e.g., Partheniades, 1965):

$$E_{w,t}(z,B,\mathrm{MPB},U_w,t) = \frac{e}{\rho_b} I(B) \frac{\tau(\mathcal{D}(t),U_w) - \tau_c(\mathrm{MPB})}{\tau_c(\mathrm{MPB})} \tag{2.8}$$

$\mathcal{D}(t) = h(t) - z$ is the instantaneous water depth (with $h(t)$ the instantaneous tidal elevation with respect to local MSL); e is an erosion coefficient characteristic of sediment type and structure (here $e = 10^{-4}$ kg/m^2/s, e.g., van Ledden *et al.* (2005)); $I(B)$ is a step function, such that $I(B) = 1$ if $B = 0$ and $I(B) = 0$ if $B > 0$, accounting for the fact that wind waves are efficiently dissipated by the presence of vegetation, which thus reduces erosion to zero (Möller *et al.*, 1999; Neumeier and Ciavola, 2004; Augustin *et al.*, 2009); τ_c(MPB) is the threshold BSS for erosion, strongly dependent on the presence/absence of stabilizing polymeric biofilms produced by benthic microbes (e.g., Paterson, 1989; Amos *et al.*, 1998). Microphytobenthos growth is light-limited (MacIntyre *et al.*, 1996) and we assume that the incoming solar irradiance is sufficient for microbial photosynthetic activity starting at Mean Low Water Level (MLWL). We further assume, coherently with typical observed values (Amos *et al.*, 1998), $\tau_c = 0.4$ Pa when $z < -H$ and $\tau_c = 0.8$ Pa when $z > -H$.

We next average $E_{w,t}$ over a tidal period, to obtain the average erosion at elevation z:

$$E_w(z, B, \mathrm{MPB}, U_w) = \frac{1}{T} \int_T E_{w,t}(z, B, \mathrm{MPB}, U_w, t)\, dt \tag{2.9}$$

and finally we average E_w over the probability distribution of observed wind velocities, $f(U_w)$, to obtain the average erosion flux, $E(z, B, \mathrm{MPB})$ as a function of elevation, vegetation biomass, and MPB:

$$E(z, B, \mathrm{MPB}) = \int_{U_w} E_w(z, B, \mathrm{MPB}, u_w) f(u_w)\, du_w \tag{2.10}$$

Equation (2.2) describes the dynamics of vegetation biomass using a logistic model (Levins, 1969), with elevation-dependent parameters. The reproduction and mortality rates, $r(z)$ and $m(z)$, reflect the physiological responses of halophytic species to soil water saturation, locally represented by elevation (Silvestri *et al.*, 2005; Marani *et al.*, 2006c).

For many purposes, e.g. when studying the properties of equilibrium states,

it may be assumed that vegetation adapts to changes in elevation very quickly (e.g., Allen, 1995; Morris *et al.*, 2002; Mudd *et al.*, 2004; D'Alpaos *et al.*, 2007; Kirwan and Murray, 2007) compared to typical geomorphological time scales (often appreciable changes in local elevations occur over several years). Under this hypothesis, vegetation biomass is instantaneously adapted to soil elevation, yielding an "equilibrium vegetation model", in which B is solely a function of z. Marani *et al.* (2010) also treat in detail the solutions arising from the fully coupled dynamical system obtained by treating biomass as an independent variable according to a "dynamic-vegetation" modeling approach. We will here first confine ourselves to the case of "instantaneous" vegetation adaptation (Section 2.3) and then provide examples of model's purview of fully-coupled analyses (Section 2.4). In particular, in the former case, the two equations (2.1) and (2.2) can be decoupled, by first finding the steady-state solution, $B(z)$, of (2.2) and by substituting it back into (2.1). A trivial solution of $dB/dt = 0$ is $B = 0$, which cannot be observed in actual marshes because the presence of seed banks and the continuous input of propagules from surrounding marshes would repopulate a marsh where vegetation had temporarily disappeared (e.g., Adam, 1990; Ungar, 1991). This leaves the steady-state solution:

$$B_s(z) = B_{max}\left[1 - \frac{m(z)}{r(z)}\right] \tag{2.11}$$

which is valid for $z \geq 0$, while $B_s(z) = 0$ when $z < 0$.

Two typical, and contrasting, relations between soil aeration and vegetation biomass may be considered.

The first case ("multispecies vegetation") is characterized by biomass increasing with increasing soil elevation (between MSL, $z = 0$, and Mean High Water Level (MHWL), $z = H$) and is typical e.g. of Mediterranean tidal environments, where several species adapted to progressively more aerated conditions compete (Day *et al.*, 1999; Marani *et al.*, 2004; Silvestri *et al.*, 2005) or sites in northern continental Europe and in the UK (e.g., Allen, 1995). In the "multispecies vegetation" case we assume a reproduction rate which linearly increases with

elevation, while the mortality rate is assumed to decrease linearly with z: $r(z) = 0.5\ z/H + 0.5\ \mathrm{yr}^{-1}$; $m(z) = -0.5\ z/H + 0.5\ \mathrm{yr}^{-1}$. We also assume each plant to produce at most one daughter plant per year in the most favourable conditions, i.e. $r(H) = 1\ \mathrm{yr}^{-1}$ and $m(H) = 0\ \mathrm{yr}^{-1}$. Observations in this case indicate that biomass is equal to zero at $z = 0$ and maximum at $z = H$ (Marani *et al.*, 2004; Silvestri *et al.*, 2005). We thus take $r(0) = m(0) = 0.5\ \mathrm{yr}^{-1}$.

The second case is a *Spartina*-dominated environment, characteristic of some North-American sites (Morris and Haskin, 1990; Morris *et al.*, 2002), in which biomass is a decreasing function of elevation between $z = 0$ and $z = H$. In this case we assume $r(0) = 1\ \mathrm{yr}^{-1}$ and $m(0) = 0\ \mathrm{yr}^{-1}$, while $r(H) = m(H) = 0.5\ \mathrm{yr}^{-1}$ (such that the steady-state biomass is maximal at $z = 0$ and is zero at $z = H$). The reproduction and mortality rates are thus: $r(z) = -0.5\ z/H + 1.0\ \mathrm{yr}^{-1}$; $m(z) = 0.5\ z/H\ \mathrm{yr}^{-1}$.

In the following we explore the stable equilibrium states and transient dynamics associated with equations (2.1) and (2.2) by considering both: i) synthetic forcings (such as sinusoidal tides of varying amplitude, constant SSCs and rates of RSLR), and ii) observed tidal levels, sediment concentrations, and wind velocities, measured within a monitoring network in the Venice lagoon by the Venice Water Authority (figure. 2.1). This dataset was homogeneously upscaled at the hourly time scale for the whole 2004-2006 observation period.

2.3 Equilibrium-vegetation modeling

2.3.1 Synthetic forcings: general model behavior leads to different tidal patterns

We first consider, as a reference case, the ideal case of a system subjected to a sinusoidal tide with amplitude $H = 0.5$ m and period $T = 12$ hours, forced by a constant external SSC and by a constant rate of RSLR (Marani *et al.*, 2010). Figure 2.2 shows the rate of change of platform elevation, dz/dt, as a function of the elevation, z, for the two vegetation types considered, when a constant

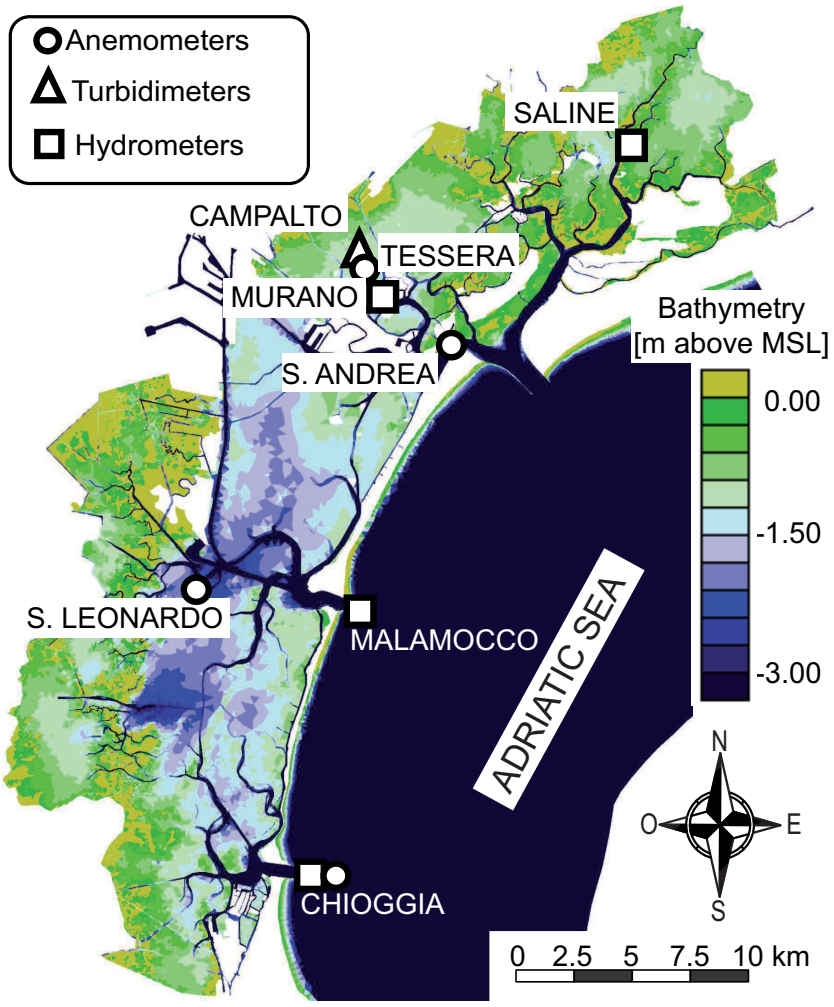

Figure 2.1: Color-coded bathymetry of the Venice Lagoon with the locations of the anemometric, turbidimetric, and mareographic stations.

SSC, C_0 =20 mg/l, and a constant rate of RSLR, R=3.5 mm/yr, are assumed. These forcings may be considered to be representative of the local RSLR for the 20^{th} Century in the Venice Lagoon (Carbognin *et al.*, 2004; Meehl, 2007; Marani *et al.*, 2007). The shape of the curves in figure 2.2 is determined by the dependence of the deposition and erosion fluxes (see eq. (2.1)) on platform elevation. For platform elevations below MLWL, $z < -H$, the settling flux is weakly dependent on z and dz/dt remains nearly constant, whereas it linearly decreases for elevations larger than MLWL, to vanish at MHWL due to the reduction in the frequency and duration of inundations. The erosion flux, Q_E, is negligible for $z < -2.5$ m because wind waves do not induce an appreciable bed shear stress in deep waters (Carniello *et al.*, 2005; Fagherazzi *et al.*, 2006; Defina *et al.*, 2007). Q_E then increases with elevation, reaching a maximum at approximately $z = -1.2$ m, to decrease again for larger values of z because of reduced wind-driven BSS and of shorter flooding times (for $z >$MLWL). Q_E vanishes as soon as $z > 0$, when the platform is encroached by halophytic plants which reduce turbulent kinetic energy (e.g., Leonard and Croft, 2006; Mudd *et al.*, 2010) and increase the critical shear stress for erosion (Möller *et al.*, 1999; Neumeier and Ciavola, 2004; Augustin *et al.*, 2009). As soon as the platform reaches an elevation which allows vegetation encroachment ($z >$MSL), the organic and trapping rates, Q_O and Q_T, respectively, contribute in determining the dependence of dz/dt on z. In the *Spartina*-vegetated case, because both Q_O and Q_T are maximum at $z = 0$ and decrease with z due to the decrease in plant biomass with marsh elevation, vegetation encroachment significantly accelerates the vertical growth of the platform (figure 2.2b), thus producing an abrupt increase in the total accretion rate. On the contrary, in the *multispecies* vegetation case (figure 2.2a), Q_O increases with z, whereas Q_T initially increases, because of the increase in biomass, to subsequently decrease at higher values of z due to the reduced SSC associated with decreased water depths and fewer inundation periods. A more gradual acceleration in the vertical growth of the marsh surface together with a smoother increase in the total accretion rate is thus observed in

the multispecies vegetation case.

Solid circles in figure 2.2 mark stable equilibrium states, which include a subtidal platform equilibrium, located at elevations lower than MLWL, and a marsh intertidal equilibrium located above MSL. These equilibria are stable because a negative (positive) perturbation of elevation produces a value $dz/dt > 0$ ($dz/dt < 0$), which tends to bring the system back to the original equilibrium state. A third solution of $dz/dt = 0$ also exists, corresponding to an unstable equilibrium state, which cannot be observed, as any perturbation drives the system away from it.

Changes in R and C_0 may lead to a different number and type of equilibria. An increase in C_0 stretches the curves in figure 2.2 and moves them upward, increasing the equilibrium elevations and possibly making the subtidal equilibrium disappear if C_0 becomes larger than a threshold (60 mg/l, in the present case). Analogously, an increase in the rate of RSLR results in a proportional downward vertical shift of the curves in figure 2.2.

From these considerations we can infer the presence of a path to pattern formation: depending on spatially-varying initial conditions and RSLR forcing different areas within the same tidal environment can manifest different equilibrium states.

2.3.2 Synthetic forcings: the role of the rate of RSLR and of organic production

The bifurcation diagram in figure 2.3 shows equilibrium platform elevations plotted as a function of the rate of RSLR, which summarizes the number and type of possible equilibria for a given value of R. In order to fully appreciate the role of vegetation, different cases of maximum organic accumulation are considered, namely the cases $\gamma = 2 \cdot 10^{-3}$ m^3/kg/yr (black line), $\gamma = 4 \cdot 10^{-3}$ m^3/kg/yr (green line), and the hypothetical case in which vegetation is absent (red line). It is seen that biomass productivity substantially affects marsh elevation, suggesting that vegetation may play here the role of ecosystem engineer

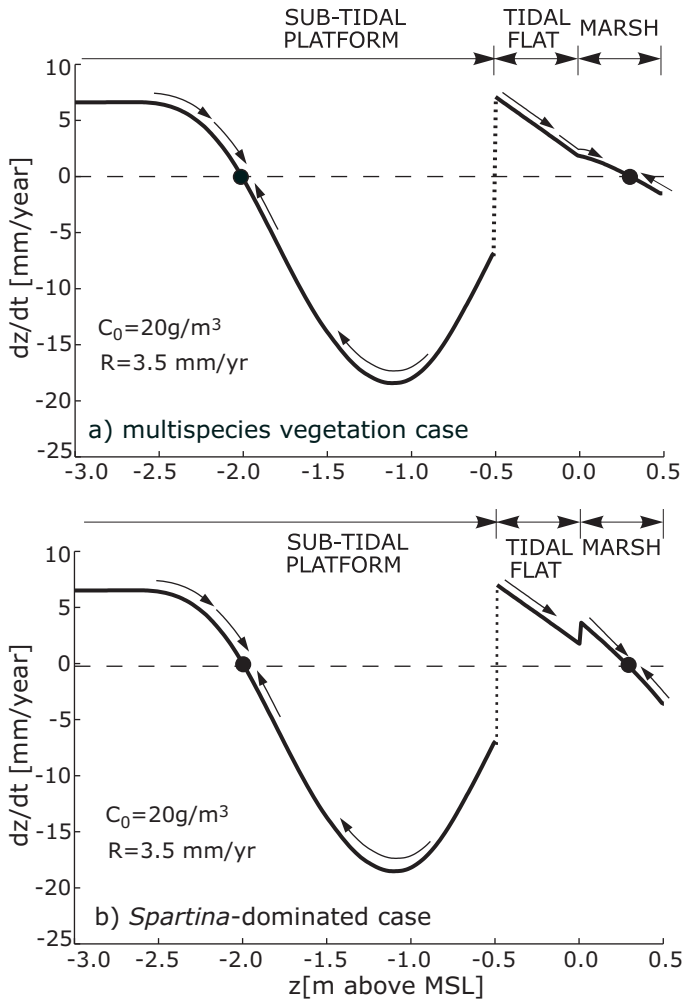

Figure 2.2: Time derivative of platform elevation, dz/dt, as a function of platform elevation, z, (a) in the *multispecies vegetation* case and (b) in the *Spartina*-dominated case, when the system is forced with a sinusoidal tide of amplitude $H = 0.5$ m, period $T = 12$ hours, wind characteristics of the Chioggia station (see figure 2.1), rate of SLR $R = 3.5$ mm/yr, and SSC $C_0 = 20$ mg/l. The elevation z is computed with respect to the local MSL.

(Jones *et al.*, 1994).

In the case of sea regression (negative values of R), no tidal equilibrium is possible for $R < -14.9$ mm/yr, suggesting the transition to a terrestrial environment. For -14.9 mm/yr $< R <$ 0.0 mm/yr only a subtidal platform equilibrium exists, as intertidal platforms are not possible as stable features. For 0.0 mm/yr $< R <$ 7.2 mm/yr the subtidal equilibrium coexists with a marsh equilibrium (when $\gamma = 2 \cdot 10^{-3}$ m^3/kg/yr), whereas for 5.4 mm/yr $< R <$ 7.2 mm/yr marsh, tidal-flat, and subtidal equilibria constitute alternative stable equilibrium states. Tidal-flat and subtidal equilibria coexist also for 7.2 mm/yr $< R <$ 10.1 mm/yr. The subtidal platform equilibrium vanishes for $R >$ 10.1 mm/yr, while all intertidal equilibria disappear for $R >$ 10.6 mm/yr, marking the transition to a marine environment. The role played by vegetation can be further appreciated by considering the effect of vegetation productivity on the possible equilibria. When $\gamma = 4 \cdot 10^{-3}$ m^3/kg/yr, the vegetated marsh can keep pace with rates of RSLR up to 9.2 mm/yr. On the contrary, in the absence of vegetation the marsh platform would drown for rates of RSLR larger than 5.4 mm/yr. The presence of vegetation thus significantly increases the capability of marshes to survive increasing rates of RSLR and decreasing sediment availability, allowing existing vegetated surfaces to sustain rates of RSLR and sediment supply that would preclude marsh surfaces from developing in the first place (Marani *et al.*, 2010; D'Alpaos, 2011; Kirwan *et al.*, 2011; Mudd, 2011).

2.3.3 Synthetic forcings: the role of the tidal range

We now analyze the equilibria of a system forced by constant external SSC and RSLR rate, subjected to sinusoidal tides of different amplitudes with the same period $T = 12$ hours.

As the tidal amplitude increases, the intensity of wind induced erosive processes over the subtidal platform progressively decreases (figure 2.4), whereas the range of elevations potentially subjected to erosion progressively increases. To understand this behavior one must consider that the maximum BSS as a

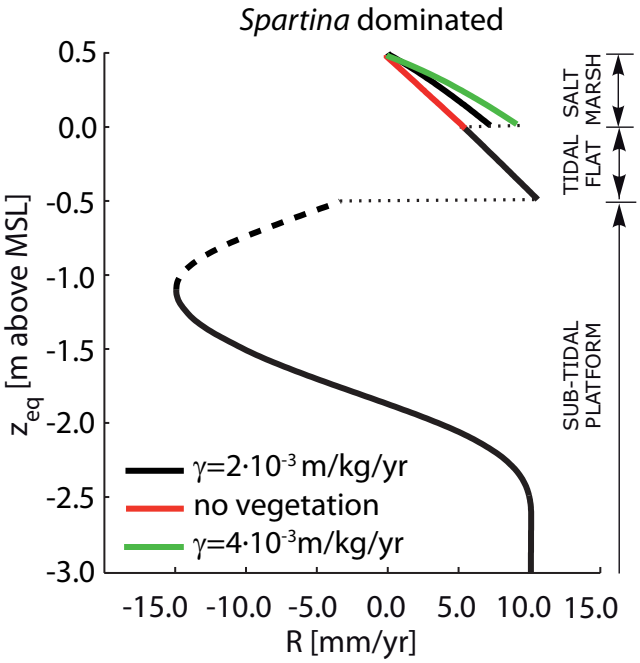

Figure 2.3: Bifurcation diagram showing equilibrium elevations, z_{eq}, as a function of the rate of RSLR, R, in the case of a *Spartina*-dominated system forced with a sinusoidal tide with period $T = 12$ hours, amplitude $H = 0.5$ m, and SSC $C_0 = 20$ mg/l. Two possible scenarios for organic production are also considered (namely $\gamma = 2.0 \cdot 10^{-3}$ m^3/yr/kg and $\gamma = 4.0 \cdot 10^{-3}$ m^3/yr/kg) together with the hypothetical case in which vegetation is absent.

function of water depth (inset in figure 2.4a) occurs for intermediate depths. In fact, for very low depths wave height is severely limited, while for large depths the orbital velocities connected with surface waves, and the associated BSSs, become very small close to the sediment surface (e.g., Fagherazzi *et al.*, 2006). It follows that, in the limiting case of a null tidal amplitude (i.e. when the water depth is constant during the tidal cycle) platform elevations continuously experience the same BSS (in particular, elevations around -1.1 m experience the maximum BSS throughout the tidal cycle). The system therefore experiences strong erosion ($Q_{E_{max}} \approx 27$ mm/yr when $H = 0$) in a relatively narrow range of elevations. As the tidal amplitude increases, a given platform elevation experiences a wider range of BSSs during the tidal cycle (elevations around -1.1 m experience also BSSs smaller than the maximum one because of variations in the water depth with the tide – see e.g. inset in figure 2.4a) and the intensity of the erosion processes decreases ($Q_{E_{max}} \approx 10$ mm/yr when $H = 1.0$ m). This suggests that bottom erosion due to the effects of wind waves is more intense in microtidal settings rather than in meso- and macrotidal settings. The subtidal equilibrium elevations, z_{eq}, experience small variations as the tidal amplitude increases ($z_{eq} = -2.0$ m when $H = 0.2$ m; $z_{eq} = -1.75$ m when $H = 0.75$ m see solid gray circles in figure 2.4b). Interestingly, no subtidal equilibria are possible for tidal amplitudes larger than 0.75 m (when $C_0 = 20$ mg/l and wind observations at S. Leonardo are considered), due to the increase in the settling rate and to the concurrent decrease in the erosion rate, for increasing tidal amplitudes (figure 2.4b). Considering more severe wind focings (e.g. wind characteristics at Chioggia, see also Section 2.3.5) produces a general lowering of subtidal equilibria (see solid white circles in figure 2.4b). Finally, a decrease in the available sediment increases the depth of subtidal equilibria which exist for a wider range of tidal amplitudes (see solid gray pentagons in figure 2.4b). Marani *et al.* (2010) showed that subtidal equilibrium elevations are relatively less sensitive to increasing rates of RSLR rather than to decreases in the SSC. Here we emphasize that the range of existence of subtidal equilibria is relatively

less sensitive to variations in the wind forcings rather than to decreases in the available sediment.

We also analyzed the influence of the tidal range on tidal-flat and salt-marsh equilibria (figure 2.5). The equilibrium elevation of the marsh within the tidal frame increases with the tidal amplitude: for prescribed forcing SSCs and rates of RSLR, marshes in high tidal ranges are higher in the tidal frame (i.e. relative to the respective MHWL) than marshes in low tidal ranges. Moreover, marshes populated by a variety of vegetation species ("multispecies vegetation" case), in which biomass increases with marsh elevation, are higher in the tidal frame than *Spartina*-populated marshes, characterized by a decrease in biomass as marsh elevation increases. This suggests that marshes in high tidal ranges are more stable, and therefore more resilient to increasing rates of RLSR, than those in low tidal ranges, in agreement with recent findings by Kirwan and Guntenspergen (2010), Kirwan *et al.* (2010), and D'Alpaos *et al.* (2011b). Moreover, the existence of a variety of vegetation species which populate the marsh increases the stability and resilience of these morphological structures. Different vegetation type are also characterized by interesting differences both in the type and number of equilibria. In the cases considered here ($C_0 = 20$ mg/l and $R = 3.5$ mm/yr), no marsh equilibria exist in the "multispecies vegetation" case for tidal amplitudes smaller than 0.5 m. On the contrary, in the *Spartina*-dominated case, a marsh equilibrium and a tidal-flat equilibrium coexist for tidal amplitudes smaller than 0.5 m.

2.3.4 Observed forcings: the role of the tidal regime

We study here the stable equilibrium states emerging from eq. (2.1) when the system is forced with observed tidal levels, sediment concentrations, and wind velocities. To this end we consider the "multispecies vegetation" case, typical of the Venice Lagoon, and the observed 20^{th}-century rate of RLSR for the Venice Lagoon, $R = 3.5$ mm/yr (Carbognin *et al.*, 2004; Meehl, 2007; Marani *et al.*, 2007). Figure 2.6(a) shows dz/dt versus z and the corresponding stable equilibria

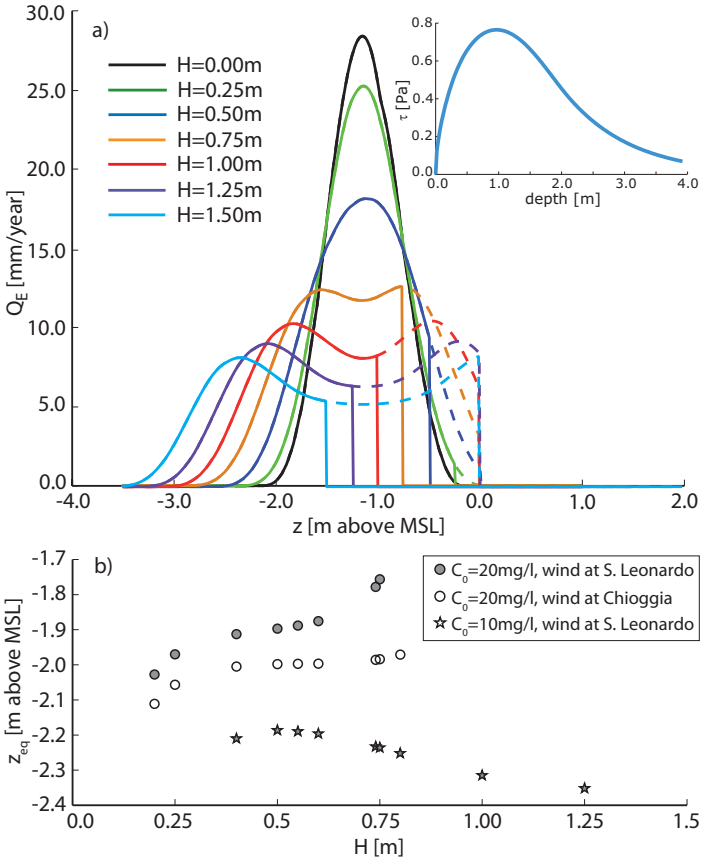

Figure 2.4: a) Erosion rate, Q_E, and b) sub-tidal platform equilibrium elevations, z_{eq}, computed for different tidal amplitudes when the system is forced with a sinusoidal tide with period $T = 12$ hours, rate of SLR $R = 3.5$ mm/yr, wind characteristics at different stations (see figure 2.1), and different SSCs. Solid lines in figure 2.4a, computed by considering wind characteristics at the S. Leonardo station, represent the case in which MPB and vegetation are both present and increase the value of the critical shear stress for erosion; dashed lines show the case in which the polymeric biofilm due to MPB is disrupted by human activity or bioturbation (e.g., invertebrates) and only vegetation contributes to increase the threshold shear stress for erosion. Inset in figure 2.4a: Dependence of the bottom shear stress, τ, on water depth computed for a wind speed of 15 m/s. Solid gray circles in figure 2.4b are obtained when considering wind at the S. Leonardo station and $C_0 = 20$ mg/l; solid white circles: wind at the Chioggia station and $C_0 = 20$ mg/l; solid gray pentagons: wind at the S. Leonardo station and $C_0 = 10$ mg/l.

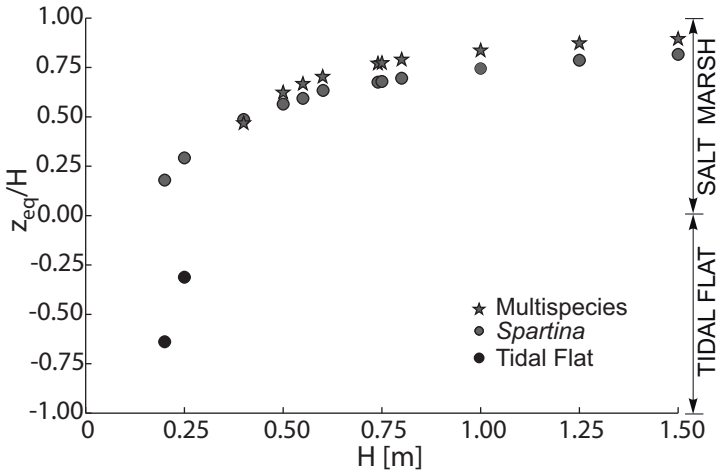

Figure 2.5: Salt-marsh and tidal-flat equilibrium elevations made dimensionless with the tidal amplitude, z_{eq}/H, versus the tidal amplitude, H, computed for different tidal amplitudes when system is forced with a sinusoidal tide with period $T = 12$ hours, rate of SLR $R = 3.5$ mm/yr, and SSC $C_0 = 20$ mg/l.

computed on the basis of tidal observations at Murano (figure 2.7a), wind regime at Tessera, and suspended sediment concentrations at Campalto (see figure 2.1). For a rate of RLSR $R = 3.5$ mm/year we find two stable equilibria: a subtidal platform equilibrium ($z = -1.38$ m) and a salt-marsh equilibrium ($z = 0.30$ m), values which are consistent with observed geomorphic features in the Venice lagoon. If $R = 7.3$ mm/yr, representing a somewhat extreme IPCC projection for RSLR in the next Century, the elevations of both the subtidal and marsh equilibria are substantially decreased. However, it is worth noting that the nature of these equilibria remains unchanged, for this set of tidal, wind, and sediment forcings. In particular, there is no transition from a salt-marsh (vegetated) equilibrium to an unvegetated tidal flat equilibrium ($z < 0$). A detailed inspection of figure 2.6a makes it possible to determine the threshold rate of RSLR for marsh drowning, $R = 10.5$ mm/yr, the limit value for which a marsh transitions to a tidal flat. If $R > 16.2$ mm/yr, such that no solution to $dz/dt = 0$ exists, the system transitions to a marine environment. This analyses show that the available equilibrium states are relatively insensitive to

a variability in the rate of RSL change, at least when the actual forcings from a network of stations in this area are considered. It should however be noted that the model postulates that the incoming flux of suspended sediment, i.e. the sources of $C_0(t)$, remains constant, whatever change may occur. This means that any accretion may occur only at the expenses of other morphological structures, if no sediment input from rivers of the sea is present (as in the case of the Venice lagoon). In order to properly describe the response of the system to large values of R further feedbacks should thus be included in the model.

Figure 2.6b represents the accessible stable equilibria for the same forcings as in figure 2.6a, except that the astronomical tide (figure 2.7b), rather than the observed tide (figure 2.7a), was imposed. The exclusion of meteorological contributions to the tide causes a general lowering of the equilibrium elevations, due to the generally lower water levels characterizing the astronomical tide, as indicated in figure 2.7.

To understand why the sub-tidal platform equilibrium elevation is decreased one must recall the relationship between the maximum bottom shear stress and water depth (inset in figure 2.4a). If frequent tidal levels are reduced, as in this case, so is the elevation for which the maximum erosion occurs and thus the equilibrium elevation for which erosion, deposition and sea level rise balance one another. The elevation of the marsh equilibrium is also reduced, but the mechanism leading to this reduction does not involve the erosion flux, as in the previous case, since erosion over marshes is inhibited by the presence of vegetation, independent of elevation (within the elevation interval allowing the development of halophytic plants). In this case a reduced frequency of high tidal levels implies a reduced sediment deposition at high elevations and thus a reduction of the soil elevation for which deposition, trapping and organic sediment production balance the rate of RSLR.

The comparison of figure 2.6a and b shows that the sensitivity of the observable bio-geomorphic equilibria to changes in the tidal regimes is quite strong. Relatively small differences in the prevalent tidal levels (compare figures 2.7a

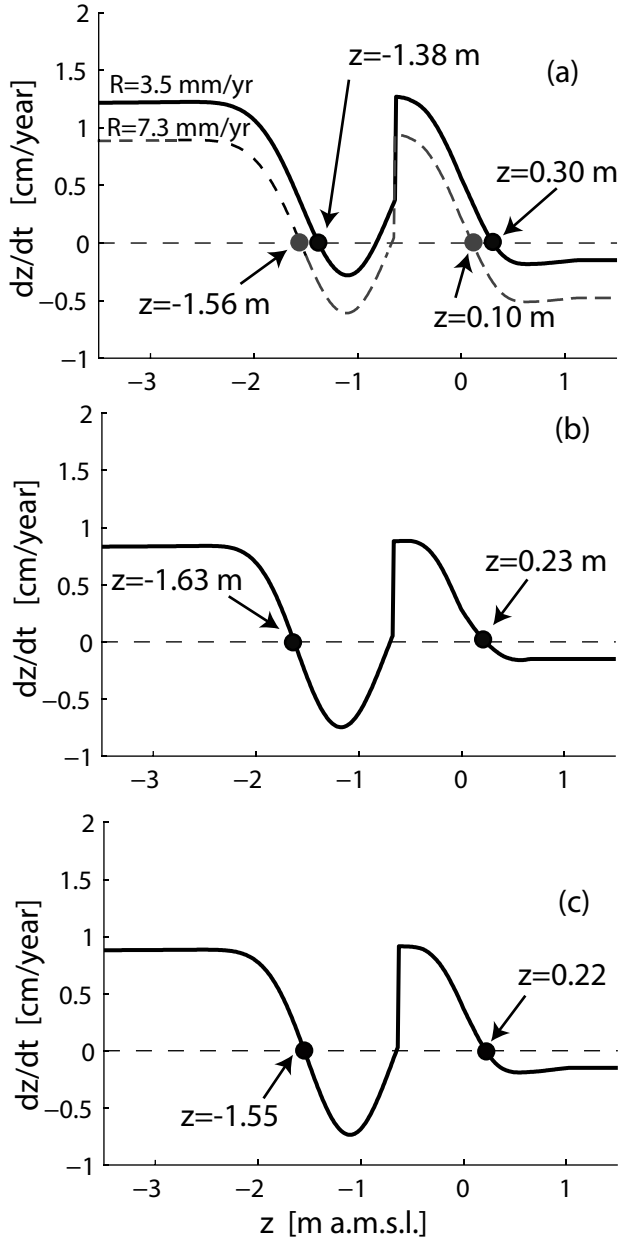

Figure 2.6: Stable equilibrium states in the oxygen-limited vegetation case with (a) tidal observations at "Murano", wind at "Tessera" and suspended sediment concentration $C_0(t)$ at "Campalto"; (b) same as in (a) except that the astronomic tide (i.e. with no meteorological component) is prescribed; (c) same as in (a) except that tidal observations at "Saline" are used.

and b) are responsible for relevant changes in the elevations of both salt-marsh and subtidal equilibrium states. On the other hand, similar changes in equilibrium elevations occur as a result of increases in R which are quite extreme within the range of the IPCC projections (figure 2.6a). One must therefore conclude that the tidal system studied is potentially more exposed to changes in the tidal regime than to changes in the rate of RSLR. The strong sensitivity of system equilibria to the characteristics of the local tide are emphasized by figure 2.6c, which shows the results of using the same wind and suspended sediment forcing as in figure 2.6c and b, and the tidal observations at the "Saline" tide gauge (see figure 2.1 for the location and figure 2.7c for the probability density function of tidal levels). The differences between figure 2.6a and figure 2.6c indeed show that the local tide can decisively influence the elevation of the available equilibrium states.

2.3.5 Observed forcings: the role of the wind regime

Figure 2.8 shows a comparison between the probabilities of exceedance of wind velocity measured at four different sites in the Venice Lagoon (see figure 2.1). Differences can obviously occur only in sub-tidal equilibria (or in tidal flats, if present, figure 2.9), as wind-driven waves are assumed to be completely dissipated by marsh vegetation. It is also worthwhile recalling (Marani *et al.*, 2007, 2010) that wind waves are likely to produce BSS values exceeding typical threshold values for sediment erosion (e.g. $\tau > \tau_c = 0.4$ Pa) only for wind velocities larger than about 5 m/s. As a consequence, differences in the probability distributions for wind velocities $u_w < 5$ m/s will not produce differences in the subtidal equilibrium elevations. Chioggia is characterized by more frequent high winds ($u_w > 5$ m/s) with respect to all the other stations, as shown in figure 2.9, leading to the lowest subtidal equilibrium elevation (figure 2.9a), because of the greatest erosion rates. As the probability of exceedance of high winds decreases (compare the Chioggia and S. Leonardo distributions) the elevation of the subtidal platform increases (figure 2.9b), because a higher elevation reduces

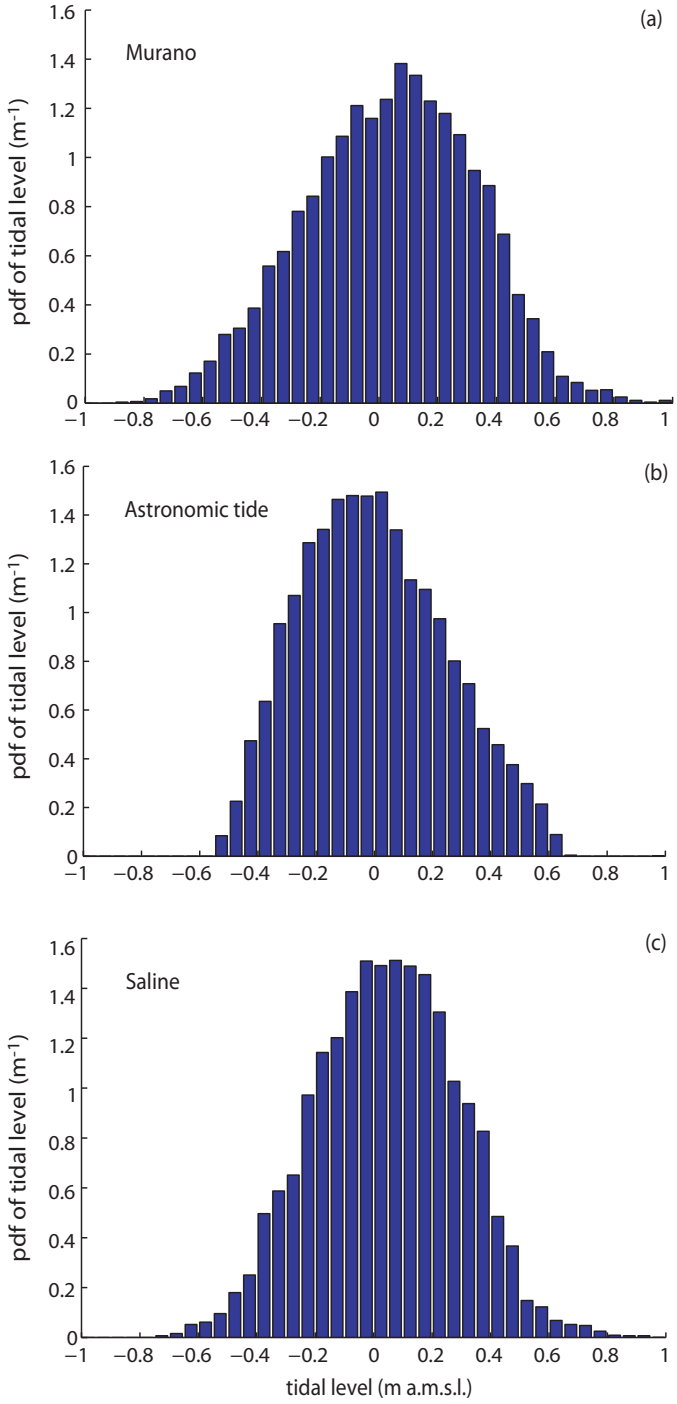

Figure 2.7: Probability density functions of Tidal levels for (a) observations at "Murano", (b) astronomic tide, (c) observations at "Saline".

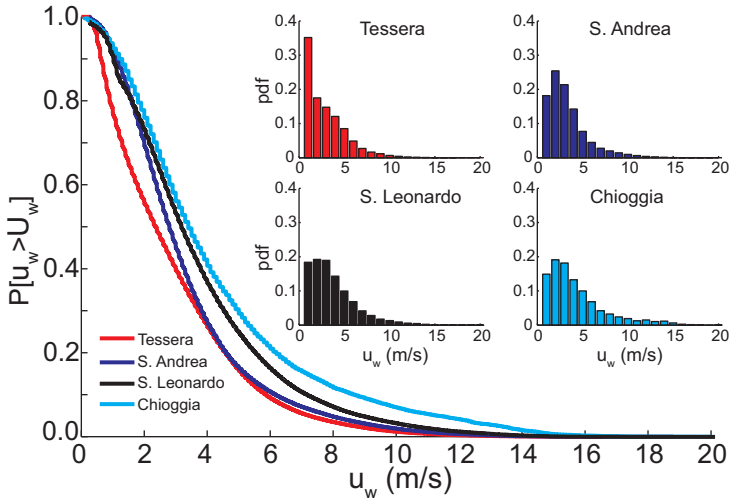

Figure 2.8: Probability of exceedance of wind velocity according to the Tessera, S. Andrea, S. Leonardo, and Chioggia anemometers. Inset: frequency distributions of wind velocity.

the erosion flux thus restoring the balance with the deposition rate and the rate of RSLR. Finally, it is worth noting that the winds measured at S. Andrea and Tessera, which are characterized by quite similar probability distributions for $u_w > 4$ m/s (figure 2.8), lead to almost the same equilibrium elevation of the subtidal platform (compare figures 2.9c and d).

2.4 Dynamic-vegetation modeling

We finally provide some examples of the model's capability to describe the fully coupled dynamics of the system based on the simultaneous solution of equations (2.1) and (2.2). For the sake of illustration we consider six different initial elevations and biomass values, and force them with a sinusoidal tide, a constant rate of RSLR and a constant sediment supply, to describe their evolution toward a stable equilibrium, as jointly determined by physical and biological processes. We first consider the case in which both the reproduction and mortality rates vary as a function of marsh elevation (i.e. $r(z) = -0.5\ z/H + 1.0\ \mathrm{yr}^{-1}$ and $m(z) = 0.5\ z/H\ \mathrm{yr}^{-1}$). Figure 2.10 portrays the evolution of the system both

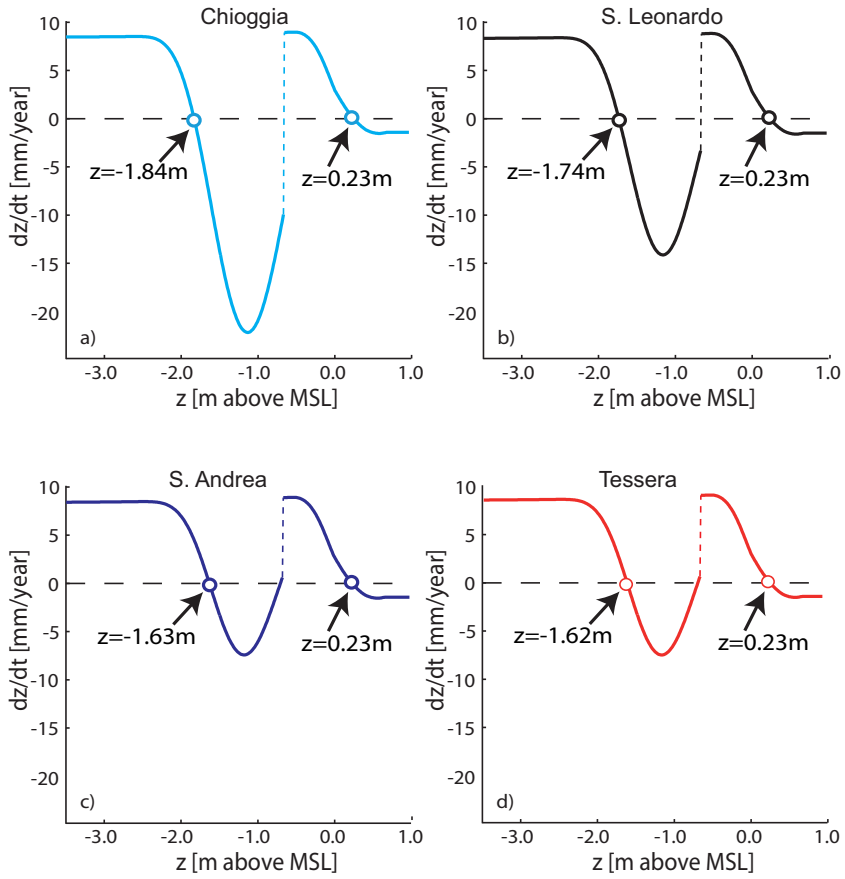

Figure 2.9: Effects of tidal regimes on the available equilibrium states. dz/dt vs. z and the associated stable equilibria on the basis of the astronomic tide, suspended sediment concentration $C_0(t)$ at Campalto, and wind velocity at Chioggia (a); S. Leonardo (b); S. Andrea (c); and Tessera (d).

in terms of variations in bottom elevations, z (figure 2.10a), and vegetation biomass, B (figure 2.10b). The six different marshes considered in this experiment will tend to the same marsh equilibrium elevation, $z_{eq} = 0.50$ m above MSL (figure 2.10a) at which the total accretion rate matches the imposed rate of RSLR (figure 2.10c). Simultaneously, the value of the vegetation biomass characterizing these marshes will tend to the same equilibrium value, $B = 500$ gm^{-2}, at which $dB/dt = 0$ (figure 2.10b). This dynamic-vegetation modeling experiment allows us to emphasize that during the transient phase, vegetation is not necessarily in equilibrium with the current forcing and adapts to changes in elevation according to its own characteristic timescale. Transient dynamics can also be analyzed by considering the evolution of these six trajectories in the phase-space (figure 2.10d). Often, when the system is far from equilibrium, the paths followed in phase space to reach the equilibrium state are characterized by nearly vertical trajectories. This occurs until the system attains the steady state biomass, $B_s(z)$ (black solid line in figure 2.10d), which is a function of elevation (see eq. (2.11)). In subsequent stages the marsh evolves by varying both biomass and elevation following the steady state biomass curve, $B_s(z)$, until it reaches equilibrium (figure 2.10d). We also consider a second scenario in which the reproduction rate, r, is assumed to be constant and equal to 1 yr^{-1} (i.e., each plant produces one daughter plant per year) and the mortality rate is assumed to increase with marsh elevation, $m(z) = z/H$ yr^{-1} (figure 2.11). According to this scenario the equilibrium biomass $B_s(z)$ (see eq. (2.11)) becomes a linearly decreasing function of marsh elevation (e.g., Mudd *et al.*, 2004; D'Alpaos *et al.*, 2007). Also in this case the system will tend to the same marsh equilibrium elevation, $z_{eq} = 0.48$ m above MSL, with an equilibrium biomass $B = 350$ gm^{-2} (figure 2.11a and b). Furthermore, also in this case the paths followed in phase space to reach the equilibrium state are characterized by nearly vertical trajectories (figure 2.11d). We also compute the time it takes for marsh elevations to be within 3% of the equilibrium elevation starting from different initial conditions, both with the "dynamic vegetation" model (i.e. by simultaneously solving

equations (2.1) and (2.2)) and with the "equilibrium vegetation" model (e.g. by considering the steady state biomass $B_s(z)$ provided by eq. (2.11)) when the birth and the mortality rates are assumed to vary with elevation (as in figure 2.10) and when the birth rate is kept constant and the mortality rate increases with elevation (as in figure 2.11). Figure 2.12 shows a comparison between the time lags required to reach equilibrium starting from different initial conditions in the above cases, and emphasizes that differences in the time lags computed by considering the "dynamic vegetation" and the "equilibrium vegetation" models, are in the range 1-15%. Such a behavior further confirms that in many cases one can realistically assume an instantaneous adaptation of vegetation to the current platform elevation.

2.5 Observations

By generalizing a fully-coupled point model of marsh biogeomorphic evolution (Marani *et al.*, 2007, 2010) we have further explored the stable equilibrium states of tidal structures and their dependence, in terms of equilibrium types and number, on biological processes and physical forcings. Model results emphasize the importance of accounting for the main interacting biological and physical components in order to obtain realistic representations of the system dynamics. Our numerical experiments allows us to point to the following main observations:

i) The number and the elevation of the equilibrium states, both in the subtidal and in the intertidal zones, depend, jointly, on a number of processes of physical and biological nature, such as: the rate of relative sea level rise, sediment supply, biomass productivity, wind climate, and the tidal range.

ii) Biomass productivity crucially affects both the equilibrium marsh elevation and marsh resilience to accelerations in RSLR, showing how a detailed understanding of biological processes is required to understand the

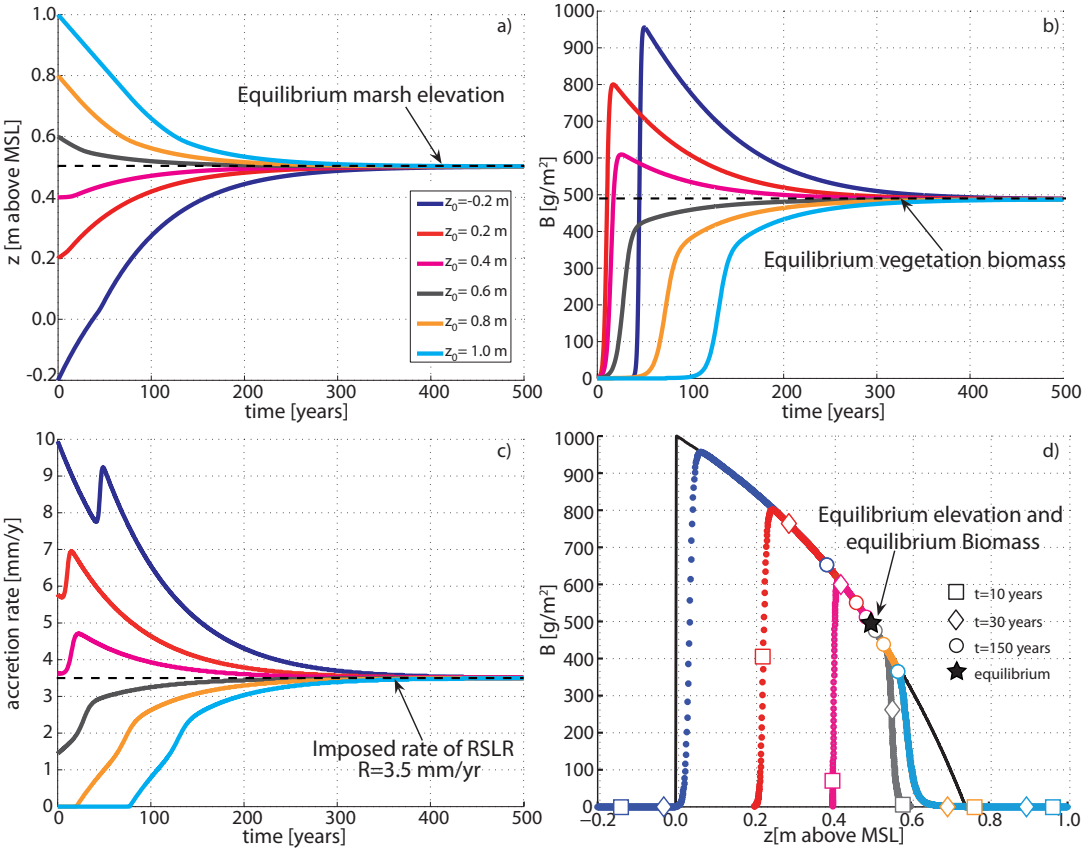

Figure 2.10: Evolution in time of (a) platform elevations, (b) vegetation biomass, (c) accretion rates, and (d) phase portrait describing the dynamics of the system, for different initial conditions. We considered the case of a *Spartina*-dominated system forced with a sinusoidal tide with $T = 12$ hours, $H = 0.75$ m, $C_0 = 20$ mg/l, and $R = 3.5$ mm/yr, when both the reproduction and mortality rates vary as a function of marsh elevation (i.e. $r(z) = -0.5\ z/H + 1.0\ \mathrm{yr}^{-1}$ and $m(z) = 0.5\ z/H\ \mathrm{yr}^{-1}$). In all panels the depicted stable state correspond to a vegetated marsh with $z = 0.50$ m above MSL and $B = 500$ g/m^2.

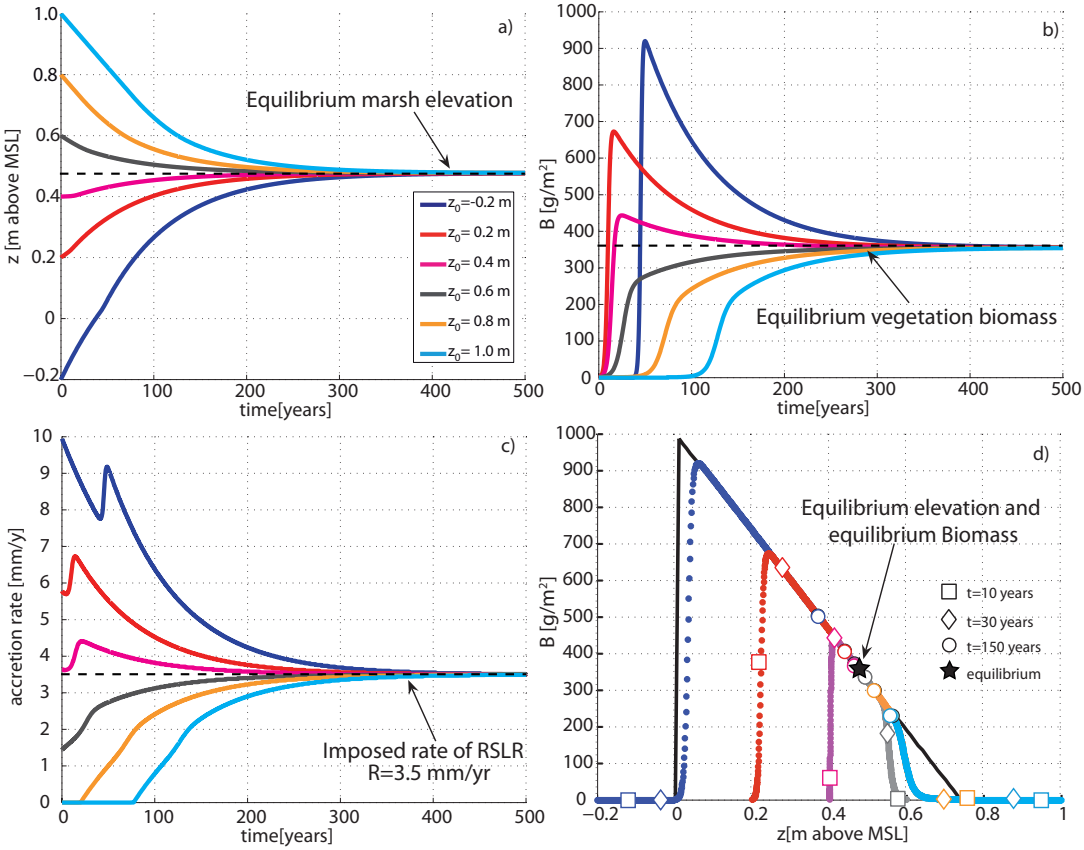

Figure 2.11: Evolution in time of (a) platform elevations, (b) vegetation biomass, (c) accretion rates, and (d) phase portrait describing the dynamics of the system, for different initial conditions. We considered the case of a *Spartina*-dominated system forced with a sinusoidal tide with $T = 12$ hours, $H = 0.75$ m, $C_0 = 20$ mg/l, and $R = 3.5$ mm/yr, when the reproduction is assumed to be constant ($r = 1.0$ yr^{-1}) and the mortality rate increases with marsh elevation (i.e. $m(z) = z/H$ yr^{-1}). In all panels the depicted stable state correspond to a vegetated marsh with $z = 0.48$ m above MSL and $B = 350$ g/m^2.

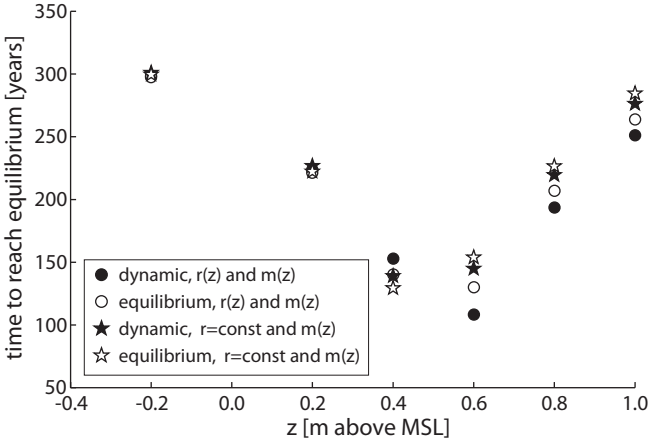

Figure 2.12: Time required for marsh elevations to reach within 3% of the equilibrium elevation starting from different initial conditions, with the "dynamic vegetation" model (i.e. by solving equations (2.1) and (2.2)) and with the "equilibrium vegetation" model (e.g. based on eq. (2.11)) when the birth and the mortality rates are assumed to vary with elevation (as in figure 2.10) and when the birth rate is constant and the mortality rate increases with elevation (as in figure 2.11).

response of tidal bio-geomorphic systems to anthropogenic and natural forcings.

iii) As the tidal amplitude increases, the intensity of erosion processes on the subtidal platform decreases and the elevation of the marsh platform, relative to the tidal frame, increases. Bottom erosion due to the effects of wind waves is more intense in microtidal settings than in meso- and macrotidal environments. Marsh resilience to environmental changes, and in particular to increasing rates of RSLR, increases with the tidal range. Marshes in macrotidal areas are therefore characterized by higher thresholds rates of RSLR resulting in marsh drowning.

iv) The existence and characteristics of equilibrium states depend quite strongly on the local tidal regime even within the same tidal system. In particular, the tide observed at different sites within the Venice lagoon, which differ as a result of propagation and dissipation of the tidal wave, yield

rather different equilibrium elevations. This circumstance also points to the importance of the meteorological contribution to tidal levels, which significantly alters the characters of the local tide, with important biogeomorphic implications.

v) In the sub-tidal range the effect of tidal fluctuations is linked to the fact that more frequent high tidal levels increase the platform elevation at which erosion by wind-waves is maximum. Consequently, the equilibrium elevation at which erosion, deposition and sea level rise are in balance is also correspondingly increased;

   The effect of tidal fluctuations in the intertidal zone are entirely due to a more effective transport of sediment at high elevations when tidal oscillations are increased. A broader probability distribution of tidal levels thus produces higher marsh elevation values;

vi) The local wind regime very importantly affects the elevation of the sub-tidal equilibrium state. Sub-tidal equilibria resulting from wind observations at sites separated by a few kilometers show, in fact, important elevation differences.

vii) Vegetation dissipates wind-waves, such that marsh equilibria are not affected by differences in wind regimes.

Chapter 3

Bio-morphological 1D model

In this Chapter we describe the 1D model developed to investigate the role of the inorganic and organic accretion rates which shape the tidal shaping the tidal landforms and develop of tidal patterns. As we did for the 0–D model, here we present the two main parts according to which the model is developed: the morphological/hydrodynamical and the biological part.

3.1 Deposition fluxes and climate change

The 1D biomorphodynamic model couples geomorphic dynamics and species competition in a spatially extended setting. The model describes the long-term biogeomorphic coupled evolution of sedimentation and vegetation patterns along a salt-marsh transect, oriented in a direction perpendicular to the nearest channel adjacent to the marsh platform (see figure 3.1).

The evolution in time of marsh topography is governed by the sediment continuity equation which reads

$$\frac{\partial z}{\partial t} = Q_s(x,t) + Q_o(x,t) - R \tag{3.1}$$

where t is time; $z(x,t)$ is the local bottom elevation (computed with respect to mean sea level, hereinafter MSL); x is the spatial coordinate along the transect; $Q_s(x,t)$ is the local annually-averaged inorganic sediment deposition

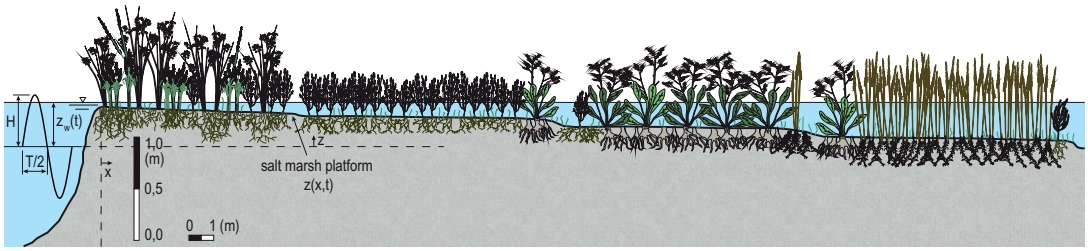

Figure 3.1: Sketch of the salt-marsh transect considered in the proposed 1-D model. The landscape-forming tide is assumed to be a sinusoidal tide with period $T = 12$ hours and amplitude $H = 0.5$ m. Bottom elevations, $z(x,t)$, and water surface fluctuations, $z_w(t)$, are computed with respect to the local mean sea level (MSL). The sketch, which portrays the biogeomorphic patterns of actual marshes, emphasizes the existence of intertwined vegetation and topographic patterns in which vegetation patches are shown to develop at different marsh elevations. Although salt marshes are commonly thought to as flat structures, field observations show the existence of small elevation differences associated to the encroachment of different vegetation types.

rate; $Q_o(x,t)$ the local annually-averaged organic accretion rate; and R is the rate of relative sea level rise (hereinafter RSLR), i.e., sea level variation plus local subsidence. We neglect particle capture on plant stems and leaves, consistently with recent findings of Marani *et al.* (2010) and Mudd *et al.* (2010) who showed that particle settling largely dominates capture for flow velocities commonly observed in tidal marshes (up to 0.05 m s^{-1}). We also neglect the erosion flux because neither tidal currents nor wind-waves usually produce bottom shear stresses high enough to erode the vegetated marsh bottom, mainly due to the presence of halophytes which both damp waves (Möller *et al.*, 1999; Augustin *et al.*, 2009; Carniello *et al.*, 2005) and protect the surface against erosion by currents (Christiansen *et al.*, 2001; Neumeier and Ciavola, 2004). It is worth noting that because temporal variations in the bottom profile occur over timescales typical of morphological changes, i.e. timescales of one to several years, equation (3.1) need be regarded as the annually-averaged mass balance equation, consistently with the presence of yearly-averaged sediment fluxes, Q_s and Q_o, in the right-hand side of equation (3.1). The latter fluxes are obtained

by averaging over a tidal cycle and by multiplying by the number of tidal cycles in one year.

In equation (3.1), at any time during the evolution, the local inorganic sediment deposition rate, $Q_s(x,t)$, is computed as

$$Q_s(x,t) = \frac{w_s}{\rho_b}\frac{n_T}{T}\int_T C(x,t)dt \tag{3.2}$$

where $C(x,t)$ is the local instantaneous suspended sediment concentration (hereinafter, SSC) within the water column; T is the tidal period, over which the averaging is performed ($T = 12$ hours); n_T is the number of tidal periods in a year; $w_s = 0.2$ mm/s is the settling velocity (estimated on the basis of a typical sediment size of 20 μm (Gibbs, 1985)); $\rho_b = \rho_s \cdot (1-\lambda)$ is the bulk density, with $\rho_s = 2650$ kg/m^3 and porosity $\lambda = 0.5$. Equation (3.2) shows that the local inorganic sediment deposition rate, $Q_s(x,t)$, can be determined only once the local, instantaneous SSC, $C(x,t)$, is know everywhere along the transect. To this end we consider the following advection-dispersion equation along the transect (which is solved at short time scales, i.e. one single tidal cycle)

$$\frac{\partial(yC)}{\partial t} + \frac{\partial}{\partial x}\left(uCy - k_d y\frac{\partial C}{\partial x}\right) = -w_s C \tag{3.3}$$

where $y(x,t) = z_w(t) - z(x,t)$ is the local instantaneous water depth; $z_w(t)$ is the spatially uniform instantaneous water elevation obtained by assuming a semidiurnal sinusoidal fluctuation of the tidal level (i.e., $z_w(t) = H \cdot sin(2\pi t/T)$, with $H = 0.5$ m typical of microtidal settings); k_d is the dispersion coefficient (assumed here to be 1.5 m^2/s (Elder, 1959)); and $u(x,t)$ is the local instantaneous fluid advective velocity.

The flow field is obtained by considering a quasi-static propagation of tidal levels along the transect and determining the advective velocity, $u(x,t)$, from the continuity equation

$$\frac{\partial y}{\partial t} + \frac{\partial(yu)}{\partial x} = 0 \tag{3.4}$$

Equations (3.3) and (3.4) make it possible to decouple are solved through a finite volume numerical method over a tidal cycle, by setting the following

boundary conditions: $y(0,t) = z_w(t) - z(0,t)$ and $u = 0|_{x=L}$ in equation (3.4); and $\frac{\partial C}{\partial x}\big|_{x=L} = 0$ and $C(0,t) = C_0$ in equation (3.3). It is worth noting that because bottom topography usually evolves on a much longer timescale than the water motion does, the solution of the hydrodynamic field (equation (3.4)) and of sediment transport dynamics (equation (3.3)) during a tidal cycle are decoupled from the morphological evolution (equation (3.1)).

The local organic accretion rate, $Q_o(x,t)$, is assumed to be proportional to the local annually-averaged aboveground biomass, $B_i(x,t) = B_i(z)$, of the vegetation species i, which colonizes the considered location, x, along the transect:

$$Q_o(x,t) = \gamma B_i(z) \tag{3.5}$$

where $\gamma = 2.5 \cdot 10^{-6}$ m^3/yr/g incorporates both typical vegetation characteristics and the density of the organic soil produced (Marani *et al.*, 2010; Mudd *et al.*, 2009). Such an assumption (i.e. the production of organic matter, Q_o, proportional to the local annually averaged aboveground biomass, $B_i(z)$) is commonly adopted in salt-marsh biomorphodynamic models (Randerson, 1979; Morris *et al.*, 2002; Mudd *et al.*, 2004; D'Alpaos *et al.*, 2006; Kirwan and Murray, 2007; Marani *et al.*, 2007).

The local annually-averaged plant biomass of a given species, $B_i(z)$, may, in turn, be expressed through a *fitness function*, $f_i(z)$, that describes how species i is adapted to different topographic elevations, $z(x,t)$, and to the associated edaphic conditions

$$B_i(z) = B_0 \cdot f_i(z) \tag{3.6}$$

where B_0 is the maximum biomass density of a fully vegetated salt-marsh area. The fitness function, $f_i(z)$, synthetically accounts for the physiological characteristics of each species, because it describes biomass production rate, and the reproductive ability, at different elevations.

Model simulations start with a random distribution of a few species whose fitness functions cover in an approximately homogeneous manner elevations between MSL and mean high water level (hereinafter MHWL=H), and with an initial topographic profile (e.g. linearly decreasing from the channel to the divide,

or horizontal. Different initial profiles have been explored leading to immaterial differences in the eco-geomorphic properties of the final equilibrium configurations).

For a given configuration of elevations and vegetation distribution along the transect, relative to a given stage t_j, the coupled biogeomorphic evolution is performed according to the following rules:

1. At every instant of the tidal cycle, we determine the hydrodynamic field from equation (3.4) and the local SSC, $C(x,t)$. This allows us to compute (from equation (3.3)) the annually-averaged inorganic deposition rate, $Q_s(x,t_j)$, for the current topographic profile (i.e. relative to time t_j);

2. The organic deposition rate, $Q_o(x,t_j)$, is therefore computed along the transect by considering biomass production (related to the *fitness function*) of the species i that occupies the site x at the current stage of evolution, t_j;

3. The topographic profile is therefore updated, on the basis of Exner's equation (3.1), according to the value of $\partial z/\partial t = Q_s(x,t_j) + Q_o(x,t_j) - R$. Everywhere along the transect the new elevation is determined as follows: $z(x,t_j+\Delta t) = z(x,t_j) + \partial z/\partial t(x,t_j)\cdot\Delta t$ (where $\Delta t = 1$ year);

4. Finally the distribution of different vegetation species along the transect is updated, to account for changed edaphic conditions and interspecific competition or mutations. This occurs either through the "fittest-takes-it-all" competition mechanism or the "stochastic competition" mechanism (see Section 3.2.1) or the "mutation" mechanism (see Section 3.2.2).

Steps from 1 to 4 are repeated until no changes in elevation and species distribution along the transect are found.

3.2 Evolutionary vegetation model

We consider in the vegetation model a different number of species that initially randomly colonize the topography. The main physiological characteristics of each species are described by the *fitness function* $f_i(z)$ (Marani *et al.*, 2012). It is commonly observed that the fitness function takes a maximum value at a small range of elevations (characteristic of each plant) and decreases as elevation depart from this optimal range (Morris, 2006, 2007). This *function* describes the biomass productivity depending on the bottom topographic elevation computed with respect the local MSL and the associated edaphic conditions. Many functions were taken into account to describe the different species properties: discrete functions, continuous beta-distributions, continuous bi-exponential distributions, continuous hyperbolic secant functions. Here we focus on the description of the discrete functions (Section 3.2.3) used as an initial modeling of the *fitness function* and secondly a more detailed description of the continuous hyperbolic secant functions (Section 3.2.4), chosen in the model for further analysis.

In the vegetation model we adopt two different evolution mechanisms to self organize the species distribution over the salt marsh. The first one is a spatial mechanism that consists in redistributing the species, following a competition criterion among the "stronger" species (i.e. more adapted to different elevation–conditions) (Section 3.2.1); the second one is a mutation mechanism (Section 3.2.2), according to which new species born from the existing ones and enter in the competition cycle. These two evolution criteria (competition and mutation) are studied in the model both separately and in order to emphasize the role of the two mechanisms and their coupled effect.

3.2.1 Competition mechanism

Changes in the distribution of bottom elevations along the transect are coupled in a two-way fashion to changes in species distribution which occur as a

consequence of inter–specific spatial competition.

The species distributed over the salt marsh may compete with each other, to conquer a small niche in the territory and establish. We account in the model for two different ways in the competition process, i.e. two different possible evolution strategies, namely, "fittest-takes-it-all" and "stochastic competition".

When the "fittest-takes-it-all" competition mechanism is adopted we select, at each site with coordinate x_k, the species i for which $f_i(z_k)$ is maximum; when the "stochastic competition" mechanism is considered, we randomly select, at each site with coordinate x_k, a species with a probability proportional to $f_i(z_k)$:

$$p(i, x_k) = \frac{f_i(z_k)}{\sum_j f_j(z_k)} \tag{3.7}$$

to represent the several stochastic factors influencing the outcome of competition (e.g. local soil properties, microtopography, meteorological conditions, etc.). From year to year natural selection by competition modifies the species colonization.

3.2.2 Mutation mechanism

Mutation is a significant phenomenon in many aspects of life on Earth and is one of the principal means by which evolutionary change takes place. Generally, mutation indicates a response to an outside factor changing.

Mutation, in biology, is a sudden, random change in a gene, or unit of hereditary material, that can alter an inheritable characteristic. New mutations can be deleterious, neutral, or advantageous. Most mutations are not beneficial, since any change in the delicate balance of an organism, having a high level of adaptation to its environment, tends to be disruptive, quickly eliminated. As the environment changes, however, mutations can prove advantageous and thus soon fixed by natural selection and contribute to evolutionary change in the species (Mitchell-Olds and Clauss, 2002).

The mutation may interest the *phenotype* of the species, i.e. the composite of an organism's observable characteristics or traits such as its morphology,

development, biochemical or physiological properties. In this case the mutations may be frequent in time. Many recent studies have reported "rapid evolution" in contemporary populations facing environmental change. We prefer the term "contemporary evolution" in reference to evolutionary changes observable over less than a few hundred years, few hundred generations, heritable trait evolution observed in contemporary time (Stockwell *et al.*, 2003). Such rates can indeed be "rapid" but this assertion is empty without actually quantifying and comparing evolutionary rates.

The mutation may also interest the *genotype* of the species, the inherited instructions within its genetic code; in this case the frequency of mutation is longer because many years are necessary to fix a different genotype character in a species.

In Sections 3.2.3 and 3.2.4 we describe in detail how the evolution evolves according to the different *fitness functions* used; however, the basic concept consists in generating new species, modifying their basic characters.

3.2.3 Discrete fitness function

We discretized the marsh elevation in the tidal frame dividing it into elevation classes. To every elevation discretized value, correspond a *fitness* value. The values randomly span a range from 0 to 1, with the constraint that $\sum_k f_i(z_k) \leq 1$. This constrain is assumed because vegetation species have in general limited own resources and then they have to redistribute them satisfying the more limiting needs.

In figure 3.2 we propose an example of four different discrete *fitness functions*. These *fitness* may be more or less specialized to a narrow range of elevations z and may have a different discretization degree.

As to the "mutation process", how does it occur? Fixed the frequency of mutation (every year, every 50, 100 years as example), we randomly choose a site of the 1D marsh transect and randomly change a character of the "mother" *fitness function*, generating a daughter species. Only if the general condition, i.e.

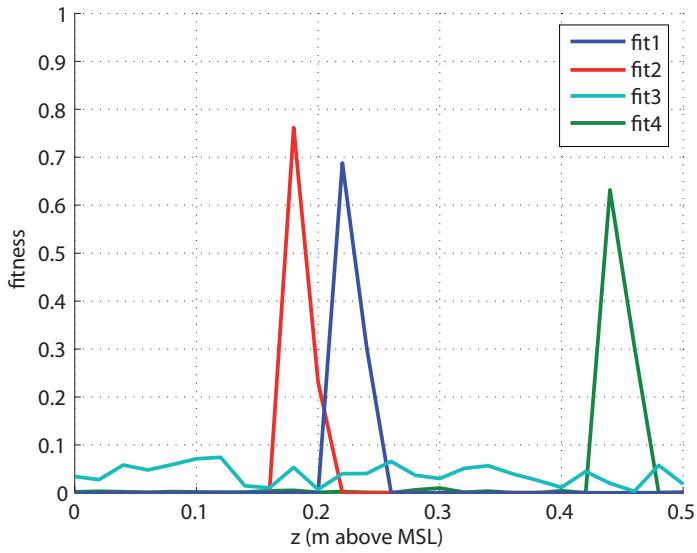

Figure 3.2: Representative discrete *fitness functions*

$\sum_k f_i(z_k) \leq 1$, the mutation, and accordingly the "daughter" species, is accepted entering in the competition spatial process, otherwise, another random changes are necessary to satisfy the constrain.

The use of the discrete function turned out to be unsuitable to exhaustively describe the species characters; being discrete, the functions have proven to be influenced by the discretization step. They are used in the initial model analysis and later replaced with the continuous functions. Some of the results show in fact that the number of species covering the salt marsh was influenced by the discretization step, and also they are not as flexible as the continuous functions. Despite of these observations, the discrete description is useful to begin to interpret the initial model response.

3.2.4 Continuous fitness function

We finally adopt in the model the following analytical general expression for the *fitness function* of the generic species i:

$$f_i(\zeta) = \frac{2}{exp(\lambda_R(\zeta - \zeta_{i0})) + exp(-\lambda_L(\zeta - \zeta_{i0}))} \tag{3.8}$$

where $\zeta = z/H$, $\zeta_{i0} = z_{i0}/H$ is the adimensional elevation where the function

is equal to one, and λ is the scale parameter, expressing the rate at which the fitness function tends to zero (left and right) away from its maximum. A prefactor $P = (f_i(\zeta_{iM}))^{-1}$ allows to impose that $f_i(\zeta_{iM}) = 1$. $\zeta_{iM} = \zeta_{i0} + ln(\lambda_L/\lambda_R)/(\lambda_L + \lambda_R)$ corresponds to the adimensional elevation where the *the fitness function* assumes the maximum value. If the *fitness function* is symmetric, $\lambda_L = \lambda_R$, $\zeta_{iM} = \zeta_{i0}$ and the prefactor P is not necessary because geometrically the maximum is equal to one.

In this Thesis we assume the symmetric condition, but also other configurations may be used.

Therefore, the *fitness function* expression becomes:

$$f_i(\zeta) = \frac{2}{exp(\lambda_i(\zeta - \zeta_{i0})) + exp(-\lambda_i(\zeta - \zeta_{i0}))} \tag{3.9}$$

Equation (3.9) is a flexible function to describe the different species properties (Morris, 2006) but other expressions were studied (e.g. beta continuous functions, bi-exponential continuous functions) leading to very similar results.

When the scale parameter is large, the considered species is very specialized, and therefore it is very fit in a narrow range of elevations. On the contrary, when the scale parameter is small, the species is not specialized and it may be well adapted over a large range of elevations.

We may also consider a prefactor C which multiply equation (3.9) accounting that a species can or not produce the maximum biomass per unit area. $0 < C < 1$, if $C = 0$ then there is no biomass productivity, if $C = 1$ then the species produce the maximum areal biomass.

In figure 3.3 there are some representation of generic *fitness functions*, symmetric or not, with unitary maximum or not, with different modes.

Looking to the "mutation process", and considering the continuous *fitness*, the mutation dynamics are a little different, but basically the main concept is the same. The possible way of mutations improve, because of the increasing in the number of the parameters describing the continuous functions, and could be

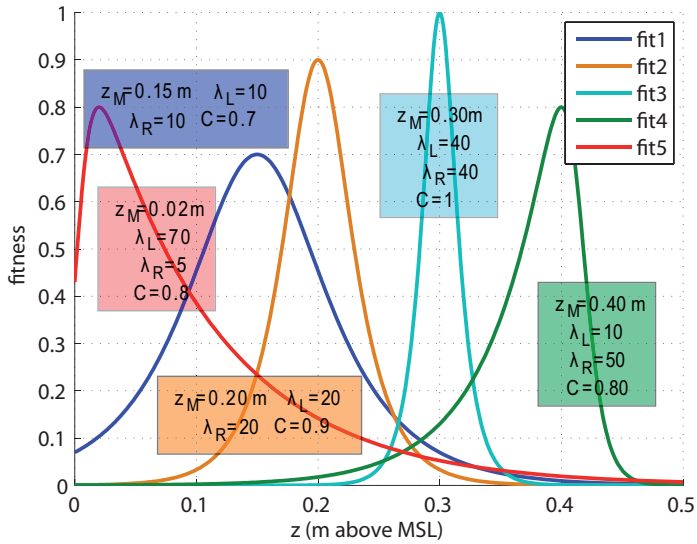

Figure 3.3: Representative continuous hyperbolic secant *fitness functions*. λ is the scale parameter (left or right), C is an optional prefactor from 0 to 1, to impose the maximum less or equal to one, index of the maximum possible areal biomass productivity, z_M is the function mode.

one of the following or a combination of these:

i) We may change just the mode of the function: in this sense, the fitness shape remains the same during the process of mutation but the new species generated is well adapted to a different range of elevation, keeping the same shape of the mother species which generates it.

ii) Another way of mutation consists in a random changing of the maximum possible areal biomass productivity (i.e. changing the parameter C);

iii) Random changing of the *asymmetry* of the function (not shown here) defined as $A = (\lambda_L - \lambda_R)/(\lambda_L + \lambda_R)$.

iv) Random changing of the *variation* of the function defined as $V = 1/\lambda_R + 1/\lambda_L$ and in the case of symmetric function it becomes $V = 2/\lambda$. Changing the *variation* we may assume that the "daughter" species is more or less flat than the "mother", i.e. more or less specialized.

In figure 3.4 we show some schematic representation of different ways of speciation, the most frequent adopted in our analysis.

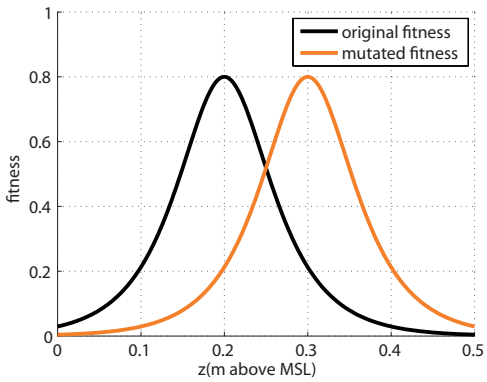

(a) Schematic species mutation: elevation mode changing

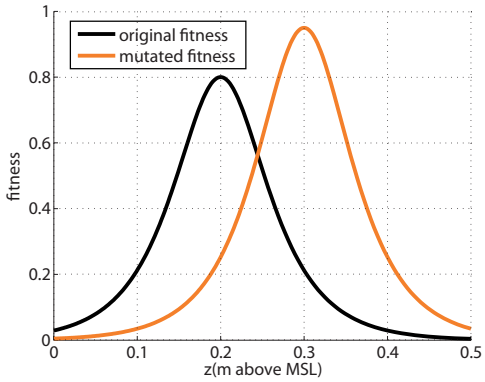

(b) Schematic species mutation: elevation mode and prefactor C changing

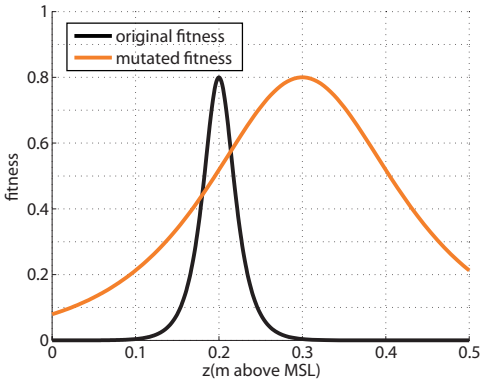

(c) Schematic species mutation: elevation mode and variation V changing

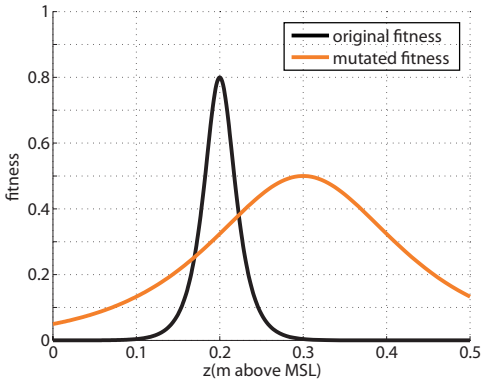

(d) Schematic species mutation: elevation mode, variation V and prefactor C changing

Figure 3.4: Schematic species mutations of the continuous *fitness function* describing the species characteristic.

Chapter 4

1–D: marsh–scale biogeomophic patterns formation

It is now interesting to explore the mechanisms that lead to the formation of well–known smaller scale patterns associated with marsh vegetation species distributions. We find here that zonation is, in fact, a biogeomophological pattern, rather than simply a biological one, and that it is the visible symptom of the underlying feedbacks between biomass productivity and soil accretion. In the first Section we present the emerging patterns using an initial discrete approach in the biological description, in the following Sections we describe how different species, adapted to different edaphic conditions, competing among them, lead to a set of almost discrete equilibria. Thus, we analyze the robustness of marsh–scale biogeomorphic features to changes in forcings, with implications for marsh ecosystem resilience to anthropogenic pressures. Finally we explore a series of analyzes that couple mutations to spatial competitions in the species evolution dynamic.

4.1 Discrete fitness functions: analysis

In this Section we present some observations using a discrete description of the fitness plant functions. We consider an initial case in which we assume

a fixed linearly decreasing salt marsh topography: $z = 0.40$ m in $x = 0$ and $z = 0.30$ m in $x = L = 40$ m. We assume an elevation discretization of 0.02 m in the range 0-0.50 m above MSL which is the semi-tidal sinusoidal amplitude. Starting from three randomly distributed and randomly generated species, we allow two evolving mechanisms: the first one is the yearly spatial selection and the second one is the yearly mutation mechanism.

The yearly spatial selection allows to redistribute the species following the "fittest-takes-it-all" formulation; the mutation mechanism, instead, allows a randomly speciation of a single species every year, changing one of the fitness function character. The constraints adopted are that $f_i(z_k) \leq 1$ and $\sum_k f_i(z_k) \leq 1$, indicating as i the different species, as k the different spatial sites and as z the different elevations of each k site.

In figures 4.1 and 4.2 we show three time steps of the evolving fitness functions and the spatial distribution of species over the constant linearly decreasing topography (figure 4.1) or over an exponential linearly decreasing topography (figure 4.2). The transect in figure 4.1 has a less steep topography than the one in figure 4.2, especially next to the channel (left of the transect). Over time, if the spatial gradient is small (i.e. small dz/dt), there is no an incentive for the species to produce a lot of biomass at a large range of elevations; on the other hand, looking to figure 4.2, where the spatial gradient is bigger (i.e. big dz/dt), there the species, adapted to large ranges of elevations, are promoted. Their fitness functions, in fact, are more flatt (i.e. less specialized to specific elevations) than the fitness functions shown in figure 4.1. If hypothetically, we consider a topography almost flat, we will observed few species very specialized. Over time, all the species tend to maximize their own productivity, i.e. tend to increase the maximum value of the fitness: when a new daughter species appears, it will survive only if it is better than the others alive above the transect, otherwise, if less good than others, it is replaced .

We consider now a complete time evolution system (i.e. maximum-fitness

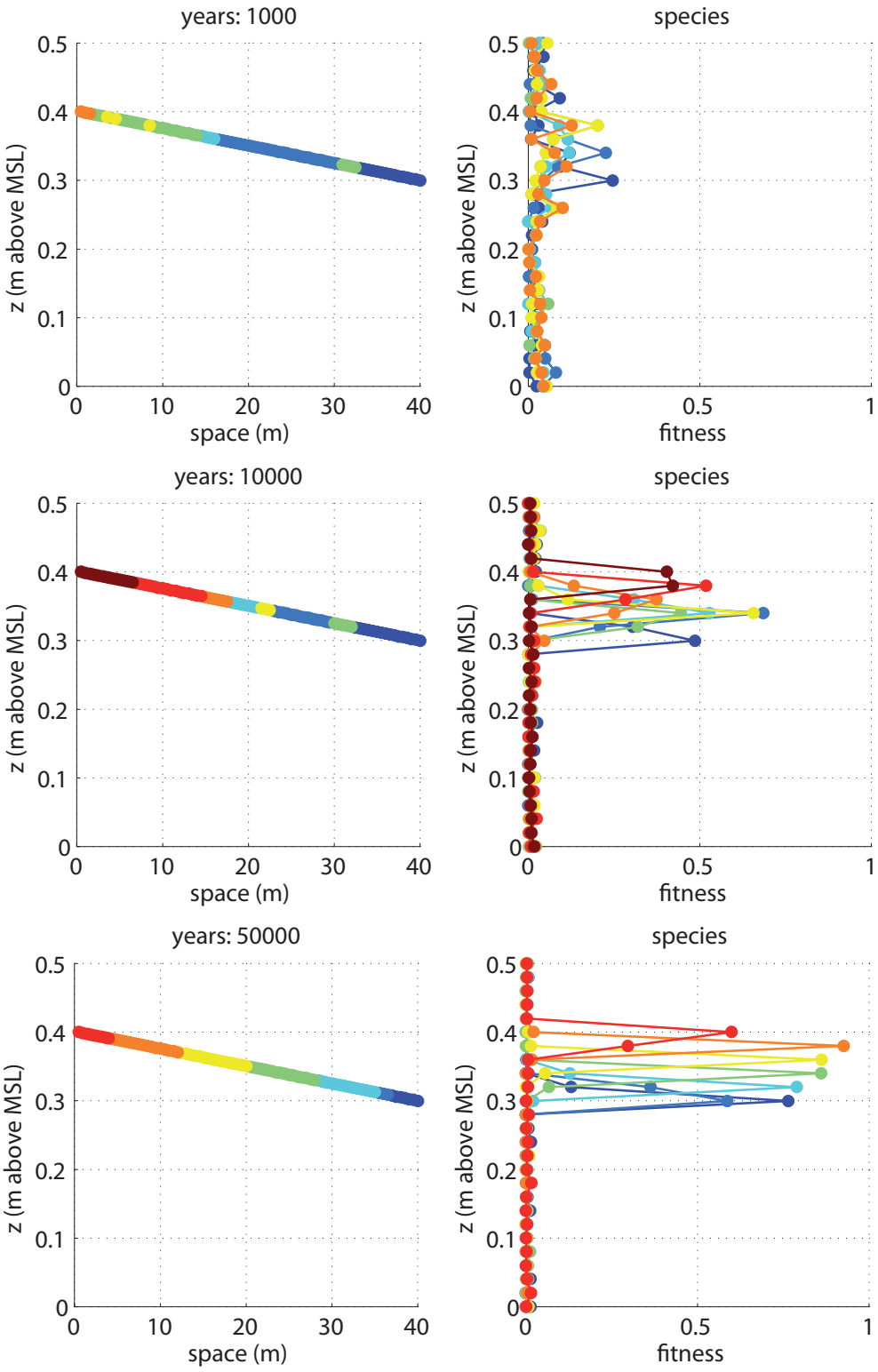

Figure 4.1: Time constant topography linearly decreasing (left) and fitness function representation (right). Each color identifies a different species (red color for species adapted to high elevations, blue color for species adapted to low elevations). Spatial yearly selection mechanism and yearly mutation on.

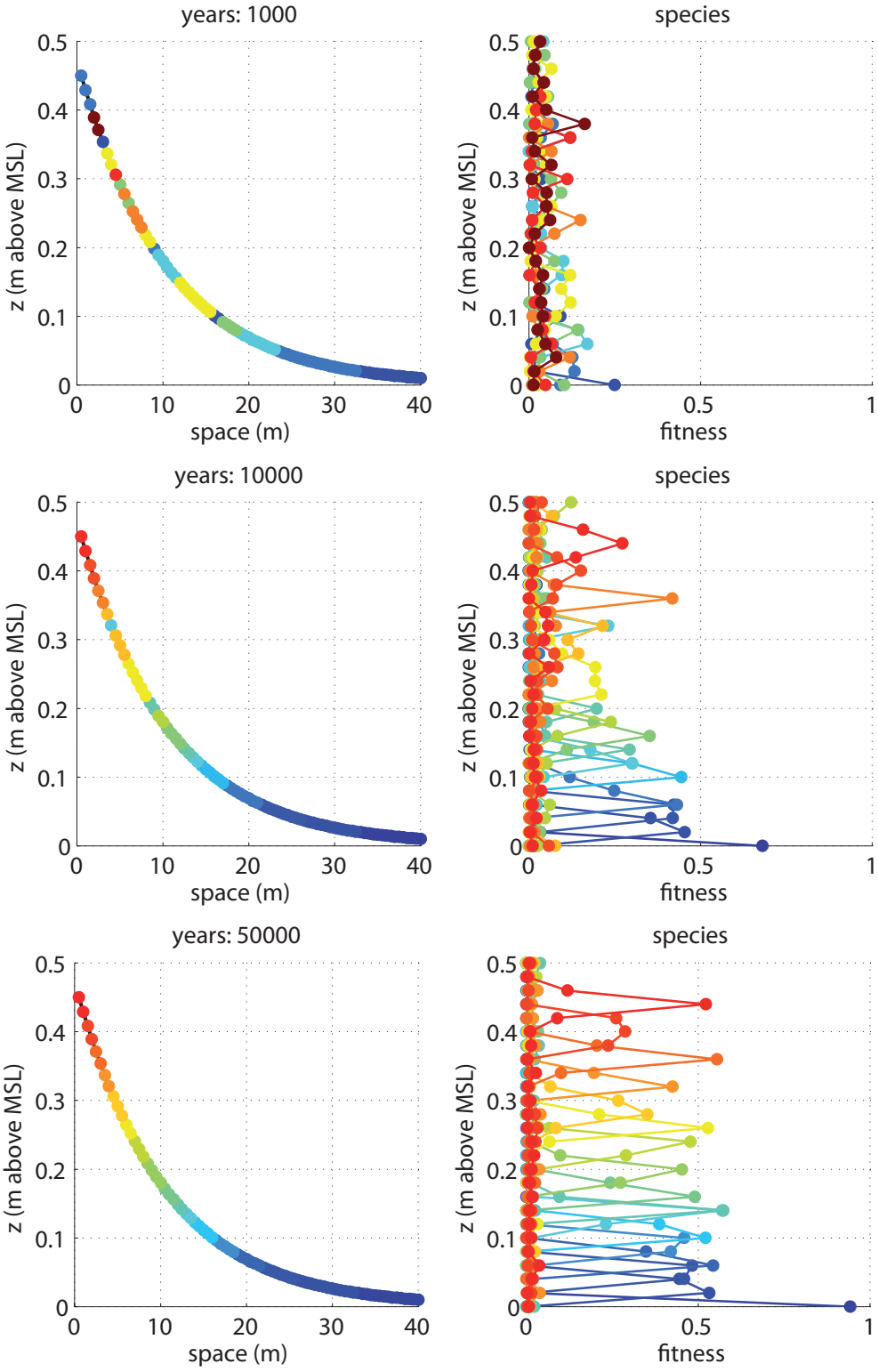

Figure 4.2: Time constant topography exponentially decreasing (left) and fitness function representation (right). Each color identifies a different species (red color for species adapted to high elevations, blue color for species adapted to low elevations). Spatial yearly selection mechanism and yearly mutation on.

colonization mechanism plus mutation mechanism plus topography evolution over time) (figure 4.3). We start from a constant topography and three randomly distributed and generated species. As external conditions we assume a sinusoidal tidal with semi-amplitude $H = 0.50$ m and period $T = 12$ hrs and a sediment suspend concentration (SSC) $C_0 = 40$ mg/l in the channel. Following the spatial competition mechanism and the mutation mechanism, the system is free to evolve with a mutual interaction from the topography condition to the biomass condition and viceversa. Looking to figure 4.3, it is evident the mutual relationship that appears in the bio-morphodynamic system. Entering more deeply in this concept (we will talk more about it, with further details, in Section 4.2), we can say that the topography condition influences the species colonization and redistribution above the transect, but, from the species point of view, they do not passively adapt to the morphology condition, rather, they engineer the topography producing other organic sediment deposition, producing organic soil. The "dynamic" species seem to tune the topography with a sort of an inverse feedback. The final topography in figure 4.3 appears quite flat (series plotted with different scale axes) but some terraces-like structures appear over it. This "terraces" are the result of the engineering species capability. The marsh profile is characterized by mostly tabular areas, colonized by a single vegetation species. This is the first important result, but it is also the starting point to develop other further analysis to explain the vegetation pattern formation.

Also in this case, the constraints adopted for the mutation mechanism are that $f_i(z_k) \leq 1$ and $\sum_k f_i(z_k) \leq 1$, indicating as i the different species, as k the different spatial sites and as z the different elevations of each k site. However, in this case we introduce a new parameter λ to control the fitness slopes. We impose that $\sum_k f_i(z_k) \leq (\lambda \cdot dz)^{-1}$, $dz = 0.02$ m and $\lambda = 50$. Introducing this new parameter, we are able to adjust the species specialization degree. Considering lower values of λ, implicitly we allow the less specialization, i.e. more flat fitness function.

figure 4.4 displays all the fitness shapes colonizing the sites of the transect,

from the species well adapted to the low elevations (blue color), to the species adapted to the high elevations (red color). The species do not maximize the biomass production as we can see looking to the value of the biomass (bottom right of figure 4.4), which reaches 500, 600 g/m^2, fixed the maximum areal biomass productivity equal to 1000 g/m^2.

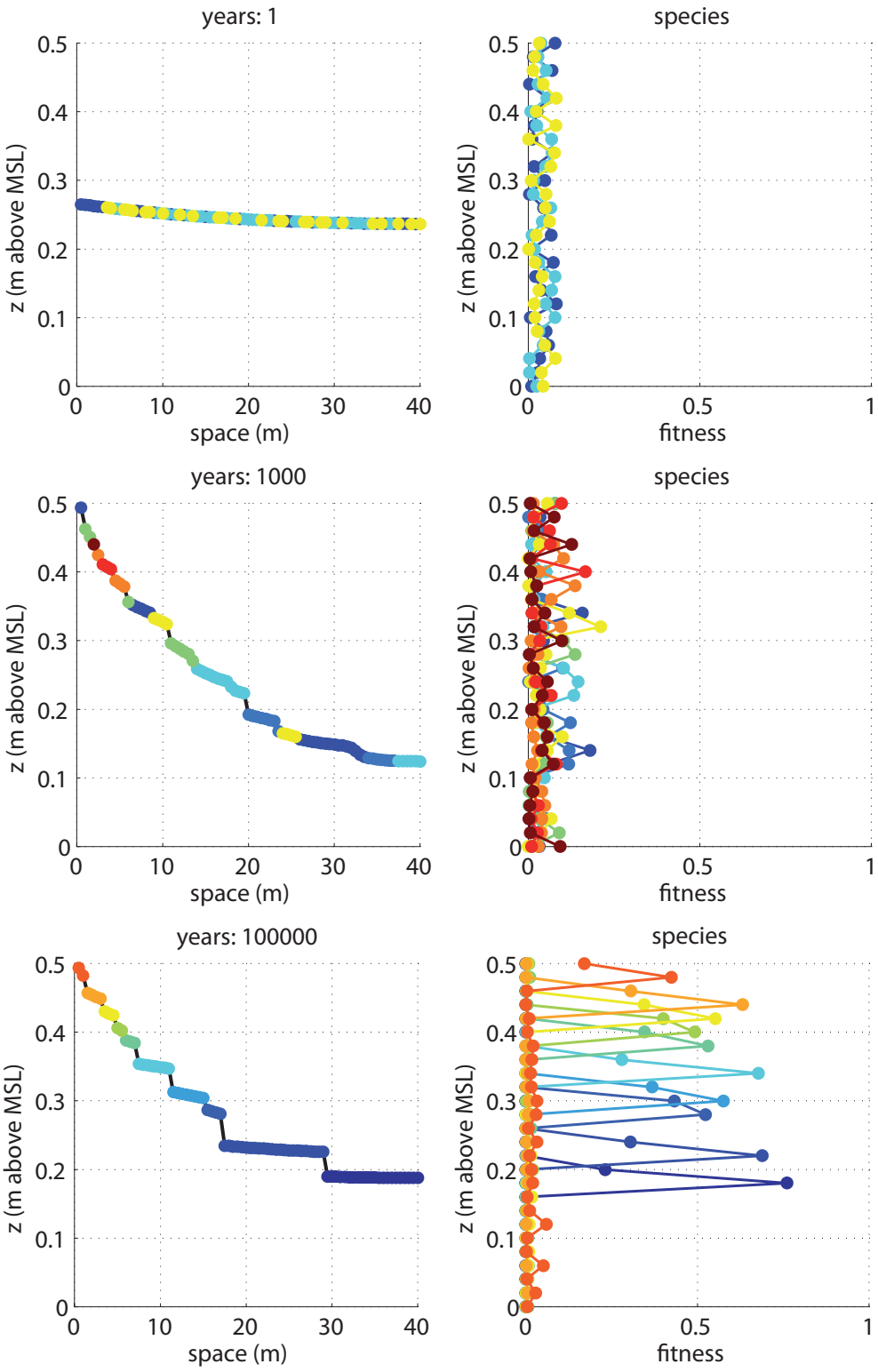

Figure 4.3: Time topography evolution (left) and fitness function representation (right). Starting constant topography condition. Each color identifies a different species (red color for species adapted to high elevations, blue color for species adapted to low elevations). Spatial yearly selection mechanism and yearly mutation on.

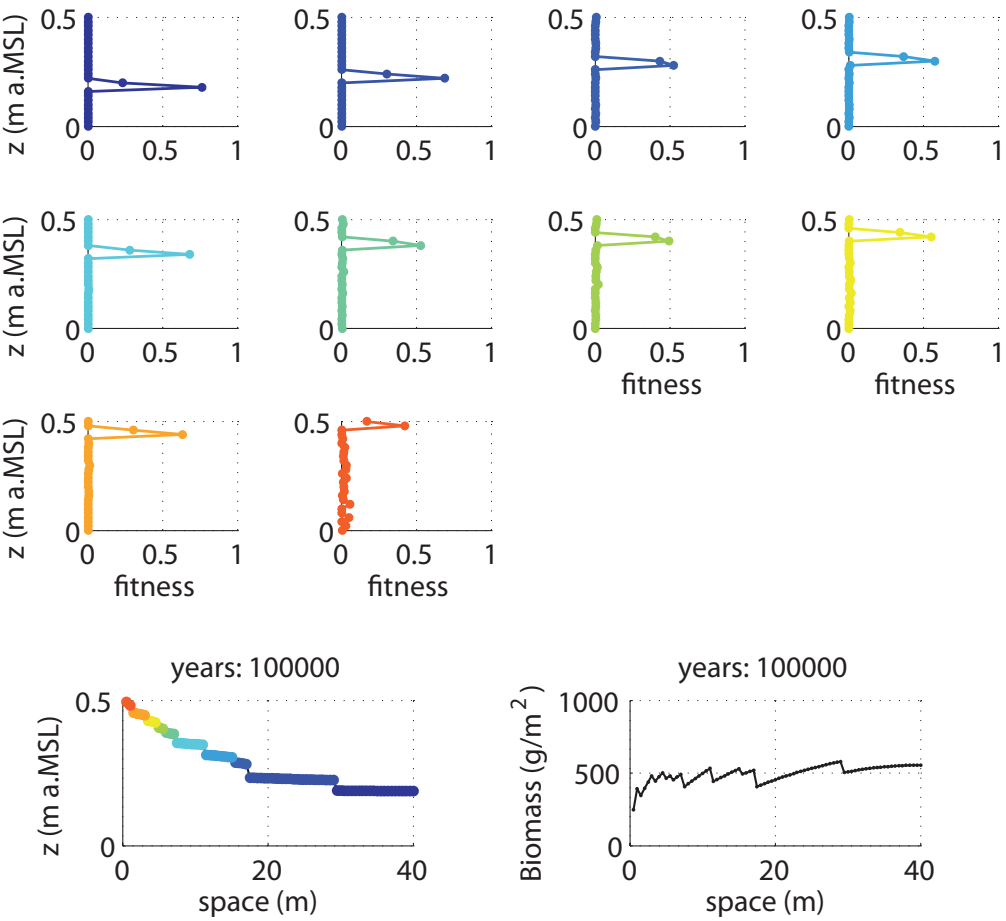

Figure 4.4: Representation of the species fitness shape after one thousand years, from species adapted to the low elevations (blue), to species adapted to high elevations (red). At the bottom of figure there are the transect topography (left) and the biomass production (right).

4.2 Training of zonation: general model behavior

We show here that zonation is, in fact, a biogeomorphological pattern, rather than simply a biological one, and that it is a visible symptom of the underlying feedbacks between biomass productivity and soil accretion (Da Lio *et al.*, 2012).

Following (Marani *et al.*, 2012), we first consider a reference case (figure 4.5*a*) in which the platform is flooded by a tidal oscillation of period $T = 12$ hours and amplitude $H = 0.50$ m, and is forced with a SSC $C_0 = 20$ mg/l and a rate of RSLR $R = 3.5$ mm/yr, the latter condition being representative of the local rate of RSLR for the 20th Century in the Venice Lagoon (Carbognin *et al.*, 2004; Marani *et al.*, 2007). Moreover, in the reference case, we consider continuous fitness functions and the vegetation dynamics along the transect is modelled on the basis of the the maximum-fitness colonization mechanism ("fittest-takes-it-all").

Starting from a configuration characterized by linealy decreasing elevations from the channel towards the end of the transect, the marsh platform evolves displaying, at equilibrium, the emergence of stable states characterized by sharp transitions between neighboring bio-geomorphic terrace-like structures, as shown in figure 4.5*a*. In the final marsh configuration, mostly tabular areas occur which are colonized by a single vegetation species (as emphasized by the red, green, blue colors in figure4.5*a*). These zonation patters are a typical feature of actual salt-marsh landscapes and can be observed in the field although being characterized by small differences in elevation, as we shall discuss in the following.

One then wonders what physical and biological processes are responsible for the development of zonation patterns in salt-marsh landscapes. This can be explained through the joint analysis of bottom elevations along the transect (figure 4.5*a*), total accretion rates ($\partial z/\partial t = Q_s(z) + Q_o(z) - R$) as a function of marsh elevation (figure 4.5*b*), and vegetation *fitness functions* (figure 4.5*c*) which are proportional to vegetation biomass on the basis of eq. (3.6). In the

reference case, we have considered three vegetation species with the same degree of specialization, i.e. the same scale parameter ($\lambda = 5$), but displaying optimal ranges at different elevations ($z = 0.10$ m above MSL for the blue species, $z = 0.25$ m above MSL for the green species, and $z = 0.45$ m above MSL for the red species.

The analysis of figure 4.5, together with the quantitative information provided by the governing equations (3.1 and 3.9), highlights that zonation structures emerge as a result of ecogeomorphic feedbacks involving inorganic deposition and organic accretion (via biomass production), which lead to pairs of stable and unstable equilibrium states. This can be illustrated by considering the middle species in figure 4.5*a* (species $i = 2$, in green) and in particular the lowest site within the patch occupied by this species (with coordinate, say, $\hat{x}_2$), whose equilibrium elevation, $\hat{z}_2 = z(\hat{x}_2)$, corresponds to the condition $\partial z/\partial t = Q_s(\hat{z}_2) + Q_o(\hat{z}_2) - R = 0$. By recalling equations (3.5) and (3.6), it follows that the above equilibrium condition can be rewritten as $f_2(\hat{z}_2) = (R - Q_s(\hat{z}_2))/(\gamma \cdot B_0)$. The latter equation gives two solutions: a stable equilibrium with elevation $z_2^{(s)}$ (above the maximum of $f_2(z)$, solid green circle in figure 4.5*b*,*c*) and an unstable equilibrium with elevation $z_2^{(u)}$ (below the maximum of $f_2(z)$, open green circle). The numerical solutions of the Exner's equation (3.1), carried out for a set of transect configurations obtained by perturbing the elevation at $\hat{x}_2$ within a range of values around $z_2^{(s)}$ (figure 4.5*b*), shows that this is a stable equilibrium. A perturbation which increases the elevation at $\hat{x}_2$ above $z_2^{(s)}$, generates a decrease in biomass production and in the related organic accretion (figure 4.5*c*), together with a decrease in the inorganic deposition rate, Q_s, as a consequence of the increased local velocity. As a consequence, the total accretion rate becomes negative, $\partial z/\partial t < 0$ (figure 4.5*b*), thus leading to a decrease in the elevation and bringing the system back to the original equilibrium. Similarly, a perturbation which decreased the elevation at $\hat{x}_2$ below $z_2^{(s)}$ would induce an increase in the biomass production and in the related organic accretion rate (figure 4.5*c*), as well as an increase in Q_s. The

total accretion rate would therefore become positive, $\partial z/\partial t > 0$ (figure 4.5*b*), thus increasing the elevation at $\hat{x}_2$ and bringing the system back to the stable equilibrium. This analysis can be summarized by noting that $\partial/\partial z(\partial z/\partial t) < 0$ at $z_2^{(s)}$, which defines the condition for a stable equilibrium. Note that the inorganic deposition rate, Q_s, varies along the transect, depending on the local instantaneous SSC (see eq. 3.3), and therefore stable equilibrium elevations at other sites within the same vegetation patch are slightly different from the elevation at $\hat{x}_2$, $z_2^{(s)}$, generating a mildly sloping geomorphic structure.

The second equilibrium solution, $z_2^{(u)}$, is an unstable equilibrium (open green circle in figure 4.5*b*, *c*). Let us, in fact, consider a site with elevation equal to $z_2^{(u)}$. A postive perturbation increasing the elevation of such a site, enhances the organic accretion rate, Q_o (figure 4.5*c*), while reducing inorganic deposition, Q_s, as a cosequence of a higher flow velocity. However, the increase in Q_o outweighs the decrease in Q_s, thereby making $\partial z/\partial t > 0$ (figure 4.5*b*) and driving the elevation of the site away from $z_2^{(u)}$ towards $z_2^{(s)}$. On the contrary, a perturbation which acted to decrease the elevation of the site, would promote a decrease in the organic accretion rate, Q_o, stronger than the increase in the inorganic deposition rate, Q_s, thus making $\partial z/\partial t < 0$ (figure 4.5*b*) and therefore pushing the elevation to even lower values, towards the stable equilibrium, $z_3^{(s)}$, of the vegetation species $i = 3$ (blue solid circle in figure 4.5*b*).

We note that in the case of the "green" species ($i = 2$) (as well as for the lower "blue" species) $\partial Q_s/\partial z << \partial Q_o/\partial z$ and therefore the stability of this equilibrium state is not influenced by variations in Q_s induced by perturbations of z because $\partial/\partial z(\partial z/\partial t) \cong \partial Q_o/\partial z$. In fact, the stability of these equilibria can be established by studying $f_i(z)$ alone (we reacall that $Q_o(z) = \gamma \cdot B_0 \cdot f_i(z)$), the condition $df_i/dz < 0$ denoting a stable equilibrium. This is not the case for the portion of the marsh nearest to the margin (red in figure 4.5*a*, *b*, *c*), where the inorganic deposition rate, Q_s, is very sensitive to changes in the local elevation. We may, in fact, note that the equilibrium state in the upper marsh zone (red in figure 4.5*a*, *b*, *c*) lies on the branch of the fitness function located

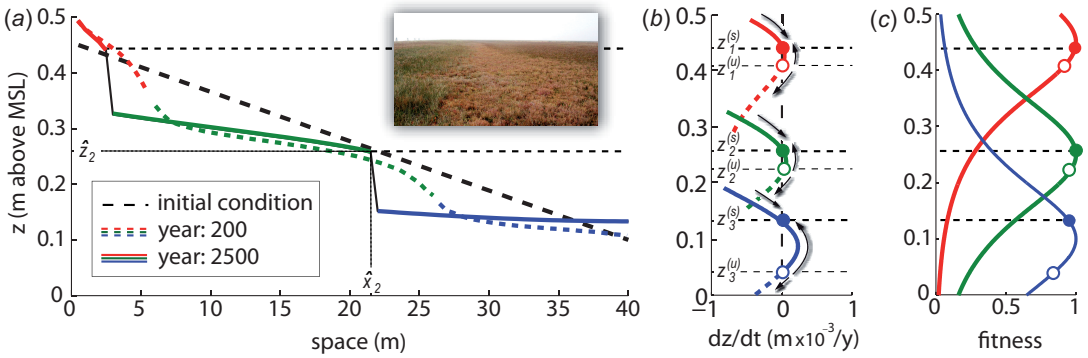

Figure 4.5: Reference case. Zonation patterns generated by the model. (a) The time evolution of transect topography was here started from a linear initial condition but several other initial conditions were explored with analogous results. Monospecific vegetation patches, very similar to observed zonation patterns (see inset), and terrace-like topographic structures emerge as a result of multiple stable states defined by $\partial z/\partial t = 0$ and $\partial/\partial z(\partial z/\partial t) < 0$. (b) Sites with initial elevation comprised between $z_i^{(u)}$ and $z_i^{(s)}$ move towards $z_i^{(s)}$, while sites whose initial elevation is located below $z_i^{(u)}$ move towards $z_j^{(s)}$, j being the species with optimal elevation located immediately below that of species i. (c) Shows the fitness function of the species populating the marsh, which defines the rate of organic soil production as $Q_o = \gamma \cdot B_0 \cdot f_i(z)$ (γ incorporates typical vegetation characteristics and the density of the organic soil produced, B_0 is the biomass density of a fully vegetated marsh).

below the maximum, where $df_i/dz > 0$ (figure 4.5c), seemingly implying an unstable equilibrium. However, because $\partial Q_s/\partial z > \partial Q_o/\partial z$ here, the stability of the equilibrium is controlled by inorganic deposition, which decreases with elevation, determining a value $\partial/\partial z(\partial z/\partial t) < 0$ and indicating an inorganic sediment-controlled stable equilibrium.

In figure 4.6a we represent the accretion rate $dz/dt = Qs(x,t) + Qo(x,t) - R$ along the transect almost equal to 10^{-5}, i.e. the equilibrium elevation state; in figure 4.6b we can see the trend of the respective inorganic flux (continuous line) and organic flux (dashed line). The sum of these two fluxes complement the rate of the relative see level rise. The trends of the two fluxes are specular: in primis we can see that there are three main trends that reflect the three

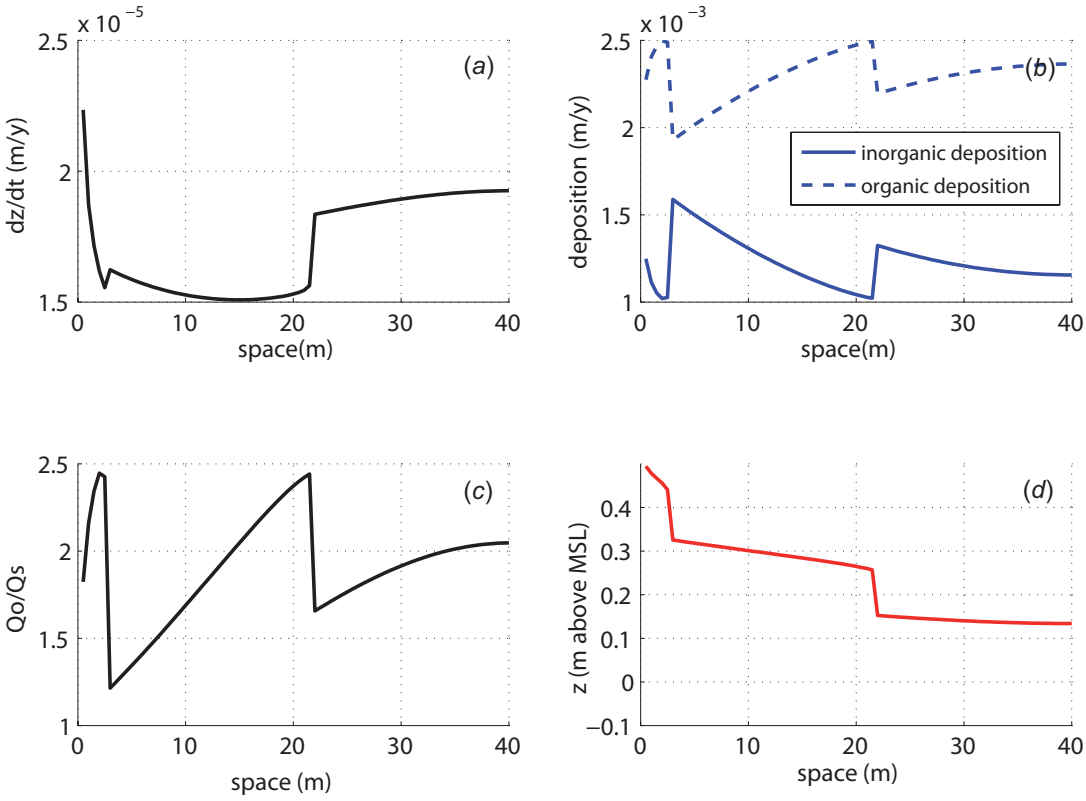

Figure 4.6: Reference case. (a) Accretion rate dz/dt, function of elevation; (b) organic $(Q_o(x,t))$ and inorganic $(Q_s(x,t))$ fluxes along the transect; (c) organic flux compared with the inorganic one; (d) transect equilibrium topography

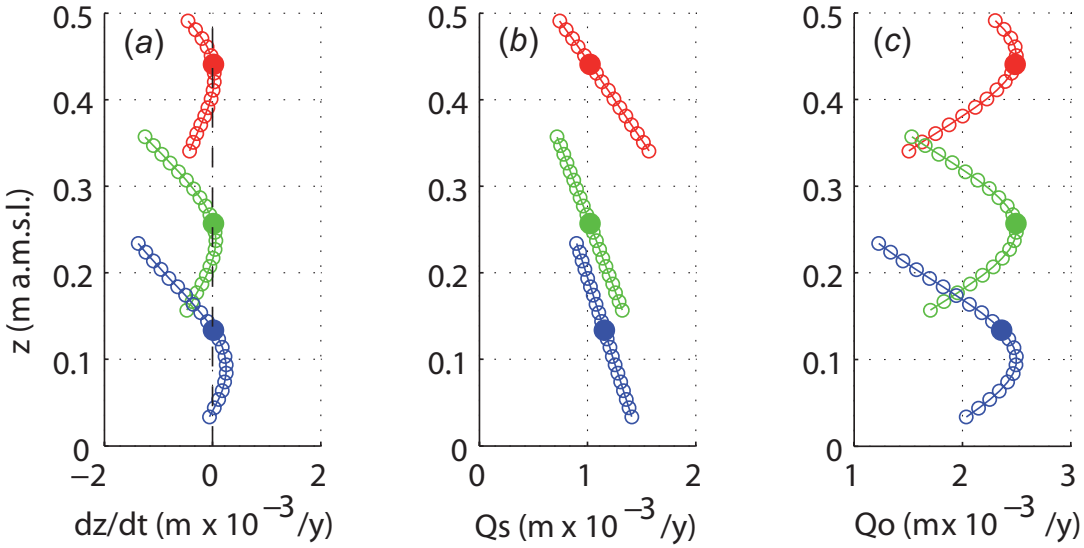

Figure 4.7: Reference case. (a) Accretion rate, function of elevation. Solid circles represent the stable elevation equilibria; (b) Shows the rate of inorganic soil production as Q_s almost linearly decreasing as the elevation increases. Solid circles represent the stable elevation equilibria; (c) Shows the rate of organic soil production as $Q_o = \gamma \cdot B_0 \cdot f_i(z)$ (γ incorporates typical vegetation characteristics and the density of the organic soil produced, B_0 is the biomass density of a fully vegetated marsh, $f_i(z)$ is the fitness function). Solid circles represent the stable elevation equilibria

terraces structures developing over the salt marsh. You can see how each pattern is similar to other: from the channel to the no flux boundary, the inorganic flux decreases because of the moving away from the channel input sediment. Respectively, the organic flux increases over each pattern because each elevation terrace decreases: decreasing in elevation in fact, we tend to the maximum value of the fitness function and thus an increasing of the organic production, reaching the maximum value of $B_o = 1000$ g/m^2 and $Q_o = 2.5$ mm/yr. We can also appreciate the ratio between the organic and the inorganic flux (figure 4.6c), big at the end of the terraces sign that at the end of the terraces the organic flux is predominant among the sediment fluxes. The last subplot (figure 4.6d) represents the elevation topography like in figure 4.5a.

We note that, in all cases, the terrace-like structures lie for the most part above the elevation for which maximum biomass production occurs (see fig-

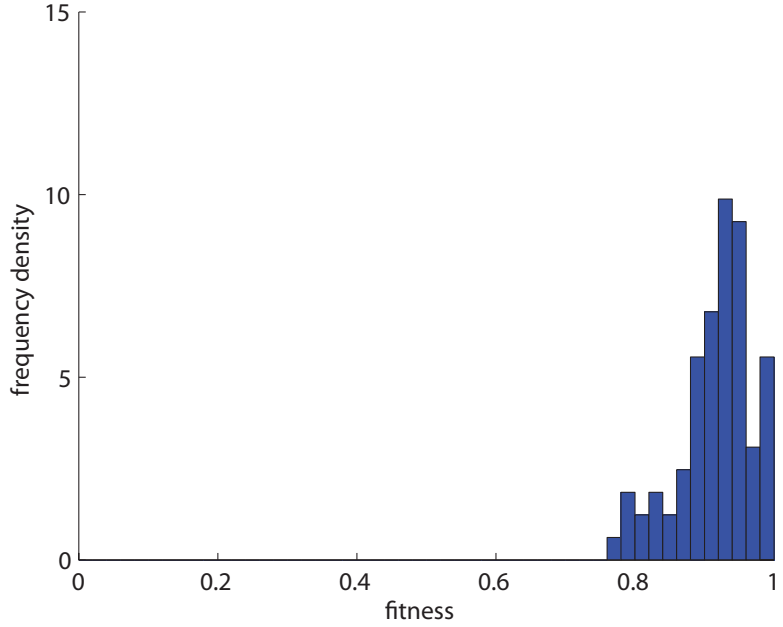

Figure 4.8: Reference case: frequency density of the fitness functions

ure 4.5*c*), suggesting that zonation patterns may be associated with a higher morphological stability at the expense of a reduced productivity. In figure 4.8 we represent the frequency density of the fitness functions showing the sub-optimality (the more frequent values are in the range $0.92 - 0.94$) of the organic production in a stable state morphological condition and in figure 4.9 we show the frequency of each species colored them with the three different colors.

Focusing now on the last node of the transect colonized by the red species, we remember that it is a stable equilibrium, although it is located on the branch of the fitness function below the maximum, where $df_i/dz > 0$ (figure 4.5*c*), seemingly implying an unstable equilibrium. However, because $\partial Q_s/\partial z > \partial Q_o/\partial z$ here, the stability of the equilibrium is controlled by inorganic deposition, which decreases with elevation, determining a value $\partial/\partial z(\partial z/\partial t) < 0$ and indicating an inorganic sediment-controlled stable equilibrium. The analysis presented in figure 4.11 and 4.12 perturb the elevation of this node indicated with a red solid circle; in figure 4.10 there is the reference case, already presented in figure 4.6*b*, highlighting the node subjected to perturbation.

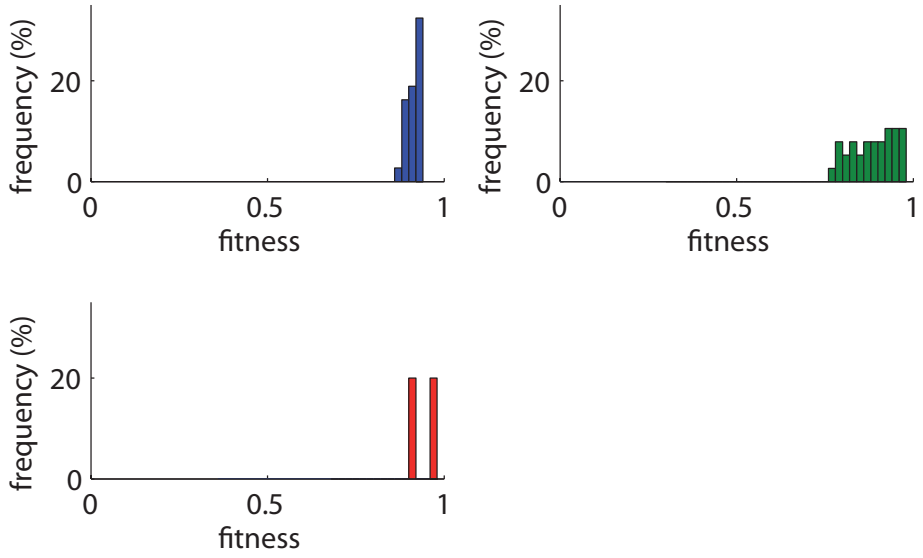

Figure 4.9: Reference case: frequency density of each species ("blue", "green", "red") fitness functions

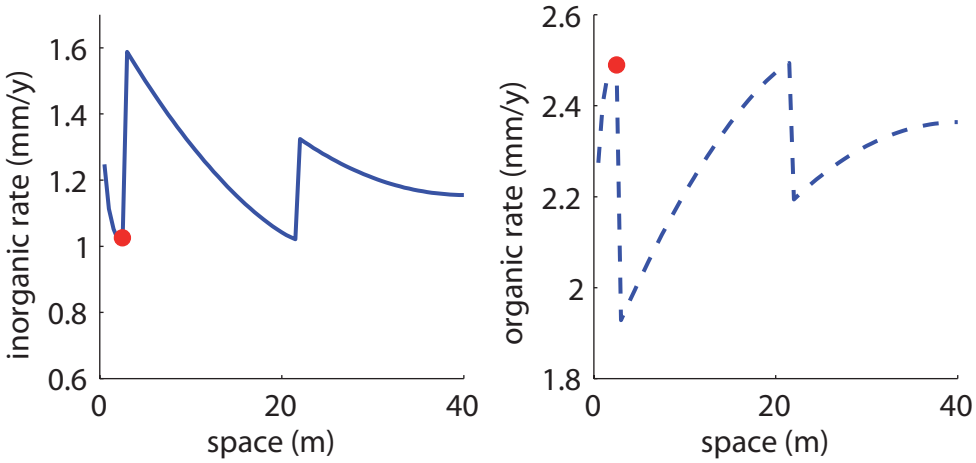

Figure 4.10: Reference case. Inorganic and organic flux (left and right respectively); the red solid circle represents the last site colonized by the red species.

In the perturbation N∘1 we reduce by 5 cm $z = z_{eq} - 0.05 = 0.3907$ m the stable equilibrium elevation of the node#6 ($z_{eq} = 0.4407$ m). Because of this reduction, the inorganic sediment deposition increases from 1.026 mm/y to 1.299 mm/yr (almost +27%) because the increased depth; conversely, the organic deposition decreases from 2.489 mm/yr to 2.117 mm/yr.

In the perturbation N∘2 we increase by 5 cm $z = z_{eq} + 0.05 = 0.4907$ m the stable equilibrium elevation of the node#6 ($z_{eq} = 0.4407$ m). This increase in elevation produces a reduction of the inorganic flux from 1.026 mm/yr to 0.743 mm/yr (almost -38%) and an increase in organic flux from 2.489 mm/yr to 2.306 mm/yr. Looking to the mean sediment suspend concentration (SSC) over a tidal cycle, we can appreciate that there is no an important variation among the three cases analyzed: in the reference case the mean SSC over a tidal cycle is equal to to 0.1536 mg/l, in the case "perturbation N∘1" equal to 0.1545 mg/l and in the last case ("perturbation N∘2") equal to 0.1497 mg/l. The difference among these values is very small, but, despite this fact, the differences in terms of inorganic sediment deposition flux, function of the SSC, are much bigger. In fact, the model is written, requiring that at the end of a tidal cycle, all the suspended sediment present, is instantly deposited at the bottom of salt marsh according to $Q_s(x,t) = h(x,t) \cdot C(x,t)$, where $h(x,t)$ is the instant depth, because the water basin becomes empty during the reflux tidal phase. As the depth increases, the inorganic sediment deposition flux increases too, as we can read in Table 4.1 referring to the last tidal instant; the inorganic deposition over a tidal cycle is almost the same in the three cases (see Table 4.1, tidal cycle*). figure 4.13 displays the mean SSC over a tidal cycle in the three different configurations taken into account obviously decreasing by the continuous sediment charging of the channel.

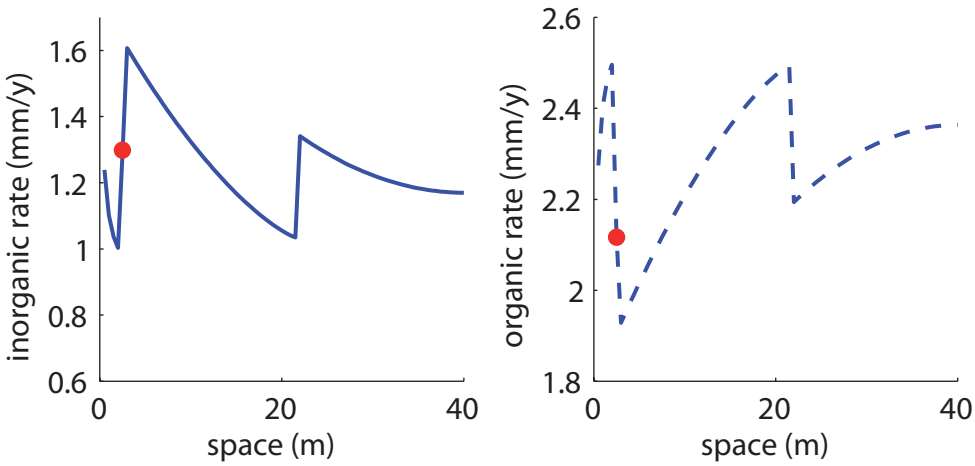

Figure 4.11: Perturbation N◦1. Inorganic and organic flux (left and right respectively); the red solid circle represents the last site colonized by the red species in the case in which we perturb the site equilibrium elevation z_{eq} from the equilibrium state $z = z_{eq} - 0.05$m decreasing the equilibrium elevation

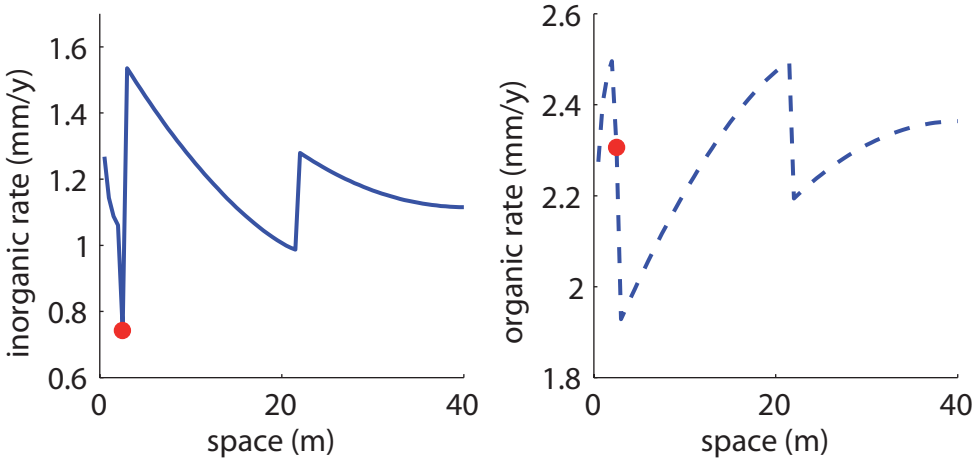

Figure 4.12: Perturbation N◦2. Inorganic and organic flux (left and right respectively); the red solid circle represents the last site colonized by the red species in the case in which we perturb the site equilibrium elevation z_{eq} from the equilibrium state $z = z_{eq} + 0.05$m increasing the equilibrium elevation

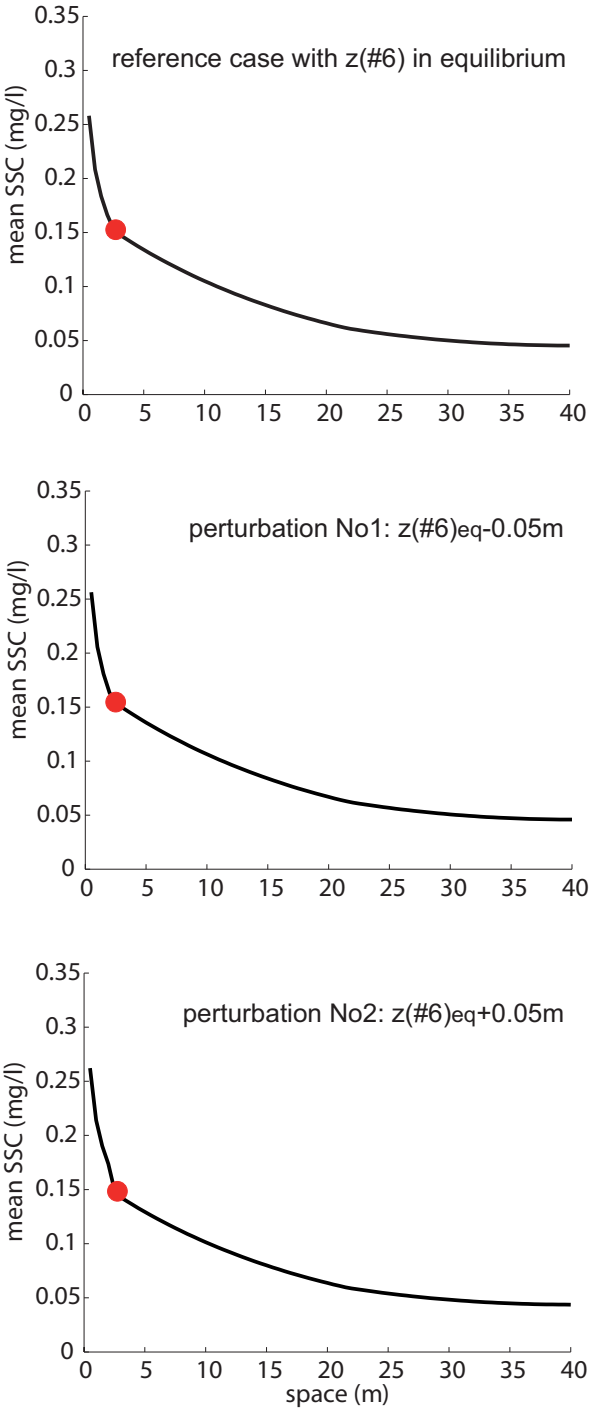

Figure 4.13: Mean suspend sediment concentration over a tidal cycle in three different elevation topography configuration. In red solid circle we indicate the site#6 of the salt marsh transect, subjected to perturbation

Table 4.1: Inorganic deposition, organic deposition and mean SSC in three different elevation topography configurations. We perturb the elevation of a site of the salt marsh transect to see the effect on the deposition fluxes

	Q_s(#6)(mm/yr)	Q_o(#6)(mm/yr)	mean SSC(#6)(mg/l)
	1.026	2.489	0.1536
z_{eq}	0.718 tidal cycle*		
	0.308 last ist.		
	1.299	2.117	0.1545
$z_{eq} - 0.05m$	0.722 tidal cycle*		
	0.577 last ist.		
	0.743	2.306	0.1497
$z_{eq} + 0.05m$	0.700 tidal cycle*		
	0.043 last ist.		

* total inorganic deposition during all the instants of the tidal cycle except the last time instant when the first salt mash node is uncovered by the water

4.3 The role of the rate of RSLR

We now analyse the bio-geomorphic patterns emerging when the marsh is subjected to the same forcing considered in the reference case and to increasing rates of RSLR, namely $R = 5$ mm/yr and $R = 7$ mm/yr. In the case of $R = 5$ mm/yr, the bio-geomorphic features of the equilibrium patterns are qualitatively similar to those of the reference case, although some differences emerge (figure 4.14*a*). The comparison of the two equilibrium profiles shows that as the rate of RSLR increases, the equilibrium marsh elevations tend to decrease, in agreement with the results of other modelling approaches (Kirwan *et al.*, 2010; Marani *et al.*, 2007; Morris *et al.*, 2002; D'Alpaos *et al.*, 2011a,b). It should be noted that, under increased RSLR conditions, the equilibria of the two highest geomorphic structures (red and green in figure 4.14*a*) lie on the branch of the fitness functions where $df_i/dz > 0$ and hence $dQ_o/dz > 0$, very close to the maximum value (figure 4.14*c*). Because $\partial(\partial z/\partial t)/\partial z < 0$ (figure 4.14*b*), this suggests that the stability of the equilibria are here governed by the inorganic deposition flux, i.e. $\partial Q_s/\partial z > \partial Q_o/\partial z$. On the contrary, the equilibrium elevation in the lowest patch belongs to the branch of the fitness curve where $dQ_o/dz < 0$ (figure 4.14*c*), and is therefore governed by the organic flux, as in the reference case (i.e., $\partial Q_o/\partial z > \partial Q_s/\partial z$). Interestingly, the general lowering of the equilibrium elevations induced by an increased rate of RSLR causes a sort of cascade effect, in which areas that, for a lower value of R, belonged to higher elevation structures now abruptly transitioned to lower equilibrium states. As a result, the area colonized by the species adapted to the lowest elevations is larger under increased R, with a corresponding reduction in the area of the higher vegetation patches. A further increase in the rate of RSLR, however, may drastically change marsh patterns, due to the lowest sites in the lowest patch becoming unstable and switching abruptly to a lower yet (unvegetated) equilibrium state (figure 4.14*d*, *e*, *f*).

Figures 4.15 and 4.16 show the deposition fluxes according to RSLR=5 mm/yr and RSLR=7 mm/yr respectively. In according to the previous re-

sults, when the topography is lower than the MSL, i.e. there is a transition from the salt marsh to tidal flat equilibria, the organic deposition is absent (see figure 4.16) and the inorganic deposition balances the rate of the RSLR. When RSLR=5 mm/yr is considered, the inorganic deposition is greater than the organic toward all the transect, different from the equilibrium–fluxes configuration observed in the reference case (see figure 4.6*b*). This is due to the lower (on average) bottom elevations toward the transect. In fact, the inorganic flux $Q_s(z)$ is founded (through numerical simulation) to be a monotonically decreasing function of z: as z increases, the amount of the "precipitable" suspended sediment $C \cdot D = C \cdot (h - z)$ decreases, decreasing the flux of inorganic sediment deposited during a tidal cycle (remember that C is the SSC, D is the water depth and h is the instantaneous tidal water free surface).

4.4 The role of the sediment supply

We then analyzed the role of sediment supply in dictating the emerging biogeomorphic patterns. When the SSC is reduced, compared to the reference case, to $C_0 = 5$ mg/l (figure 4.17*a*, *b*, *c*) we observe that only the portion of the transect closest to the channel (distance $<$ 10m) is able to keep pace with the imposed rate of RSLR (3.5 mm/yrr in this case). On the contrary, because a decrease in the available SSC leads to a decrease in the settling rate across the transect, portions of the platform farthest from the channel progressively drown below MSL reaching a subtidal equilibrium at elevations lower than MLWL. The reduction in the SSC from $C_0 = 20$ mg/l to $C_o = 5$ mg/l has stronger effects on marsh topography than the increase in the rate of RSLR from $R = 3.5$ mm/yr to $R = 7$ mm/yr (see figures 4.14*d*, *e*, *f*) and therefore the equilibrium configuration is reached at elevations lower than MLWL, where the increased settling rate can balance the imposed rate of RSLR. The first portion of the transect is able to keep pace with the imposed rate of RSLR and displays the formation of vegetation patches which are colonized by single vegetation species

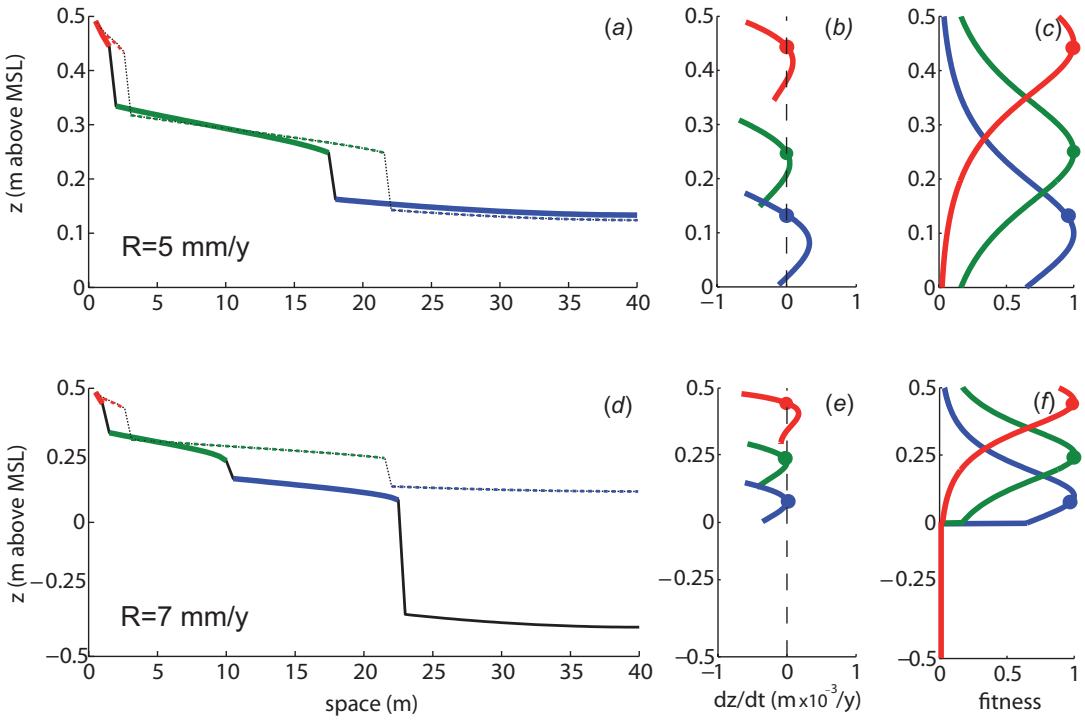

Figure 4.14: (*a*) Equilibrium topography; terrace structures develop due to the existence of multiple stable states. As external forcings we assume $C_0 = 20$ mg/l and $R = 5.0$ mm/yr. The dashed line represents the equilibrium elevation state in figure 4.5*a*; (*b*) Accretion rate as a function of perturbations in the local elevation. Solid circles represent the stable elevation equilibria, open circles the unstable equilibria. External forcings assumed: $C_0 = 20$ mg/l and $R = 5.0$ mm/yr; (*c*) Fitness functions of the species populating the transect (scale parameter $\lambda = 5$) with $C_0 = 20$ mg/l and $R = 5.0$ mm/yr. Solid circles represent the stable elevation equilibria, open circles the unstable equilibria; (*d*) The same as (*a*) except $R = 7$ mm/yr; (*e*) The same as (*b*) except $R = 7$ mm/yr; (*f*) The same as (*c*) except $R = 7$ mm/yr;

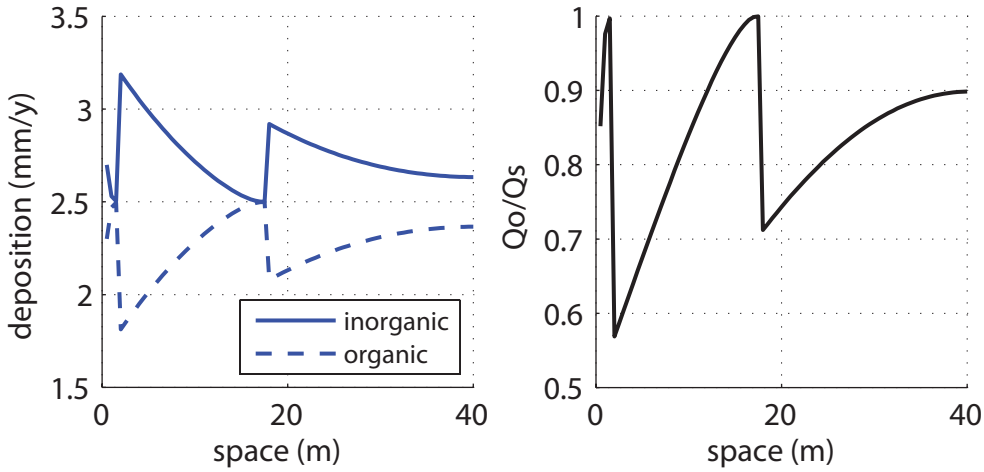

Figure 4.15: Case RSLR=5 mm/yr. Deposition fluxes (inorganic and organic) over the salt marsh transect (left); relation between the organic and the inorganic flux (right)

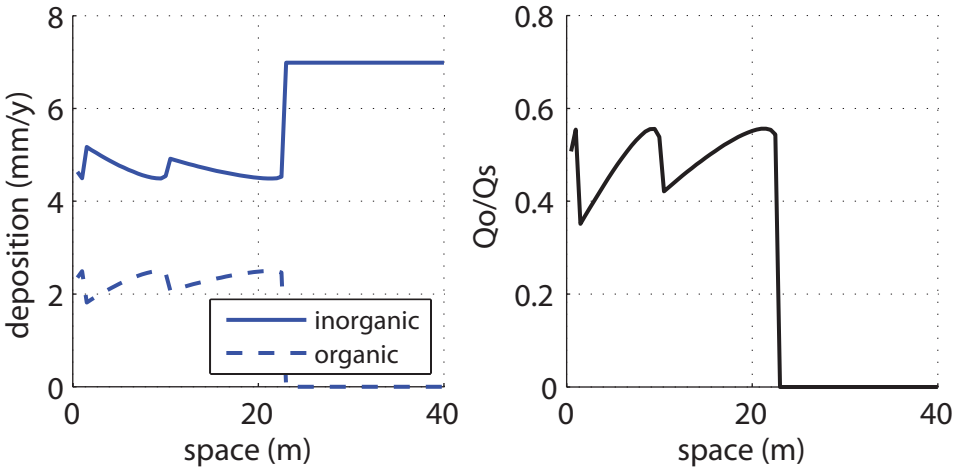

Figure 4.16: Case RSLR=7 mm/yr. Deposition fluxes (inorganic and organic) over the salt marsh transect (left); relation between the organic and the inorganic flux (right)

and characterized by elevations that decrease towards the inner part of the transect. We can appreciate the big spatial topography variability: with a so poor sediment concentration in the channel ($C_0 = 5$ mg/l), the entire transect length is too much long to be able to be a salt marsh, so, what happens is that in a part of it there's a transaction from marsh stable equilibria to subtidal stable equilibria in which there is no vegetation. This is similar to what happened in the case with $R = 7$ mm/yr, but now the spatial topography variability is more accentuated. Despite of this, the vegetation still imposes its balance to the marsh topography, what changes is the spatial dimension where it is able to do its influence. Figure 4.18 shows the inorganic and organic flux considering $C_0 = 5$ mg/l: the organic flux is null where the transect topography is lower than the MSL and the inorganic flux, in a stable condition, is equal to the rate of the RSLR.

If the forcing SSC is increased to $C_0 = 30$ mg/l (figures 4.17*d*, *e*, *f*), or $C_0 = 40$ mg/l (figures 4.17*g*, *h*, *i*) or $C_0 = 50$ mg/l (figures 4.17*l*, *m*, *n*) no significant differences occur with respect to the reference case. This is probably because with high SSC, the topography rises up very quickly and then obstructs the sediment flux coming from the channel. Thus, organic and inorganic rate in figures 4.19, 4.20 and 4.21 are very similar among them and to the reference case rates, previously commented.

4.5 The role of vegetation specialization

We have shown that vegetation acts as a landscape engineer by producing particular morphological-biological patterns in salt-marsh ecosystems. One might then wonder how vegetation characteristics influence the biogeomorphic features of salt-marsh landscapes. To address this question, we have considered vegetation species with different degrees of specialization, i.e. species capable of adapting to narrower or broader ranges of marsh elevations, as represented by different values of the scale parameter λ in equation (3.9). In particular,

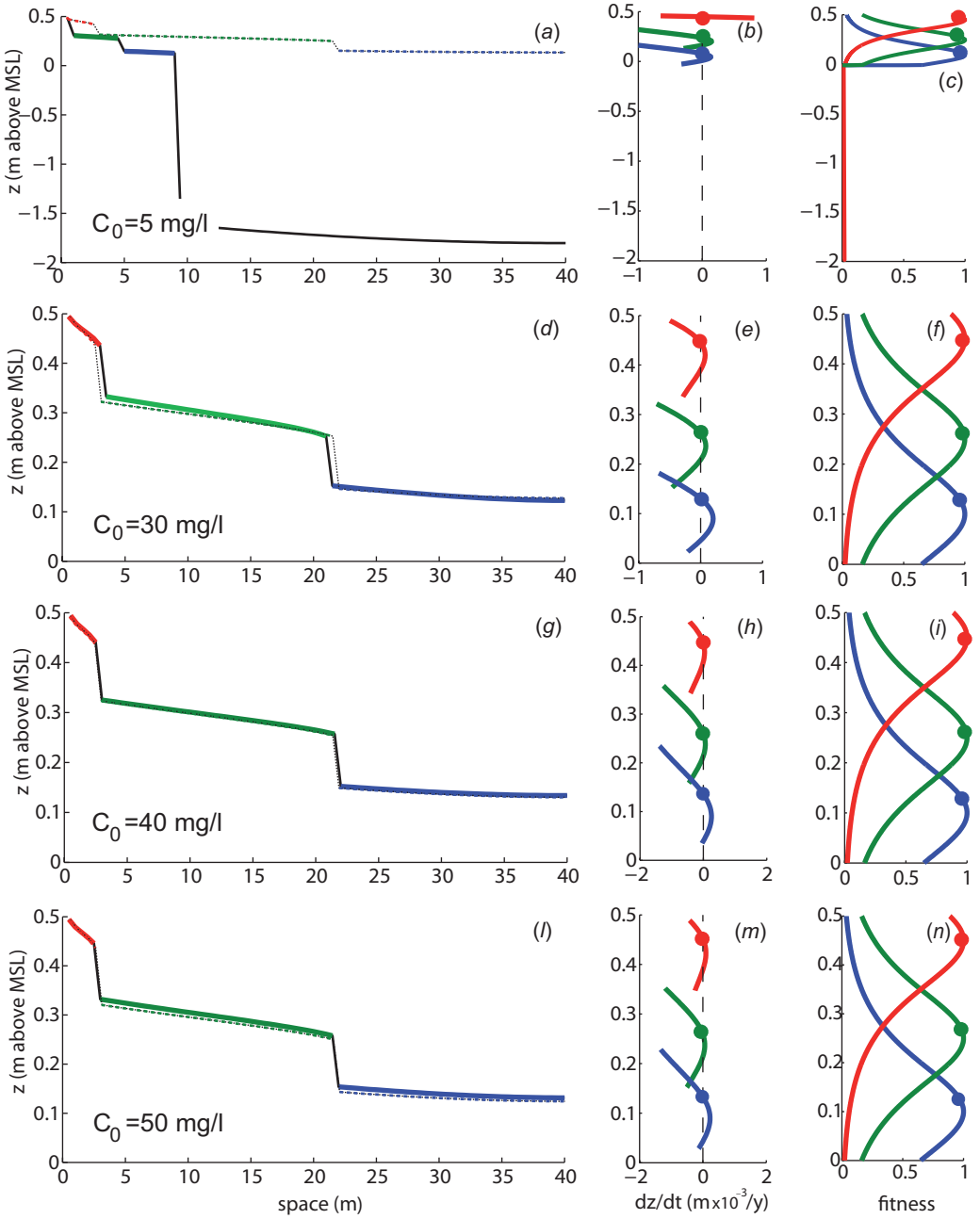

Figure 4.17: (a) Equilibrium topography for $C_0 = 5$ mg/l and $R = 3.5$ mm/yr. The dashed line represent the equilibrium topography for the reference case (figure 4.5a); (b) Accretion rate as a function of perturbations in the local elevation. Solid circles represent the stable elevation equilibria. (c) Fitness functions of the species assumed to populate the transect (scale parameter $\lambda = 5$). Solid circles represent the stable elevation equilibria; (d), (g) and (l) The same as (a) with $C_0 = 30$, $C_0 = 40$, $C_0 = 50$ mg/l respectively; (e), (h) and (m) The same as (b) with $C_0 = 30$, $C_0 = 40$, $C_0 = 50$ mg/l respectively; (f), (i) and (n) The same as (c) with $C_0 = 30$, $C_0 = 40$, $C_0 = 50$ mg/l respectively;

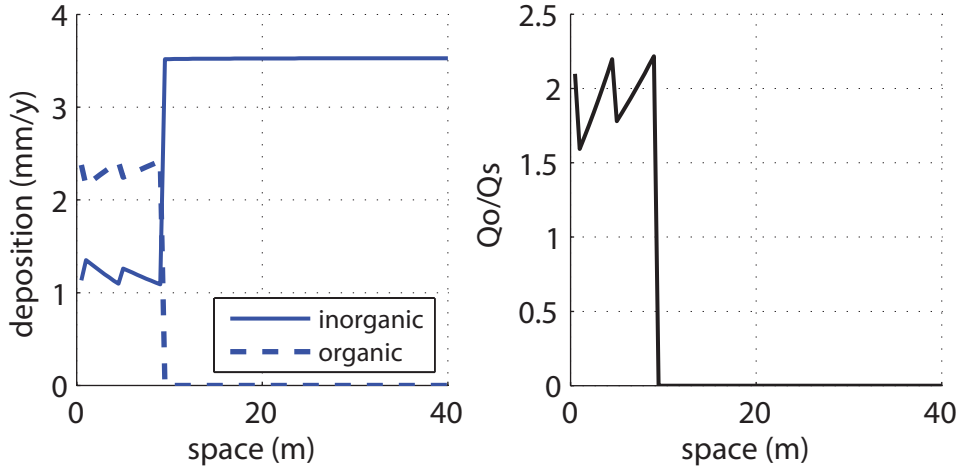

Figure 4.18: Case $C_o = 5$ mg/l. Deposition fluxes (inorganic and organic) over the salt marsh transect (left); relation between the organic and the inorganic flux (right)

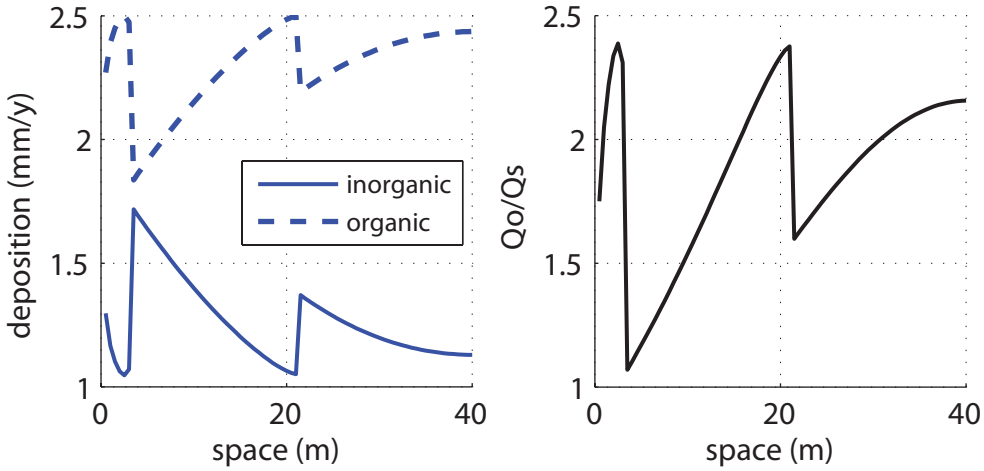

Figure 4.19: Case $C_o = 30$ mg/l. Deposition fluxes (inorganic and organic) over the salt marsh transect (left); relation between the organic and the inorganic flux (right)

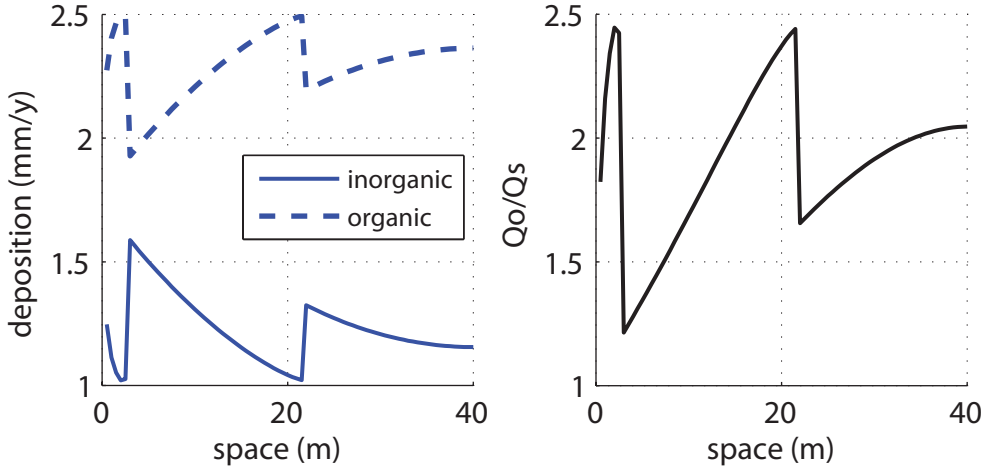

Figure 4.20: Case $C_o = 40$ mg/l. Deposition fluxes (inorganic and organic) over the salt marsh transect (left); relation between the organic and the inorganic flux (right)

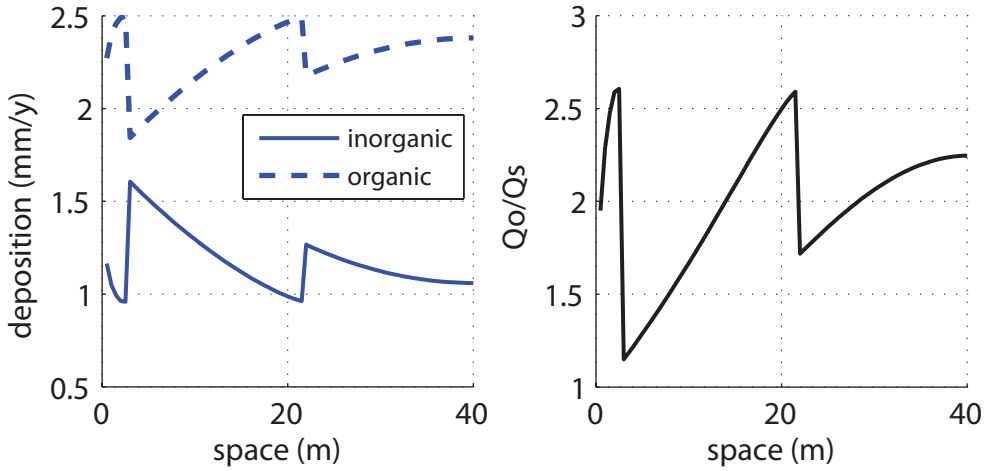

Figure 4.21: Case $C_o = 50$ mg/l. Deposition fluxes (inorganic and organic) over the salt marsh transect (left); relation between the organic and the inorganic flux (right)

we consider here vegetation species which are both more specialized ($\lambda = 10$) and less specialized ($\lambda = 2$) than the reference case ($\lambda = 5$). The maximum productivity elevations are in all cases kept the same ($z = 0.10$, $z = 0.25$, and $z = 0.45$ m above MSL).

Model results show that when vegetation species are assumed to be more specialized (figures 4.22*a*, *b*, *c*) the emerging biogeomorphic structures are more "focused" within narrow elevation ranges with smaller topographic gradients, the evidence of a stronger vegetation control on morphodynamic processes. Such a behaviour can be illustrated by comparing the slope of the fitness functions, df_i/dz, for the reference case and the case of more specialized vegetation species in figure 4.22*c*. As the degree of specialization increases, the slope of the fitness function increases (compare dashed and solid lines in figure 4.22*c*). Therefore, smaller variations in the topographic elevation are required to determine the changes in Q_o necessary to match the spatial gradients of Q_s and balance the rate of RSLR. When less specialized (i.e. $\lambda = 2$) vegetation species are considered topographies displaying smoother, and possibly more realistic, transitions between patches are obtained (figure 4.22*d*, *e*, *f*). Interestingly, because of the reduced vegetation control on elevation, topographic gradients are greater for less specialized vegetation, suggesting the possibility of reading the morphological signature of vegetation physiological adaptations to environmental conditions. Our results, in fact, suggest that the slope of a vegetation patch may be indicative of the breadth of the range of elevations to which the colonizing vegetation species is adapted.

Comparing figure 4.23 and figure 4.24, emerges that $\partial Q_o/\partial x$ is greater in the case of species very specialized than the case of species less specialized and thus, considering $\lambda = 10$, the maximum organic productivity is just close to the end of the "terraces" (especially for the "red" and "green" species), instead, considering $\lambda = 2$, the organic productivity is close to its maximum value over all the transect, always bigger than the inorganic rate.

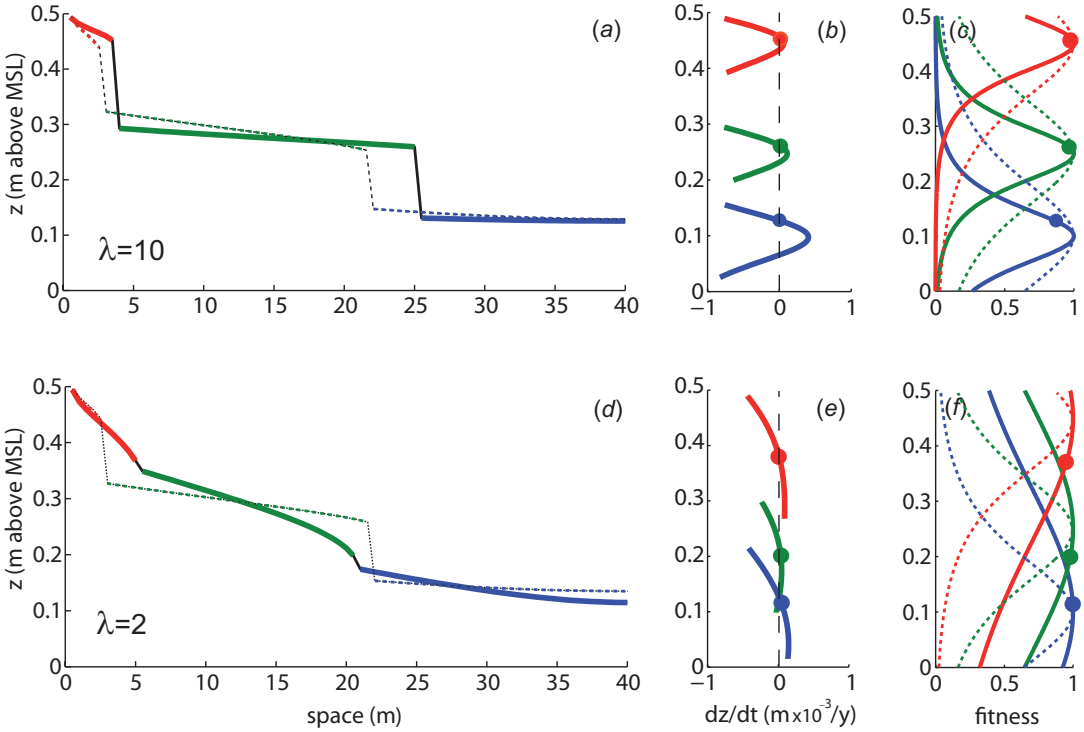

Figure 4.22: (a) Equilibrium topography with terrace structures developing. Multiple stable states emerge assuming $C_0 = 20$ mg/l and $R = 3.5$ mm/yr. The dashed line represent the equilibrium elevation state in figure 4.5a; (b) Accretion rate as a function of perturbations in the local elevation. Solid circles represent the stable elevation equilibria. External forcings assumed: $C_0 = 20$ mg/l and $R = 3.5$ mm/yr; (c) Fitness functions of the species populating the transect with scale parameter $\lambda = 10$, $C_0 = 20$ mg/l and $R = 3.5$ mm/yr. Solid circles represent the stable elevation equilibria; (d) The same as (a) considering the scale parameter $\lambda = 2$; (e) The same as (b) considering the scale parameter $\lambda = 2$; (f) The same as (c) considering the scale parameter $\lambda = 2$;

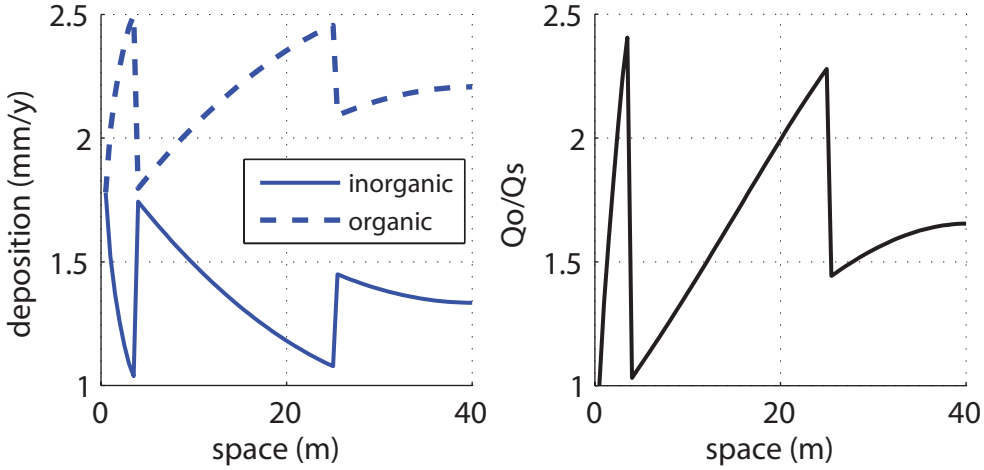

Figure 4.23: Case $\lambda = 10$. Deposition fluxes (inorganic and organic) over the salt marsh transect (left); relation between the organic and the inorganic flux (right)

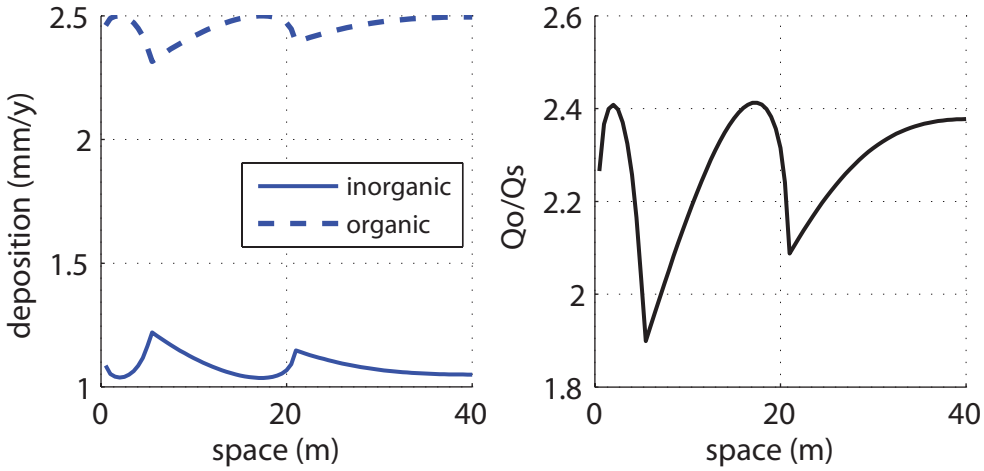

Figure 4.24: Case $\lambda = 2$. Deposition fluxes (inorganic and organic) over the salt marsh transect (left); relation between the organic and the inorganic flux (right)

4.6 The role of the initial topography condition

In this analysis we consider three different initial topographic conditions: i) a constant initial topography at 0.20 m above the MSL (figure 4.25*a*); ii) a random initial topography generated from a uniform distribution (figure 4.25*d*); iii) a random initial topography, produced from a normal distribution with *mean*=0.20 m above MSL and *st.dev.*=0.05 m above MSL (figure 4.25*g*).

Starting from a very random topography, and in particular with very large jumps of topography between neighboring nodes (see figure 4.25*d*), what happens is that very low elevations of nodes positioned at about half transect length, gradually over time receive a limited contribution of inorganic sediment and belong to the branch of the stable organic curve $\partial Q_o/\partial z < 0$ (figure 4.25*f*). Focusing on these nodes, colonized by the "blue" species between "green" species, and imaging that these elevations increase over time, possibly colonized by the "green" species: if it happens (because of organic or inorganic contributions), $\partial Q_o/\partial t < 0$ because $\partial Q_o/\partial z < 0$ and $\partial Q_s/\partial t < 0$ because reducing depth. In this sense being $\partial z/\partial t < 0$, the elevations tends to decrease and remain colonized by the "blue" species. Conversely, for the nodes positioned close to the channel and colonized by the "blue" species at the beginning, receive a lot of inorganic sediment and tend to increase their elevations, moving in the branch of the *fitness function* "green" curve where $\partial Q_o/\partial z > 0$; in this sense if the elevations increase, $\partial Q_o/\partial t > 0$ and $\partial Q_s/\partial t < 0$ because reducing depth, but, $|\partial Q_s/\partial z| << |\partial Q_o/\partial z|$ thus, $\partial z/\partial t > 0$ till $\partial/\partial z(\partial z/\partial t) < 0$, i.e. condition for a stable equilibrium.

If we start the simulation with again a random topography, but with small jumps between neighboring nodes (figure 4.25*g*), the inorganic deposition is more homogeneous towards the transect and then, at the beginning, all the elevations tend to increase their elevation. Over time the transect is first colonized by "red" and "green" species, but then, the elevations for which $\partial Q_o/\partial z > 0$ (unstable branch) with $|\partial Q_s/\partial z| << |\partial Q_o/\partial z|$ (because far from the channel), move down and become colonized by the "blue" species. In this case patches with mixed

vegetation are not present.

The constant initial topography condition (figure 4.25*a*) produce a topography almost similar to the reference case (figure 4.5*a*).

As usual we report the organic and the inorganic depositions towards the transect in the equilibrium configuration for the three initial different topography conditions (see Figures 4.26, 4.27, 4.28).

4.7 The role of the settling velocity

Considering (figure 4.29*a,b,c*) a settling velocity lower than the one adopted in the reference case (see figure 4.5, $w_s = 0.2$ mm/s), the sediment may reach the end of the transect conveyed by the water flow. Taking $w_s = 0.1$ mm/s, allows the increasing in the elevation topography, especially at the end of the transect, far from the channel. The increasing in terms of elevation, lead to the disappearance of the "blue" species specialized at the low elevations. Almost all of the transect is at 30 cm above the MSL, colonized by the "green" species. In figure 4.30 there is the representation of the inorganic and organic fluxes after having achieved the equilibrium configuration.

If we instead increase the settling velocity ($w_s = 0.4$ mm/s) greater than the reference case, the most of the sediment stops and settles at the beginning of the transect without reaching the end of it. Accordingly, the elevation topography quite decreases and the most of the transect moves from a salt marsh environment to a subtidal environment. Furthermore in figure 4.31 the organic flux is equal to zero in the above mentioned transect part, while the inorganic flux balances the rate of the RSLR, leading to the equilibrium state, namely, $dz/dt = 0$.

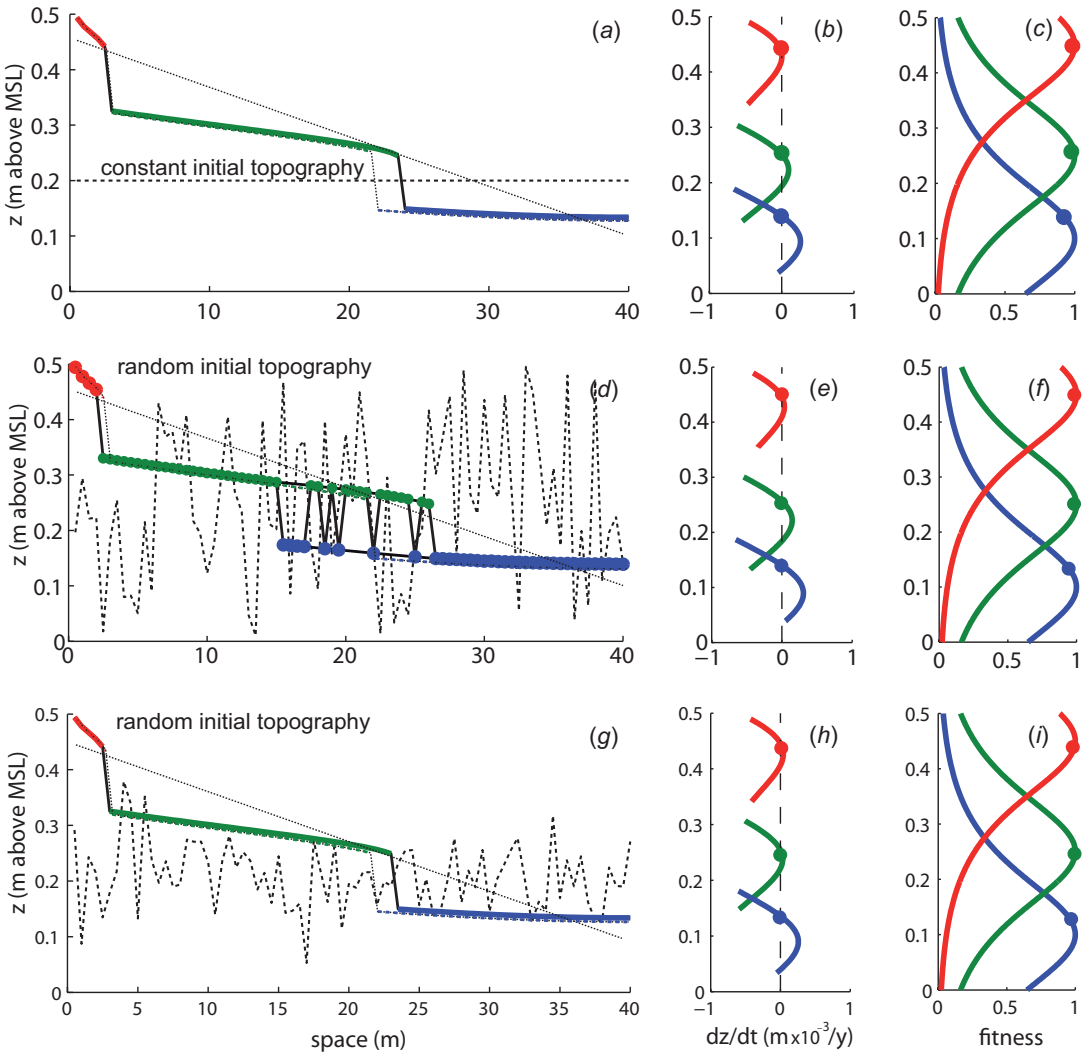

Figure 4.25: (*a*) Equilibrium topography with terrace structures developing. Multiple stable states emerge assuming $C_0 = 20$ mg/l, $R = 3.5$ mm/yr and a constant ($z = 0.20$ m above MSL) initial topography (black dashed line). Dashed line represent the equilibrium topography (colour line) and the initial topography (black line) of the reference case; (*b*) Accretion rate as a function of perturbations in the local elevation. Solid circles represent the stable elevation equilibria; (*c*) Fitness functions of the species populating the transect with scale parameter $\lambda = 5$. Solid circles represent the stable elevation equilibria; (*d*) and (*g*) The same as (*a*) considering a random initial topography from a uniform distribution and from a normal distribution respectively (black dashed line); (*e*) and (*h*) The same as (*b*) considering a random initial topography from a uniform distribution and from a normal distribution respectively (black dashed line); (*f*) and (*i*) The same as (*c*) considering a random initial topography from a uniform distribution and from a normal distribution respectively (black dashed line)

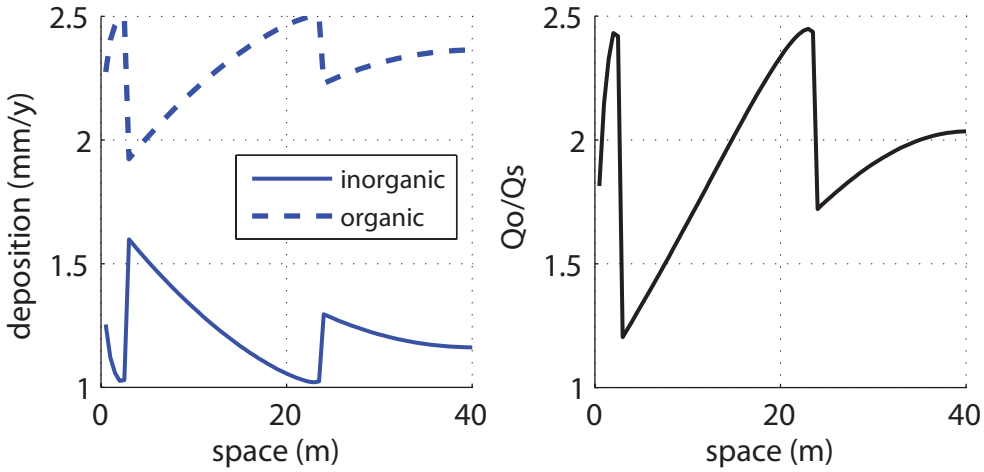

Figure 4.26: Case constant initial topography. Deposition fluxes (inorganic and organic) over the salt marsh transect (left); relation between the organic and the inorganic flux (right)

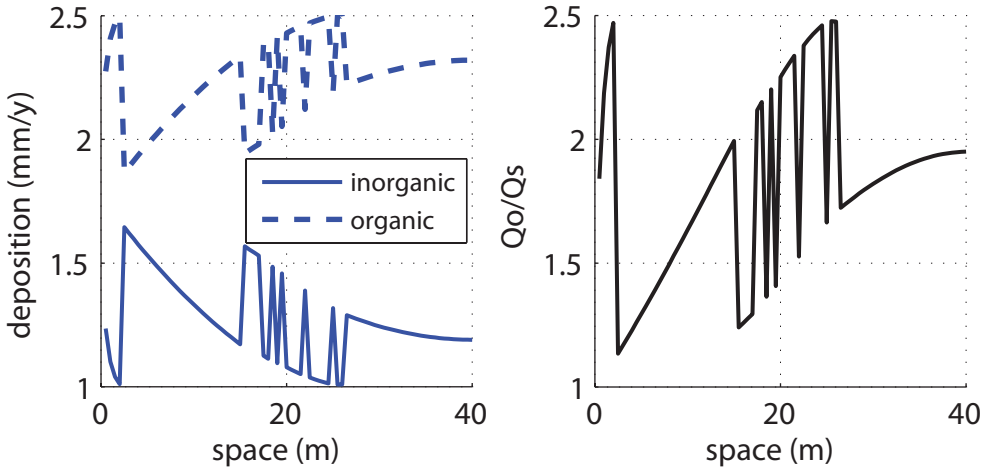

Figure 4.27: Case random initial topography from a uniform distribution. Deposition fluxes (inorganic and organic) over the salt marsh transect (left); relation between the organic and the inorganic flux (right)

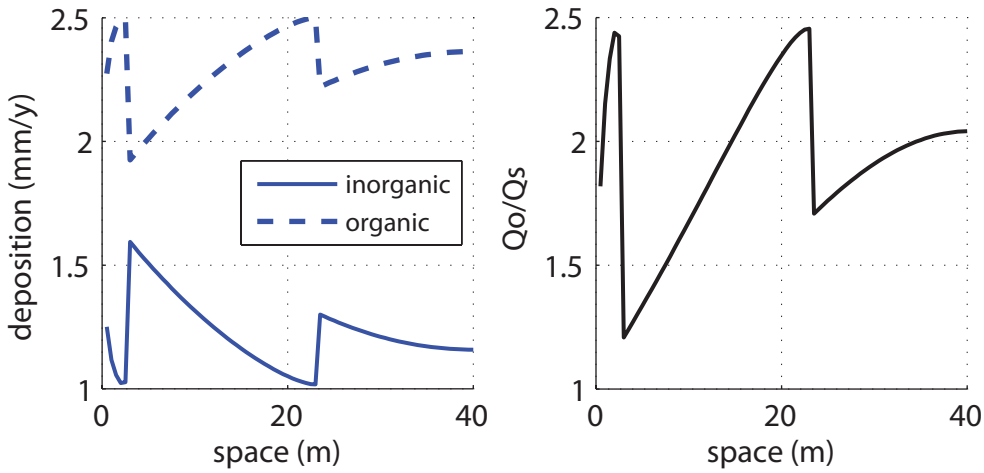

Figure 4.28: Case random initial topography from a normal distribution. Deposition fluxes (inorganic and organic) over the salt marsh transect (left); relation between the organic and the inorganic flux (right)

4.8 The role of the maximum areal biomass productivity

In the reference case we assumed a maximum biomass areal productivity equal to $B_0 = 1000$ g/m^2. If we decrease this value and consider $B_0 = 500$ g/m^2, the maximum organic flux is equal to $Q_{o\ max}(x,t) = \gamma \cdot B_0 \cdot f_i(z_M) = 1.25$ mm/yr, being z_M the mode elevation of the *fitness function* and $f_i(z_M) = 1$. In this case the organic flux is much lower than the inorganic flux (see figure 4.33) over the entire length of the transect unlike what was observed in the reference case (figure 4.6*c*). Moreover, the first part of the transect colonized by the "blue" species (figure 4.32*a*), in the reference case was colonized by the "green" one. Considering $B_0 = 500$ g/m^2, in fact, at the end of the transect there are an already reduced inorganic deposition because of the distance from the channel plus a less organic deposition than the case "$B_0 = 1000$ g/m^2".

Considering as second case the maximum areal biomass productivity equal to $B_0 = 2000$ g/m^2, the topography shape changes a lot than the reference case presented (figure4.5*a*). As we can observe in figure 4.32*d*, the elevations of the sites close to the channel exceed the semi-tidal amplitude ($H = 0.50$ m):

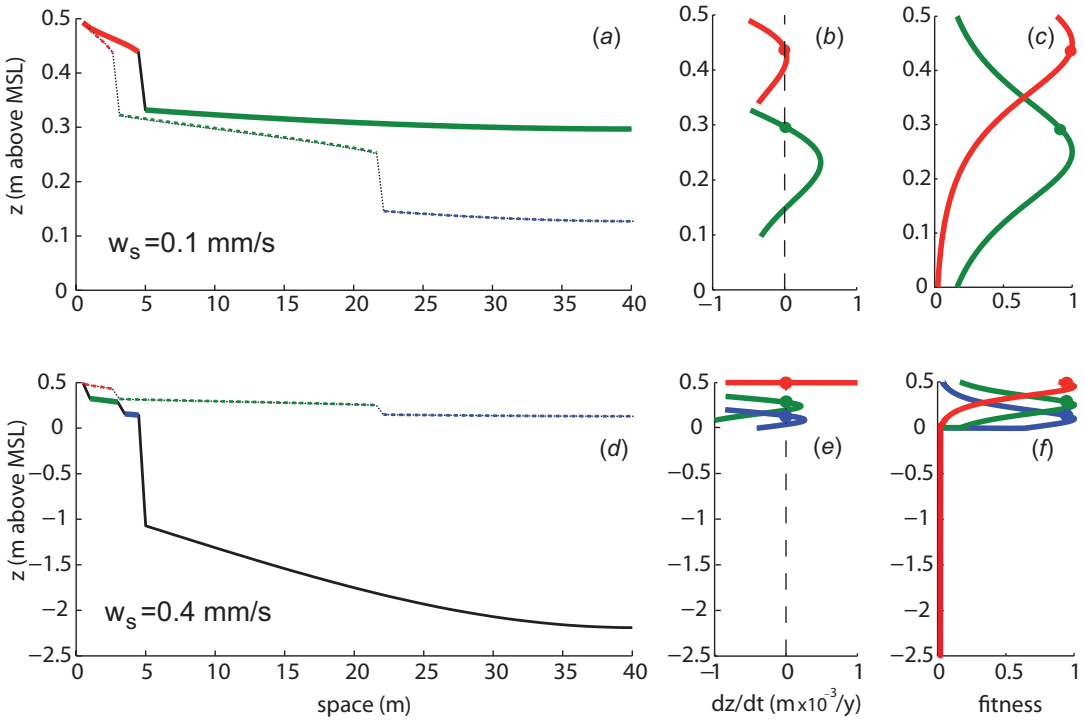

Figure 4.29: (a) Equilibrium topography with terrace structures developing. Multiple stable states emerge assuming $C_0 = 20$ mg/l, $R = 3.5$ mm/yr and $w_s = 0.1$ mm/s. In dashed line we represent the equilibrium elevation state in figure 4.5a; (b) Accretion rate as a function of perturbations in the local elevation. Solid circles represent the stable elevation equilibria. External forcings assumed: $C_0 = 20$ mg/l, $R = 3.5$ mm/yr and $w_s = 0.1$ mm/s; (c) Fitness functions of the species populating the transect (scale parameter $\lambda = 5$) with $C_0 = 20$ mg/l, $R = 3.5$ mm/yr and $w_s = 0.1$ mm/s. Solid circles represent the stable elevation equilibria; (d) The same as (a) with $w_s = 0.4$ mm/s; (e) The same as (b) with $w_s = 0.4$ mm/s; (f) The same as (c) with $w_s = 0.4$ mm/s;

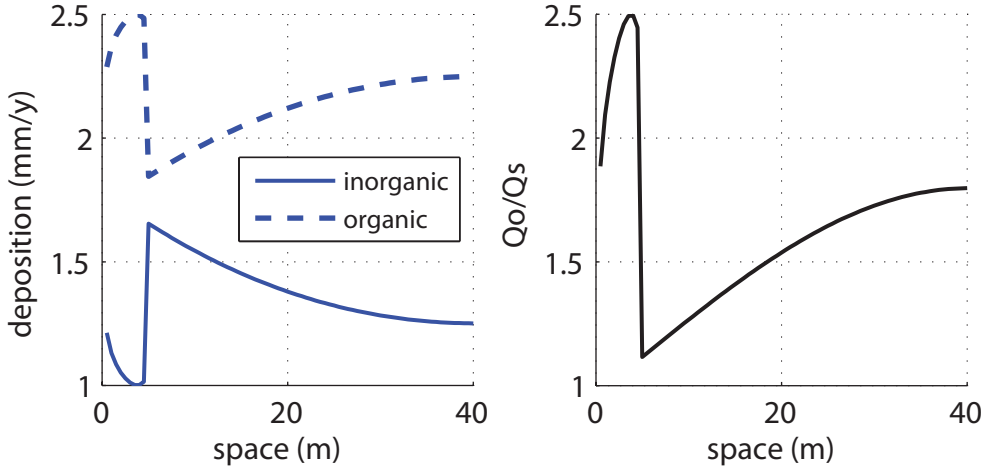

Figure 4.30: Case $w_s = 1$ m/s. Deposition fluxes (inorganic and organic) over the salt marsh transect (left); relation between the organic and the inorganic flux (right)

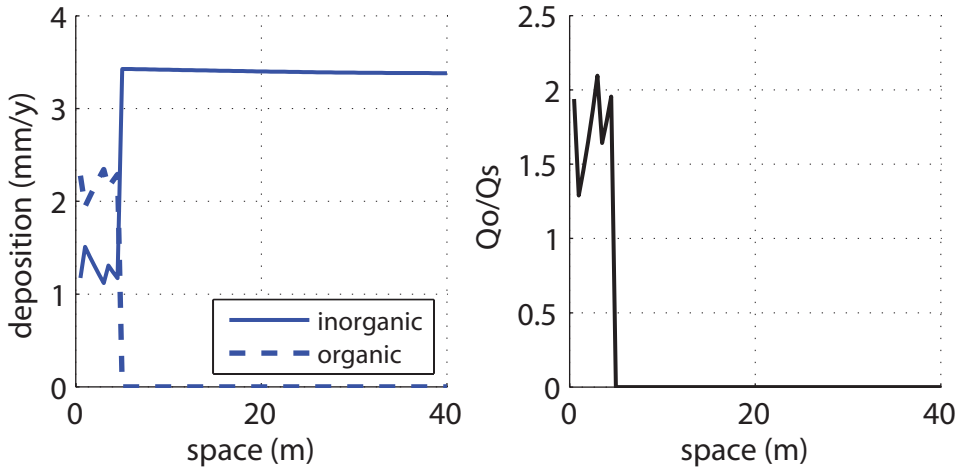

Figure 4.31: Case $w_s = 4$ m/s. Deposition fluxes (inorganic and organic) over the salt marsh transect (left); relation between the organic and the inorganic flux (right)

this fact obstructs the inflow of sediment conveyed by the channel, then the inorganic sediment flux becomes equal to zero over all the transect. The only deposition flux active on the system is the organic one. Because $dz/dt > 0$ when Q_s becomes equal to zero, the elevations increase over time as long as the organic deposition balances the rate of the RSLR. In fact, in figure 4.34, we can see that $Q_s = 0$ over all the transect, instead $Q_o = 3.5$ mm/yr equal to R, then $dz/dt = 0$ i.e. equilibrium state. According to the model the biomass productivity above the high water level follows the fitness function as shown in figure 4.32*c*. Two species colonize the transect in the equilibrium configuration.

4.9 The role of the tidal amplitude

Considering the influence of the sinusoidal tidal amplitude, we compare two different values to the reference semi–tidal amplitude equal to $H = 0.50$ m. The first value is half the reference one and the second value is 4 times it.

Referring to figure 4.35*a*, the maximum elevation obviously reaches the semi–tidal value $H = 0.25$ m. The most of the transect shifts from salt marsh equilibria to subtidal equilibria because the decrease of the tidal amplitude, decreases the flooding period.

For a fixed bottom elevation, $\hat{z}$, the instant depth may be expressed as $D(\hat{z}, t) = \eta(t) - \hat{z}$ where $\eta(t)$ is the water free surface. The flooding period during which the bottom is submerged by the water may be calculated from the solution of the equation (4.1)

$$D(\hat{z}, t) = \eta(t) - \hat{z} = 0 \tag{4.1}$$

where $\eta(t) = -H \cdot cos(\omega t)$.

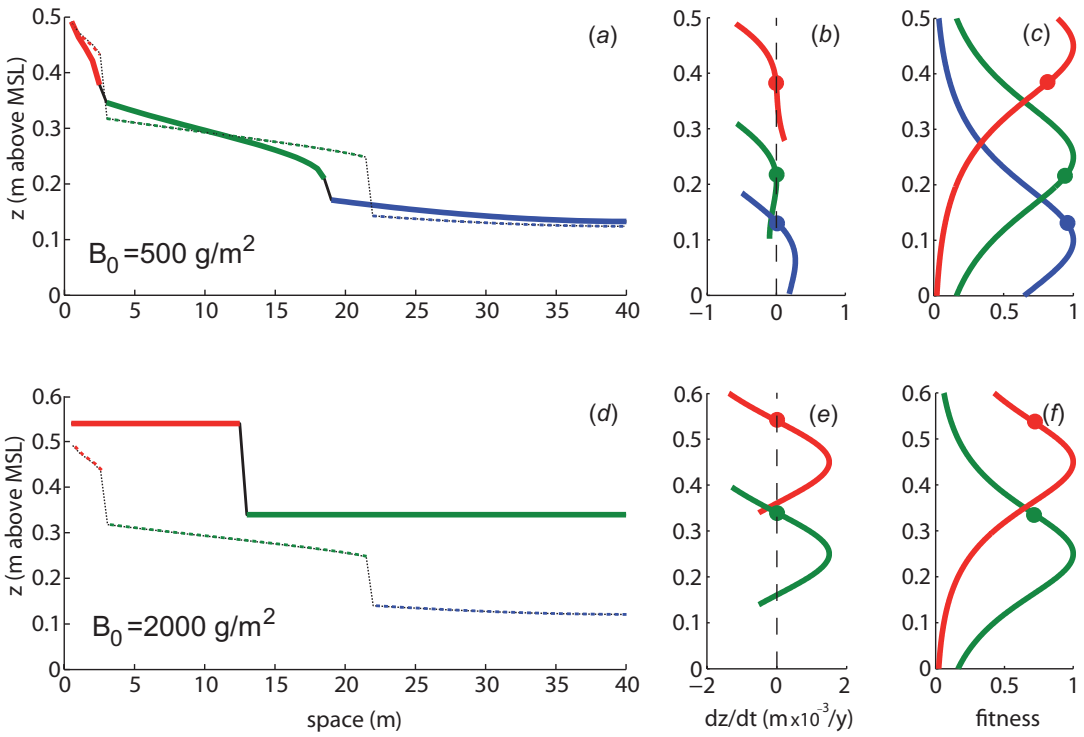

Figure 4.32: (a) Equilibrium topography with terrace structures developing. Multiple stable states emerge assuming $C_o = 20$ mg/l, $R = 3.5$ mm/yr and $B_0 = 500$ g/m^2. Dashed line represent the equilibrium elevation state in figure 4.5a; (b) Accretion rate as a function of perturbations in the local elevation. Solid circles represent the stable topography. External forcings assumed: $C_0 = 20$ mg/l, $R = 3.5$ mm/yr and $B_0 = 500$ g/m^2; (c) Fitness functions of the species populating the transect (scale parameter $\lambda = 5$) with $C_0 = 20$ mg/l, $R = 3.5$ mm/yr and $B_0 = 500$ g/m^2. Solid circles represent the stable topography; (d) The same as (a) with $B_0 = 2000$ g/m^2; (e) The same as (b) with $B_0 = 2000$ g/m^2; (f) The same as (c) with $B_0 = 2000$ g/m^2;

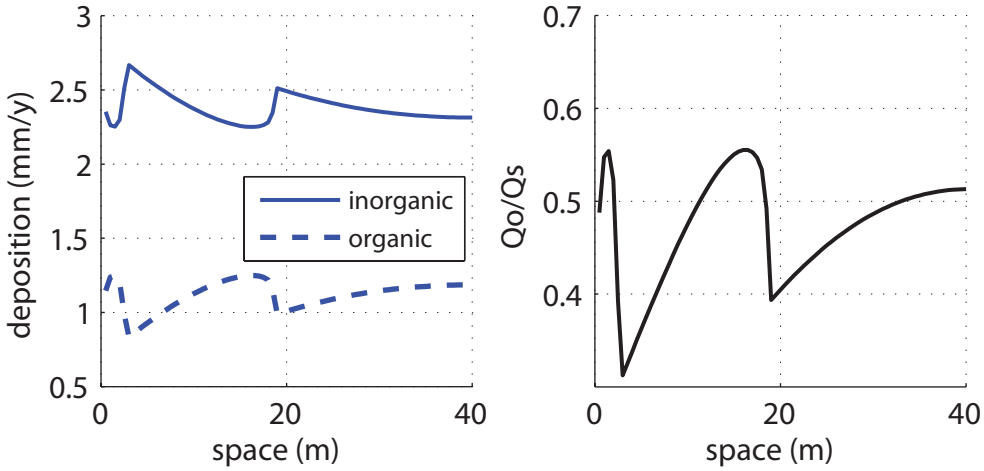

Figure 4.33: Case $B_o = 500$ g/m^2. Deposition fluxes (inorganic and organic) over the salt marsh transect (left); relation between the organic and the inorganic flux (right)

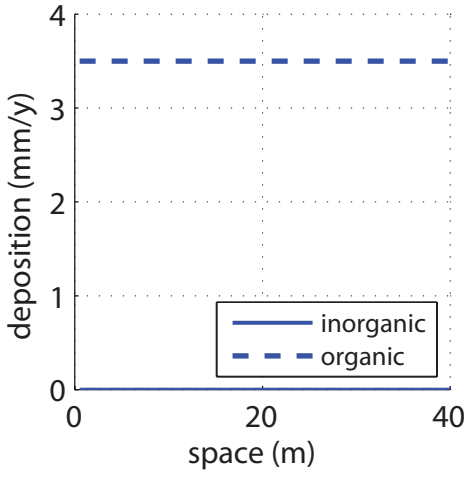

Figure 4.34: Case $B_o = 2000$ g/m^2. Deposition fluxes (inorganic and organic) over the salt marsh transect (left); relation between the organic and the inorganic flux (right)

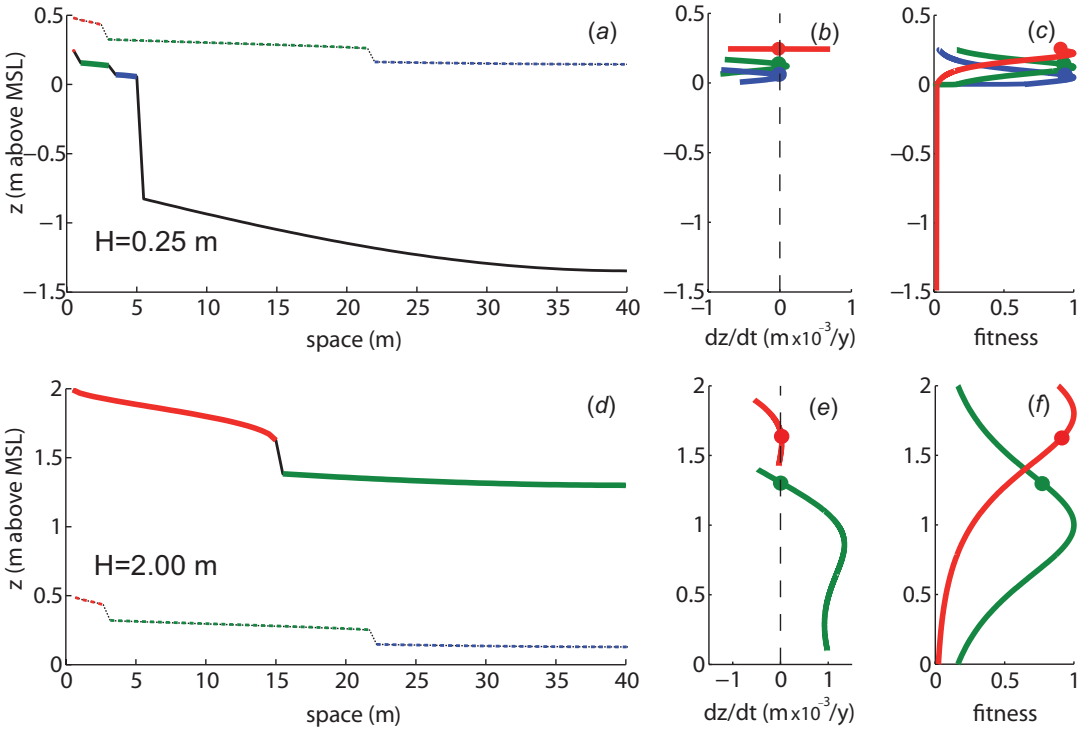

Figure 4.35: (a) Equilibrium topography with terrace structures developing. Multiple stable states emerge assuming $C_o = 20$ mg/l, $R = 3.5$ mm/yr and $H = 0.25$ m. In dashed line we represent the equilibrium elevation state in figure 4.5a; (b) Accretion rate as a function of perturbations in the local elevation. Solid circles represent the stable elevation equilibria. External forcings assumed: $C_0 = 20$ mg/l, $R = 3.5$ mm/yr and $H = 0.25$ m; (c) Fitness functions of the species populating the transect (scale parameter $\lambda = 5$) with $C_0 = 20$ mg/l, $R = 3.5$ mm/yr and $H = 0.25$ m. Solid circles represent the stable elevation equilibria; (d) The same as (a) with $H = 2.00$ m; (e) The same as (b) with $H = 2.00$ m; (f) The same as (c) with $H = 2.00$ m;

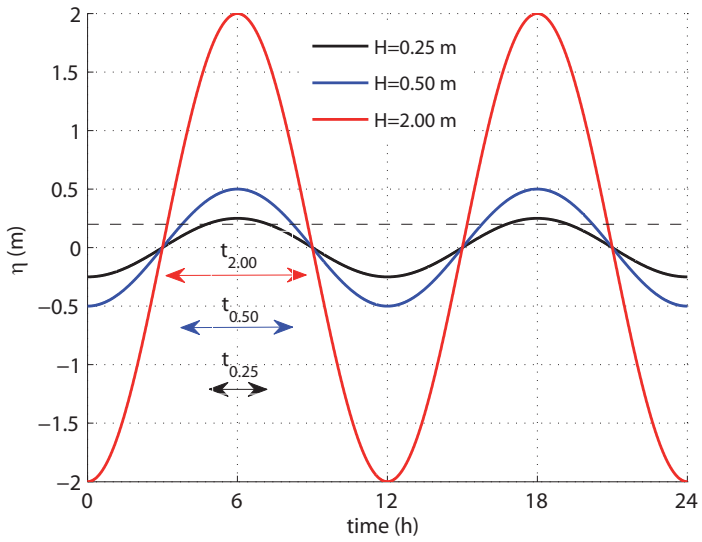

Figure 4.36: Time interval of submersion with different tidal amplitudes for a fixed elevation $\hat{z}$ (dashed line).

We have (see also figure 4.36):

$$\begin{aligned}
\text{if } D = 0 \quad &\Rightarrow \quad -H \cdot cos(\omega t) = \hat{z} \\
&\Rightarrow \quad cos(\omega t) = \tfrac{-\hat{z}}{H} \\
&\Rightarrow \quad t_1(\hat{z}) = arccos\left(\tfrac{-\hat{z}}{H}\right) \cdot \tfrac{1}{\omega} = \\
&\qquad = arccos\left(\tfrac{-\hat{z}}{H}\right) \cdot \tfrac{T}{2\pi} \\
&\Rightarrow \quad t_2(\hat{z}) = T - t_1 = \\
&\qquad = T - arccos\left(\tfrac{-\hat{z}}{H}\right) \cdot \tfrac{T}{2\pi} =
\end{aligned}$$

And then:

$$\Delta t(\hat{z}) = t_2 - t_1 \quad = \frac{T \cdot \left(\pi - arccos\left(\tfrac{-\hat{z}}{H}\right)\right)}{\pi} \tag{4.2}$$

The organic rate of deposition is null where the elevation is lower than the MSL, therefore the inorganic rate Qs matches the rate of the RSLR (figure 4.37).

In general the vegetation still imposes its balance to the marsh topography developing the characteristic terraces-like structures, what changes is the spatial dimension where it is able to do its influence.

Considering $H = 2.00$ m, the period of submersion is greater than the period we had with $H = 0.50$ m, as displayed in figure 4.36 (red line). The elevation of the salt marsh may reaches the semi–tidal amplitude of 2.00 m above the

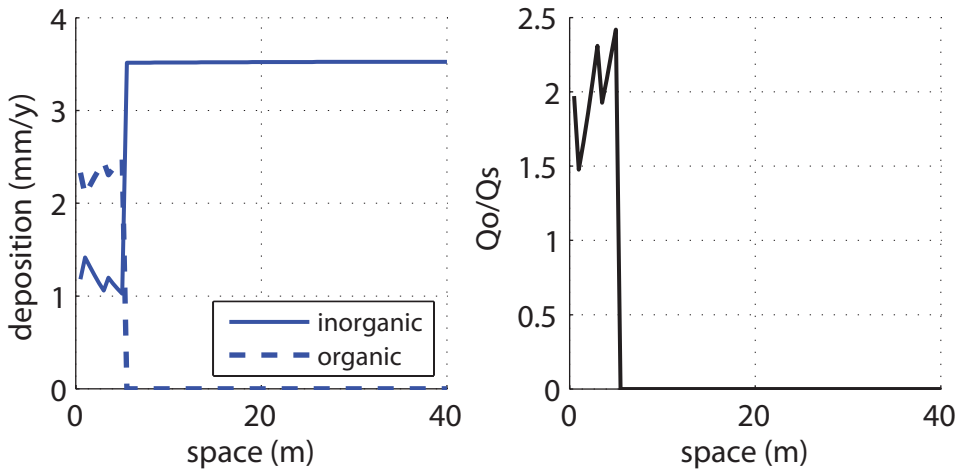

Figure 4.37: Case $H = 0.25$ m. Deposition fluxes (inorganic and organic) over the salt marsh transect (left); relation between the organic and the inorganic flux (right)

MSL close to the channel, and the other part of the transect is at almost 1.5 m above the MSL. Two species colonize the salt marsh and the phenomenon of the zonation is still present. The *fitness functions* are rescaled according to the semi–tidal amplitude: the ratio between the elevation where the fitness function is maximum and the semi–tidal amplitude is kept constant. As we did considering the semi–tidal amplitude equal to $H = 0.25$ m, the constant ratios are the following: $\zeta_M^{(1)} = 0.20$ (blue species), $\zeta_M^{(2)} = 0.5$ (green species), $\zeta_M^{(3)} = 0.90$ (red species) and the relative elevation mode (in m above the MSL) is equal to $z_M^{(i)} = \zeta^{(i)} \cdot H$ for $i = 1 : n$ species considered. In figure 4.38 we show the rate of the inorganic and organic flux: the second one is almost always greater than the first one, especially at the beginning of the transect.

4.10 Stochastic competition formulation

We finally took into account the possible role of the various stochastic components which influence the outcome of species competition, such as, e.g., heterogeneities of soil properties and marsh microtopography. The role of the heterogeneous geomorphological constraints on the bio-geomorphic emerging patterns is therefore modeled on the basis of the "stochastic competition" mechanism,

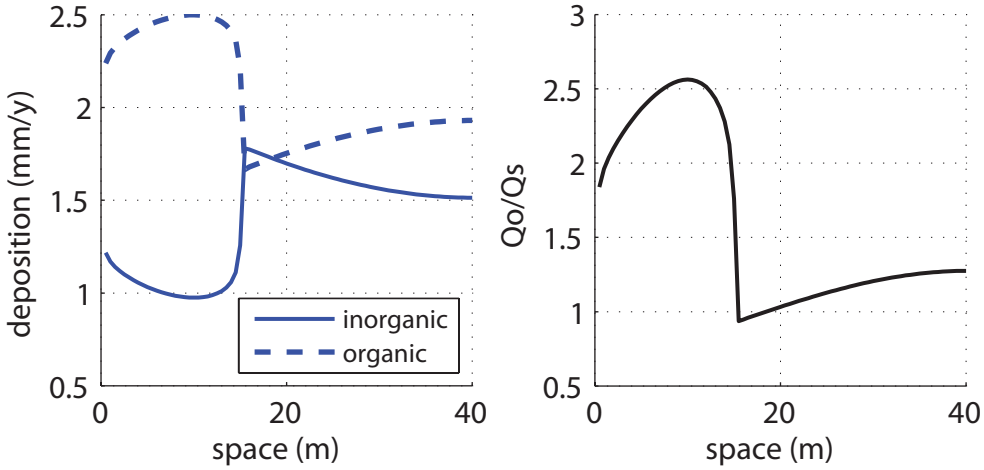

Figure 4.38: Case $H = 2.00$ m. Deposition fluxes (inorganic and organic) over the salt marsh transect (left); relation between the organic and the inorganic flux (right)

almost more similar to the real interspecific competition. Figure 4.40*a* shows that when the stochastic competition is adopted, more realistic dynamics and less regular patterns are obtained. The resulting marsh topography, although displaying decreasing elevations from the channel towards marsh interior, as in the reference case, is characterized by a more irregular trend, whereas vegetation patches populated by single species are replaced by patches of mixed vegetation species.

The irregularity in the species distribution is reflected in the shape of the organic rate (figure 4.39) towards the marsh.

The role of biogeomorphic feedbacks in forming the observed zonation patterns may still be identified by studying the probability distribution of bottom elevations along the transect. Figure 4.40*b* shows the frequency density of bottom elevations encroached by different vegetation species, where color-coded bars identify different species (the same species considered in the reference case with their *fitness functions*). Each colored bar represents the most-abundant species within each elevation interval. A multimodal distribution emerges which suggests the existence of engineered preferential elevation ranges for the different vegetation species: a clear signature of the governing feedback between biomass productionand elevation even when vegetational and topographic patterns are

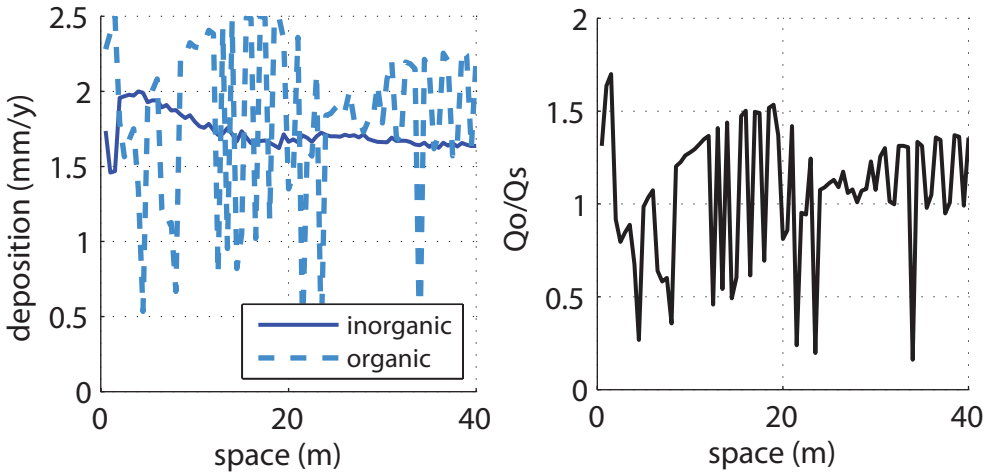

Figure 4.39: Case "stochastic formulation". Deposition fluxes (inorganic and organic) over the salt marsh transect (left); relation between the organic and the inorganic flux (right)

significantly less visually evident (figure 4.40*a*).

Imaging in fact, to delete the organic contribution in the fluxes balance, but maintain the stochastic spatial competition: the topography appears almost exponentially decreasing, with the disappearance of the characteristic "terraces" structures (figure 4.41*a*). Furthermore, in figure 4.41*b* the multimodal characteristic of the probability distribution of the bottom elevations is replaced with a single mode (lower elevations are more frequent than the higher ones), signature of the loss of the feedback between the elevations and the vegetation.

The sub-optimality, previously showed with the fittest-takes-it-all mechanism, considering the stochastic competition among the species, is less evident, because of the irregularity in the topography. figure 4.42 and figure 4.43 show the frequency density of all the species fitness functions and of each fitness function respectively, considering one year sample. Accounting the yearly morphology changes because the species colonization changing, figure 4.44 shows a more probable frequency density of the species fitness, considering ten years sample. With a bigger years sample we can appreciate the different frequency trend, less peaked than what represented in figure 4.42; this highlights that the majority part of the values are probable, directly linked with the "stochastic competition"

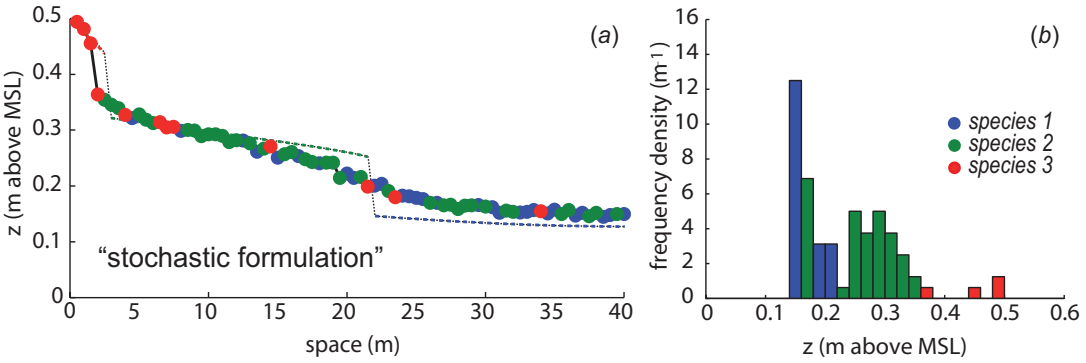

Figure 4.40: (a) Multiple stable states assuming as external forcings $C_0 = 20$ mg/l, $R = 3.5$ mm/yr. "Stochastic formulation" is assumed as spatial competition mechanism. In dashed line we indicate the topography reference case (figure 4.5a), where we adopted the "fittest-takes-it-all formulation"; (b) Multimodal frequency distribution of topographic elevations. Each peak (color-coded, according to the most abundant species in each interval) is associated with the unique species that generates it;

mechanism, but the remarkable thing is that there is no a single mode close to the maximum value of the fitness.

Similarly, we represent the frequency density of the fitness function of less specialized species (i.e. $\lambda = 2$) considering one year sample (figure 4.45) or ten years sample (figure 4.46) with the "stochastic competition" mechanism. In figure 4.47 there are the frequencies of each species fitness functions. With less specialized species, the frequency density of the fitness functions is more "peaked" close to the maximum value (see Figures 4.45 and 4.46) because of their lower slope where for a large elevation range, the fitness values are close to the maximum value. This is also the reason why there is not a big different trend between the Figures 4.45 and 4.46, like we saw considering more specialized species (i.e. $\lambda = 5$).

Our analyses show that zonation structures are largely determined by the degree of species adaptation to varying elevations, inducing a tuning of marsh elevation by vegetation. We now seek the signature of this bio-geomorphic coupling in real marshes. We performed detailed marsh topographic observations

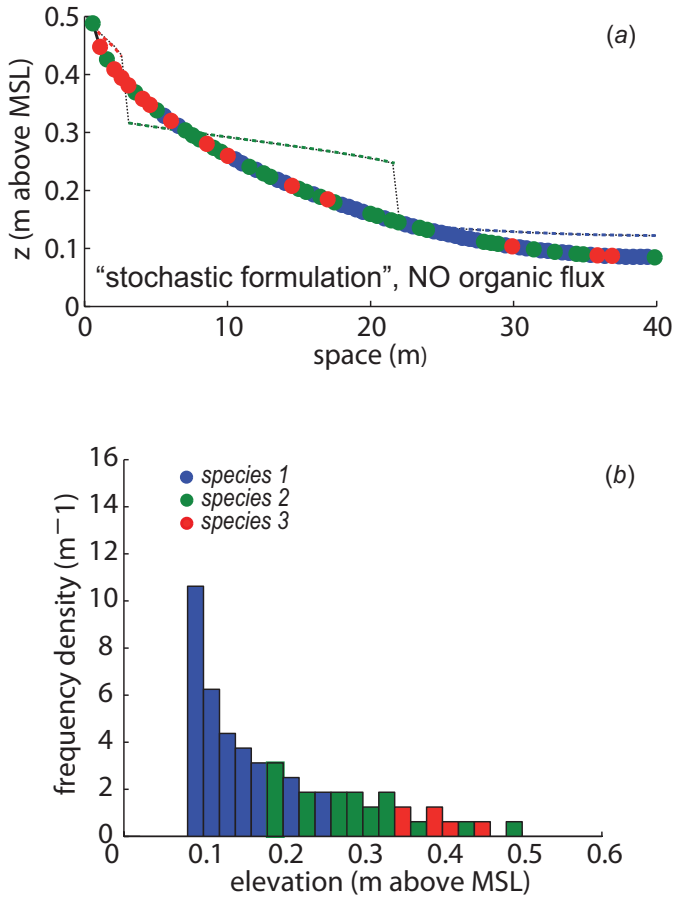

Figure 4.41: (a) Multiple stable states assuming as external forcings $C_0 = 20$ mg/l, $R = 3.5$ mm/yr. "Stochastic formulation" is assumed as spatial competition mechanism. In dashed line we indicate the topography reference case (figure 4.5a), where we adopted the "fittest-takes-it-all formulation"; (b) Frequency distribution of topographic elevations considering no organic deposition flux. Each peak (color-coded, according to the most abundant species in each interval) is associated with the unique species that generates it.

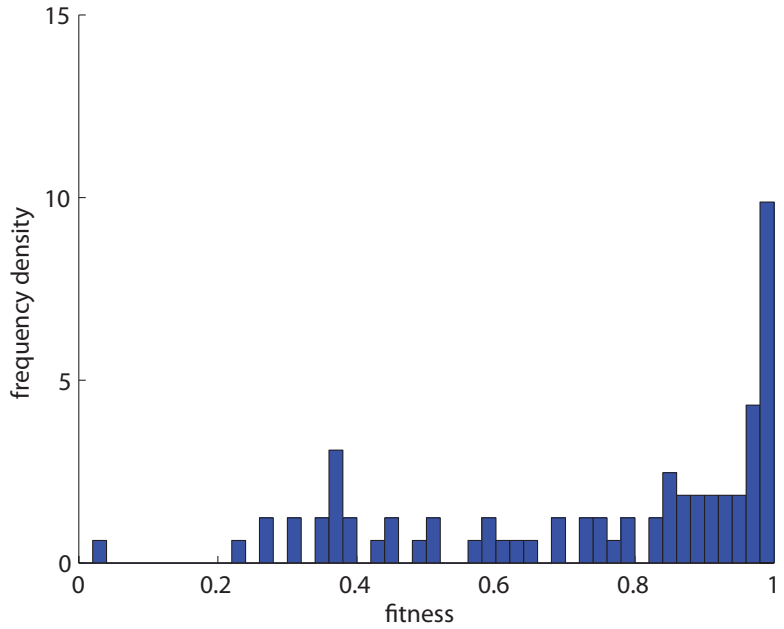

Figure 4.42: Case "stochastic competition": frequency density of the fitness functions considering one year sample

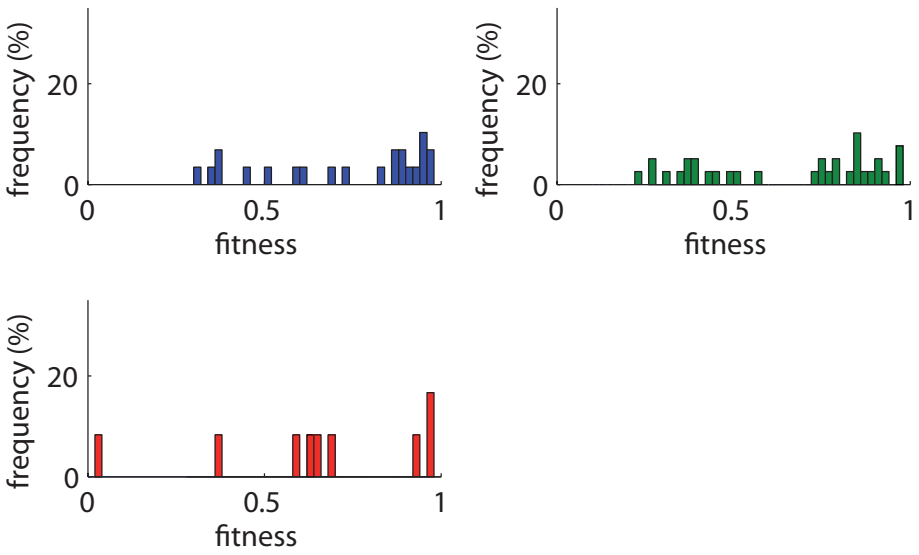

Figure 4.43: Case "stochastic competition": frequency density of each fitness functions

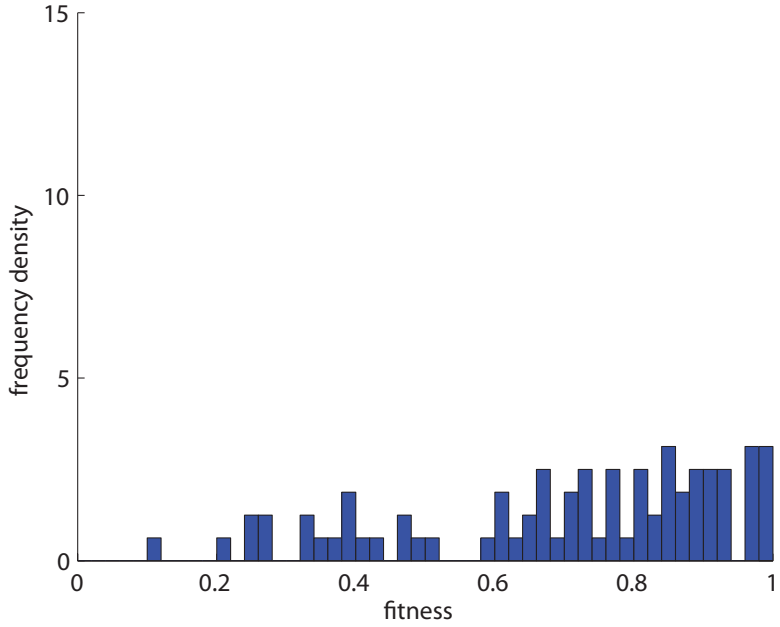

Figure 4.44: Case "stochastic competition": frequency density of the fitness functions considering ten years sample

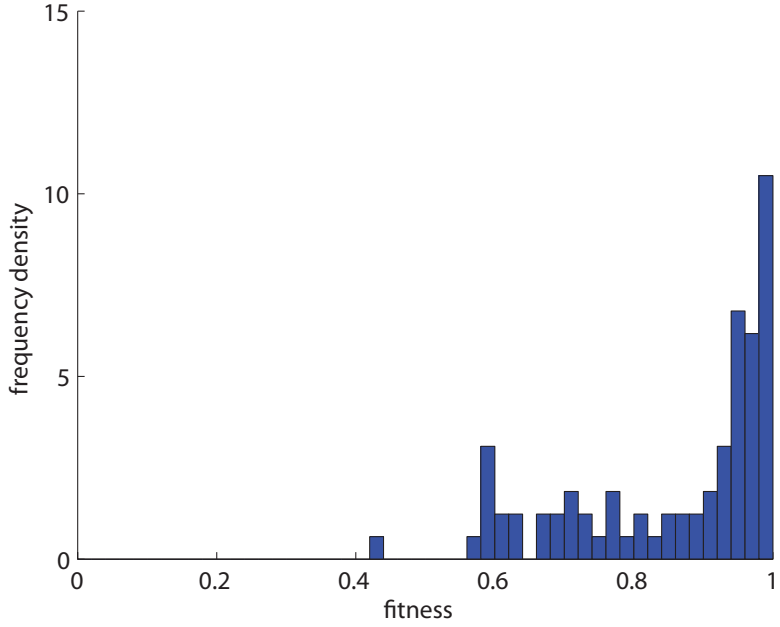

Figure 4.45: Case "stochastic competition" considering less specialized species ($\lambda = 2$): frequency density of the fitness functions considering one year sample

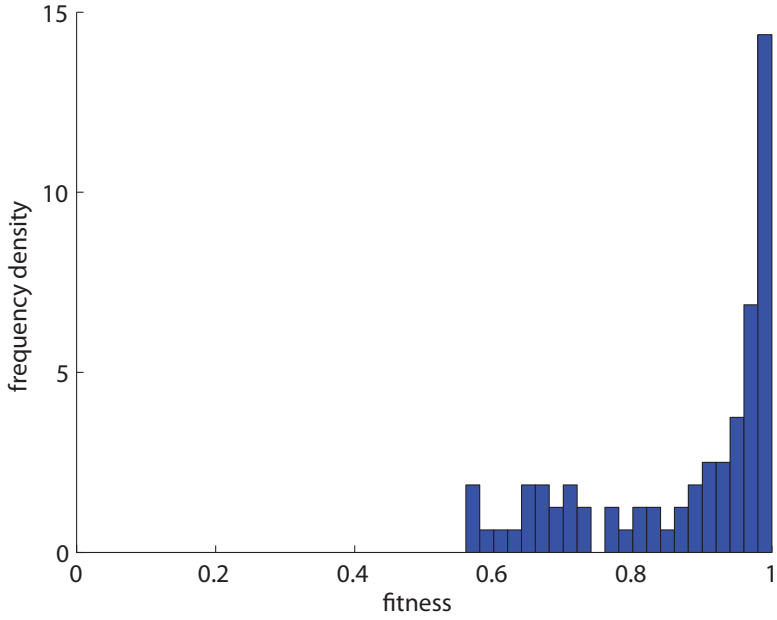

Figure 4.46: Case "stochastic competition" considering less specialized species ($\lambda = 2$): frequency density of the fitness functions considering ten years sample

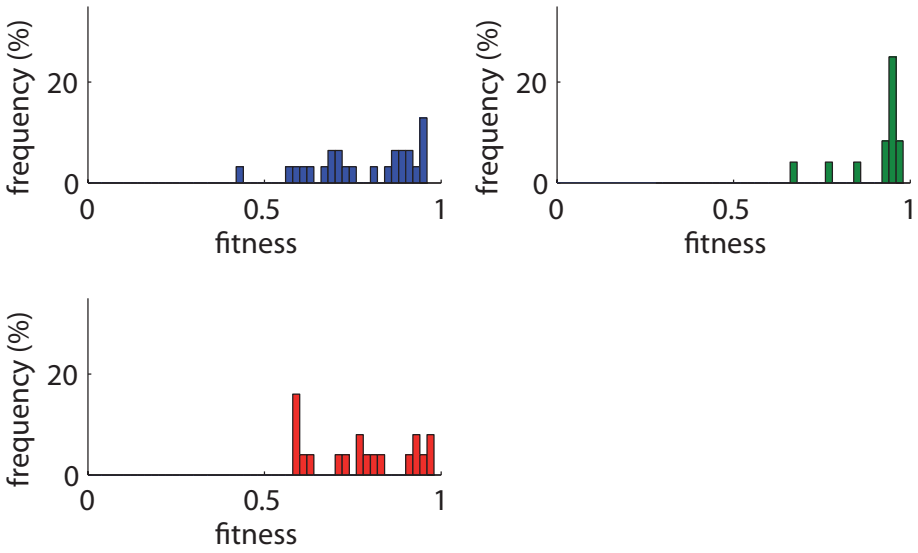

Figure 4.47: Case "stochastic competition" considering less specialized species ($\lambda = 2$): frequency density of each fitness functions

to support our analysis of coupled biogeomorphic dynamics as the determinant of marsh zonation patterns (Figures 4.48 and 4.49). A detailed survey of marsh elevations in the Venice lagoon, performed with a total station (i.e. an electronic theodolite with accuracy better than 1 mm), indeed shows the presence of previously undetected multimodal distributions of topographic elevation. Each peak in the elevation distribution is associated with a different species, a signature of the biomass-elevation feedback locking the system into a set of almost discrete preferential elevation ranges.

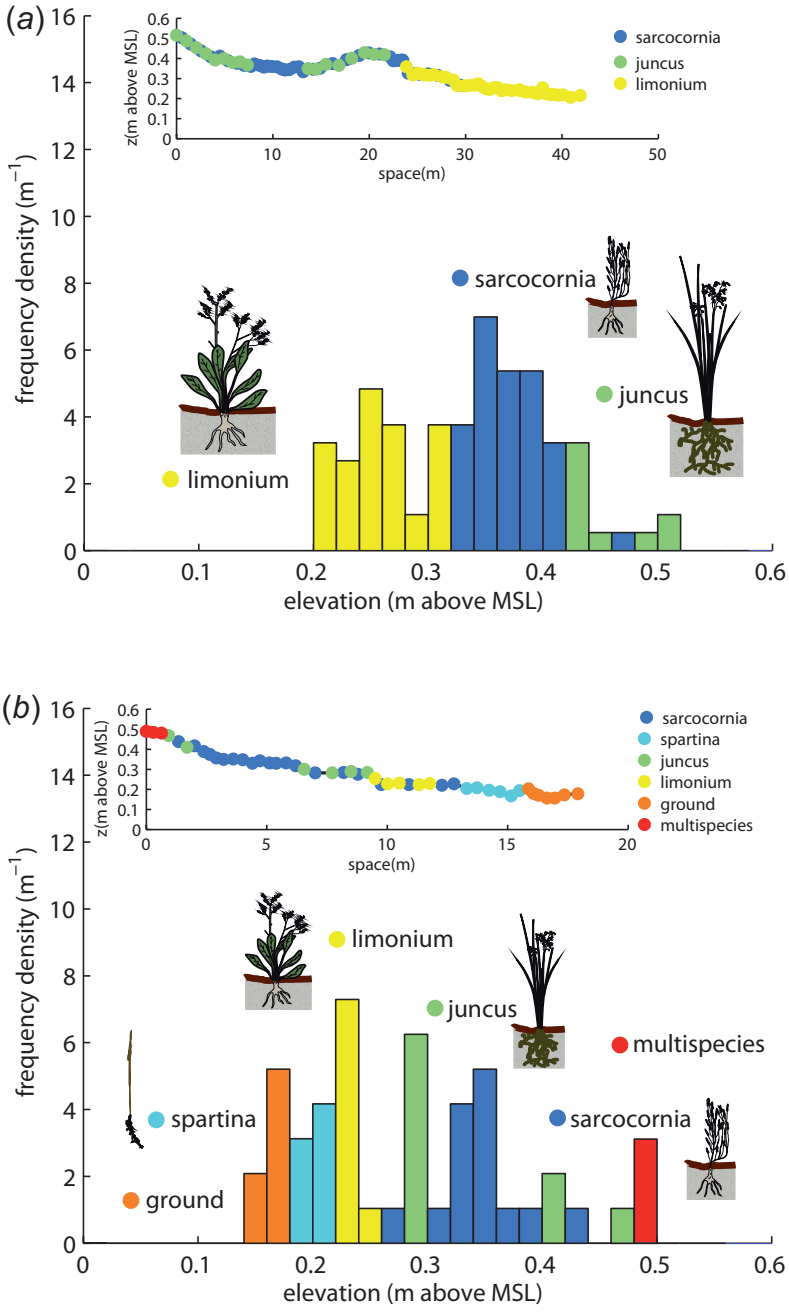

Figure 4.48: PART I (*a*–*b*) Observed zonation patterns. An accurate topographic survey (uncertainty smaller than 1 mm) reveals a multimodal frequency distribution of soil elevation, highly suggestive of the major role played by the biomass-elevation feedback in tuning marsh topography. Each bar is color-coded according to the vegetation species which is most abundant within the pertinent elevation interval, showing that indeed elevation ranges are characteristic of the vegetation species (or of a typical mix of species at high elevations) which maintain them.

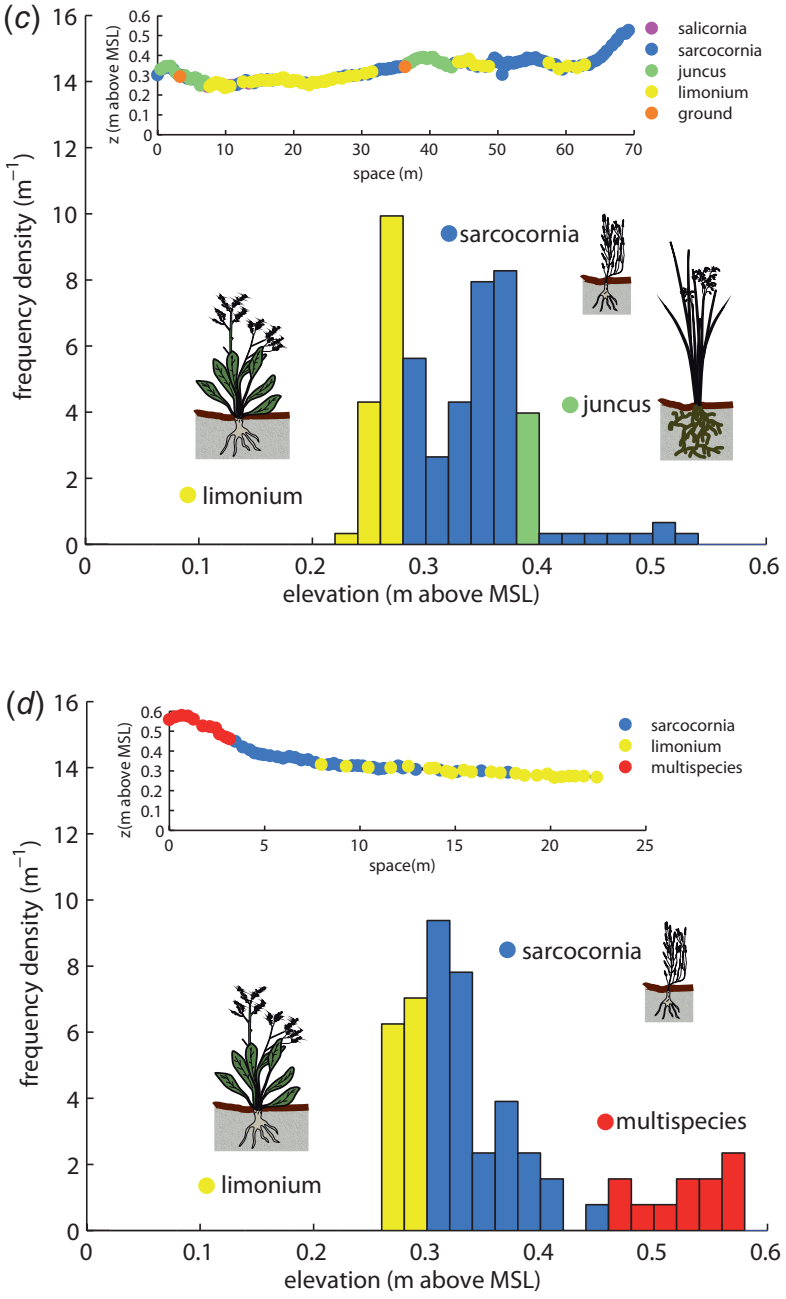

Figure 4.49: PART II (*c–d*) Observed zonation patterns. An accurate topographic survey (uncertainty smaller than 1 mm) reveals a multimodal frequency distribution of soil elevation, highly suggestive of the major role played by the biomass-elevation feedback in tuning marsh topography. Each bar is color-coded according to the vegetation species which is most abundant within the pertinent elevation interval, showing that indeed elevation ranges are characteristic of the vegetation species (or of a typical mix of species at high elevations) which maintain them.

4.11 Mutation coupled with spatial competition

In this Section we present some results obtained using the continuous fitness function in the description of the species characteristics, and coupling the competition spatial mechanism to the mutation mechanism in the species time evolution. We experiment a lot of configurations: different initial conditions, different sediment suspend concentration, different ways or frequencies of mutation. The aim of these simulations is to observe the feedbacks between the morphology and the biology, and moreover to allow the self developing of the species: with the mutation mechanism, the species are able to reproduce themselves. These couple mechanisms show not only how the species colonize the marsh, but also how the natural mutation develops and how it holds up over time.

Despite the numerous attempts, we were not able to set up a stable configuration, namely, with the mutation mechanism working in the model, to obtain a topography stable configuration. What in fact happens is that a small perturbation to a random elevation of the transect (influenced by the new species generated), influences probably all the other transect elevations because of the different inorganic flux. The sites far from the channel have the lowest inorganic intake, accordingly a freeble equilibrium, compounded by the continuous renewal of species upstream. According to the spatial selection, the new fittest or one of the most new fit species, replaces the old species, producing more organic matter and consequently changing the marsh elevation.

So far, we have not been able to find a valid method to ensure that the mutation influenced not so onerous the entire topography feature.

In the following we present a collection of some of the most significant tests examined, numbering them in numerical order. In all of the analysis, we set $R = 3.5$ mm/yr, $H = 0.50$ m and also we assume that the mother species competes with the daughter one: in the spacial competition, if the daughter

is fitter that the mother, it replaces the mother, otherwise not. In general we assume also the sediment suspend concentration $C_0 = 20$ mg/l, except where it is specified.

4.11.1 Analysis: 1

In this first analysis (see figure 4.50), in the mutation process we change both the fitness function mode and its maximum value in a random way. The mode changing is equal to $z_{M(new)} = z_{M(old)} \pm 20\%\ z_{M(old)}$ then, high elevations change more that the low ones. The time step of mutation is equal to 50 years, i.e. a mutation every 50 years. As usual, we start from a linearly decreasing topography condition and three different species randomly distributed above the marsh transect. We set symmetric fitness functions with $\lambda_1 = 20$, $\lambda_2 = 30$, $\lambda_3 = 40$ from low to high elevations, less specialized species at the low elevations and $C_i = 1$ for the i species. The species also spatial compete following the fittest-takes-it all rule, i.e. the fittest one is preferred.

As shown in figure 4.50, the species with the greater value of maximum are preferred in the evolutionary dynamic, the number of species increase over time, but as said above, this number is influenced by the instable marsh topography. Just born a new species, if it is fitter than the others above the transect, replaces them and changes the elevation of the sites. The quite big step of mutation seems to change too quickly the topography and this probably contributes to the instability displayed in figure 4.50 (bottom) at one thousand years.

All of the other time–configurations, not shown here, are in the supplementary material:

`Analysis_cited\RUN_03_04_2012_AnnualSpec_allSel_40_050dx_sechlR=1LVfixed_C_3SPini_mother_Mutation50`

4.11.2 Analysis: 2

In the second analysis (see figure 4.51), as the first case, in the mutation process we change both the fitness function mode and its maximum value in a

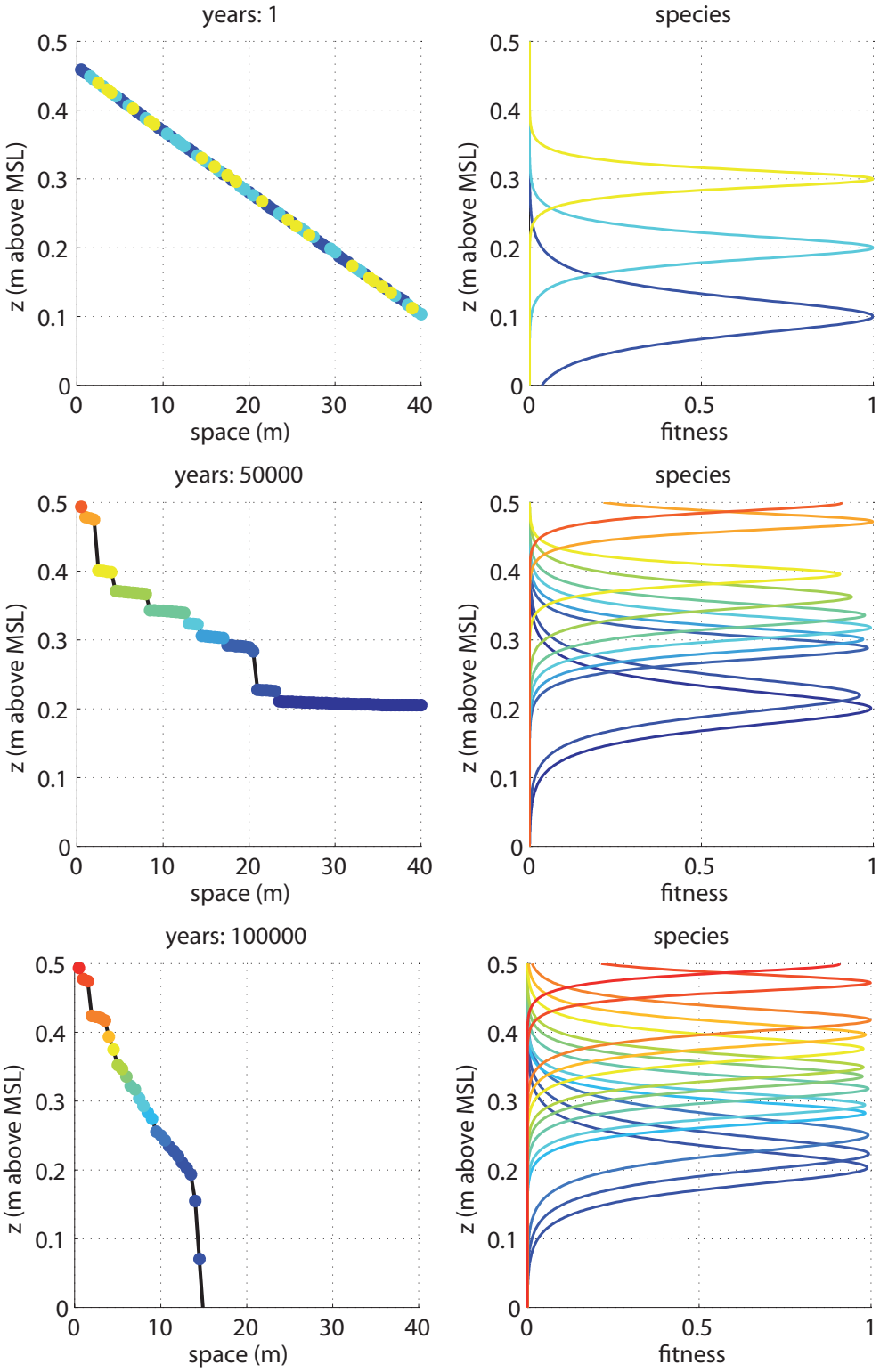

Figure 4.50: Analysis: 1. Time evolution of topography (left) and species (right). Rate of mutation adopted: 50 years. Mutation based on changing the fitness function mode and the maximum value. More details in the supplementary material.

random way every 10 years. The increasing (or decreasing) in the elevation mode is a random value in the interval $[-0.005; +0.005]$m. Unlike the first case, the mode moving is uniformly distributed both for the low and the high elevations, thus, the species are more stable over time because of their reduced shift mode and adaptation to different ranges of elevation.

We consider three initial species i whose scale parameter is equal to $\lambda_i = 5$ and it remains unchanged during the evolution process like $C_i = 1$. The species also spatial compete following the fittest-takes-it all rule.

Supplementary material about this analysis:

`Analysis_cited\RUN_03_04_2012_AnnualSpec_allSel_40_050dx_sechlR=lLVfixed_C_3SPini_mother_Mutation10_deltaz_fMax`

4.11.3 Analysis: 3

The third analysis (see figure 4.52) consider as the previous analysis $C_0 = 20$ mg/. In the mutation process we change both the fitness function mode and its maximum value in a random way every 50 years like Analysis 1. The increasing (or decreasing) in the elevation mode is a random value in the interval $[-0.005; +0.005]$m. Unlike the first case, the mode moving is uniformly distributed both for the low and the high elevations. The low frequency of mutation plus the low mode elevation changing, lead to very small variations both in terms of species and of topography. The general evolution is so slowed, that's why the topography seems to be stable.

We consider three initial species i whose scale parameter is equal to $\lambda_i = 5$ and it remains unchanged during the evolution process. Spatial competition following the fittest-takes-it all rule.

Supplementary material about this analysis:

`Analysis_cited\RUN_03_04_2012_AnnualSpec_allSel_40_050dx_sechlR=lLVfixed_C_3SPini_mother_Mutation50_deltaz_fMax`

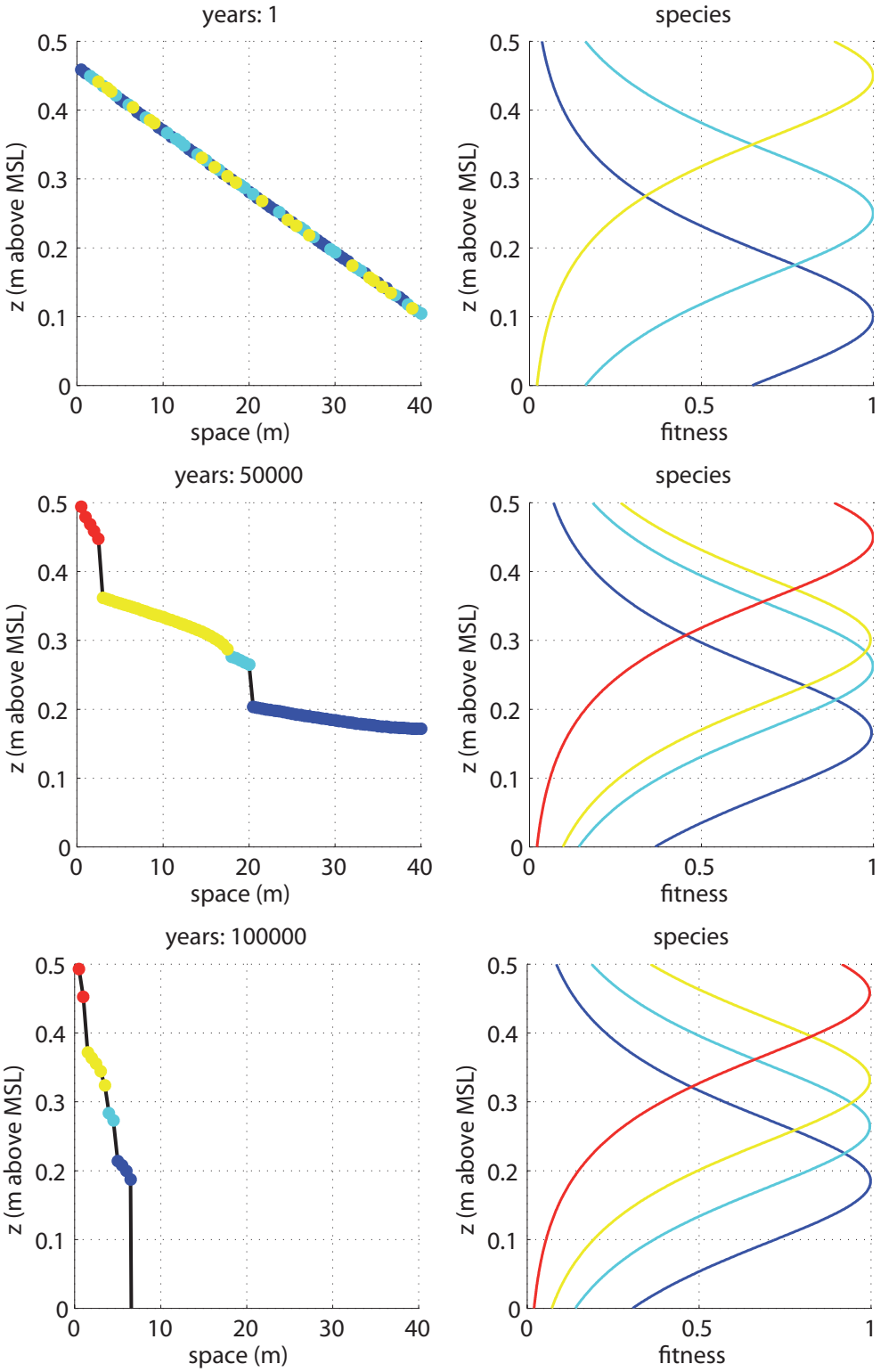

Figure 4.51: Analysis: 2. Time evolution of topography (left) and species (right). Rate of mutation adopted: 10 years. Mutation based on changing the fitness function mode and the maximum value. More details in the supplementary material.

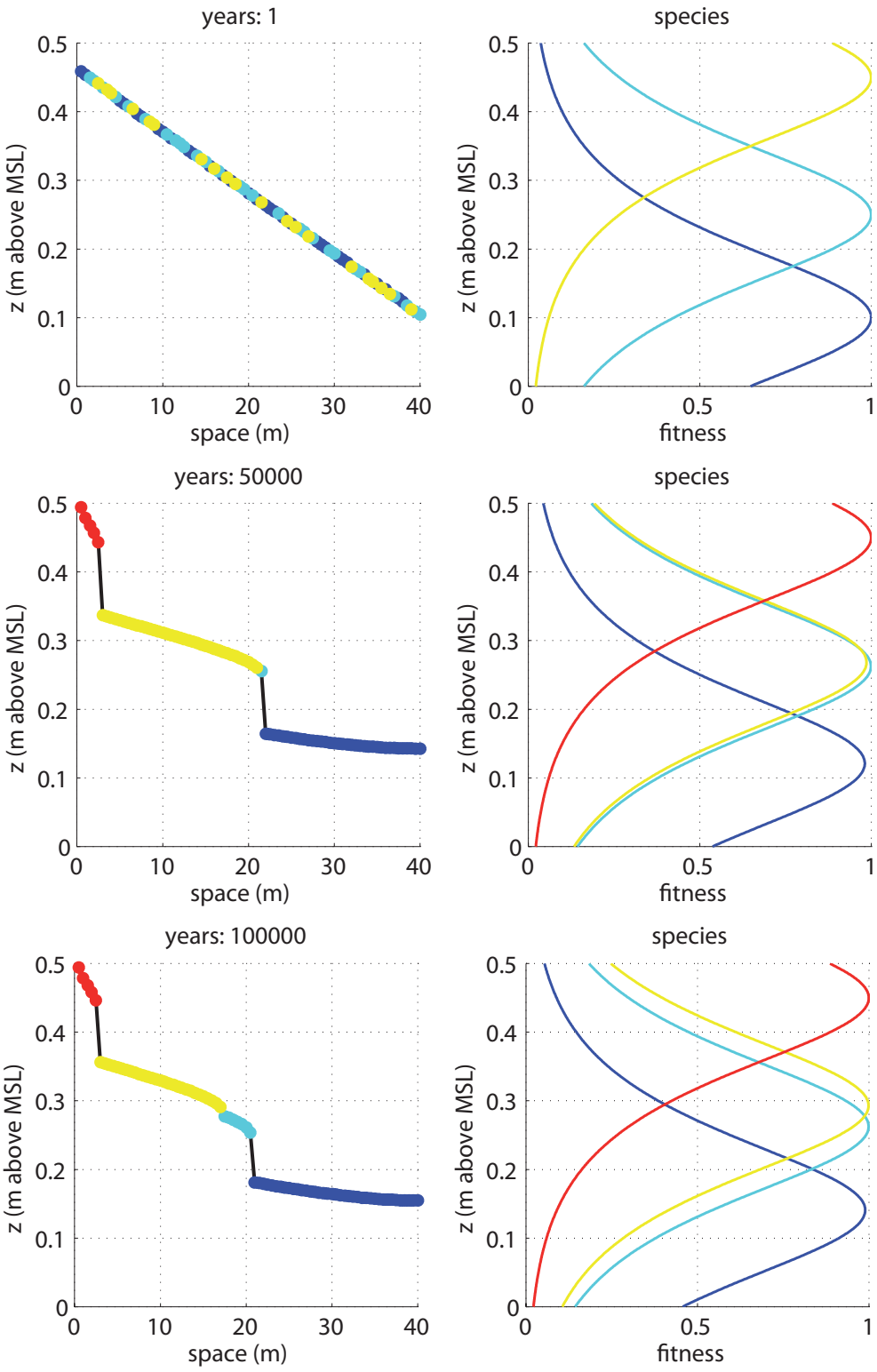

Figure 4.52: Analysis: 3. Time evolution of topography (left) and species (right). Rate of mutation adopted: 50 years. Mutation based on changing the fitness function mode (different from Analysis 1) and the maximum value. More details in the supplementary material

4.11.4 Analysis: 4

In figure 4.53 we show three time step configurations. The data are the same as in Analysis 3 except the initial species. Here we set, from low to high elevations, $\lambda_1 = 5$, $\lambda_2 = 10$, $\lambda_3 = 20$ (less specialized species at the low elevations) and $C_1 = 0.3$, $C_2 = 0.7$, $C_3 = 0.6$ as the maximum initial fitness values (less biomass productivity at the low elevations). We remember that $B_i(x,t) = f_i(z) \cdot B_0$, i is the generic species, B_0 is the maximum areal biomass productivity equal to 1000 g/m^2. The fittest species is chosen in the spatial competition as before. In the mutation process we change both the fitness function mode and its maximum value in a random way.

Supplementary material:

`Analysis_cited\RUN_03_04_2012_AnnualSpec_allSel_40_050dx_sechlR=lLVfixed_C_3SPini_mother_Mutation50_deltaz_fMax_rndSPini`

4.11.5 Analysis: 5

Analysis 5, 6 and 7 differ in the characteristic of the initial species adopted. In figure 4.54 the mutation process changes both the fitness function mode and its maximum value in a random way every 5 years. The increasing (or decreasing) in the elevation mode is a random value in the interval $[-0.02; +0.02]$m, greater than the one assumed in Analysis 2, 3, 4. Here we set, from low to high elevations, $\lambda_1 = 10$, $\lambda_2 = 10$, $\lambda_3 = 5$ (less specialized species at the high elevations) and $C_1 = 0.7$, $C_2 = 0.5$, $C_3 = 0.3$ as the maximum initial fitness values (less biomass productivity at the high elevations).

Supplementary material:

`Analysis_cited\RUN_03_04_2012_AnnualSpec_allSel_40_050dx_sechlR=lLVfixed_C_3SPini_mother_Mutation5_deltazAUM_fMax_rndSPini_3`

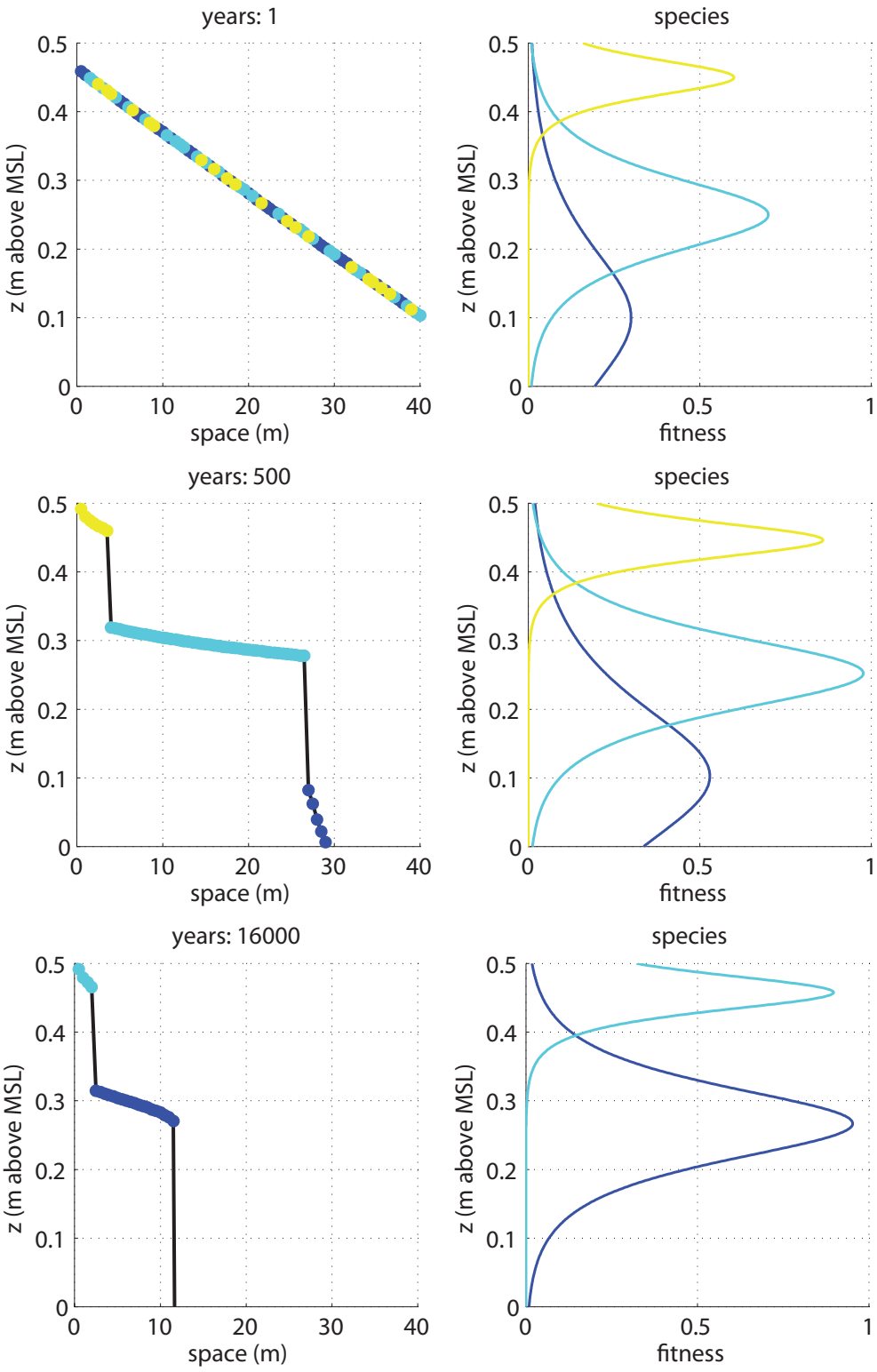

Figure 4.53: Analysis: 4. Time evolution of topography (left) and species (right). Rate of mutation adopted: 50 years. Mutation based on changing the fitness function mode and the maximum value. Initial species differ from Analysis 3. More details in the supplementary material

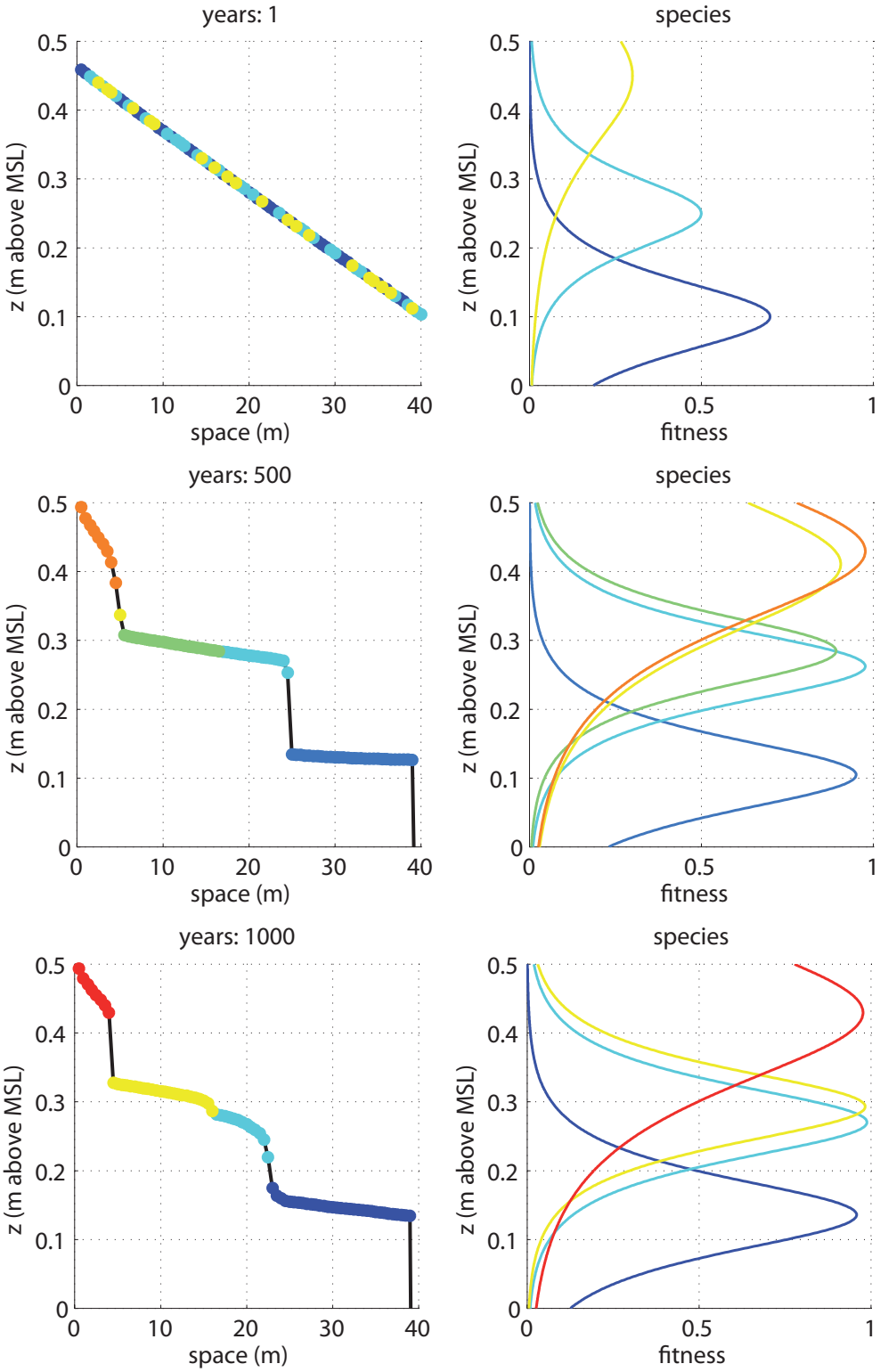

Figure 4.54: Analysis: 5. Time evolution of topography (left) and species (right). Rate of mutation adopted: 5 years. Mutation based on changing the fitness function mode and the maximum value. More details in the supplementary material

4.11.6 Analysis: 6

Analysis 6 (see figure 4.55) is the same as Analysis 5 except the fitness functions shape. Here we set, from low to high elevations, $\lambda_1 = 5$, $\lambda_2 = 10$, $\lambda_3 = 10$ (less specialized species at the low elevations) and, as Analysis 5, $C_1 = 0.7$, $C_2 = 0.5$, $C_3 = 0.3$ as the maximum initial fitness values (less biomass productivity at the high elevations).

In the mutation process we change both the fitness function mode (as Analysis 5) and its maximum value in a random way from 0 to 1.

Supplementary material:

`Analysis_cited\RUN_03_04_2012_AnnualSpec_allSel_40_050dx_sechlR=lLVfixed_C_3SPini_mother_Mutation5_deltazAUM_fMax_rndSPini_4`

4.11.7 Analysis: 7

Analysis 7 (see figure 4.56) has the same characteristic as Analysis 5 and 6 except the fitness functions shape. Here we set, for all the species i, $\lambda_i = 5$ and $C_i = 0.3$ as the maximum initial fitness values.

In the mutation process we change both the fitness function mode (as Analysis 5 and 6) and its maximum value in a random way from 0 to 1.

The salt marsh time instability is very quick (less then 5 hundred years) because the small biomass productivity chosen for the initial species; we remember that $B_i(x,t) = f_i(z) \cdot B_0$, B_0 is the maximum areal biomass productivity equal to 1000 g/m^2, then the initial species produce just 300 g/m^2.

Supplementary material:

`Analysis_cited\RUN_03_04_2012_AnnualSpec_allSel_40_050dx_sechlR=lLVfixed_C_3SPini_mother_Mutation5_deltazAUM_fMax_rndSPini_6`

4.11.8 Analysis: 8

Analysis 8 (see figure 4.57) has the same characteristic as Analysis 3 except the way of speciation about the mode fitness elevation. In this Analysis we

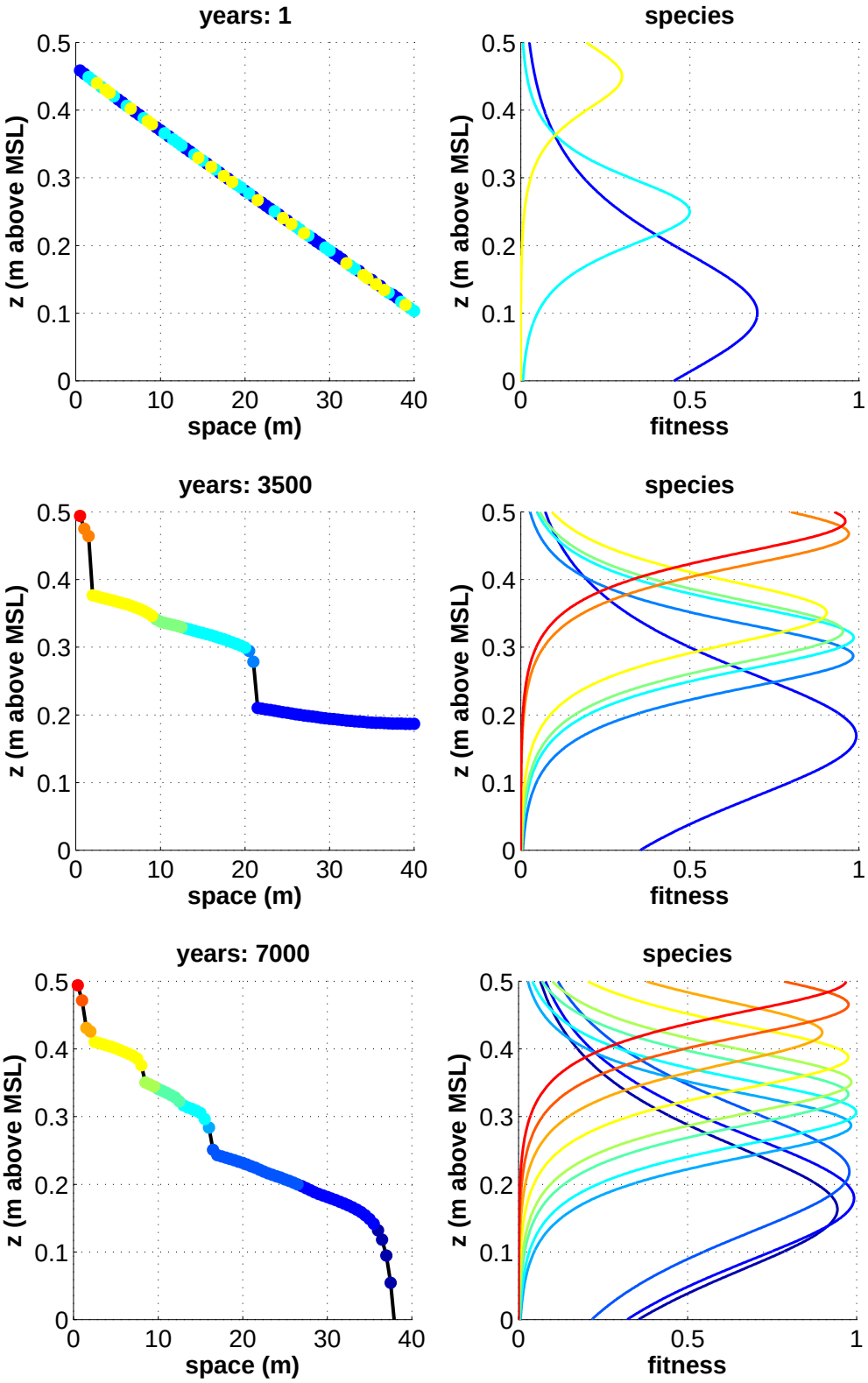

Figure 4.55: Analysis: 6. Time evolution of topography (left) and species (right). Rate of mutation adopted: 5 years. Mutation based on changing the fitness function mode and the maximum value. Initial species differ from Analysis 5. More details in the supplementary material

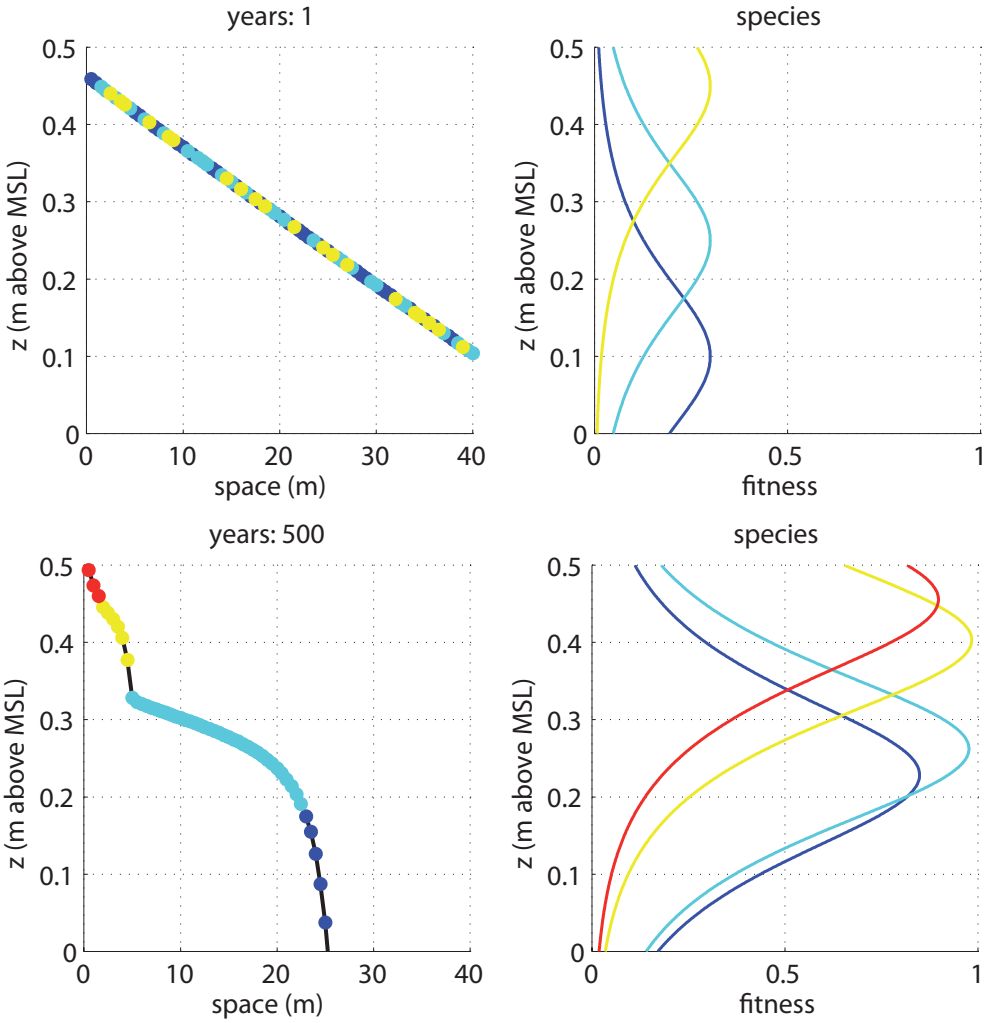

Figure 4.56: Analysis: 7. Time evolution of topography (left) and species (right). Rate of mutation adopted: 5 years. Mutation based on changing the fitness function mode and the maximum value. Initial species differ from Analysis 5 and 6. More details in the supplementary material

assume that the increasing (or decreasing) in the elevation mode is a random value in the interval $[-0.02; +0.02]$m, instead in Analysis 3, we remember that $z_{M(new)} = z_{M(old)} \pm 20\%\ z_{M(old)}$. Here we set, for all the species i, $\lambda_i = 5$ and $C_i = 1$ as the maximum initial fitness values.

In the mutation process we change both the fitness function mode and its maximum value in a random way from 0 to 1.

Supplementary material:

`Analysis_cited\RUN_03_04_2012_AnnualSpec_allSel_40_050dx_sechlR=lLVfixed_C_3SPini_mother_Mutation50_deltazAUM_fMax`

4.11.9 Analysis: 9

Analysis 9 (see figure 4.58) has the same characteristic as Analysis 8 except the the value C_i assumed for the initial fitness functions. Here we set, for all the species i, $\lambda_i = 5$ (like Analysis 8) and $C_i = 0.3$ as the maximum initial fitness values.

In the mutation process we change both the fitness function mode and its maximum value in a random way from 0 to 1.

Supplementary material:

`Analysis_cited\RUN_03_04_2012_AnnualSpec_allSel_40_050dx_sechlR=lLVfixed_C_3SPini_mother_Mutation50_deltazAUM_fMax_rndSPini_5`

4.11.10 Analysis: 10

In Analysis 10 (see figure 4.59) we assume a time interval of mutation equal to 2 years. In this Analysis we assume that the increasing (or decreasing) in the elevation mode is a random value in the interval $[-0.005; +0.005]$m. Here we set, for all the species i, $\lambda_i = 5$ and $C_i = 1$ as the maximum initial fitness values. The suspend sediment concentration here is equal to $C_0 = 40$ mg/l, double than the reference value used.

In the mutation process we change both the fitness function mode and its maximum value in a random way from 0 to 1.

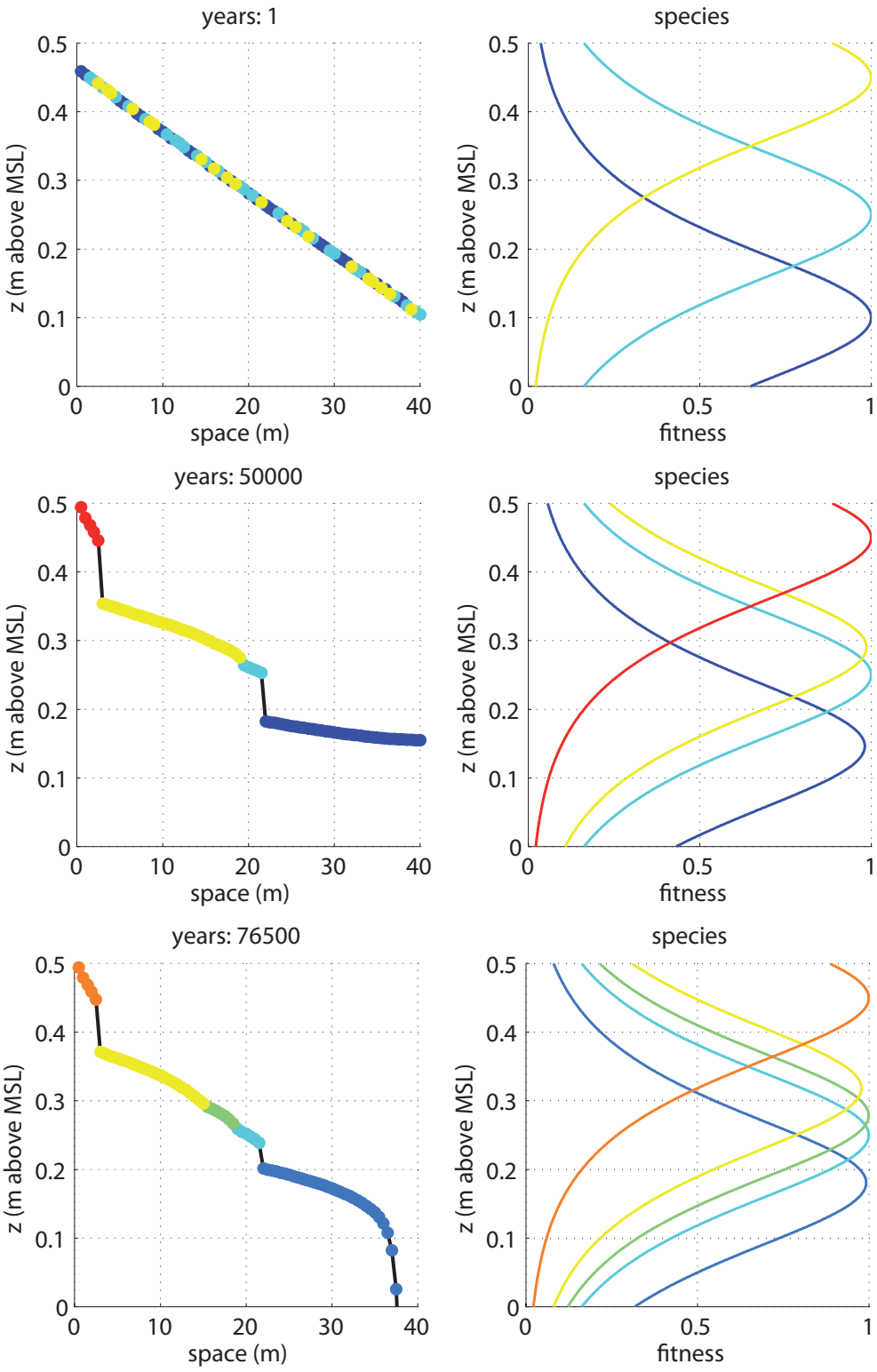

Figure 4.57: Analysis: 8. Time evolution of topography (left) and species (right). Rate of mutation adopted: 50 years. Mutation based on changing the fitness function mode (more than Analysis 3) and the maximum value. More details in the supplementary material

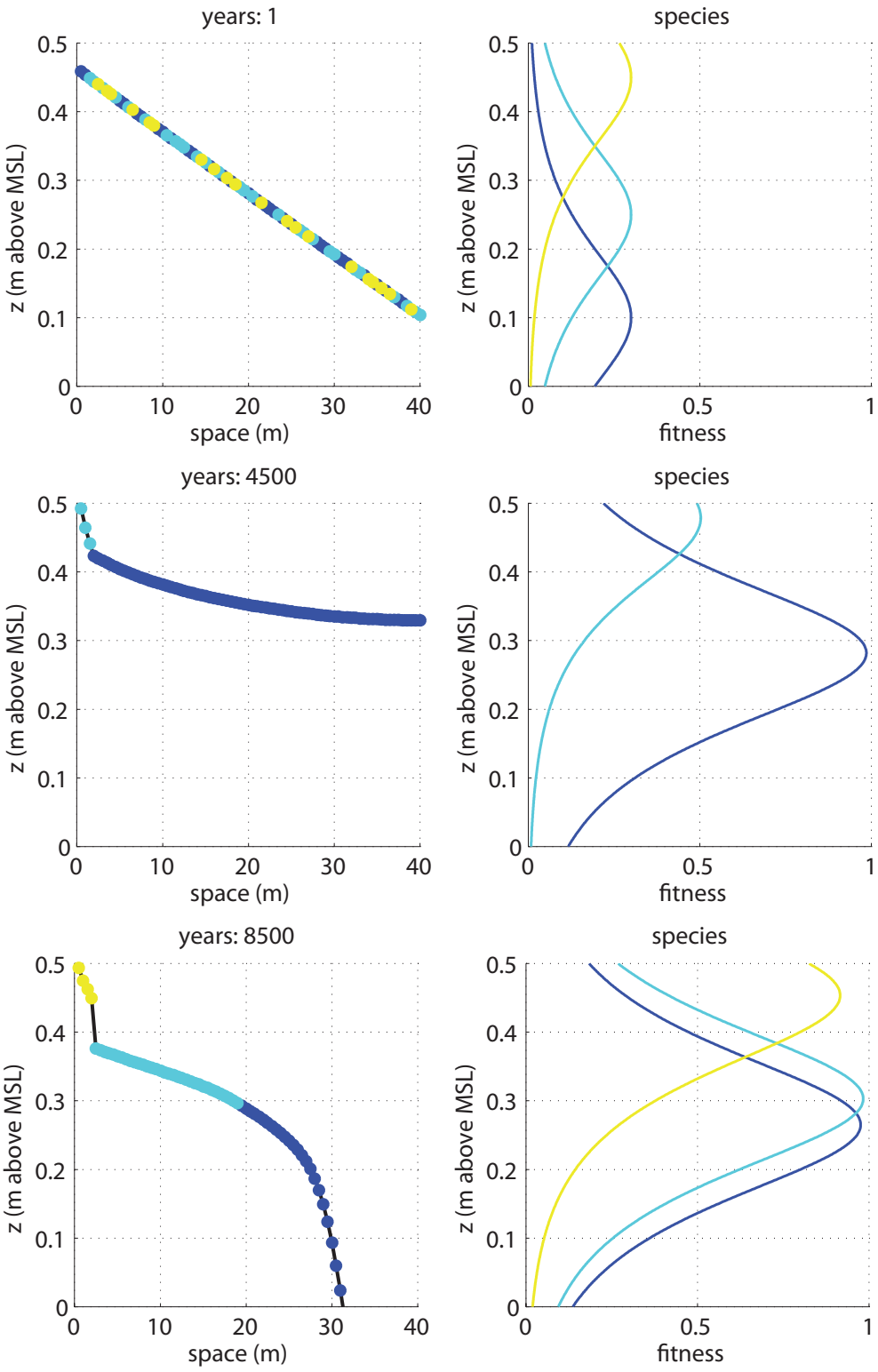

Figure 4.58: Analysis: 9. Time evolution of topography (left) and species (right). Rate of mutation adopted: 50 years. Mutation based on changing the fitness function mode (like Analysis 8) and the maximum value. Initial species differ from Analysis 8. More details in the supplementary material

Supplementary material:

`Analysis_cited\RUN_03_04_2012_AnnualSpec_allSel_40_050dx_sechlR=lLVfixed_C_3SPini_mother_Mutation2_deltaz_C040_CORRETTO`

4.11.11 Analysis: 11

In Analysis 11 (see figure 4.60) is the same as Analysis 10 except the frequency of mutation: here we assume a time interval equal to 10 years. For all the species i, $\lambda_i = 5$ and $C_i = 1$ as the maximum initial fitness values. The suspend sediment concentration (as Analysis 10) is equal to $C_0 = 40$ mg/l.

In the mutation process we change both the fitness function mode and its maximum value in a random way from 0 to 1.

Supplementary material:

`Analysis_cited\RUN_03_04_2012_AnnualSpec_allSel_40_050dx_sechlR=lLVfixed_C_3SPini_mother_Mutation10_deltaz_C040_CORRETTO`

4.11.12 Analysis: 12

In Analysis 12 (see figure 4.61), in the mutation process we change both the fitness function mode and its maximum value in a random way every 50 years. The increasing (or decreasing) in the elevation mode is a random value in the interval $[-0.005; +0.005]$m.

We consider three initial species i whose scale parameter is equal to $\lambda_i = 5$ and $C_i = 1$. The species here, spatial compete randomly selecting a species with a probability proportional to $f_i(z_k)$: $p(i, x_k) = f_i(z_k)/\sum_j f_j(z_k)$ ("stochastic competition" mechanism), k-site, x-spatial coordinate, z-elevation, i-, j-species.

At the beginning of the evolution process, the topography is quite irregular and more similar to the real topography observed, but over time it becomes quite flat, probably correlated with the way of changing the species (e.g. frequency of mutation, elevation mode changing or type of competition mechanism).

Supplementary material:

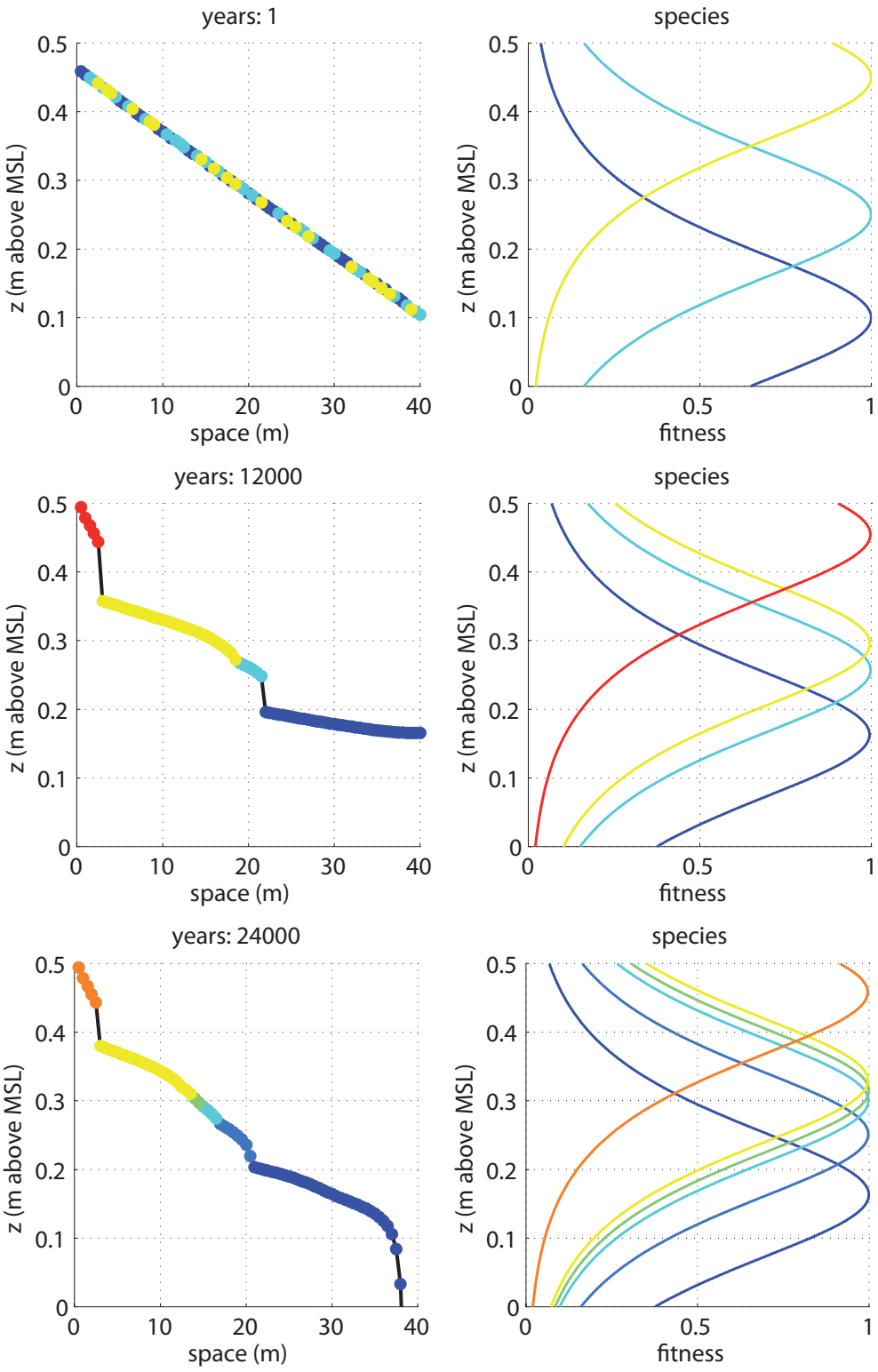

Figure 4.59: Analysis: 10. Time evolution of topography (left) and species (right). Rate of mutation adopted: 2 years. Mutation based on changing the fitness function mode and the maximum value. $C_0 = 40$ mg/l. More details in the supplementary material

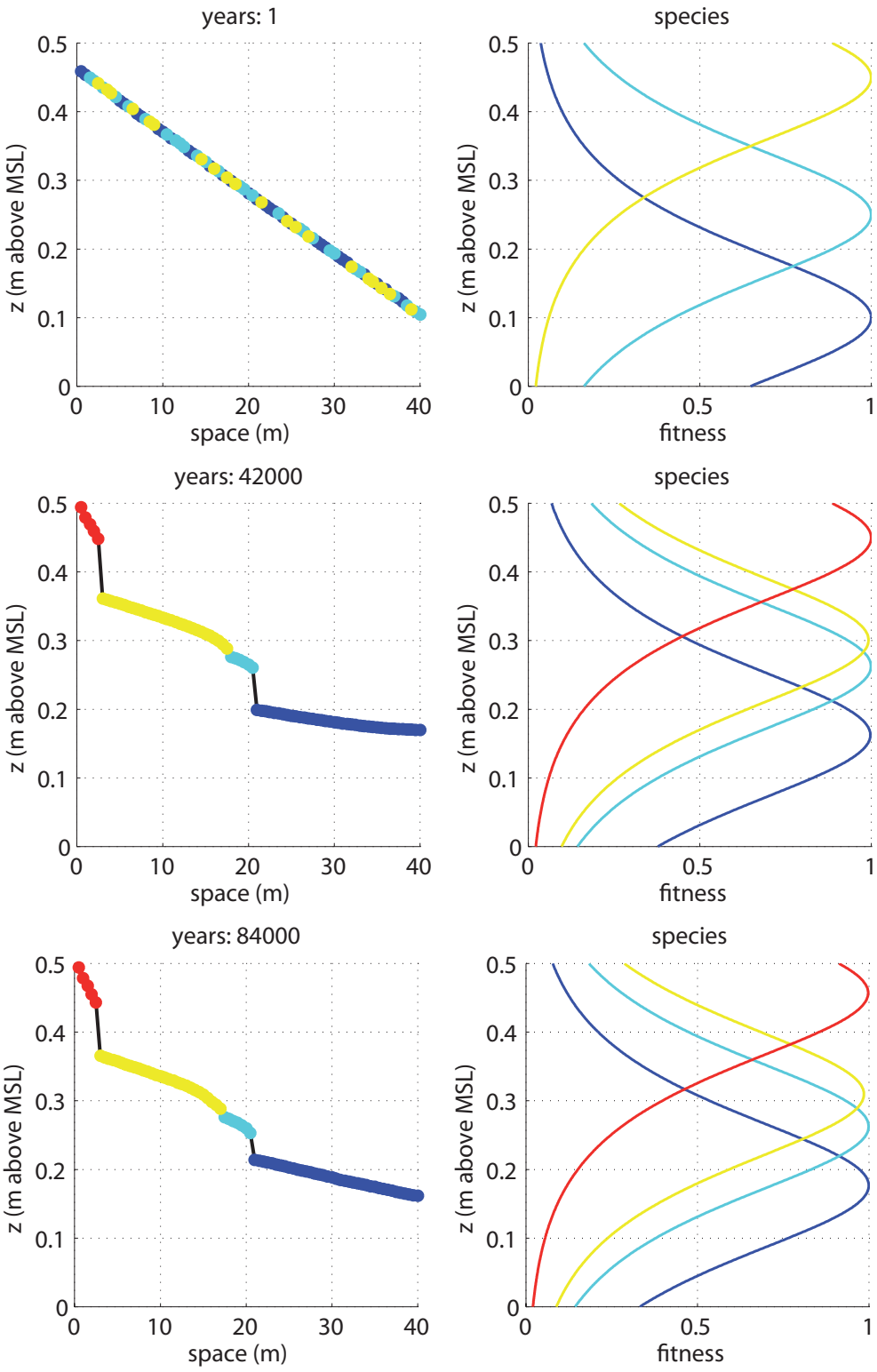

Figure 4.60: Analysis: 11. Time evolution of topography (left) and species (right). Rate of mutation adopted: 10 years. Mutation based on changing the fitness function mode and the maximum value. $C_0 = 40$ mg/l. More details in the supplementary material

`Analysis_cited\RUN_03_04_2012_AnnualSpec_allSel_40_050dx_sechlR=lLVfixed_C_3SPini_mother_Mutation50_deltaz_cumulata`

4.11.13 Analysis: 13

In Analysis 13 (see figure 4.62), in the mutation process we change both the fitness function mode and its maximum value in a random way every 50 years. The increasing (or decreasing) in the elevation mode is a random value in the interval $[-0.005; +0.005]$m.

We consider three initial species i whose scale parameter is equal to $\lambda_i = 5$ and $C_i = 1$. Differ from Analysis 12, here, the species spatial compete randomly selecting a species with a probability proportional to $f_i(z_k)$: $p(i, x_k) = f_i^2(z_k)/\sum_j f_j^2(z_k)$ (non linear "stochastic competition" mechanism), k-site, x-spatial coordinate, z-elevation, i-, j-species.

Supplementary material:

`Analysis_cited\RUN_03_04_2012_AnnualSpec_allSel_40_050dx_sechlR=lLVfixed_C_3SPini_mother_Mutation50_deltaz_cumulata^2`

4.11.14 Analysis: 14

Analysis 14 (see figure 4.63), is similar to Analysis 13 except the spatial competition mechanism. Here, the species spatial compete randomly selecting a species with a probability proportional to $f_i(z_k)$: $p(i, x_k) = f_i^5(z_k)/\sum_j f_j^5(z_k)$ (non linear "stochastic competition" mechanism), k-site, x-spatial coordinate, z-elevation, i-, j-species. In this way, about the spatial competition, we tend to maximize the big probability and minimize the small one. In fact, the terraces-like structures reappear as when we adopt the "fittest-takes-it-all" competition mechanism.

Supplementary material:

`Analysis_cited\RUN_03_04_2012_AnnualSpec_allSel_40_050dx_sechlR=lLVfixed_C_3SPini_mother_Mutation50_deltaz_cumulata^5`

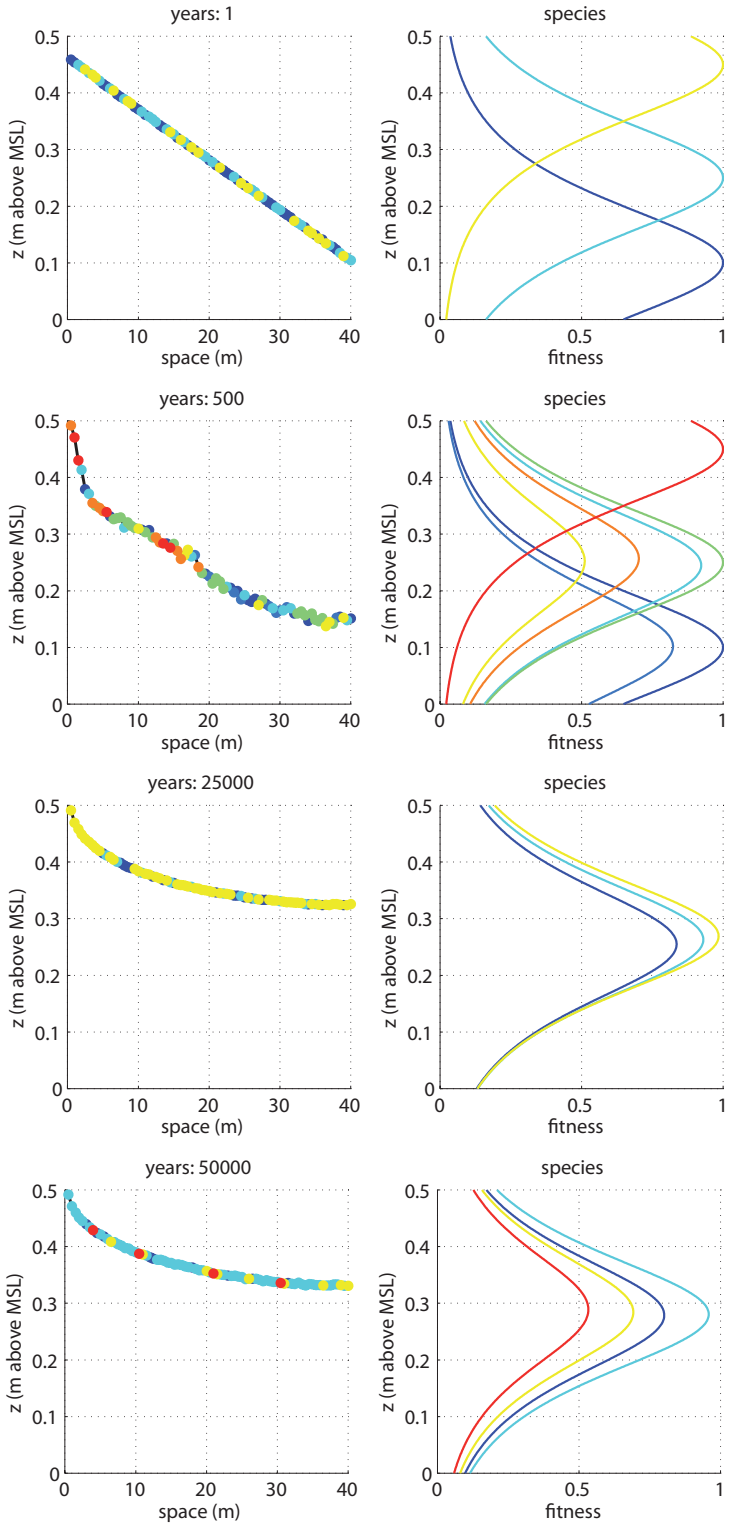

Figure 4.61: Analysis: 12. Time evolution of topography (left) and species (right). Rate of mutation adopted: 50 years. Mutation based on changing the fitness function mode and the maximum value. Linear stochastic formulation adopted in the spatial competition. More details in the supplementary material

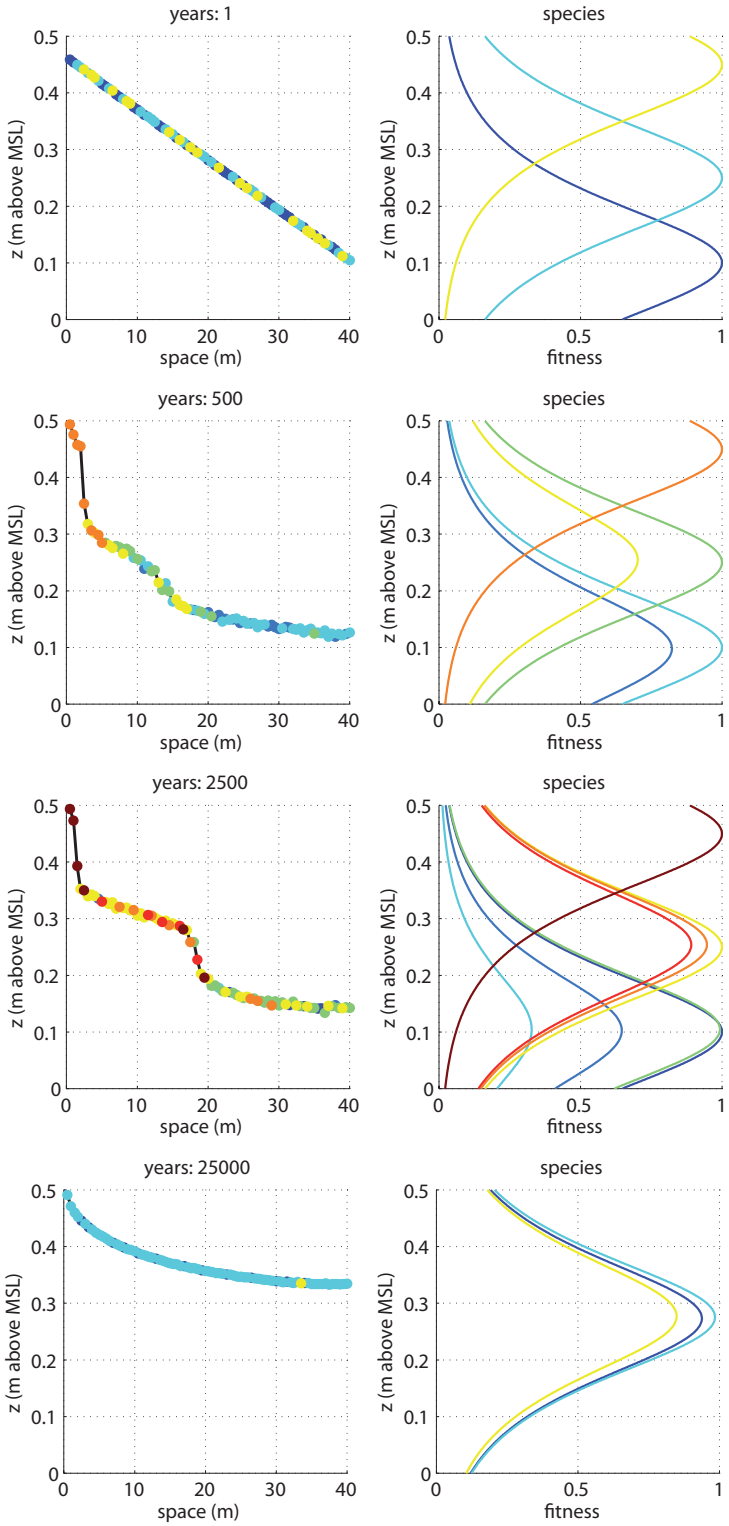

Figure 4.62: Analysis: 13. Time evolution of topography (left) and species (right). Rate of mutation adopted: 50 years. Mutation based on changing the fitness function mode and the maximum value. Non-linear stochastic formulation adopted in the spatial competition (differ from Analysis 12). More details in the supplementary material

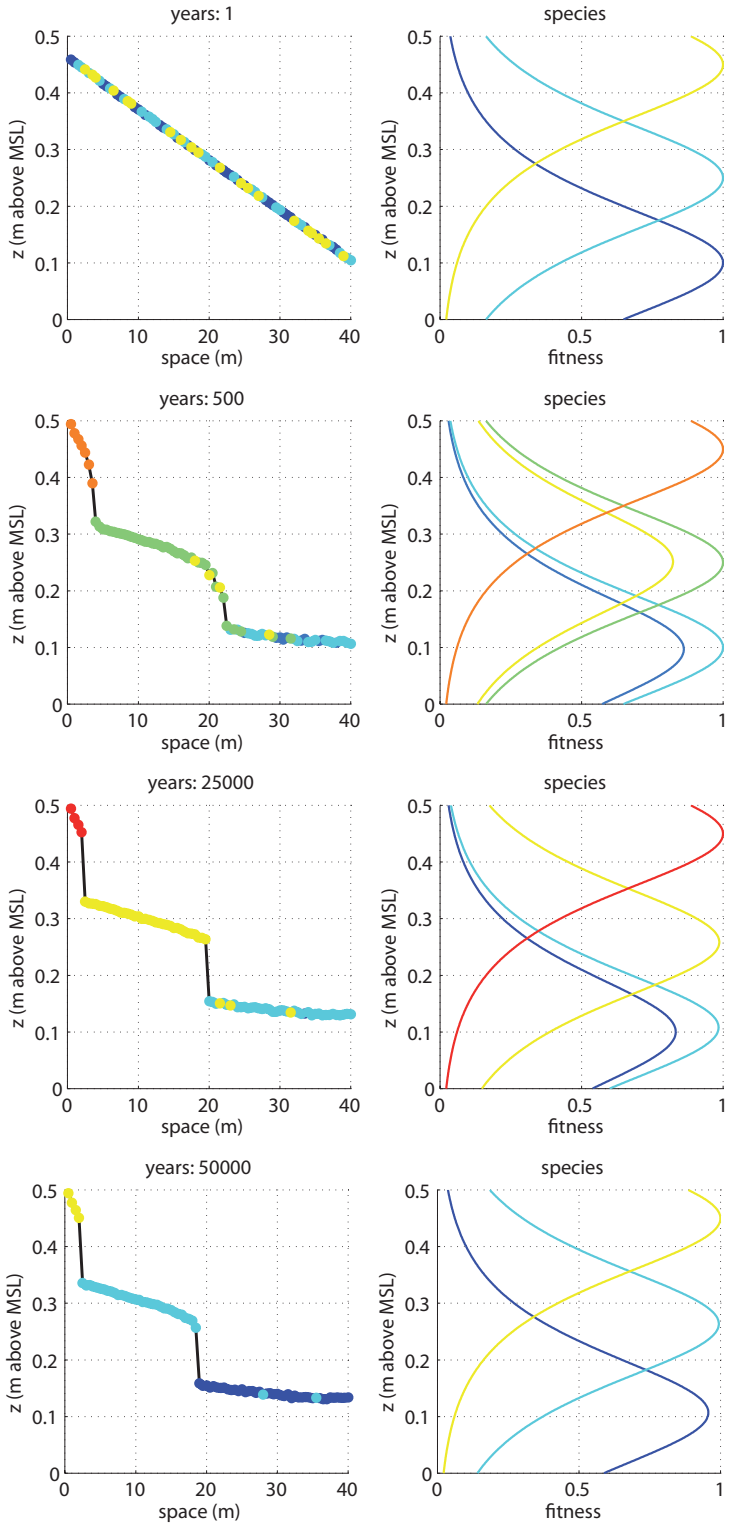

Figure 4.63: Analysis: 14. Time evolution of topography (left) and species (right). Rate of mutation adopted: 50 years. Mutation based on changing the fitness function mode and the maximum value. Non-linear stochastic formulation adopted in the spatial competition (differ from Analysis 12 and 13). More details in the supplementary material

4.11.15 Analysis: 15

Analysis 15 (see figure 4.64), is similar to Analysis 13 and 14, except the spatial competition mechanism.
Here, the species spatial compete randomly selecting a species with a probability proportional to $f_i(z_k)$: $p(i, x_k) = f_i^{10}(z_k)/\sum_j f_j^{10}(z_k)$ (non linear "stochastic competition" mechanism), k-site, x-spatial coordinate, z-elevation, i-, j-species. As in Analysis 14, we maximize the big probability and minimize the small one, tending to the case in Analysis 3, where we select the species with the "fittest" rule.

Supplementary material:

`Analysis_cited\RUN_03_04_2012_AnnualSpec_allSel_40_050dx_sechlR=lLVfixed_C_3SPini_mother_Mutation50_deltaz_cumulata^10`

4.11.16 Analysis: 16

In figure 4.65 the mutation process changes only the fitness function mode every year. The mode changing is equal to $z_{M(new)} = z_{M(old)} \pm 20\%\ z_{M(old)}$ then, high elevations change more than the low ones. Here we set, from low to high elevations, $\lambda_1 = 20$, $\lambda_2 = 30$, $\lambda_3 = 40$ (less specialized species at the low elevations, but in general very specialized species) and $C_i = 1$, as the maximum initial fitness values (constant during the simulation, not subjected to change during the evolution process).

Being the frequency of mutation so high, what happens is that every year a new species is able to colonize a small elevation niche in the topography shape because the "daughter" species are very fruitful ($C = 1$ for all the species during the simulation). This is why we observe a sort of continuous spectrum of species perfect adapted both to the low elevations and to the high ones.

Supplementary material:

`Analysis_cited\RUN_03_04_2012_AnnualSpec_allSel_40_050dx_sechlR=lLVfixed_3SPini_mother`

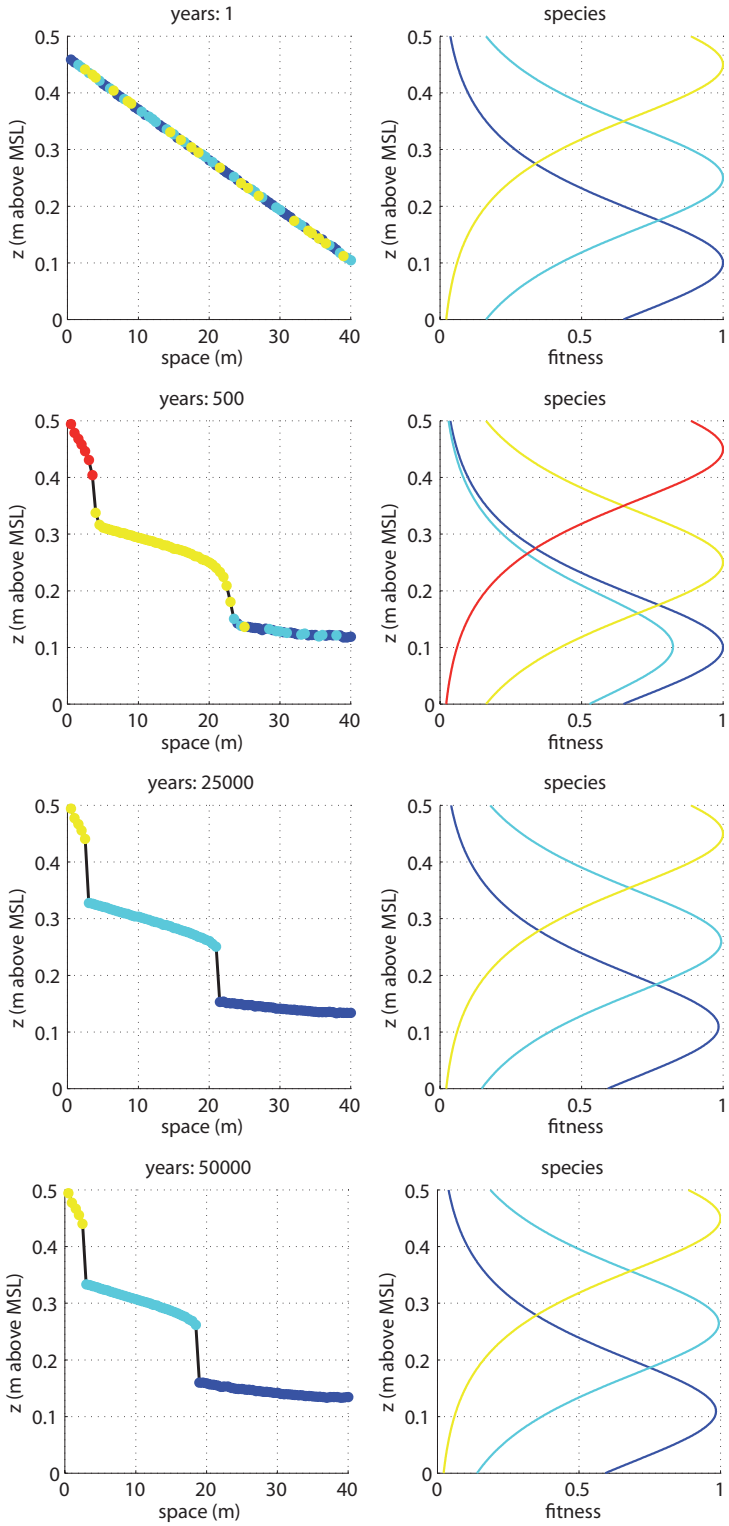

Figure 4.64: Analysis: 15. Time evolution of topography (left) and species (right). Rate of mutation adopted: 50 years. Mutation based on changing the fitness function mode and the maximum value. Non-linear stochastic formulation adopted in the spatial competition (differ from Analysis 12, 13 and 14). More details in the supplementary material

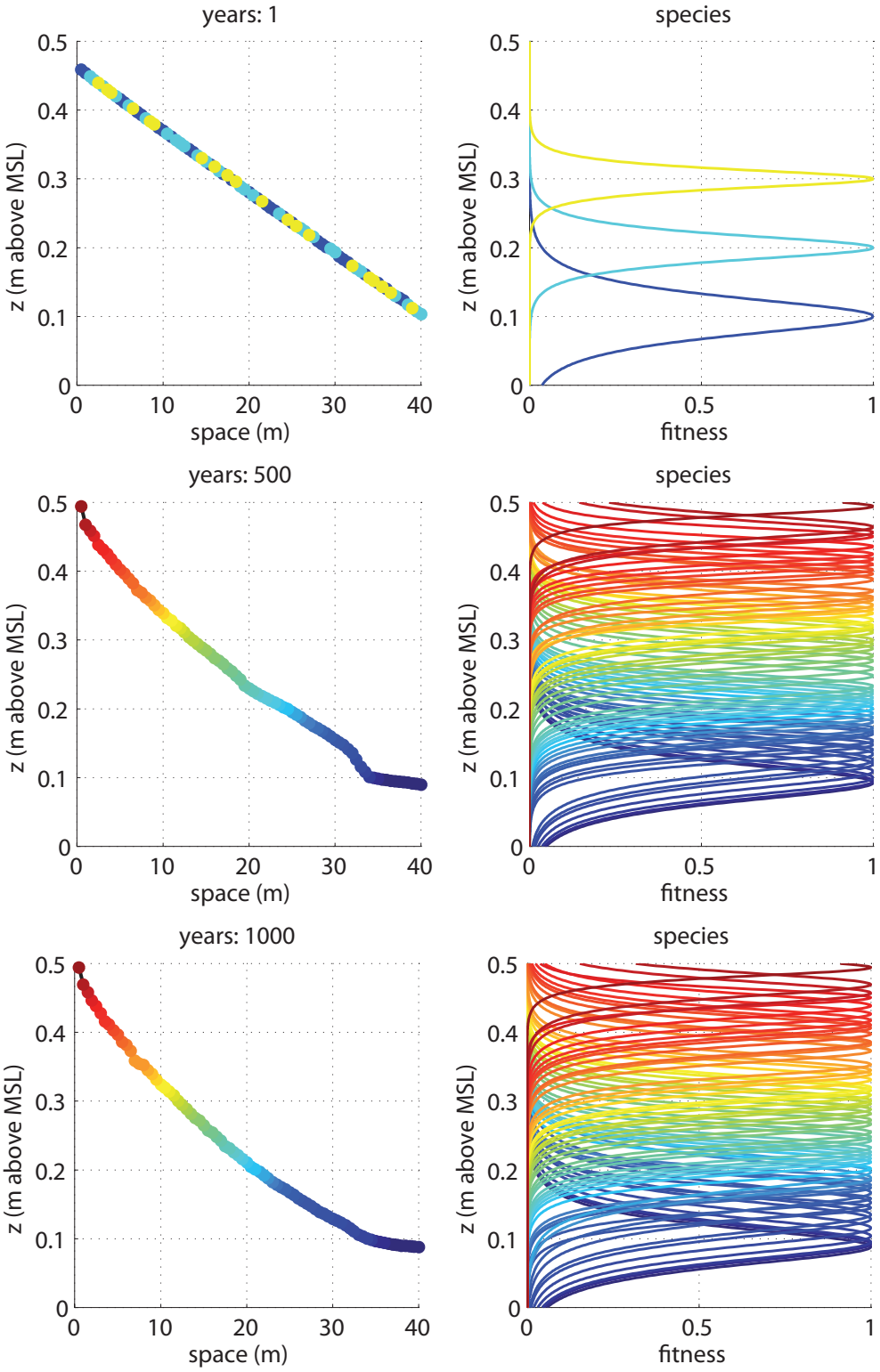

Figure 4.65: Analysis: 16. Time evolution of topography (left) and species (right). Rate of mutation adopted: 1 years. Mutation based on changing the fitness function mode. More details in the supplementary material

4.11.17 Analysis: 17

In figure 4.66 the mutation process changes the fitness function mode and the maximum value every year. The mode changing is equal to $z_{M(new)} = z_{M(old)} \pm 20\%\ z_{M(old)}$ then, high elevations change more that the low ones. Here we set, from low to high elevations, $\lambda_1 = 20$, $\lambda_2 = 30$, $\lambda_3 = 40$ (as Analysis 16) and $C_i = 1$ for the initial species.

Also in this Analysis, like the 16^{th}, every year a new species is generated. We observe a sort of continuous spectrum of species perfect adapted to the low elevations as to the high ones, but, because of the "daughter" species could be not so fruitful, like the case in which the maximum value of the "daughter" species was equal to 1 (Analysis 16), here the species are not so good to colonize a small elevation niche in the topography shape every year. This is why the salt marsh topography is not time stable as in Analysis 16.

Supplementary material:

`Analysis_cited\RUN_03_04_2012_AnnualSpec_allSel_40_050dx_sechlR=1LVfixed_C_3SPini_mother`

In figure 4.67 we present the time sequence when the elevation of the last site goes down under the mean sea level.

4.11.18 Analysis: 18

Analysis 18 (see figure 4.68) is similar to Analysis1 except the time frequency of mutation adopted. Here, the time step of mutation is equal to 100 years, i.e. a new mutation every 100 years. In the mutation process we change both the fitness function mode and its maximum value in a random way. The mode changing is equal to $z_{M(new)} = z_{M(old)} \pm 20\%\ z_{M(old)}$ then, high elevations change more than the low ones.

We set symmetric fitness functions with $\lambda_1 = 20$, $\lambda_2 = 30$, $\lambda_3 = 40$ from low to high elevations, less specialized species at the low elevations and $C_i = 1$ for the i species. In the spatial competition, the fittest species is preferred in the evolution theory.

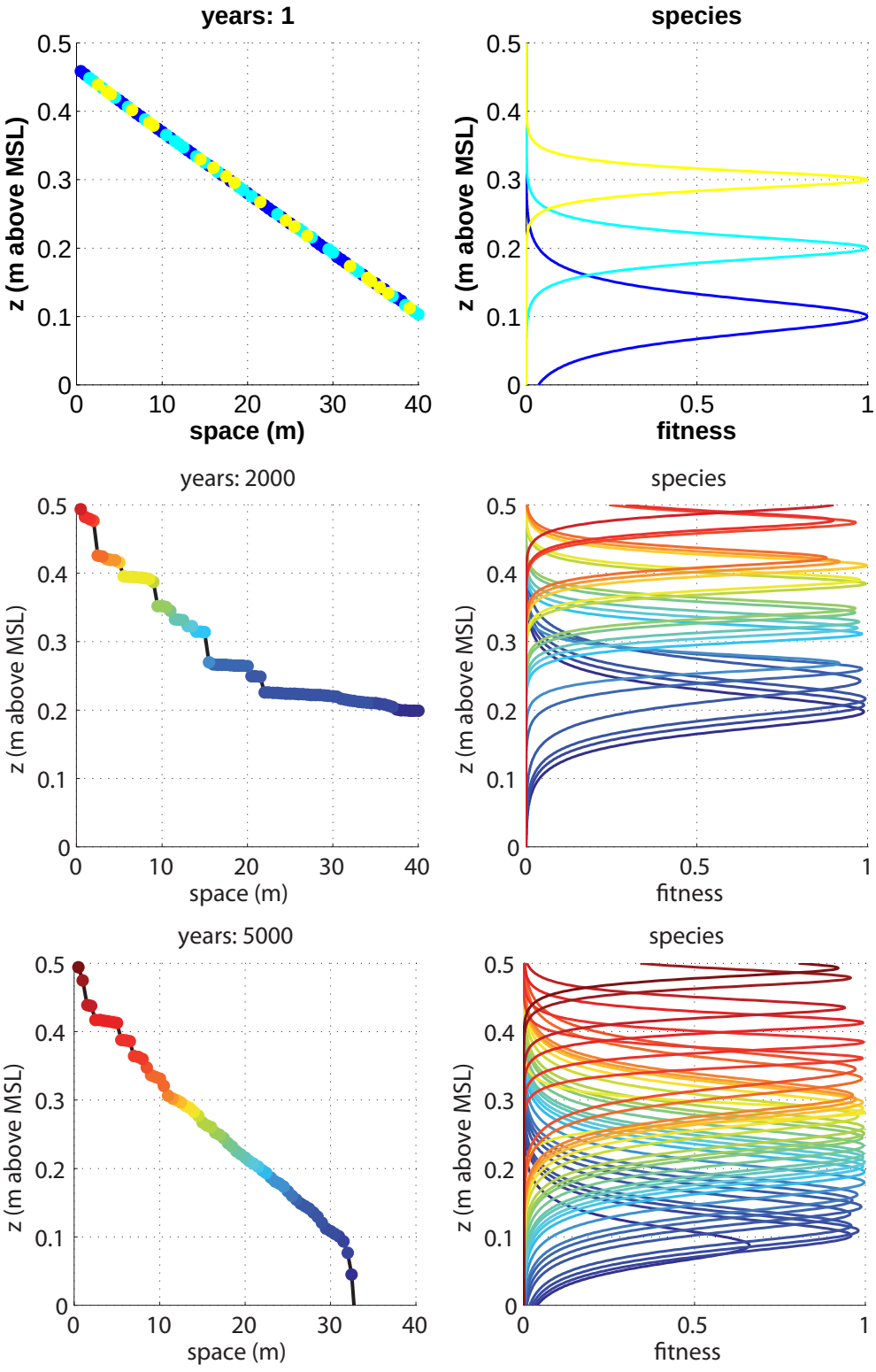

Figure 4.66: Analysis: 17. Time evolution of topography (left) and species (right). Rate of mutation adopted: 1 years. Mutation based on changing the fitness function mode and the maximum value. More details in the supplementary material

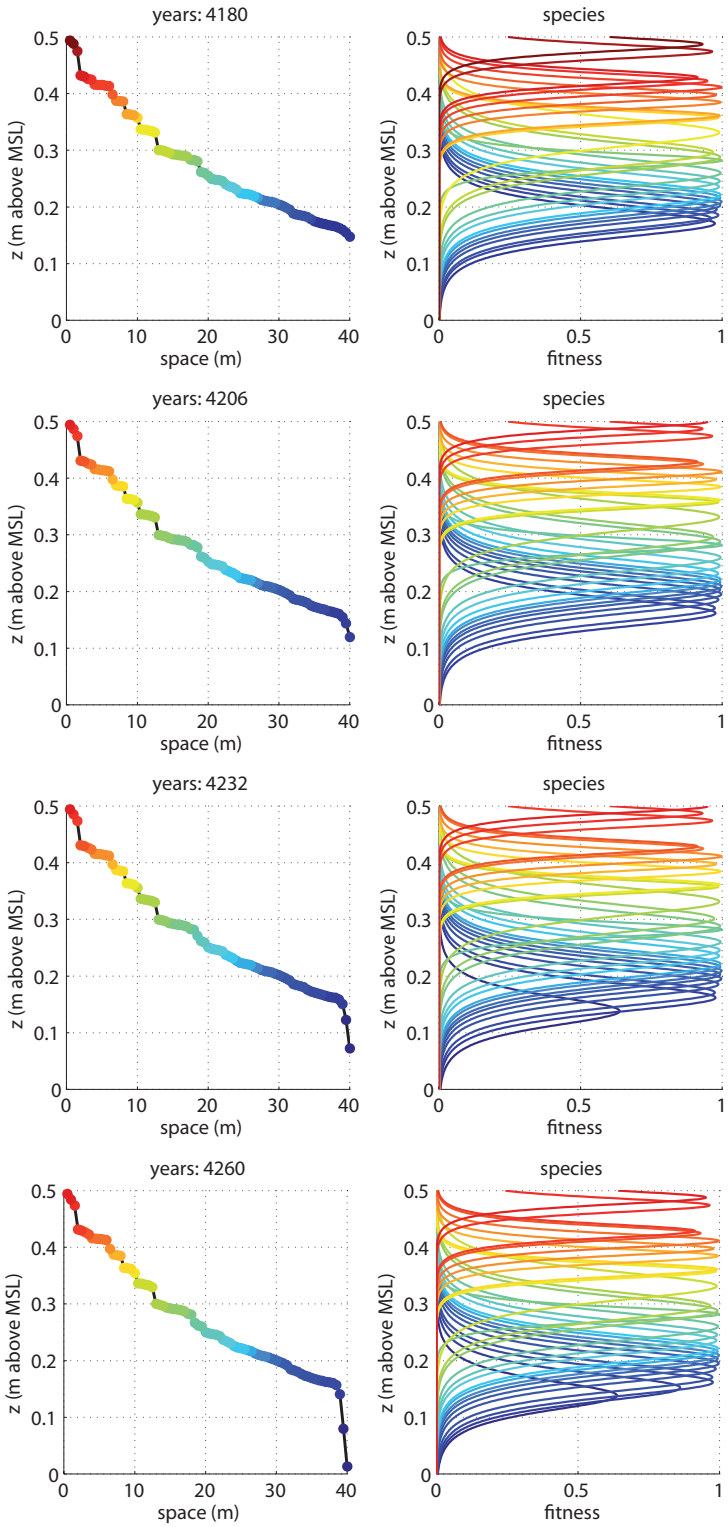

Figure 4.67: Analysis: 17 – time sequence. Time evolution of topography (left) and species (right). Time sequence when the elevation of the last site goes down under the mean sea level. More details in the supplementary material

Supplementary material:

`Analysis_cited\RUN_03_04_2012_AnnualSpec_allSel_40_050dx_sechlR=lLVfixed_C_3SPini_mother_Mutation100`

4.11.19 Analysis: 19

In Analysis 19 we consider three coupled ways of mutation: every 100 year we change the elevation mode of the fitness functions (like in Analysis 1), the maximum value of them (uniformly random between 0 and 1) and finally we generate a random value of the variation in the interval $[0.05; 0.4]$, thus the scale parameter in between the minimum value $\lambda = 5$ and the maximum one $\lambda = 40$, remembering that $V = 2/\lambda$ with symmetric fitness functions. Here the simulation begin with three different species whose $\lambda = 5$ and $C = 1$. The species also spatial compete following the fittest-takes-it all rule.

Supplementary material:

`Analysis_cited\RUN_03_04_2012_AnnualSpec_allSel_40_050dx_sechlR=lLVvariable_C_3SPini_mother_Mutation50_lambda5`

4.11.20 Analysis: 20

Analysis 20 is the same as Analysis 19 except the initial scale parameter value. Here we assume $\lambda = 20$.

Supplementary material:

`Analysis_cited\RUN_03_04_2012_AnnualSpec_allSel_40_050dx_sechlR=lLVvariable_C_3SPini_mother_Mutation50_lambda20`

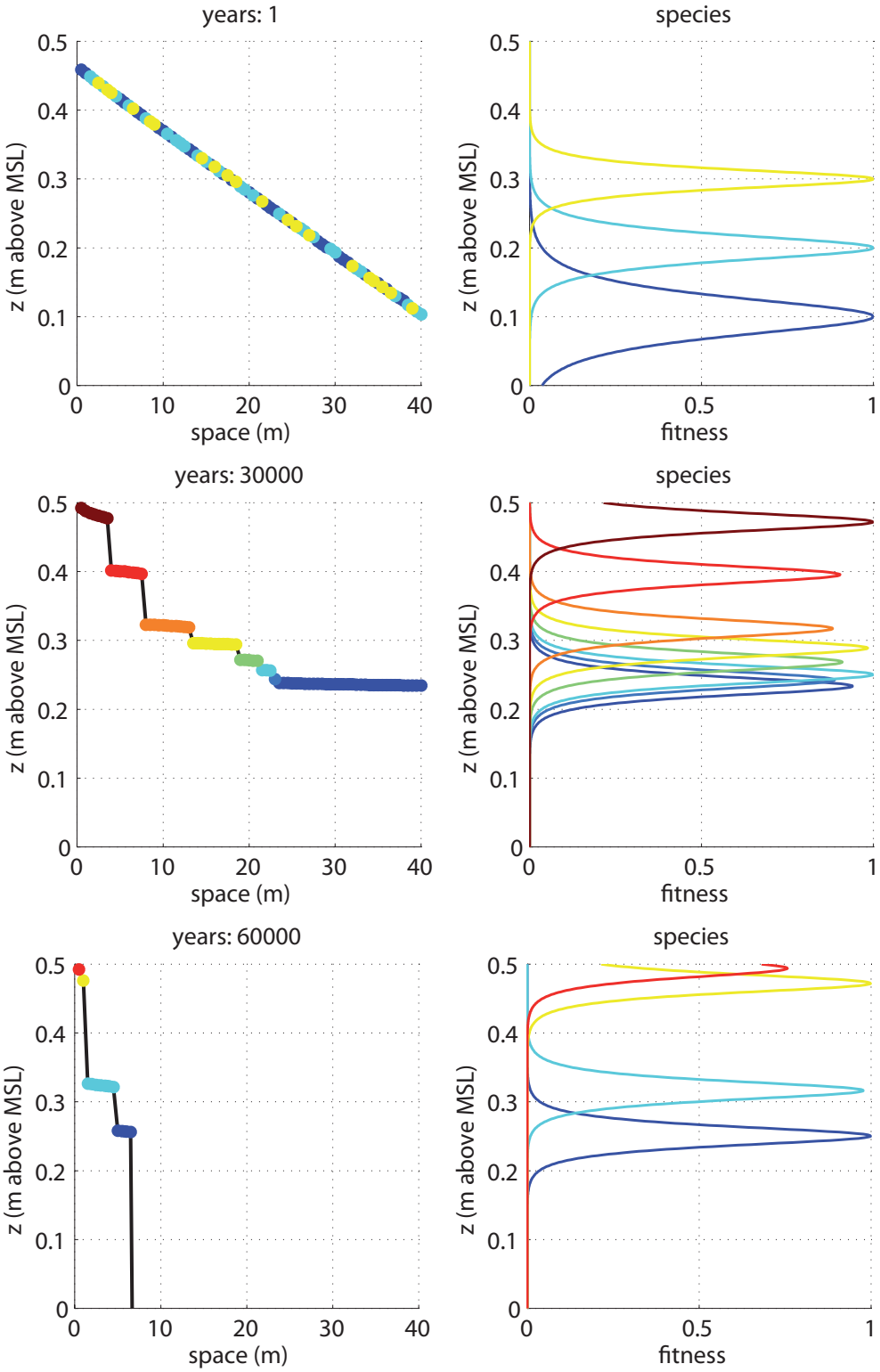

Figure 4.68: Analysis: 18. Time evolution of topography (left) and species (right). Rate of mutation adopted: 100 years. Mutation based on changing the fitness function mode and the maximum value. More details in the supplementary material

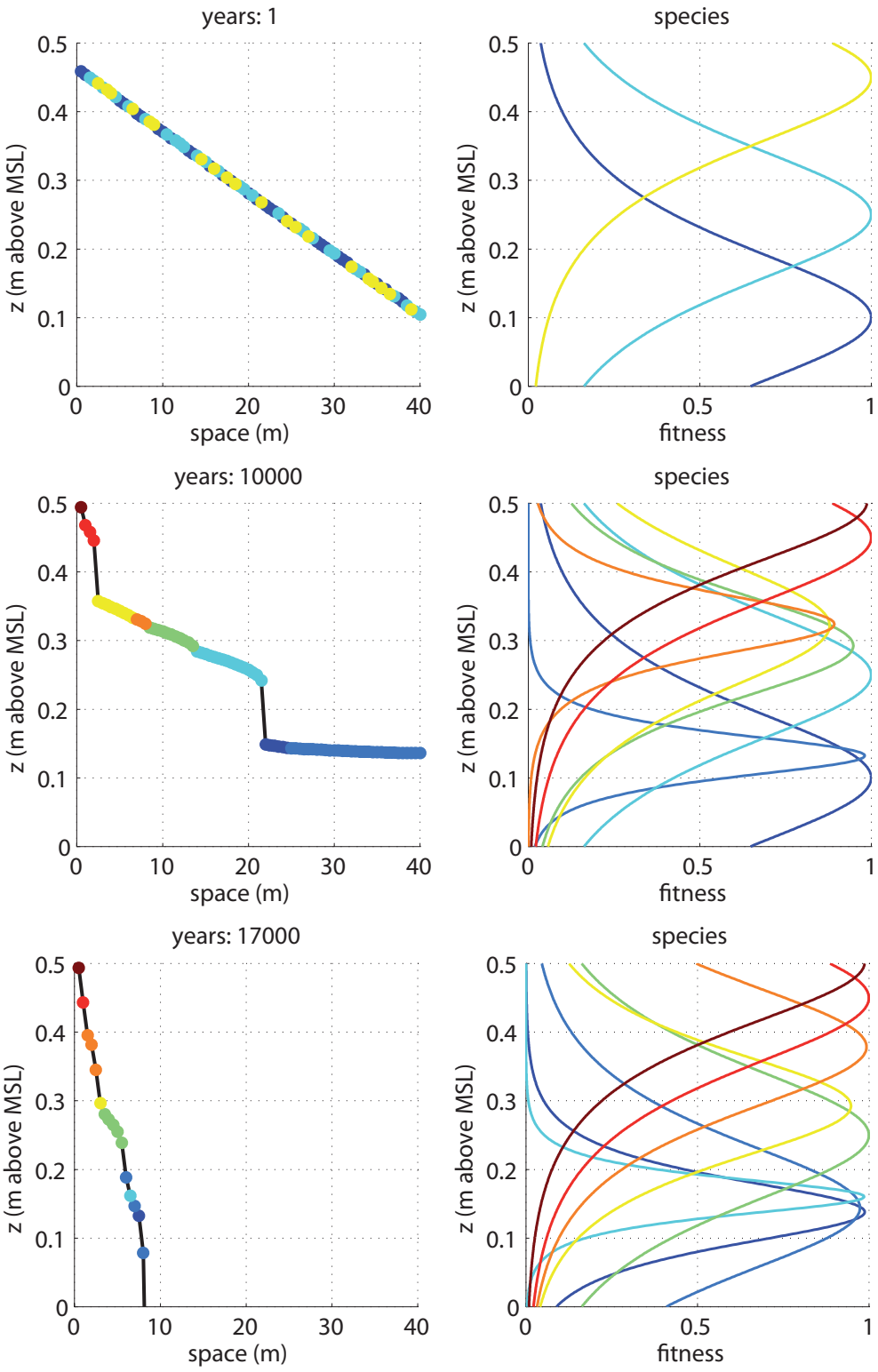

Figure 4.69: Analysis: 19. Time evolution of topography (left) and species (right). Rate of mutation adopted: 50 years. Mutation based on changing the fitness function mode, the maximum value and the variation value. More details in the supplementary material

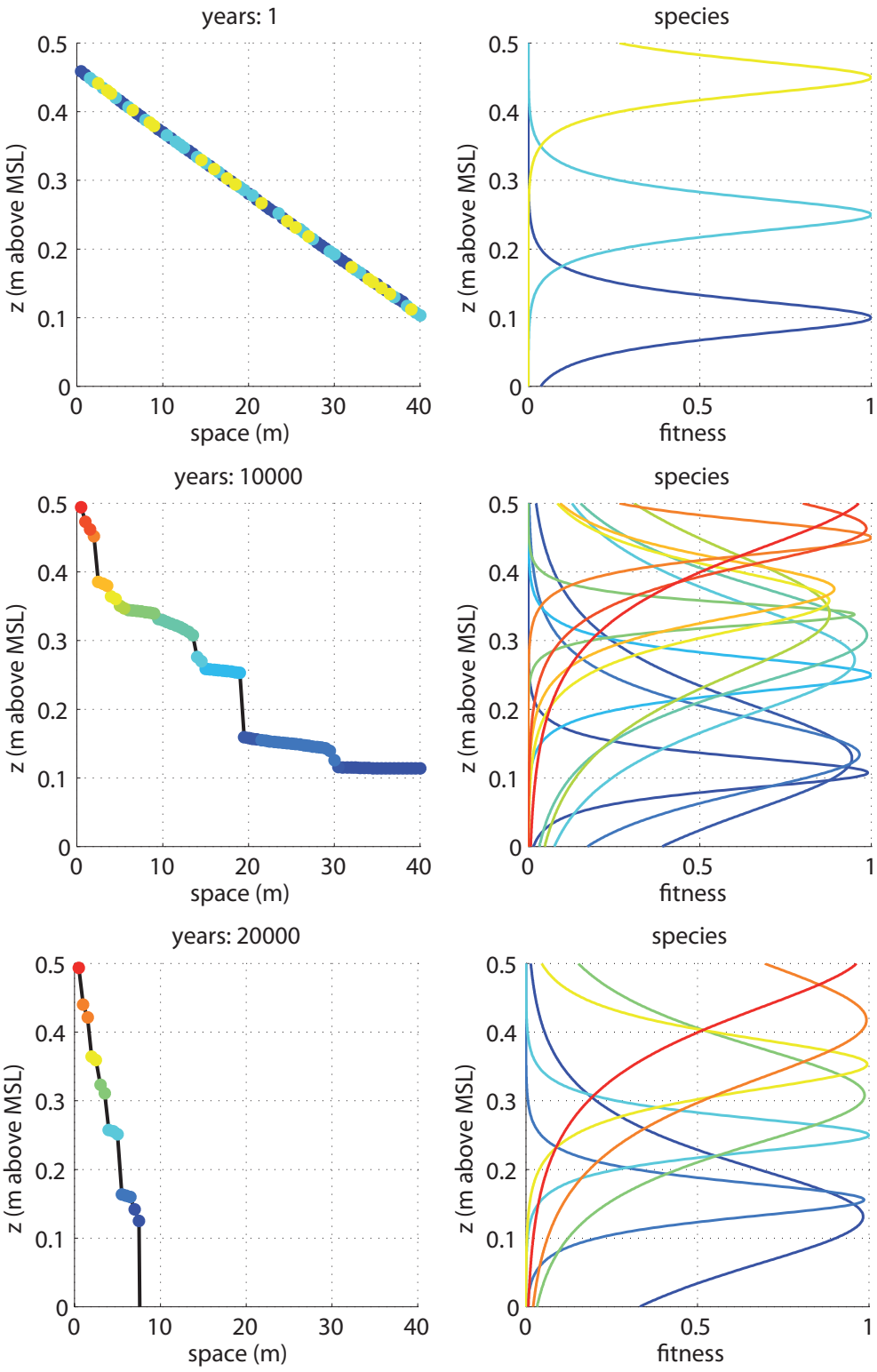

Figure 4.70: Analysis: 20. Time evolution of topography (left) and species (right). Rate of mutation adopted: 50 years. Mutation based on changing the fitness function mode, the maximum value and the variation value. Initial species differ from Analysis 19. More details in the supplementary material

4.12 Observations

Using a 1-D bio-geomorphological model, we explored the stable spatial equilibrium states (inorganic–controlled or organic–controlled) of marsh tidal environments. The 1-D model accounts the spatially environmental setting, the spatial biological and interspecific dynamics between the halophytic plants that live in the tidal environments, studies the biological-morphological interactions between the vegetation species and the topography, forming striking vegetation patterns. Hence, we explored the response of intertidal geomorphologies to different external forcings. Our analysis bring us to the following main observations:

i) A one-dimensional description of tidal biogeomorphology shows that biogeomorphic feedbacks are also responsible for the occurrence of smaller scale patterns characterized by the spatial distribution of marsh vegetation. Zonation patterns are shown to emerge as a result of the feedbacks between inorganic deposition and organic accretion, via biomass production. We highlight the crucial role of vegetation in shaping the tidal landscape: marsh vegetation acts as a landscape engineer by tuning platform elevation, leading to the formation of zonation structures.

ii) The tight feedback between primary productivity and topography suggests the possibility of decoding the signature of physiological plant adaptations in observed tidal marsh morphologies. In fact, we show here that specialized vegetation species, highly fit only within a narrow range of marsh elevations, exert a strong control on topography and constrain elevation within similarly narrow ranges. In contrast, vegetation species which are relatively well adapted to a broader range of marsh elevations more loosely tune the marsh landscape and produce more gradual transitions between adjacent vegetation patches.

iii) Vegetation controls on topography also hold in the presence of more realistic heterogeneous environmental forcings, such as soil properties and marsh

microtopography. Biogeomorphic patterns are less sharply defined in this case, but the underlying presence of multiple equilibria as the pattern-generating mechanism can still be detected via the presence of multiple peaks in the frequency distribution of topographic elevation. The one-to-one correspondence between such peaks and species abundance is the unique signature of vegetation as a landscape constructor.

iv) Possible biogeomorphic equilibria and the associated patterns are sensitive to changes in the forcings. Changes in the rate of RSLR, as example, produce the migration of marsh biogeomorphic patterns, eventually leading to their selective or complete disappearance when a critical rate of RSLR is exceeded. Because of the external prohibitive forcings, a part of the salt marsh could disappear but, in the remaining part, the stable salt marsh terraces-structures are still present, sign that the vegetation still imposes its balance on the marsh topography.

v) Even if, in this configuration, the model is not stable, the evolutionary dynamic is further developed introducing the species speciation. Coupling the spatial interspecific competition to the mutation mechanism, is interesting to see that the patterns formation is a strong characteristic in the evolutionary dynamic of tidal systems. We remark the crucial role of vegetation: marsh vegetation acts as a landscape engineer by tuning platform elevation, even more, with the mutation mechanism introduction. The species, able to compete among them, are free to evolve over time: this implies that only the new fit species can survive and contribute to the production of organic soil. In turn, the topography influences the kind of species appointed to colonize a small niche in the space system. The introduction of mutation allows not to prescribe the species a priori and allows to create a system totally free to evolve with the clearly two–way feedback between vegetation and topography discussed before.

Conclusions

We have analyzed the spatial distribution of biogeomorphic patterns characterizing tidal environments over a wide range of scales. Our key result is that multiple competing stable states, governed by two-way biogeomorphic feedbacks, provide a unifying framework to explain the formation of patterns in tidal environments from the system large–scale to the marsh small–scale.

In this Thesis we developed and applied a point coupled model which allows the identification of equilibrium conditions and transient dynamics that characterize marsh surfaces, tidal flats and subtidal platform. Model results emphasize the importance of accounting for the main interacting biological and physical components in order to obtain realistic representations of the system dynamics.

The number and the elevation of the equilibrium states, both in the sub-tidal and in the intertidal zones, depend, jointly, on a number of processes of physical and biological nature, such as: the rate of relative sea level rise, sediment supply, biomass productivity, wind climate, and the tidal range.

We relaxed some of the previous simplifying assumptions and explored the response of intertidal geomorphologies to realistic tidal forcings, time-varying sediment suspended concentrations and wind characteristics obtained from observations in the Venice Lagoon in order to address the crucial role of actual forcings on the equilibrium states.

Furthermore we developed a 1–D bio-geomorphic model accounting the spatial competition among different vegetation species also allowing the "free" mutation of species over time. Our model and observational analyses show that widely occurring zonation patterns are largely the result of ecological engineer-

ing performed by marsh vegetation species through the biomass-elevation feedback. When competition is assumed to operate according to a deterministic fittest-take-it-all mechanism, i.e. selecting the species whose organic–elevation productivity is maximum, the resulting bio-geomorphic zonation structures are located within relatively narrow and well-separated elevation ranges, colonized by single elevation species. Abrupt steps separate adjacent zonation patches in this extreme end-member case. When stochasticity in competition processes is accounted for, by assigning a probability of success proportional to the fitness of each competing species, the emerging spatial bio-geomorphic structures become less "quantized" and topographic and vegetational boundaries are more blurred, similarly to what is observed in nature. However, we show that, even when bio-geomorphic patterns become more subtle because of stochasticity, the signs of the governing feedbacks can still be detected by studying the possible presence of multimodality in the frequency distribution of marsh elevations. Topographic multimodality, in fact, can only arise if vegetation species tune soil elevation within ranges dictated by the local inorganic sediment availability and their preferred range of physiological adaptation.

We thus conclude that the existence of the competing stable states represents the large–scale pattern formation mechanism for tidal landscapes. Moreover, at marsh–scale, observed vegetation zonation structures are not simply induced by topography, to which vegetation species passively adapt, but rather by an active tuning of topography according to the elevational dependence of species fitness.

Bibliography

Adam, P. (1990). *Salt-marsh ecology*. Cambridge, UK, Cambridge Univ. Press.

Allen, J. R. L. (1995). Salt marsh growth and flandrian sea level: implication of a simulation model for flandrian coastal stratigraphy and peat-based sea-level curves. *Sedimentary Geology*, **100**, 21–45.

Allen, J. R. L. and Pye, K. (1992). *SALTMARSHES Morphodynamics, Conservation and Engineering Significance*. Cambridge University Press, New York.

Amos, C., Brylinsky, M., Sutherland, T., O'Brien, D., Lee, S., and Cramp, A. (1998). The stability of a mudflat in the humber estuary, south yorkshire, uk. *Geological Society, London, Special Publications*, **139**, 25–43.

Augustin, L., Irish, J., and Lynett, P. (2009). Laboratory and numerical studies of wave damping by emergent and near-emergent wetland vegetation. *Coastal Engineering*, **56**(3), 332–340.

Belluco, E., Camuffo, M., Ferrari, S., Modenese, L., Silvestri, S., Marani, A., and Marani, M. (2006). Mapping salt-marsh vegetation by multispectral and hyperspectral remote sensing. *Remote Sensing of Environment*, **105**, 54–67.

Bertness, M. and Ellison, A. (1987). Determinants of pattern in a new england salt marsh plant community. *Ecol. Mon., 57(2), 129-147.*

Bertness, M., Gough, L., and Shumway, S. (1992). Salt tolerances and the distribution of fugitive salt marsh plants. *Ecology 73:1842-1851. http://dx.doi.org/10.2307/1940035.*

Bockelmann, A., Bakker, J., Neuhaus, R., and Lage, J. (2002). The relation between vegetation zonation, elevation and inundation frequency in a wadden sea salt marsh. *Aquatic Botany, 73, 211-221.*

Bohannon, J. (2007). A sinking city yields some secrets. *Science*, **309**, 1978–1980.

Bruno, J. F., Stachowicz, J. J., and Bertness, M. D. (2003). Inclusion of facilitation into ecological theory. *Trends in Ecology and Evolution, 18, 199-125.*

Callaway, R., Jones, S., Ferrenn, W. R., , and Parikh, A. (1990). Ecology of a mediterranean-climate estuarine wetland at carpinteria, california: plant distributions and soil salinity in the upper marsh. *Canadian Journal of Botany 69:1139-1146.*

Carbognin, L., Teatini, P., and Tosi, L. (2004). Eustacy and land subsidence in the venice lagoon at the beginning of the new millennium. *Journal of Marine Systems*, **51**, 345–353.

Carniello, L., Defina, A., Fagherazzi, S., and D'Alpaos, L. (2005). A combined wind wave-tidal model for the venice lagoon, Italy. *Journal of Geophysical Research*, **110**(F04007). doi:10.1029/2004JF000232.

Carniello, L., D'Alpaos, A., and Defina, A. (2011). Modeling wind waves and tidal flows in shallow micro-tidal basins. *Estuarine, Coastal and Shelf Science*, **92**, 263–276. doi:10.1016/j.ecss.2011.01.001.

Chapman, V. (1976). *Coastal Vegetation.* second ed. Pergamon Press, Oxford, 292 pp.

Christiansen, T., Wiberg, P., and Milligan, T. (2001). Flow and sediment transport on a tidal salt marsh surface. *Estuarine Coastal Shelf Science*, **50**, 315–331.

Corenblit, D., Baas, A., Bornette, G., Delmotte, S., Francis, R., Gurnell, A., Julien, F., Naiman, R., and Steiger, J. (2011). Feedbacks between geomorphology and biology controlling earth surface processes and landforms: a review of foundation concepts and current understandings. *Earth-Science Reviews 106, 307-331.*

Costa, C., Marangoni, J., and Azevedo, A. (2003). Plant zonation in irregularly flooded salt marshes: relative importance of stress tolerance and biological interactions. *Journal of Ecology 91, 951-965.*

Da Lio, C., D'Alpaos, A., and Marani, M. (2012). Emergent bio-geomophic patterns in tidal environments. *Phil. Trans. R. Soc. A.* Under Review.

D'Alpaos, A. (2011). The mutual influence of biotic and abiotic components on the long-term ecomorphodynamic evolution of salt-marsh ecosystems. *Geomorphology*, **126**, 269–278. doi:10.1016/j.geomorph.2010.04.027.

D'Alpaos, A., Lanzoni, S., Mudd, S., and Fagherazzi, S. (2006). Modelling the influence of hydroperiod and vegetation on the cross-sectional formation of tidal channels. *Estuarine Coastal Shelf Science*, **69**, 311–324. doi:10.1016/j.ecss.2006.05.002.

D'Alpaos, A., Lanzoni, S., Marani, M., and Rinaldo, A. (2007). Landscape evolution in tidal embayments: modeling the interplay of erosion sedimentation and vegetation dynamics. *Journal of Geophysical Research*, **112**(F01008). doi:10.1029/2006JF000537.

D'Alpaos, A., Da Lio, C., and Marani, M. (2011a). Biogeomorphology of tidal landforms: physical and biological processes shaping the tidal landscape. *Ecohydrol.*, **5**, 550–562. doi: 10.1002/eco.279.

D'Alpaos, A., Mudd, S. M., and Carniello, L. (2011b). Dynamic response of marshes to perturbations in suspended sediment concentrations and rates of relative sea level rise. *Journal of Geophysical Research.* doi:10.1029/2011JF002093.

Day, J., Rybczyk, J., Scarton, F., Rismondo, A., Are, D., and Cecconi, G. (1999). Soil accretionary dynamics, sea-level rise and the survival of wetlands in venice lagoon: a field and modelling approach. *Estuarine, Coastal and Shelf Science, 49, 607-628.*

Day, J., Boesch, D., Clairain, E., and et al. (2007). Restoration of the mississippi delta: Lessons from hurricanes katrina and rita. *Science*, **315**(5819), 1679–1684. doi:10.1126/science.1137030.

Defina, A., Carniello, L., Fagherazzi, S., and D'Alpaos, L. (2007). Self organization of shallow basins in tidal flats and salt marshes. *Journal of Geophysical Research*, **112**(F03001). doi:10.1029/2006JF000550.

D'Odorico, P., Laio, F., Porporato, A., Ridolfi, L., Rinaldo, A., and Rodriguez-Iturbe, I. (2010). Ecohydrology of terrestrial ecosystems. *Bioscience*, **60**(11), 898–907. doi:10.1525/bio.2010.60.11.6.

Elder, J. W. (1959). The dispersion of marked fluid in turbulent shear flow. *J. Fluid Mech., 5, 544-560.*

Fagherazzi, S., Marani, M., and Blum, L. K. (2004). *The coupled evolution of geomorphological and ecosystem structures in salt marshes, in The Ecogeomorphology of Tidal Marshes.* Coastal Estuarine Stud., vol. 59, edited by S. Fagherazzi,M.Marani, and L. K. Blum, pp. 1-5, AGU, Washington, D. C.

Fagherazzi, S., Carniello, L., D'Alpaos, L., and Defina, A. (2006). Critical bifurcation of shallow microtidal landforms in tidal flats and salt marshes. *Proceedings of the Natural Academy of Sciences U.S.A.*, **103**(22), 8337–8341. doi:10.1146/annurev.earth.35.031306.140128.

Fagherazzi, S., Kirwan, M., Mudd, S., Guntenspergen, G., Temmerman, S., D'Alpaos, A., van de Koppel, J., Rybczyk, J., Reyes, E., Craft, C., and Clough, J. (2012). Numerical models of salt marsh evolution: ecological, geomorphic, and climatic factors. *Rev. Geophys., 50(RG1002), 1-28.*

Feola, A., Belluco, E., D'Alpaos, A., Lanzoni, S., Marani, M., and Rinaldo, A. (2005). A geomorphic study of lagoonal landforms. *Water Resources Research*, **41**(W06019). doi:10.1029/2004WR003811.

Gibbs, R. (1985). Estuarine flocs e their size, settling velocity and density. *J. Geophys. Res.*, **90**, 3249–3251.

Grace, J. and Wetzel, R. (1981). Habitat partitioning and competitive displacement in cattails (typha): experimental field studies. *The American Naturalist, 118, 463-74.*

Jones, C., Lawton, J., and Shachak, M. (1994). Organisms as ecosystem engineers. *Oikos*, **69**, 373–386.

Jones, C., Lawton, J., and Shachak, M. (1997). Positive and negative effects of organisms as physical ecosystem engineers. *Ecology, 78, 1946-1957.*

Kirwan, M. and Guntenspergen, G. (2010). Influence of tidal range on the stability of coastal marshland. *Journal of Geophysical Research*, **115**(F02009). doi:10.1029/2009JF001400.

Kirwan, M. and Murray, A. (2007). A coupled geomorphic and ecological model of tidal marsh evolution. *Proceedings of the Natural Academy of Sciences U.S.A.*, **104**(15), 6118–6122. doi:10.1073/pnas.0700958104.

Kirwan, M., Murray, A., and Boyd, W. (2008). Temporary vegetation disturbance as an explanation for permanent loss of tidal wetlands. *Geophysical Research Letters*, **35**(L05403). doi:10.1029/2007GL032681.

Kirwan, M., Guntenspergen, G., D'Alpaos, A., Morris, J., Mudd, S., and Temmerman, S. (2010). Limits on the adaptability of coastal marshes to rising sea level. *Geophysical Research Letters*, **37**(L23401). doi:10.1029/2010GL045489.

Kirwan, M. L., Murray, A. B., Donnelly, J. P., and Corbett, D. R. (2011). Rapid wetland expansion during european settlement and its implication for marsh

survival under modern sediment delivery rates. *Geology*, **39**(5), 507–510. doi: 10.1130/G31789.1.

Krone, R. B. (1987). *A method for simulating historic marsh elevations, in: Coastal Sediments 87, edited by N.C. Krause*. Am. Soc. Civ. Eng., New York.

Larsen, L. and Harvey, J. (2010). How vegetation and sediment transport feedbacks drive landscape change in the everglades and wetlands worldwide. *Am. Nat.*, **176**(3), E66–E79. doi: 10.1086/655215.

Leeuw, J. D., Munck, W. D., Olff, H., and Bakker, J. (1993). Does zonation reflect the succession of salt-marsh vegetation? a comparison of an estuarine and a coastal island marsh in the netherlands. *Acta Botanica Neerlandica 42, 435-445.*

Leonard, L. A. and Croft, A. L. (2006). The effect of standing biomass on flow velocity and turbulence in *Spartina alterniflora* canopies. *Estuarine Coastal Shelf Science*, **69**, 325–336.

Levine, J., Brewer, J., and Bertness, M. (1998). Nutrients, competition and plant zonation in a new england salt marsh. *Journal of Ecology, 86: 285-292. doi: 10.1046/j.1365-2745.1998.00253.x.*

Levins, R. (1969). Some demographic and genetic consequences of environmental heterogeneity for biological control. *Bulletin of the Entomological Society of America*, **15**, 237–240.

MacIntyre, H., Geiger, R., and Miller, D. (1996). Microphytobenthos: The ecological role of the secret garden of unvegetated, shallow-water marine habitats: 1. distribution, abundance and primary production. *Estuaries*, **19**(2A), 186–201.

Marani, M., Belluco, E., D'lpaos, A., Defina, A., Lanzoni, S., and Rinaldo, A. (2003). On the drainage density of tidal networks. *Water Resources Research 39, 1040, doi:10.1029/2001WR001051.*

Marani, M., Lanzoni, S., Silvestri, S., and Rinaldo, A. (2004). Tidal landforms, patterns of halophytic vegetation and the fate of the lagoon of venice. *Journal of Marine Systems*, **51**, 191–210. doi:10.1016/j.jmarsys.2004.05.012.

Marani, M., Belluco, E., Ferrari, S., Silvestri, S., D'Alpaos, A., Lanzoni, S., Feola, A., and Rinaldo, A. (2006a). Analysis, synthesis and modelling of high-resolution observations of salt-marsh ecogeomorphological patterns in the venice lagoon. *Estuarine Coastal Shelf Science*, **69**(3-4), 414–426. doi:10.1016/j.ecss.2006.05.021.

Marani, M., Zillio, T., Belluco, E., Silvestri, S., and Maritan, A. (2006b). Non-neutral vegetation dynamics. *PLoS ONE, 1, 1-5.*

Marani, M., Silvestri, S., Belluco, E., Ursino, N., Comerlati, A., Tosatto, O., and Putti, M. (2006c). Spatial organization and ecohydrological interactions in oxygen-limited vegetation ecosystems. *Water Resources Research*, **42**(W07S06). doi:10.1029/2005WR004582.

Marani, M., D'Alpaos, A., Lanzoni, S., Carniello, L., and Rinaldo, A. (2007). Biologically controlled multiple equilibria of tidal landforms and the fate of the venice lagoon. *Geophysical Research Letters*, **34**(L11402). doi:10.1029/2007GL030178.

Marani, M., D'Alpaos, A., Lanzoni, S., Carniello, L., and Rinaldo, A. (2010). The importance of being coupled: Stable states and catastrophic shifts in tidal biomorphodynamics. *Journal of Geophysical Research*, **115**(F04004). doi:10.1029/2009JF001600.

Marani, M., Da Lio, C., and D'Alpaos, A. (2012). The secret gardener: marsh vegetation as a landscape constructor. *Proc. Natl. Acad. Sci. U. S. A.* In press.

Matthews, B., Narwani, A., Hausch, S., Nonaka, E., Peter, H., Yamamichi, M., Sullam, K. E., Bird, K. C., Thomas, M. K., Hanley, T. C., and Turner, C. B.

(1997). Toward an integration of evolutionary biology and ecosystem science. *Ecology Letters, 14: 690-701. doi: 10.1111/j.1461-0248.2011.01627.x.*

Meehl, G. A. e. a. (2007). *Global climate projections, in: Climate Change 2007: The Physical Science Basis: Contribution of Working Group I to the Fourth Assessment Report of the Intergovernmental Panel on Climate Change, edited by S. Solomon et al.* Cambridge Univ. Press, Cambridge, U. K.

Middelburg, J., Barranguet, C., Boschker, T., Herman, P., Moens, T., and Heip, C. (2000). The fate of intertidal microphytobenthos carbon: An in situ 13c-labeling study. *Limnol. Oceanogr. 45: 1224-1234.*

Miller, D., Geider, R., and MacIntyre, H. (1996). Microphytoberthos: The ecological role of the "secret garden" of unvegetated, shallow-water marine habitats. ii. role in sediment stability and shallow-water food webs. *Estuaries 19:202-212.*

Mitchell-Olds, T. and Clauss, M. J. (2002). Plant evolutionary genomics. *Current Opinion in Plant Biology, 5, 74-79.*

Möller, I., Spencer, T., French, J., Leggett, D., and Dixon, M. (1999). Wave transformation over salt marshes: A field and numerical modelling study from north norfolk, england. *Estuarine, Coastal and Shelf Science*, **49**, 411–426.

Morris, J. T. (2006). Competition among marsh macrophytes by means of geomorphological displacement in the intertidal zone. *Estuarine, Coastal and Shelf Science*, **69**, 395–402, doi:10.1016/j.ecss.2006.05.025.

Morris, J. T. (2007). Ecological engineering in intertidial saltmarshes. *Hydrobiologia, 577, 161-168.*

Morris, J. T. and Haskin, B. (1990). A 5-yr record of aerial primary production and stand characteristics of *Spartina alterniflora*. *Ecology*, **7**(16), 2209–2217.

Morris, J. T., Sundareshwar, P. V., Nietch, C. T., Kjerfve, B., and Cahoon, D. R. (2002). Responses of coastal wetlands to rising sea level. *Ecology*, **83**, 2869–2877.

Mudd, S. M. (2011). The life and death of salt marshes in response to anthropogenic disturbance of sediment supply. *Geology*, **39**(5), 511–512. 10.1130/focus052011.1.

Mudd, S. M., Fagherazzi, S., Morris, J. T., and Furbish, D. J. (2004). *Flow, sedimentation, and biomass production on a vegetated salt marsh in South Carolina: toward a predictive model of marsh morphologic and ecologic evolution, in: The Ecogeomorphology of Tidal Marshes, Coastal and Estuarine Studies, edited by Fagherazzi, S., M. Marani, and L.K. Blum*, volume 59. AGU, Washigton, D.C.

Mudd, S. M., Howell, S. M., and Morris, J. T. (2009). Impact of dynamic feedbacks between sedimentation, sea-level rise, and biomass production on near surface marsh stratigraphy and carbon accumulation. *Estuarine, Coastal and Shelf Science*, **82**(3), 377–389.

Mudd, S. M., D'Alpaos, A., and Morris, J. T. (2010). How does vegetation affect sedimentation on tidal marshes? Investigating particle capture and hydrodynamic controls on biologically mediated sedimentation. *Journal of Geophysical Research*, **115**(F03029). doi:10.1029/2009JF001566.

Muneepeerakul, R., Bertuzzo, E., Rinaldo, A., and Rodriguez-Iturbe, I. (2008). Patterns of vegetation biodiversity: the roles of dispersal directionality and river network structure. *Journal of Theoretical Biology*, **252**(2), 221–229. doi: 10.1016/j.jtbi.2008.02.001.

Murray, A., Knaapen, M. A. F., Tal, M., and Kirwan, M. L. (2008). Biomorphodynamics: Physical-biological feedbacks that shape landscapes. *Water Resources Research*, **44**(W11301). doi:10.1029/2007WR006410.

Neubauer, S. (2008). Contributions of mineral and organic components to tidal freshwater marsh accretion. *Estuarine Coastal and Shelf Science*, **78**(1), 78–88. 10.1016/j.ecss.2007.11.011.

Neumeier, U. and Ciavola, P. (2004). Flow resistance and associated sedimentary processes in a *Spartina maritima* salt marsh. *Journal of Coastal Research*, **20**(2), 434–447.

Nyman, J. A., Walters, R. J., Delaune, R. D., and Patrick, W. H. (2006). Marsh vertical accretion via vegetative growth. *Estuarine Coastal and Shelf Science*, **69**(3-4), 370–380.

Partheniades, E. (1965). Erosion and deposition of cohesive soils. *Journal of the Hydraulics Division, ASCE*, **91**(HY2), 105–138.

Paterson, D. (1989). Short-term changes in the erodibility of intertidal cohesive sediments related to the migratory behaviour of epipelic diatoms. *Limnology and Oceanography*, **34**, 223–234.

Pennings, S. and Callaway, R. (1992). Salt marsh plant zonation: the relative importance of competition and physical factors. *Ecology, 73(2), 681-690.*

Pignatti, S. (1966). *La vegetazione alofila della laguna veneta.* Istituto Veneto di Scienze, Lettere ed Arti, Memorie, Volume 33(1), Venezia.

Randerson, P. F. (1979). *A simulation model of salt-marsh development and plant ecology. In: Estuarine and Coastal Land Reclamation and Water Storage, edited by B. Knights and A. J. Phillips.* Farnborough, Saxon House.

Reinhardt, L., Jerolmack, D., Cardinale, B., Vanacker, V., and Wright, J. (2010). Dynamic interactions of life and its landscape: feedbacks at the interface of geomorphology and ecology. *Earth Surf. Process. Landforms*, **35**, 78–101. DOI: 10.1002/esp.1912.

Rinaldo, A., Fagherazzi, S., Lanzoni, S., Marani, M., and Dietrich, W. E. (1999a). Tidal networks 2. Watershed delineation and comparative network morphology. *Water Resources Research*, **35**(12), 3905–3917.

Rinaldo, A., Fagherazzi, S., Lanzoni, S., Marani, M., and Dietrich, W. E. (1999b). Tidal networks 3. Landscape-forming discharges and studies in empirical geomorphic relationships. *Water Resources Research*, **35**(12), 3919–3929.

Rogel, J., Silla, R., and Ariza, F. (2001). Edaphic characterization and soil ionic composition influencing plant zonation in a semiarid mediterranean salt marsh. *Geoderma 99, 81-98.*

Sanderson, E., Ustin, S., and Foin, T. (2000). The influence of tidal channels on the distribution of salt marsh plant species in petaluma marsh, ca, usa. *Plant Ecology 146, 29-41.*

Schneider, S. H. (1997). The rising seas. *Scientific American*, **3**, 112–118.

Silvestri, S., Defina, A., and Marani, M. (2005). Tidal regime, salinity and salt-marsh plant zonation. *Estuarine Coastal Shelf Science*, **62**, 119–130.

Stachowicz, J. J. (2011). Mutualism, facilitation, and the structure of ecological communities. *Bioscience 51, 235-246.*

Stockwell, C., Hendry, A., and Kinnison, M. (2003). Contemporary evolution meets conservation biology. *Ecology and Evolution, 18(2), 94-101.*

Sundbäck, K. and Granéli, W. (1988). Influence of microphytobenthos on the nutrient flux between sediment and water: a laboratory study. *Mar. Ecol. Prog. Ser. 43: 63-69.*

Temmerman, S., Govers, G., Meire, P., and Wartel, S. (2003). Modelling long-term tidal marsh growth under changing tidal conditions and suspended sediment concentrations, scheldt estuary, belgium. *Marine Geology*, **193**(1-2), 151–169.

Temmerman, S., Bouma, T. J., Van de Koppel, J., Van der Wal, D., De Vries, M. B., and Herman, P. M. J. (2007). Vegetation causes channel erosion in a tidal landscape. *Geology*, **35**(7), 631–634. 10.1029/2004JF000243.

Turner, R. E., Swenson, E. M., Milan, C. S., Lee, J. M., and Oswald, T. (2004). Below-ground biomass in healthy and impaired salt marshes. *Ecological Research*, **19**(1), 29–35. doi:10.1111/j.1440-1703.2003.00610.x.

Ungar, I. (1991). *Ecophysiology of Vascular Halophytes*. CRC Press, Boca Raton, Fla.

van de Koppel, J., van der Wal, D., Bakker, J., and Herman, P. (2005). Self-organization and vegetation collapse in salt marsh ecosystems. *American Naturalist*, **165**, E1–E12.

van Ledden, M., Wang, Z., Winterwerp, H., and de Vriend, H. (2005). Sandmud morphodynamics in a short tidal basin. *Ocean Dynamics*, **54**(3-4), 385–391.

Viles, H. (1988). *Biogeomorphology*. Basil Blackwell, Oxford, UK.

Wang, C., Menenti, M., Stoll, M. P., Feola, A., Belluco, E., and Marani, M. (2009). Separation of ground and low vegetation signatures in lidar measurements of salt-marsh environments. *IEEE Transactions on Geoscience and Remote Sensing*, **47**, 2014–2023.

Widdows, J. and Brinsley, M. (2002). Impact of biotic and abiotic processes on sediment dynamics and the consequences to the structure and functioning of the intertidal zone. *Journal of Sea Research 48, 143-156.*

Wilson, S. and Keddy, P. (1985). Plant zonation on a shoreline gradient: physiological response curves of component species. *J. Ecol. 73: 851-860.*

Yallop, M., Winder, B., Paterson, D., and Stal, U. (1994). Comparative structure, primary production and biogenic stabilisation of cohesive and non-cohesives marine sediments inhabited by microphytobenthos. *Estuar Coast Shelf Sci 39:565-582.*

Yoo, K., Amundson, R., Heimsath, A., and Dietrich, W. (2005). Processbased model linking pocket gopher (thomomys bottae) activity to sediment transport and soil thickness. *Geology*, **33**, 917–920.

FINITO DI SCRIVERE NEL MESE DI GENNAIO 2013